Impact of biogeochemical processes on pH dynamics in marine systems

Mathilde Hagens

Impact of biogeochemical processes on pH dynamics in marine systems

Invloed van biogeochemische processen
op de dynamiek van pH in mariene systemen
(met een samenvatting in het Nederlands)

Wpływ procesów biogeochemicznych
na dynamikę wartości pH w morskich systemach
(z polskim streszczeniem)

Proefschrift

ter verkrijging van de graad van doctor aan de Universiteit Utrecht
op gezag van de rector magnificus, prof. dr. G. J. van der Zwaan,
ingevolge het besluit van het college voor promoties in het openbaar te verdedigen op

vrijdag 26 juni 2015 des middags te 2.30 uur

door

Mathilde Hagens

geboren op 18 april 1986 te Soest

Promotoren:

Prof. Dr. J. J. Middelburg
Prof. Dr. ir. C. P. Slomp

Abstract

Uptake of anthropogenic carbon dioxide (CO_2) from the atmosphere has resulted in a range of changes in ocean chemistry, including the lowering of pH, collectively referred to as ocean acidification. Rates of coastal-zone acidification exceed those of the open ocean since coastal-ocean pH is influenced by many other processes than absorption of CO_2 alone. These processes do not only play a role in long-term acidification but also impact pH on seasonal timescales. Examples are enhanced atmospheric sulphur and nitrogen deposition, as well as eutrophication, the latter which can additionally result in the development of low-oxygen waters. The degree to which these processes induce a change in pH depends both on their rates and the extent to which the water can buffer acid production or consumption. This acid-base buffering capacity has been shown to decrease substantially in hypoxic waters, suggesting that low-oxygen conditions exacerbate ocean acidification. In this dissertation the key factors controlling the seasonal pH variability and longer-term pH changes in both the coastal and open ocean were examined, showing that buffering mechanisms play a crucial role in the impact of any biogeochemical or physical process on pH.

Monthly or seasonal water-column chemistry and process-rate measurements in a transiently hypoxic coastal marine basin indicate that, despite generally higher process rates in the surface water of the basin, the amplitude of pH variability as mainly governed by the balance between primary production and respiration is greater in the seasonally-hypoxic bottom water, due to a considerable reduction of its acid-base buffering capacity in summer. A proton budget, based on these measurements and set up for each season, shows that the net change in pH is much smaller than the flux of protons induced by each of the individual processes.

The interplay between absorption of atmospheric CO_2 and atmospheric sulphur and nitrogen deposition in the coastal ocean was found to depend on the water-column concentration of CO_2 relative to the atmosphere. If the atmospheric concentration surpasses that of the surface water, then this part of the coastal ocean is most sensitive to CO_2-induced acidification, but least affected by additional acidification resulting from atmospheric acid deposition. Although coastal seas will become up to a factor 4 more sensitive to atmospheric deposition-induced acidification between the present-day and 2100, the annual change in proton concentration will only increase by 28% at most.

Finally, a set of general expressions describing the sensitivity of pH to a change in ocean chemistry was derived. These expressions, which can include as many acid-base systems as relevant and are thus generally applicable, were tested on several long-term open ocean data sets. For each of these sites, pH can be properly predicted if seasonal cycles of temperature, salinity, total alkalinity (TA) and the total concentrations of acid-base species are known. By the end of the 21st century a change in most acid-base parameters will induce a comparably greater pH excursion. This increased vulnerability is driven by enhanced CO_2 concentrations and slightly moderated by the projected global warming.

Contents

Chapter 1:

General introduction and synopsis

"Nothing in life is to be feared, it is only to be understood. Now is the time to understand more, so that we may fear less."

Marie Skłodowska Curie

1.1   Carbon cycle

The element carbon (C) is often considered a building block of life on Earth, being one of the requirements for organic molecule formation. In addition, in its gaseous forms, carbon dioxide (CO_2) and methane (CH_4), it contributes to the quantity of infrared radiation being trapped in Earth's atmosphere (Berner and Berner, 1996). Because of this absorption, generally referred to as the greenhouse effect, Earth has a moderate temperature allowing it to evolve into a habitable planet (Ruddiman, 2001). The cycling of C is therefore of utmost importance in regulating Earth's climate (Berner and Caldeira, 1997).

The global biogeochemical C cycle (Fig. 1.1) can be divided into short-term (i.e. hundreds to thousands of years) and long-term cycles (Berner, 1991), which are naturally connected via long-term sedimentary C burial and subsequent weathering, in addition to volcanic activity (Ruddiman, 2001). It is the partitioning between the amounts of C in the various reservoirs that determines the CO_2 content of the atmosphere (Ridgwell and Zeebe, 2005). Given that the size of the atmospheric C reservoir is comparably smaller than other reservoirs in the short-term cycle, minor changes in C cycling can have a large impact on the atmospheric CO_2 content (Williams and Follows, 2011). Variations in the segmentation of C occur over several time scales, with tectonic-scale variations (i.e. over millions of years) driven by chemical weathering, thereby acting as a negative climate feedback mechanism (Ruddiman, 2001). Fluctuations in C cycling on glacial-interglacial time scales (i.e. tens to hundreds of thousands of years) are caused by the amount of incoming solar radiation, which in turn is driven by physical forcing mechanisms regulating changes in the orientation of Earth's rotational axis and the shape of its orbit around the Sun, collectively referred to as Milankovitch cycles (Berger, 1980; Milanković, 1941).

Human activity has substantially altered the global C cycle since ca. 1850 by exploiting geologically stored organic C in the form of oil, natural gas and coal and adding it to the short-term cycle (Sarmiento and Gruber, 2002). Moreover, both deforestation (Houghton et al., 1983) and cement manufacturing (Rotty, 1981) result in an additional flux of CO_2 to the atmosphere. As a result, the partial pressure of CO_2 (pCO_2) in the atmosphere has increased from its upper bound in the current glacial-interglacial cycle (Petit et al., 1999) of 280 to 400 parts per million by volume (ppmv) over the last ~200 years (Fig. 1.2). While atmospheric pCO_2 has substantially exceeded its present level several times in geological history, of which the early Palaeozoic, the Mesozoic, the Cretaceous (Berner, 1997) and the Palaeocene-Eocene Thermal Maximum (Sluijs et al., 2007) are well-known examples, the current rate of change is unprecedented in the last 22 000 years, and likely much longer (IPCC, 2013).

This unequivocal alteration of the C cycle has major implications for Earth's climate system, most prominently its warming, leading to sea level rise, diminishing of ice sheets and significantly less snow cover (IPCC, 2013). These changes would have been greater amplified if all anthropogenic CO_2 emissions were to remain in the atmosphere. However, fast turnover of C in the various compartments of the short-term C cycle (Fig. 1.1) enables partitioning of the human-induced CO_2 flux between the atmosphere (~45%), the terrestrial biosphere (~29%), and the ocean (~26%; Le

Quéré et al., 2009). The oceanic sink of atmospheric CO_2 and its implications for ocean chemistry are the focus of this dissertation.
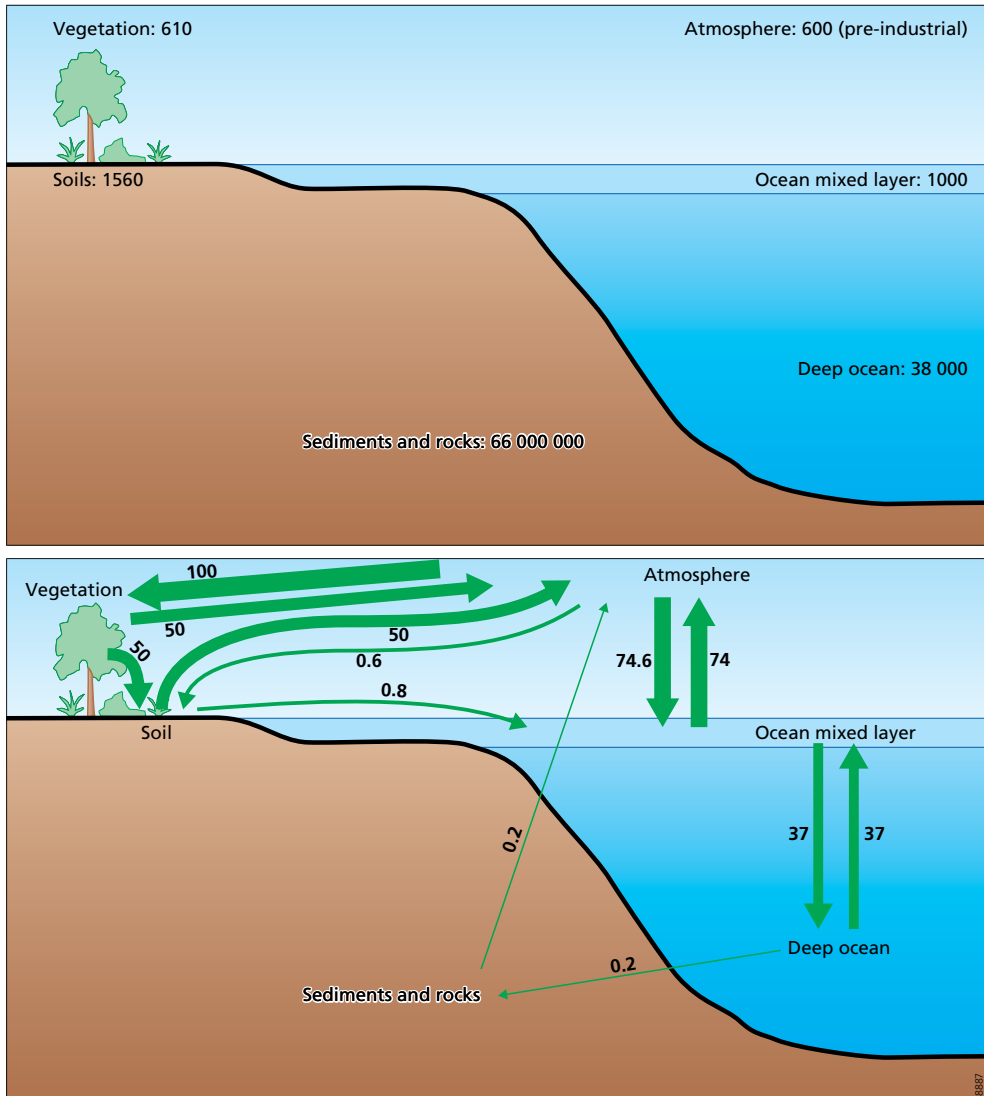
Figure 1.1 Major reservoirs of the global C cycle (Pg C; upper panel), and pre-industrial fluxes between the major reservoirs (Pg C yr^{-1}; lower panel). Prior to human activity, the exchange rates between the reservoirs of the long-term (sediments and rocks) and short-term C cycle were in balance. Figure adapted from Ruddiman (2001).
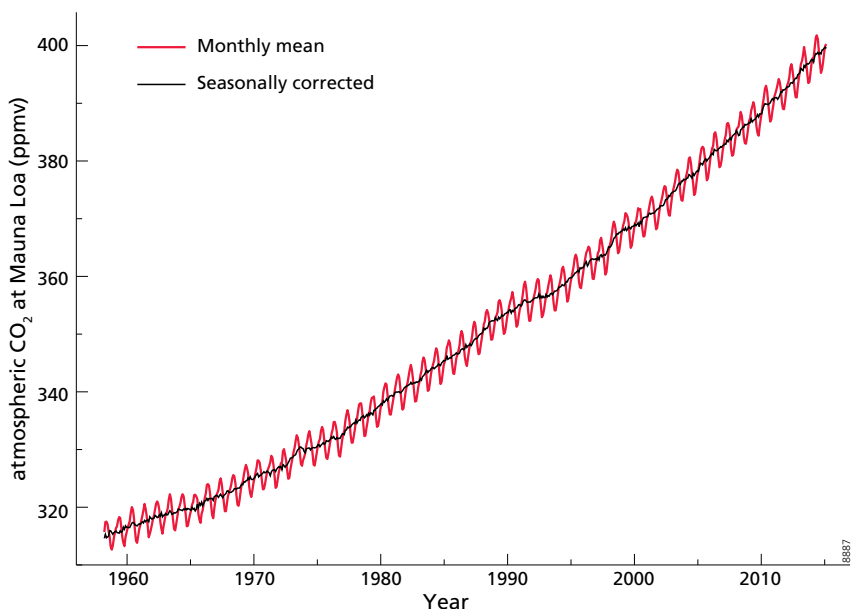
Figure 1.2 Monthly mean and seasonally corrected atmospheric CO_2 concentration (ppmv) as measured at Mauna Loa Observatory, Hawaii, USA, since March 1958. In February 2015, monthly mean CO_2 reached a concentration of 400.26 ppmv. Figure taken from Dr. Pieter Tans, NOAA/ERSL (http://www.esrl.noaa.gov/ gmd/ccgg/trends/) and Dr. Ralph Keeling, Scripps Institution of Oceanography (http://scrippsco2.ucsd. edu/).

1.2   Marine carbonate system

The transfer of C from the atmosphere to the ocean occurs in the form of CO_2 and follows Henry's law, which states that at a given temperature the solubility of CO_2 in seawater is directly proportional to atmospheric pCO_2 (Henry, 1803). This law also applies to other atmospheric gasses, thereby impacting e.g. the oxygen (O_2) content of the surface ocean (Sarmiento and Gruber, 2006). However, the equilibration time of atmospheric and oceanic CO_2 is ca. 20 times longer than that of other gasses (Sarmiento and Gruber, 2006). Furthermore, in contrast to O_2, the vast majority (~98%) of CO_2 in the combined ocean-atmosphere system is present in the oceanic reservoir (Zeebe and Wolf-Gladrow, 2001). These peculiar features are driven by unique intrinsic properties of CO_2 that convolute its partitioning between the ocean and the atmosphere. More specifically, CO_2 is not the only form of inorganic C present in seawater. On dissolving in seawater, CO_2 hydrates to form carbonic acid (H_2CO_3). Aqueous CO_2 and H_2CO_3 are chemically indistinguishable and usually denoted as a single C species, although it is known that H_2CO_3 comprises less than ~0.3% of this pool (Zeebe and Wolf-Gladrow, 2001). Here, this pool is referred to as total dissolved CO_2 and denoted CO_2. Total dissolved CO_2 is a weak acid that can donate a hydrogen ion or proton (H^+) to form bicarbonate (HCO_3^-), which, in turn, has the carbonate ion (CO_3^{2-}) as a conjugate base. The

sum of these three C species is referred to as dissolved inorganic carbon (DIC), and the acid-base system involving DIC and its contributing species is termed the carbonate system.

Dependent on acid-base equilibria, the transition between the three different species constituting DIC is determined by the concentration of H^+, usually denoted as its negative logarithm, which is better known as pH (Fig. 1.3). Pre-industrial average oceanic surface-water pH is ~8.2, from which it follows that HCO_3^- is the dominant species of DIC (~90%), followed by CO_3^{2-} (~9%; Williams and Follows, 2011). CO_2 thus comprises only ~1% of the inorganic oceanic C reservoir, explaining why the partitioning of CO_2 between the atmosphere and the ocean differs so much from that of e.g. O_2. In fact, only ca. 1 of 20 molecules of atmospheric CO_2 that dissolves in seawater will remain in this form, meaning that about 20 times more CO_2 than O_2 must be exchanged between the atmosphere and the ocean to reach equilibrium (Sarmiento and Gruber, 2006). The time scale at which CO_2 equilibrium is reached (~6 months for a 40-m thick surface layer; Sarmiento and Gruber, 2006) may be comparably longer than the time scale at which biological and physical processes act on the oceanic reservoir, implying that on seasonal time scales equilibrium is usually not reached. Presumably however, on a longer time scale the pre-industrial ocean and atmosphere may reach equilibrium (Fig. 1.1).

Assessing the amount of atmospheric CO_2 absorbed by the oceans requires accurate calculations of the oceanic carbonate system. So far six chemical properties associated with this system have been discussed (pCO_2, CO_2, HCO_3^-, CO_3^{2-}, DIC and pH), as well as four interrelating equations (two acid-base equilibria, the definition of DIC and Henry's law). Any mathematical problem can be solved if the number of unknowns is equal to the number of associated equations. Therefore, to perform calculations on the carbonate system, at least two of the six parameters mentioned above need to be known. All properties but DIC are part of an acid-base equilibrium and are thus affected by changes in state (i.e. temperature, salinity or pressure), making them more difficult to use for certain applications (Sarmiento and Gruber, 2006). Most marine chemists therefore use an additional property with a corresponding equation that is also conservative with respect to state, i.e. total alkalinity (TA).

The concept of TA is not trivial and, depending on the underlying assumptions, can be defined differently. The most commonly used definition is operationally based and states that TA is the difference between base and acid concentrations under certain reference conditions, i.e. a pH of 4.5, a temperature of 25°C, zero ionic strength (a measure of the concentration of ions in solution) and standard atmospheric pressure (Dickson, 1981). An alternative definition for TA in terms of major conservative ions and the total concentrations of acid-base species can be derived from this using the principle of electro-neutrality of solutions (Wolf-Gladrow et al., 2007). At a pH of 4.5, CO_2 is the dominant DIC species (Fig. 1.3) and thus is the reference proton level in the definition of TA (Stumm and Morgan, 1996). Therefore, its addition or removal does not change TA (MacIntyre, 1978), and both HCO_3^- and CO_3^{2-} act as bases relative to the reference species. Since HCO_3^- takes up 1 H^+ when recombining into CO_2, while CO_3^{2-} requires 2 H^+ for this process, the contribution of CO_3^{2-} to TA is twice that of HCO_3^-. In addition to the carbonate system, many other acid-base systems are present in seawater, which all contribute to TA (Dickson, 1981). The most important
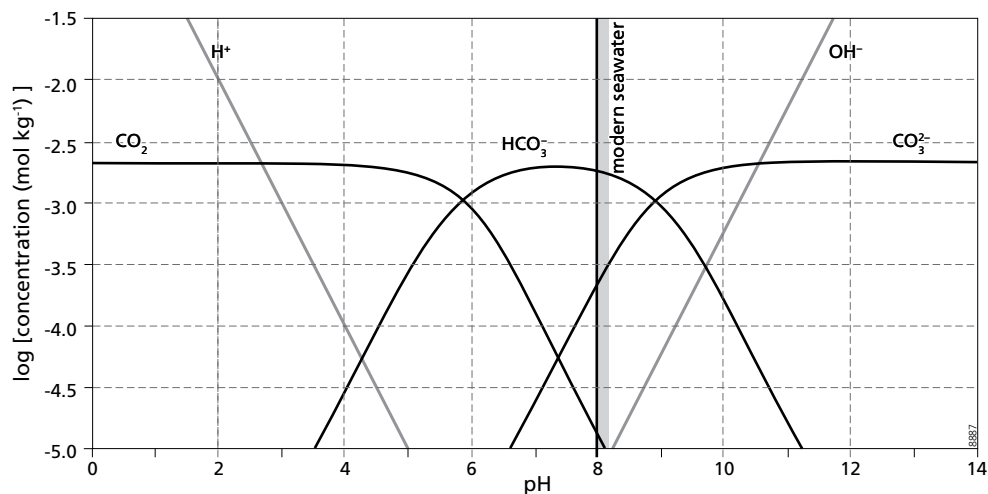
Figure 1.3 Bjerrum plot (named after N. Bjerrum who developed this graphical representation of acid-base speciation; Zeebe and Wolf-Gladrow, 2001) showing the concentrations of CO_2, HCO_3^- and CO_3^{2-}, as well as H^+ and the hydroxide ion (OH^-), as a function of pH for a DIC concentration of 2000 µmol kg^{-1}, a temperature of 20°C, a salinity of 35, and standard atmospheric pressure. The grey bar indicates the range of pH of modern seawater (8.1 – 8.2). Figure modified from Zeebe and Wolf-Gladrow (2001).

species is total borate, but also the ammonium, phosphate, nitrate, nitrite, sulphide, silicate, fluoride and sulphate systems can potentially contribute to TA (Soetaert et al., 2007). Each acid-base system of interest introduces one species more than the number of associated equations, implying that, for each of them, a total concentration must be measured for an accurate assessment of the fate of CO_2 in the ocean.

1.3 Ocean acidification

At present, the ocean absorbs CO_2 at an estimated rate of 1.4 to 2.2 Pg C yr^{-1} (Takahashi et al., 2009; Gruber et al., 2009) and part of this is CO_2 of anthropogenic origin. Consequently, the ocean has taken up about 48% of the total CO_2 emissions from fossil fuel burning and cement production since pre-industrial times (Sabine et al., 2004). This uptake has induced a range of changes in ocean chemistry: aside from the obvious increase in CO_2 content, DIC and HCO_3^- concentrations have risen, while CO_3^{2-} concentrations and pH have fallen (Gattuso and Hansson, 2011). These changes are collectively referred to as ocean acidification, or 'the other CO_2 problem', as both climate change and ocean acidification have the same underlying cause (Doney et al., 2009a). Since the Industrial Revolution, oceanic pH has decreased by ca. 0.1 unit (Orr et al., 2005) and with the 'business-as-usual' scenario RCP8.5, where the growth rate of atmospheric CO_2 continues its recent pattern (Meinshausen et al., 2011), it is expected to drop another 0.33 unit before the year 2100 (Bopp

et al., 2013). Moreover, with the potential exception of extreme events, the projected change in oceanic pH in forthcoming centuries has been unparalleled in the past 300 million years (Caldeira and Wickett, 2003). The fifth IPCC report was the first to explicitly mention the decrease in oceanic surface-water pH and associated changes (Fig. 1.4; IPCC, 2013), indicating the growing recognition of and concern for ocean acidification.

The lowering of CO_3^{2-} concentrations is particularly important when discussing effects of ocean acidification on marine biota, as it is the carbonate species incorporated in calcium carbonate ($CaCO_3$) minerals (Zeebe and Wolf-Gladrow, 2001). Three primary biogenic $CaCO_3$ minerals are found in seawater: aragonite, calcite and magnesian calcite. While aragonite and calcite are polymorphs of $CaCO_3$ with different crystal structures and correspondingly different intrinsic properties, the latter is a variety of calcite in which part of the calcium ions (Ca^{2+}) are replaced by magnesium ions (Mg^{2+}; Dickson, 2010). Because of their different structures, aragonite is about 1.5 times more soluble than calcite, whereas the solubility of magnesian calcite depends on the Mg^{2+} content (Busenberg and Plummer, 1989). However, it is ultimately the ratio between the product of Ca^{2+} and CO_3^{2-} concentrations, divided by the solubility constant K_{sp} that determines the stability of $CaCO_3$ minerals. It is thus evident that a lowering of CO_3^{2-} concentrations severely impacts $CaCO_3$ formation and dissolution and that, because of its higher solubility, aragonite is especially vulnerable to this process. There is growing evidence that ocean acidification severely impacts calcification of e.g. coccolithophores (Beaufort et al., 2011), foraminifera (Uthicke and Fabricius, 2012), coral reefs (Hoegh-Guldberg et al., 2007; Kleypas et al., 1999), and even mussels and oysters (Gazeau et al., 2007b), although results vary both within and among species (Fabry, 2008).

Aside from calcification, ocean acidification may impact many other biological and biogeochemical processes, and the number of studies focussing on this is growing exponentially (Gattuso and Hansson, 2011). To highlight just a few, ocean acidification is found to impact clownfish behaviour by hindering their neurotransmitter function (Nilsson et al., 2012). Furthermore, several studies have shown that primary production might increase under elevated CO_2 levels (Low-Décarie et al., 2014; Riebesell et al., 2007), although the response may be species-specific (Trimborn et al., 2013). The effects of ocean acidification on food webs (Fabry et al., 2008; de Kluijver et al., 2010), microbial diversity (Liu et al., 2010; Joint et al., 2011), benthic processes (Gazeau et al., 2014), and pelagic biogeochemical processes including secondary production (Li and Gao, 2012; Pedersen et al., 2014), nitrification (Fulweiler et al., 2011; Kitidis et al., 2011) and nitrogen fixation (Eichner et al., 2014) are less clear to date. Many studies so far have focussed on effects of ocean acidification on single species, highlighting that much is yet to be discovered about long-term ecosystem impacts (Guinotte and Fabry, 2008). By studying waters naturally rich in CO_2, which can be used as analogues for future ecosystems, this assessment can be supported. Examples of such ecosystems are volcanic CO_2 vents (Hall-Spencer et al., 2008) and CO_2 seeps (McGinnis et al., 2011), providing naturally occurring pH gradients on a scale of a few hundred metres, and upwelling regions (Thomsen et al., 2010).
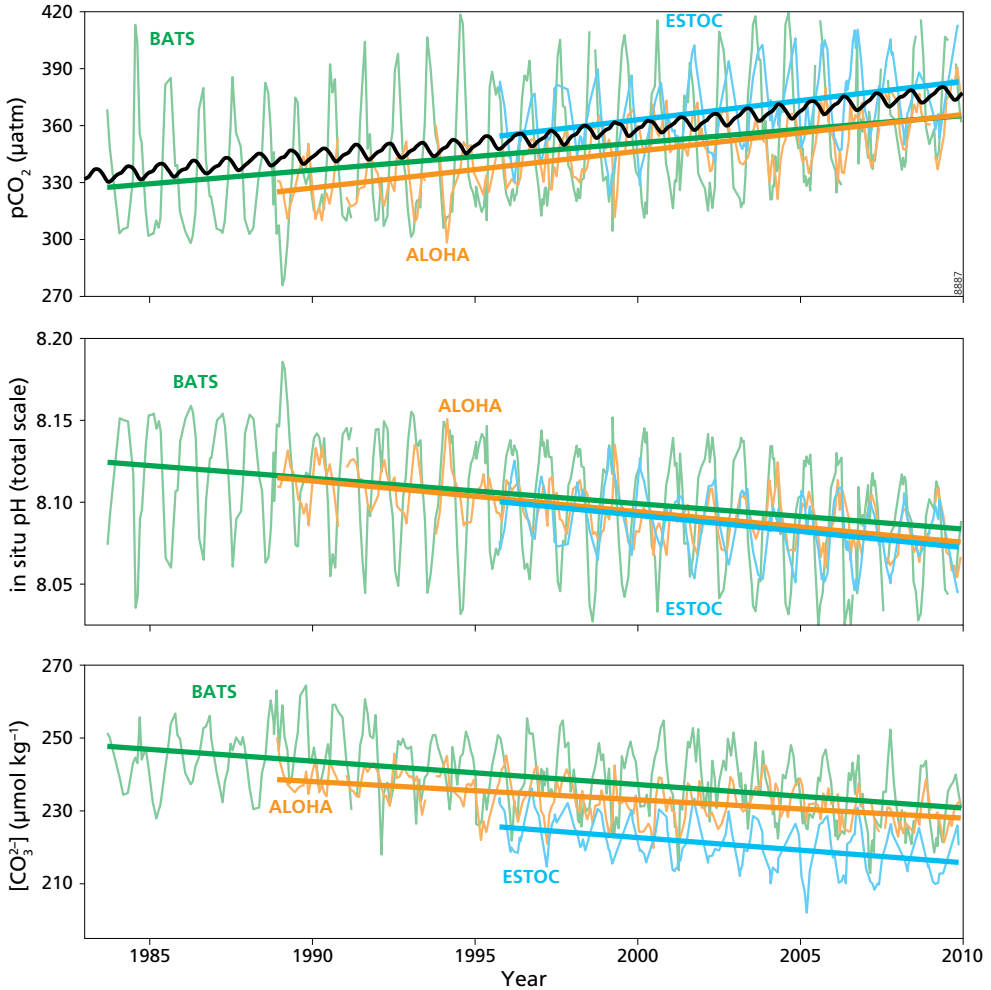
Figure 1.4 Changes in surface-water pCO_2 (µatm), pH (at in situ temperature), and concentration of CO_3^{2-} (µmol kg^{-1}) as determined at three distinct open-ocean sites: BATS (Bermuda Atlantic Time Series, western North Atlantic Ocean), ALOHA (A Long-term Oligotrophic Habitat Assessment; part of the Hawaiian Ocean Time-series program, central North Pacific) and ESTOC (European Station for Time series in the Ocean, eastern North Atlantic Ocean). Figure from IPCC (2013).

1.4 Coastal zone carbon cycling and acidification

The decline in pH of 0.0013-0.0020 unit yr^{-1} as projected by model calculations (Haugan and Drange, 1996; Orr et al., 2005) has been confirmed by global scale measurements, which show that pH decreased by 0.0018±0.0004 unit yr^{-1} between 1991 and 2011 (Lauvset et al., 2015). A comprehensive regional-scale study on open ocean sites showed that tropical and subtropical sites displayed less variability in rates of ocean acidification than high-latitude sites (Bates et al., 2014),

and high-latitude regions have indeed been identified as being most sensitive to ocean acidification (Orr et al., 2005; Steinacher et al., 2009). However, measurements spanning at least a decade in the Atlantic Ocean (Bates, 2007; Santana-Casiano et al., 2007), Pacific Ocean (Dore et al., 2009; Byrne et al., 2010), Iceland Sea (Olafsson et al., 2009) and Southern Ocean (Midorikawa et al., 2012) generally confirm the global trend. This indicates that, by using knowledge of the carbonate system, open-ocean acidification can be reasonably well predicted from atmospheric CO_2 levels. For the coastal ocean, however, the story is a bit more complicated.

The coastal ocean is that part of the marine realm that connects the terrestrial and open ocean reservoirs, in addition to interaction with the atmosphere (Gattuso et al., 1998; Fig. 1.5). It consists of several highly dynamic ecosystems that have distinct features but are tightly connected, such as rivers, estuaries, tidal wetlands and continental shelves (Bauer et al., 2013). These distinct features lead to differences in C cycling in the several sub-ecosystems of the coastal ocean, which in turn affect the net direction of CO_2 air-sea exchange. Generally, the flux of CO_2 between the atmosphere and the coastal ocean is driven by biological processes like primary production and respiration but is additionally influenced by temperature and lateral transport processes (Gattuso et al., 1998; Borges, 2003; Kitidis et al., 2012). As a result of substantial organic carbon processing, on a global scale estuaries are sources of CO_2 to the atmosphere (Frankignoulle et al., 1998), with an estimated flux of ca. 0.25 Pg C yr^{-1} (Cai, 2011). Conversely, vegetated tidal wetlands are highly productive and therefore sequester C (Chmura et al., 2003), a sink which is coined 'blue carbon' (McLeod et al., 2011). Sequestration makes tidal wetlands a sink for atmospheric CO_2 of approximately 0.2 – 0.4 Pg C yr^{-1} (Duarte et al., 2005; Bauer et al., 2013), although the magnitude of this sink is rapidly declining (Hopkinson et al., 2012). Continental shelves usually act as a sink for CO_2 via a mechanism connecting shelf water with the deeper layers of the open ocean and is
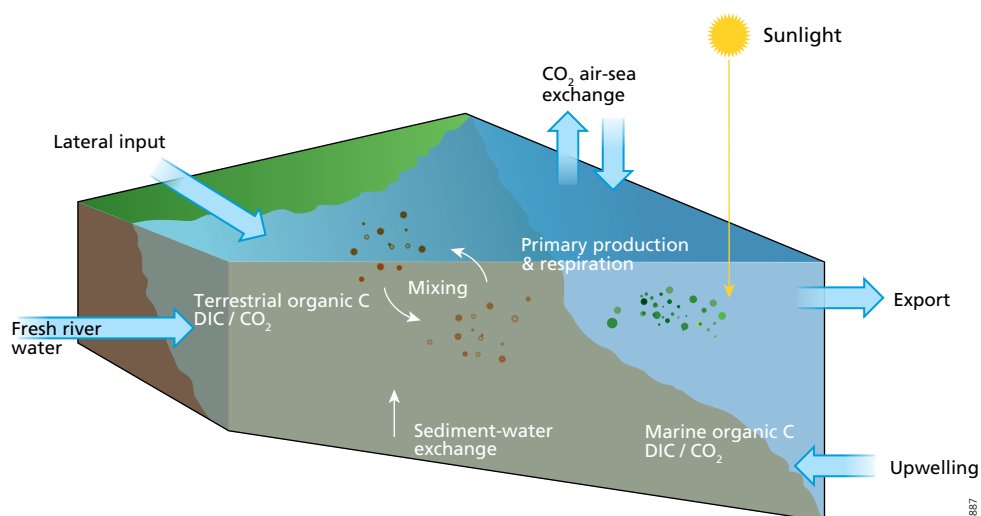

Figure 1.5 Main processes impacting coastal-ocean C cycling, as well as the major pathways connecting this cycle with the atmosphere and open ocean. Figure simplified from Bauer et al. (2013).

termed the 'continental shelf pump' (Tsunogai et al., 1999; Thomas et al., 2004). Approximations of the global magnitude of this sink illustrate a decreasing trend with time however, with the most recent estimate being 0.2 Pg C yr^{-1} (Laruelle et al., 2014; Gruber, 2014). From the onset of the Industrial Revolution, the global flux of C from the land to inland waters has increased by about 1.0 Pg C yr^{-1}, of which 90% is removed in the coastal zone before reaching the open ocean (Regnier et al., 2013). As a result of this and other inputs, the global coastal ocean has shifted from a net source to a net sink of CO_2 over the past 50 to 100 years (Bauer et al., 2013).

However, for each sub-ecosystem in the coastal zone, trends on both the regional and local scale may vary substantially from the global pattern. For example, low-latitudinal continental shelves on average release CO_2 because of high terrestrially-derived organic C input, while mid- and high-latitudinal shelves absorb CO_2 (Borges et al., 2005; Cai, 2011). This does not, however, imply that all low-latitudinal shelves are by definition a net source of CO_2 (Chen et al., 2013). Upscaling estimates of coastal-zone CO_2 air-sea exchange rates from the local to the global scale may therefore be best done using either provinces (Cai et al., 2006) or a spatially-explicit topology based on distinct features of that particular ecosystem (Laruelle et al., 2010, 2013).

As the coastal-zone C cycle is influenced by many processes other than absorption of increased atmospheric CO_2, there is no consensus of this process being the sole or main driver for coastal-zone acidification (Duarte et al., 2013a). Being a highly dynamic system, the coastal ocean shows high variations in pH at diurnal, seasonal and decadal time scales (Wootton and Pfister, 2012; Hofmann et al., 2011; Provoost et al., 2010; Johnson et al., 2013). The different trends among these and other time series of pH indicate that various drivers are responsible for these changes in pH and that their importance may differ for each type of coastal system. Suggested processes include enhanced upwelling of waters enriched in CO_2 for the California Current System (Feely et al., 2008), enhanced acidic riverine input in the Gulf of Maine (Salisbury et al., 2008), increased terrestrial input of dissolved organic carbon (Monteith et al., 2007) and enhanced atmospheric deposition of sulphur and nitrogen (Doney et al., 2007; Hunter et al., 2011). Moreover, there is growing recognition of the coupling between coastal-zone acidification and eutrophication (Borges and Gypens, 2010; Feely et al., 2010; Provoost et al., 2010; Cai et al., 2011; Wallace et al., 2014).

1.5   Eutrophication, hypoxia and coupling with acidification

Eutrophication refers to the process of increasing the supply rate of organic matter to an ecosystem (Nixon, 1995). It can result from enhanced input of either organic matter itself or the nutrients required for organic C assimilation (Berner and Berner, 1996). Increased organic matter input to estuaries mainly results from sewage and with the increasing number of sewage treatment plants, this source of eutrophication has significantly decreased over the past decades (Brosnan and O'Shea, 1996; Soetaert et al., 2006). Sewage treatment, however, is not effective in removing dissolved nutrients (Simpson et al., 1977), which are also added to the coastal ocean via other pathways driven by anthropogenic activities, including fertiliser runoff and atmospheric deposition (Galloway et al., 2008; Okin et al., 2011).

Nutrients, most notably nitrogen (N) and phosphorus (P), as well as over 50 trace elements (Williams, 1981), are essential compartments of organic molecules and are therefore requirements of organic C assimilation. Because of the tight link between the atmospheric and oceanic C reservoirs, oceanic primary production is limited by nutrient- rather than C-availability, explaining why enhanced nutrient input increases primary productivity. In most temperate estuaries, N is the limiting nutrient for primary production, although enhanced P inputs also promote eutrophication (Howarth et al., 2011). Oceanic primary production accounts for about half the total global primary production (Sakshaug et al., 1997; Falkowski, 1994) and within the marine realm, the coastal ocean is highly productive, covering ca. 7% of the surface area but accounting for 14 – 30% of total oceanic primary production (Gattuso et al., 1998). This indicates that primary production is a major process contributing to the C cycle of the coastal ocean. Similar to the direction and magnitude of air-sea CO_2 exchange, estimates of coastal-zone primary production vary widely. This is partly due to spatial and temporal variability in primary production, occurring between and within ecosystems and on time scales ranging from diurnal to interannual (Cloern et al., 2014; Gazeau et al., 2004). In addition to nutrient availability (Howarth et al., 2011), this spatial and temporal variability is driven by a combination of physical, chemical and biological factors, such as light availability (Kirk, 1994), grazing (Calbet, 2001) and temperature (Eppley, 1972). Variations in these factors may, in turn, result from tidal forcing (Blauw et al., 2012), eddy formation (Mahadevan et al., 2012) and other physical forcings. Moreover, estimates of coastal-zone primary production vary because of differences in the adopted methodologies (Laws et al., 2000; Falkowski and Raven, 2013). The methodological issues may be partly overcome by concurrent measurements of primary production employing at least two different techniques (Marra, 2002) and is the focus of Chapter 3.

Both primary production and respiration tightly link biogeochemical O_2 and C cycles. The average ratio in which C, N and P are incorporated into organic matter is 106:16:1 (Redfield, 1958) and is commonly known as the Redfield ratio. During primary production, O_2 is produced in a ratio equivalent to C incorporation, although the exact value of this so-called photosynthetic quotient depends on the form in which N is assimilated (Williams et al., 1979). Similarly, respiration consumes O_2 and releases CO_2 in a ratio referred to as the respiratory quotient. As a result, O_2 and carbonate system parameters in the coastal ocean vary concomitantly on diurnal and seasonal time scales (Frankignoulle and Distèche, 1984; Reum et al., 2014; Baumann et al., 2015). With higher rates of primary production and respiration resulting from anthropogenic nutrient input, pH variability on both diurnal (Hofmann et al., 2011) and seasonal scales (Omstedt et al., 2009) are increased. Furthermore, if eutrophication results in an imbalance of both processes, this will induce a change in pH that significantly exceeds the atmospheric CO_2-induced pH change (Borges and Gypens, 2010). This change in pH can be sustained for decades and reverts direction if the sign of the imbalance between primary production and respiration changes (Provoost et al., 2010; Duarte et al., 2013a).

From the tight coupling between biogeochemical O_2 and C cycles, it may be suspected that the observed trends in O_2 resulting from eutrophication are similar to those in the carbonate system parameters. Since the air-sea exchange of O_2 is much faster than that of CO_2, this may not always be the case in surface waters, but this tight link is observed in waters that are not directly connected

to the atmosphere, such as seasonally stratified waters (Taguchi and Fujiwara, 2010). Such waters show a clear signal of the often observed decoupling between primary production and respiration (Arístegui and Harrison, 2002), resulting from the build-up of phytoplankton biomass in spring, which subsequently sinks to the bottom water and sediment and is respired with a time lag on the order of weeks. Since the bottom water and atmosphere in such systems are not directly connected at the time of high respiratory activity, substantial drops in bottom-water pH concurrent with the initiation of hypoxia occur, as has been observed in a variety of ecosystems around the world (Cai et al., 2011; Sullivan et al., 2014; Cantoni et al., 2012; Wang et al., 2013; Zhai et al., 2012).

Hypoxia, defined as O_2 concentrations below 63 µmol L^{-1} (Rabalais et al., 2010), occurs when the oxygen consumption during organic matter degradation exceeds the supply of oxygen-rich waters. The development of low-oxygen zones is mainly driven by enhanced nutrient loads and associated higher rates of primary production and respiration, while their global distribution is tightly linked to that of developed watersheds (Rabalais et al., 2014). The decline in O_2 concentrations is faster in the coastal ocean relative to the open ocean (Gilbert et al., 2010) and as such, the number of low-oxygen zones in the coastal ocean has been rapidly increasing in the last halve century as a result of eutrophication (Diaz and Rosenberg, 2008). Most of these areas can be found along densely populated coasts in northern Europe, Japan, China, eastern North-America and the Gulf of Mexico (Rabalais et al., 2010). Hypoxia severely impacts the biogeochemical cycles of many chemical elements, including C (Rabalais et al., 2014), and the general sediment biogeochemistry (Middelburg and Levin, 2009).

Hypoxia and acidification are not only coupled but also intensify each other (Melzner et al., 2013). The number of dead zones will increase as oceanic CO_2 concentrations continue to rise, even if the concentration of O_2 remains constant (Brewer and Peltzer, 2009). Similarly, the current summertime drop in bottom-water pH of seasonally stratified waters is greater than can be expected from eutrophication and anthropogenic CO_2 uptake alone (Cai et al., 2011). A third process exacerbating both hypoxia and acidification is global warming, which not only decreases the solubility of O_2 (Sarmiento and Gruber, 2006), but also increases respiration rates (Yvon-Durocher et al., 2012). The precarious progression of climate change poses an uncertainty to the extent at which acidification, de-oxygenation and warming will occur, as each of them shows a different sensitivity to various scenarios (Cao et al., 2014). Nevertheless, these three processes are the major challenges the marine realm will face in upcoming decades and are ultimately caused by the same driver, i.e. anthropogenic CO_2 emissions (Gruber, 2011).

1.6 Oceanic buffering capacity

The additional drop in bottom-water pH found by Cai et al. (2011) and unexplained by eutrophication or acidification was attributed to a decline in the bottom-water acid-base buffering capacity, an effect that is most pronounced in eutrophied waters (Sunda and Cai, 2012). The acid-base buffering capacity, or buffer intensity, is the ability of a solution to buffer changes in pH upon

the addition of a strong acid or base (Van Slyke, 1922) and is traditionally calculated from the inverse slope of a titration curve (Stumm and Morgan, 1996; Morel and Hering, 1993).

In the context of global change, the first notion of a seawater buffer factor concerned the rate of anthropogenic CO_2 uptake by the oceans relative to the increase in DIC. Buch (1933) presented carbonate system calculations to show that, for a constant TA and temperature, the increase in pCO_2 relative to its ambient concentration is about 10 times higher than the relative increase in DIC. Using measurements of the radio-active ^{14}C isotope, Revelle and Suess (1957) were first to realise the dependency of the magnitude of this factor on ambient DIC and CO_2 concentrations. The buffer factor they derived, defined as the relative change in CO_2 concentration over the relative change in DIC, is currently known as the Revelle factor. A higher Revelle factor indicates a greater rise in CO_2 concentration per unit of DIC increase, meaning that the system is less capable of buffering atmospheric CO_2-uptake through immediate acid-base reactions that remove this species. Keeling (1973) showed that the Revelle factor increases with the progressive absorption of atmospheric CO_2. Sundquist et al. (1979) explicitly stated that the Revelle factor holds for constant TA alone and derived its analytical expression, accounting for the borate system but treating it as invariable, i.e. assuming its concentration does not vary.

The buffering mechanism described by the Revelle factor indicates a state of chemical equilibrium of the carbonate system and assumes that no heterogeneous reactions take place that may affect TA during atmospheric CO_2-uptake (Sundquist et al., 1979; Yi et al., 2001). Therefore, the Revelle factor is often referred to as a homogeneous buffer factor (Sundquist et al., 1979); this is in contrast to total buffer factors, where these heterogeneous reactions, such as $CaCO_3$ dissolution, are not by definition excluded (Sundquist and Plummer, 1981). In fact, a homogeneous buffer factor can be derived from a total buffer factor by imposing the condition that TA is constant. In addition to homogeneous and total buffer factors, the term chemical buffer factor is also frequently applied. It describes the resistance to a change in pH resulting from the addition or removal of DIC (Skirrow, 1975) or of a strong acid of base, and is the inverse of the acid-base buffering capacity (Soetaert et al., 2007). Depending on its underlying assumptions, a chemical buffer factor can be classified as either homogeneous or heterogeneous.

Frankignoulle (1994) summarised and further extended the concepts of chemical and homogeneous buffer factors. Using assumptions similar to Sundquist et al. (1979) for the borate system, he analytically derived a suite of buffer factors for the carbonate system in seawater. Among these are two chemical buffer factors that determine the change in pH due to changes in TA and dissolved CO_2, of which the latter is equivalent to a change in DIC since both changes do not influence TA and are thus homogeneous processes (MacIntyre, 1978). These two buffer factors are equivalent to two of the factors derived by Egleston et al. (2010), which determine the change in $[H^+]$ due to changes in DIC and TA. In open-ocean surface water, the buffer factors of Frankignoulle (1994) and Egleston et al. (2010) may represent the vast majority of chemically driven pH change. In coastal oceans, however, other acid-base systems may also affect pH change, such as the sulphide system below the redox-cline in anoxic, permanently stratified waters (Ulfsbo et al., 2011; Gaines Jr and Pilson, 1972; Knull and Richards, 1969). Consequently, when calculating buffer factors in

these systems, their definition needs to be extended and other acid-base systems included, which is done in Chapter 5. These newly-derived, generally applicable buffer factors are used in Chapter 6 to attribute seasonal pH variability in different oceanic settings to their governing factors.

1.7   Use of acid-base buffering capacity to quantify changes in pH

An accurate representation of the acid-base buffering capacity and other buffer factors is of utmost importance for assessing pH variability on various time scales, as well as ocean acidification, given that the effect of any physical or biogeochemical processes on pH is highly impacted by the extent to which changes in pH are attenuated (Zhang, 2000; Soetaert et al., 2007; Hofmann et al., 2010a). For any proton-producing process, the vast majority of H^+ produced is consumed by immediate acid-base reactions, thereby neutralising their acidifying effect. The acid-base buffering capacity controls the extent to which this weakening occurs. An aqueous system with a high acid-base buffering capacity consumes relatively more protons than a poorly buffered system. Hence, if two aqueous systems are exposed to the same biogeochemical process, such as primary production, at exactly the same rate, the system with the higher acid-base buffering capacity will show a comparably smaller pH change.

The modulating role of the acid-base buffering capacity makes it a central concept when studying the pH evolution of any aquatic system. Specifically, the change in pH induced by a certain process can be quantified as the product of the process rate and the amount of H^+ produced or consumed by that process, divided by the acid-base buffering capacity (Hofmann et al., 2010a). In the case of multiple processes acting concurrently, the total net change in pH is simply the sum of the change in pH induced by each individual process. For a highly productive estuary it has been shown that the net change in pH resulting from several simultaneously acting biogeochemical processes is much smaller than that induced by each of the individual processes (Hofmann et al., 2009).

If the carbonate system is quantified using DIC and TA, as is normally done (see Sect. 1.2), it can only determine the combined effect of several concurrently acting processes on pH. However, to identify and quantify the driving factors responsible for seasonal pH variability or coastal ocean acidification, it is necessary to quantify the change in pH of each individual process separately, which can only be done if pH is calculated explicitly. The details of this explicit pH method are extensively described in the dissertation of Andreas Hofmann (2009) and are summarised in Chapters 2 and 4, in which the method is applied. In Chapter 2, the explicit pH method is used to assess the driving mechanisms beyond pH variability in a seasonally hypoxic coastal marine basin, while in Chapter 4 it is employed to study the impact of atmospheric sulphur and nitrogen deposition on a variety of coastal-ocean environments during the 21st century.

1.8   Scope and outline of the dissertation

This dissertation aims at identifying key mechanisms controlling the seasonal pH variability and longer-term pH changes in the coastal and open ocean. To this end, I (1) attribute governing factors to seasonal pH changes by setting up a measurement-based proton budget in a seasonally hypoxic coastal marine basin; (2) assess the impact of various measurement techniques on estimates of the key biogeochemical process of primary production; (3) discuss the importance of atmospheric sulphur and nitrogen deposition on current and future coastal-ocean acidification; (4) define buffer factors that are generally valid and applicable to any kind of aquatic system; (5) apply these buffer factors to several open-ocean settings to assess the driving factors behind their seasonal pH variability.

The aim of **Chapter 2** is to determine the driving factors behind seasonal pH variability in a transiently hypoxic coastal marine basin, with an emphasis on the role of the acid-base buffering capacity. To achieve this aim, monthly water-column chemistry measurements were carried out in Lake Grevelingen, located in the south-western delta area of the Netherlands. In addition, rates of several processes impacting the C cycle were determined either monthly or seasonally. By calculating pH explicitly as detailed above, these measurements were used to set up of one the first seasonal proton budgets of its kind. The results clearly indicate that, while process rates are generally higher in the surface water of the basin, the amplitude of pH variability is greater in the seasonally hypoxic bottom water, due to a substantial reduction of its acid-base buffering capacity in summer. The proton budgets show that the net change in pH is much smaller than the flux of protons induced by each of the individual processes. Moreover, primary production and respiration dominate the seasonal cycle of pH in the basin.

In **Chapter 3**, primary production in Lake Grevelingen was studied in more detail, focussing especially on the role of species diversity. Three different methods of measuring primary productivity were employed concurrently, where the first of these involved measurements of C assimilation and was conducted on incubated water samples under a range of light conditions. Both other methods assessed changes in O_2 concentration: one similarly determined the evolution of O_2 in bottle incubations, and the other directly tracked O_2 concentrations at high-resolution intervals in the water column. In addition, the active fraction of the phytoplankton population was identified through the incorporation of the stable ^{13}C isotope into specific organic molecules present in all phytoplankton species and thought to represent viable organisms. The composition of these molecules, termed phospholipid-derived fatty acids (PLFA), varies per group of phytoplankton and can thus be used to study species diversity. All three methods provide similar estimates of primary productivity in Lake Grevelingen, with the overall highest estimates obtained by measuring changes in O_2 concentration in the water column. The ratio between C assimilation and O_2 production in incubation bottles depends on the rate of primary production, where the ratio increases with increasing primary productivity. Measurements of PLFA indicate distinct changes in species diversity over the year, in addition to primary productivity estimates similar in pattern to those from the other methods, although significantly smaller in magnitude. Despite the uncertainties and assumptions associated with each method, these techniques are all suitable for determining primary

productivity in the eutrophic coastal ocean. Their differences, however, cannot be unequivocally linked to species dynamics.

Chapter 4 focusses on the interplay between atmospheric CO_2 absorption and atmospheric sulphur and nitrogen deposition in the coastal ocean, emphasising their dependency on water-column biogeochemistry. A simple biogeochemical model in combination with explicit pH modelling was used to show that the relative significance of both processes to coastal-ocean acidification depends on the water-column concentration of CO_2 relative to the atmosphere. If the atmospheric concentration exceeds that of the surface water, i.e. there is a net uptake of CO_2 over the year such as in the continental shelf, then this part of the coastal ocean is comparably more sensitive to CO_2-induced acidification but less affected by additional acidification resulting from atmospheric acid deposition than a coastal water with a CO_2 concentration surpassing that of the atmosphere. The simple biogeochemical model was further used to assess the change of this vulnerability during the 21st century as a result of the projected increase in atmospheric CO_2, showing that coastal seas become up to a factor 4 more sensitive to atmospheric deposition-induced acidification. The annual change in proton concentration will however only increase by 28% at most.

In **Chapter 5** a set of general expressions was derived describing the sensitivity of pH to a change in ocean chemistry. While preceding work on buffer factors was subject to certain constraints, these newly-derived expressions can include as many acid-base systems as relevant. This makes them suitable for applications in aqueous systems where acid-base systems other than the carbonate and borate systems contribute significantly to the acid-base buffering capacity, such as anoxic bottom waters in coastal basins. The new set of buffer factors is fully consistent with the Revelle factor and other previously derived buffer factors, and provides more accurate values in such aqueous systems. The buffer factors were calculated for current global ocean surface water and, following projected changes in CO_2 and temperature, for 2100 as well, showing that a change in most acid-base parameters will induce a comparably greater pH excursion by the end of the 21st century. This increased vulnerability is driven by enhanced CO_2 concentrations and slightly moderated by global warming. Furthermore, by 2100 global ocean pH will become less sensitive to changes in temperature.

To further test the newly-derived general expressions, in **Chapter 6** they were applied to several long-term data sets with seasonal coverage encompassing a variety of physical and biogeochemical settings. After removing a long-term trend where present, all data were combined into a composite year to which a harmonic function with several different periodicities was fit. By varying all parameters over the year according to this fit, pH was calculated and compared to the observed pH. For each of the sites, pH can be properly predicted if seasonal cycles of temperature, salinity, TA and the total concentrations of acid-base species are known. The factors driving the majority of pH variability differ however per site. In the Mediterranean Sea, changes in DIC are responsible for most pH variability in winter and spring, while temperature variability is the most dominant factor driving pH trends for the rest of the year. In the Iceland Sea, variations in DIC dominate the pH signal for the majority of the year, although temperature is most important in early summer and TA variability drives most pH changes in early winter. Seasonality in pH at a site in the subtropical

Pacific Ocean close to Hawaii is almost solely driven by temperature changes. This work highlights the power of the newly-derived buffer factors in quantifying concomitantly-acting buffering mechanisms, thus showing that they can be used to gain further insight into current and future pH dynamics in marine systems.

Overall, this dissertation highlights that buffering mechanisms play a crucial role in the impact of biogeochemical or physical processes on pH in marine systems. The complexity of several concurrently-acting processes influencing pH variability in any oceanic water on various time scales requires that both the total acid-base buffering capacity and related buffer factors describing the sensitivity of pH to a certain change in water-column chemistry or physical state be properly quantified. In the course of the 21st century, when the marine realm will face the 'triple trouble' of warming, de-oxygenation and acidification, the total acid-base buffering capacity will decline. As a consequence, the sensitivity of pH to most of the physical and chemical changes occurring in the marine realm will increase, highlighting that pH variability on any given temporal scale will increase in amplitude.

Chapter 2:

Biogeochemical processes and buffering capacity concurrently affect acidification in a seasonally hypoxic coastal marine basin

Abstract

Coastal areas are impacted by multiple natural and anthropogenic processes and experience stronger pH fluctuations than the open ocean. These variations can weaken or intensify the ocean acidification signal induced by increasing atmospheric pCO_2. The development of eutrophication-induced hypoxia intensifies coastal acidification, since the CO_2 produced during respiration decreases the buffering capacity in any hypoxic bottom water. To assess the combined ecosystem impacts of acidification and hypoxia, we quantified the seasonal variation in pH and oxygen dynamics in the water column of a seasonally stratified coastal basin (Lake Grevelingen, the Netherlands).

Monthly water-column chemistry measurements were complemented with estimates of primary production and respiration using O_2 light-dark incubations, in addition to sediment-water fluxes of dissolved inorganic carbon (DIC) and total alkalinity (TA). The resulting data set was used to set up a proton budget on a seasonal scale.

Temperature-induced seasonal stratification combined with a high community respiration was responsible for the depletion of oxygen in the bottom water in summer. The surface water showed strong seasonal variation in process rates (primary production, CO_2 air-sea exchange), but relatively small seasonal pH fluctuations (0.46 units on the total hydrogen ion scale). In contrast, the bottom water showed less seasonality in biogeochemical rates (respiration, sediment-water exchange), but stronger pH fluctuations (0.60 units). This marked difference in pH dynamics could be attributed to a substantial reduction in the acid-base buffering capacity of the hypoxic bottom water in the summer period. Our results highlight the importance of acid-base buffering in the pH dynamics of coastal systems and illustrate the increasing vulnerability of hypoxic, CO_2-rich waters to any acidifying process.

Chapter 2

2.1   Introduction

The absorption of anthropogenic carbon dioxide (CO_2) has decreased the average pH of open ocean surface water by ca. 0.1 unit since the Industrial Revolution (Orr et al., 2005). In coastal areas, the problem of ocean acidification is more complex, as seawater pH is influenced by various natural and anthropogenic processes other than CO_2 uptake (Borges and Gypens, 2010; Duarte et al., 2013; Hagens et al., 2014). As a result, the signal of CO_2-induced acidification may not be readily discernible in coastal systems, as time series of pH show high variations at diurnal, seasonal and decadal timescales (e.g. Hofmann et al., 2011; Wootton and Pfister, 2012). One major anthropogenic process impacting coastal pH is eutrophication (Borges and Gypens, 2010; Provoost et al., 2010; Cai et al., 2011). Enhanced inputs of nutrients lead to higher rates of both primary production and respiration (Nixon, 1995), thereby increasing the variability in pH on both the diurnal (Schulz and Riebesell, 2013) and seasonal scales (Omstedt et al., 2009). Moreover, when primary production and respiration are not balanced, they can lead to longer-term changes in pH at rates that can strongly exceed the expected pH decrease based on rising atmospheric CO_2 (Borges and Gypens, 2010). The direction of this eutrophication-induced pH change depends on the sign of the imbalance, and the resulting pH trend can be sustained for decades (Provoost et al., 2010; Duarte et al., 2013).

A well-known effect of eutrophication is the development of hypoxia in coastal bottom waters (Diaz and Rosenberg, 2008). Such bottom-water oxygen (O_2) depletion occurs when the O_2 consumption during respiration exceeds the supply of oxygen-rich waters and typically develops seasonally as a result of summer stratification and enhanced biological activity. As respiration of organic matter produces CO_2 at a rate proportional to O_2 consumption (Redfield et al., 1963), it follows that zones of low O_2 are also zones of high CO_2 (hypercapnia) and thus show high levels of dissolved inorganic carbon (DIC) and low pH (Brewer and Peltzer, 2009; Howarth et al., 2011). In coastal bays, oxygen and carbonate system parameters co-vary on both diurnal (Burnett, 1997) and seasonal timescales (Frankignoulle and Distèche, 1984; Melzner et al., 2012), where the diurnal variability may be of similar magnitude to the seasonal variability (Yates et al., 2007). Primary production and respiration are often spatially and temporally decoupled, as phytoplankton biomass is produced during spring blooms in the surface water, subsequently sinks, and is degraded with a time lag in the bottom water and sediment. In seasonally stratified areas, this can lead to significant concomitant drops in bottom-water pH and O_2 in summer, as has been shown for the Seto Inland Sea (Taguchi and Fujiwara, 2010), the northern Gulf of Mexico and the East China Sea (Cai et al., 2011), the Bohai Sea (Zhai et al., 2012), the Gulf of Trieste (Cantoni et al., 2012), several estuarine bays across the northeastern US coast (Wallace et al., 2014), the semi-enclosed Lough Hyne (Sullivan et al., 2014) and in areas just off the Changjiang Estuary (Wang et al., 2013).

Long-term trends in pH resulting from increased prevalence of bottom-water hypoxia can be substantial compared to the pH trend resulting from anthropogenic CO_2-induced acidification. Data from the Lower St Lawrence Estuary indicate that the decrease in bottom-water pH over the past 75 years is 4-6 times higher than can be explained by the uptake of anthropogenic CO_2 alone (Mucci et al., 2011). In Puget Sound, respiration currently accounts for 51-76% of

the decrease in subsurface water pH since pre-industrial times, although this fraction will likely decrease as atmospheric CO_2 continues to increase (Feely et al., 2010). Model simulations for the northern Gulf of Mexico show that the seasonal drop in bottom-water pH has increased in the Anthropocene because of a decline in its buffering capacity (Cai et al., 2011), an effect that is most pronounced in eutrophied waters (Sunda and Cai, 2012).

The acid-base buffering capacity (β), also termed the buffer intensity or buffer factor, is the ability of an aqueous solution to buffer changes in pH or proton (H^+) concentration upon the addition of a strong acid or base (Morel and Hering, 1993; Stumm and Morgan, 1996). It is of great importance when considering the effect of biogeochemical processes on pH (Zhang, 2000; Soetaert et al., 2007; Hofmann et al., 2010a). A system with a high acid-base buffering capacity is efficient in attenuating changes in [H^+] and thus displays a smaller net pH change compared to systems with a low β. Thus, if two aqueous systems are exposed to the same biogeochemical processes at exactly the same rate, the system with the lower β will show pH excursions with larger amplitudes.

In the 21st century, seawater buffering capacity is expected to decline as a result of increasing CO_2 and the subsequent decrease in pH (Egleston et al., 2010; Hofmann et al., 2010a; Hagens et al., 2014). As a result, one would predict a greater seasonal pH variability (Frankignoulle, 1994; Egleston et al., 2010) and a more pronounced diurnal pH variability in highly productive coastal environments (Schulz and Riebesell, 2013; Shaw et al., 2013), which may additionally be modified by ecosystem feedbacks (Jury et al., 2013). In seasonal hypoxic systems, model analysis predicts more pronounced fluctuations in bottom-water pH (Sunda and Cai, 2012). However, detailed studies of the effects of seasonal hypoxia on pH buffering and dynamics are currently lacking.

Here we present a detailed study of the pH dynamics and acid-base buffering capacity in a temperate coastal basin with seasonal hypoxia (Lake Grevelingen). We quantify the impact of individual processes, i.e. primary production, community respiration, sediment effluxes and CO_2 air-sea exchange, on pH using the method developed by Hofmann et al. (2010a), which uses DIC and [H^+], rather than total alkalinity (TA), to quantify the carbonate system. From this, we construct a proton budget that attributes proton production or consumption to these processes. Our aim is to quantify seasonal changes in the acid-base buffering capacity and elucidate their importance for carbon cycling and pH dynamics in coastal hypoxic systems.

2.2   Methods

2.2.1   Site description

Lake Grevelingen, located in the southwestern delta area of the Netherlands, is a coastal marine lake with a surface area of 115 km^2 and an average water depth of 5.1 m (Nienhuis, 1978; Fig. 2.1). The bathymetry of the lake is characterised by deep gullies intersecting extended shallow areas; half of the lake is shallower than 2.6 m, and only 12.4% of the lake is deeper than 12.5 m. In the main gully, several deep basins are present, which are separated from each other by sills. The deepest basin extends down to 45 m water depth. Originally, Lake Grevelingen was an estuary with a tidal

range of about 2.3 m. A large flooding event in 1953 was the motive for the construction of two dams. The Grevelingen estuary was closed off on the landward side in 1964 and on the seaward side in 1971. This isolation led to a freshening of the system, with vast changes in water chemistry and biology (Bannink et al., 1984). To counteract these water quality problems, a sluice extending vertically between 3 and 11 m depth was constructed on the seaward side in 1978 (Pieters et al.,
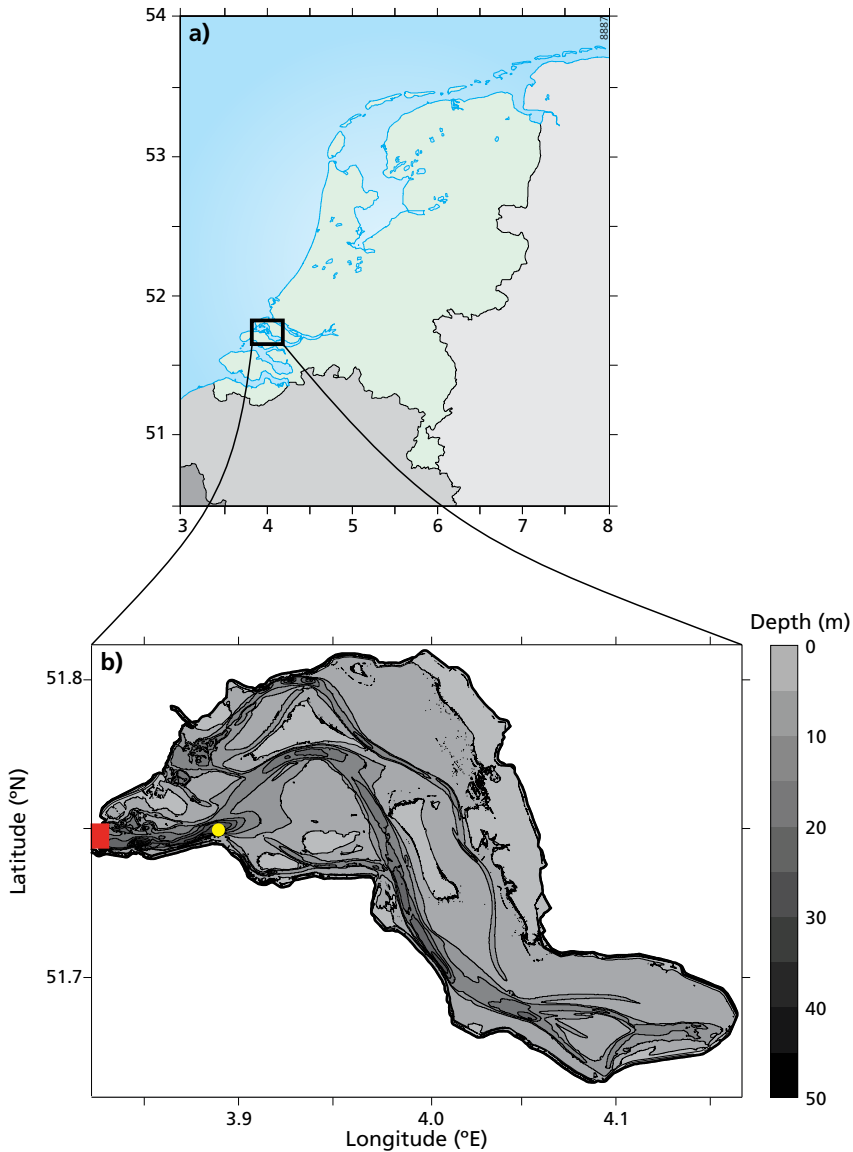

Figure 2.1 (a) Map of the Netherlands, and (b) bathymetry of Lake Grevelingen (data from the executive arm of the Dutch Ministry of Infrastructure and the Environment). Yellow dot indicates sampling location at the deepest point of the Den Osse basin (S1; 51.747°N, 3.890°E). Red bar indicates sluice location.
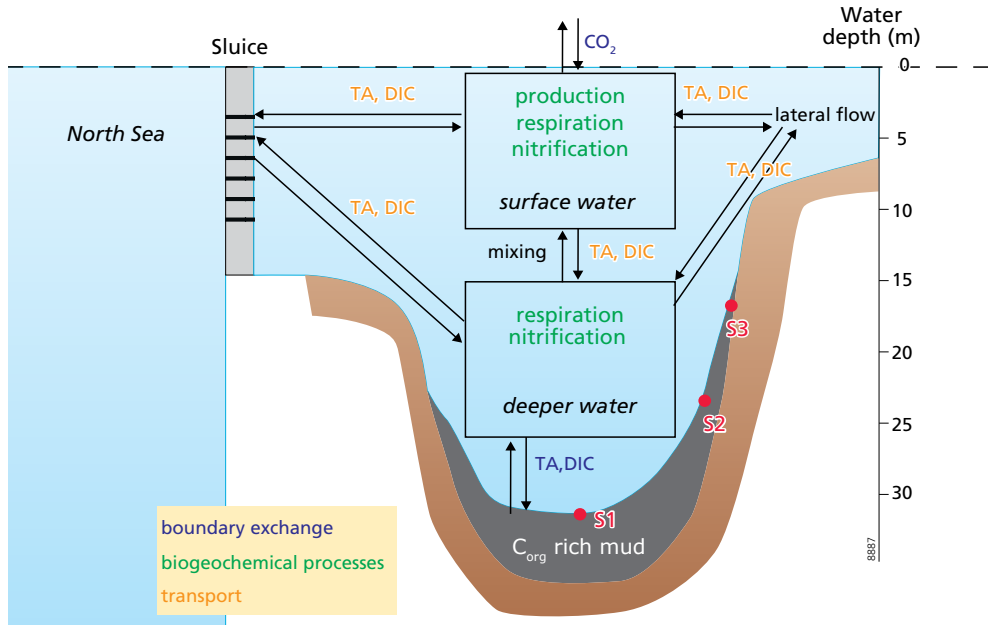
Figure 2.2 Schematic overview of the main processes affecting the Den Osse proton budget. C_{org} refers to organic carbon; see Sect. 2.2.8 for a detailed explanation of the budget.

1985). Exchange with saline North Sea water has dominated the water budget since, resulting in the lake approaching coastal salinity (29-32) and an estimated basin-wide water residence time of 229 days (Meijers and Groot, 2007). Upon intrusion, the denser North Sea water forms a distinct subsurface layer, which is then laterally transported into the lake. Yet it has been found that opening the sluice hardly affects water-column mixing (Nolte et al., 2008) and the water quality problems persist. Monthly monitoring carried out by the executive arm of the Dutch Ministry of Infrastructure and the Environment revealed that the main gully of Lake Grevelingen has experienced seasonal stratification and hypoxia since the start of the measurements in 1978, which have differed in extent and intensity annually (Wetsteyn, 2011).

Throughout 2012, we performed monthly sampling campaigns on board the R/V *Luctor*, examining water-column chemistry, biogeochemical process rates and sediment-water exchange. Sampling occurred in the Den Osse basin (maximum water depth 34 m; Fig. 2.2), a basin located in the main gully of Lake Grevelingen. Two sills surround the basin at water depths of 10 and 20 m at the landward and seaward sides, respectively. Due to its bathymetry, particulate matter rapidly accumulates within the deeper parts of the basin (sediment accumulation rate > 2 cm yr^{-1}; Malkin et al., 2014). The surface area and total volume of the Den Osse basin have been estimated at $649 \cdot 10^4$ m^2 and $655 \cdot 10^5$ m^3, respectively (Pieters et al., 1985), resulting in an average water depth of ca. 10 m. Sampling occurred at three stations along a depth gradient within the basin (Fig. 2.1b): S1 at 34 m water depth and located at the deepest point of the basin (51.747°N, 3.890°E), S2 at 23 m (51.749°N, 3.897°E) and S3 at 17 m (51.747°N, 3.898°E). Each campaign, water-column sampling

was performed at station S1. Discrete water-column samples were collected with a 12 L Niskin bottle at eight different depths (1, 3, 6, 10, 15, 20, 25 and 32 m) to assess the carbonate system parameters (pH, partial pressure of CO_2 (pCO_2), total alkalinity (TA) and DIC), concentrations of O_2, hydrogen sulphide (H_2S), dissolved organic carbon (DOC) and nutrients, and rates of community metabolism. All water samples were collected from the Niskin bottle with gas-tight Tygon tubing. A YSI6600 CTD probe was used to record depth profiles of temperature (T), salinity (S), pressure (p) and chlorophyll a (Chl a). To determine sediment-water exchange fluxes, intact, undisturbed sediment cores (6 cm Ø) were retrieved with a UWITEC gravity corer in March, May, August and November 2012 at the three stations S1, S2 and S3. Sampling usually took place mid-morning to minimise the influence of diurnal variability in determining the seasonal trend. The exact dates and times of sampling are provided in the supplementary information.

2.2.2 Stratification-related parameters

From T, S and p the water density ρ_w (kg m^{-3}) was calculated according to Feistel (2008) using the package *AquaEnv* (Hofmann et al., 2010b) in the open-source programming framework R. Subsequently, the density anomaly σ_T (kg m^{-3}) was defined by subtracting 1000 kg m^{-3} from the calculated value of ρ_w. Water density profiles were also used to calculate the stratification parameter ϕ (J m^{-3}), which represents the amount of energy required to fully homogenise the water column through vertical mixing (Simpson, 1981):

$$\phi = \frac{1}{h} \int_{-h}^{0} (\rho_{av} - \rho_w)\, gz\, dz \quad \text{with} \quad \rho_{av} = \frac{1}{h} \int_{-h}^{0} \rho_w z\, dz, \tag{1}$$

where h is the total height of the water column (m), z is depth (m), g is gravitational acceleration (m s^{-2}), and ρ_{av} is the average water-column density (kg m^{-3}).

Samples for the determination of $[O_2]$ were drawn from the Niskin bottle into volume-calibrated clear borosilicate biochemical oxygen demand (BOD) bottles of ca. 120 mL (Schott). O_2 concentrations were measured using an automated Winkler titration procedure with potentiometric end-point detection (Mettler Toledo DL50 titrator and a platinum redox electrode). Reagents and standardisations were as described by Knap et al. (1994).

During summer months we examined the presence of H_2S in the bottom water. Water samples were collected in 60 mL glass serum bottles, which were allowed to overflow and promptly closed with a gas-tight rubber stopper and screw cap. To trap the H_2S as zinc sulphide, 1.2 mL of 2% zinc acetate solution was injected through the rubber stopper into the sample using a glass syringe and needle. A second needle was inserted simultaneously through the rubber stopper to release the overpressure. The sample was stored upside down at 4°C until analysis. Spectrophotometric estimation of H_2S (Strickland and Parsons, 1972) was conducted by adding 1.5 mL of sample and 0.120 mL of an acidified solution of phenylenediamine and ferric chloride to a disposable cuvette. The cuvette was closed immediately thereafter to prevent the escape of H_2S and was allowed to react for a minimum of 30 minutes before the absorbance at 670 nm was measured. For calibration, a 2 mmol L^{-1} sulphide solution was prepared, for which the exact concentration was determined by iodometric titration.

2.2.3 Carbonate system parameters

For the determination of TA, two separate samples were collected in 50 mL centrifuge tubes. To determine the contribution of suspended particulate matter to TA, one sample was left unfiltered, while the other was filtered through a 0.45 μm nylon membrane syringe filter (Kim et al., 2006). TA was determined using the standard operating procedure for open cell potentiometric titration (Dickson et al., 2007; SOP 3b), using an automatic titrator (Metrohm 888 Titrando), a high-accuracy burette (1±0.001 mL), a thermostated reaction vessel (T = 25°C) and combination pH glass electrode (Metrohm 6.0259.100). TA values were calculated by a non-linear least-squares fit to the titration data in a custom-made script in R. Quality assurance involved regular analysis of Certified Reference Materials (CRM) obtained from the Scripps Institution of Oceanography (A.G. Dickson, batches 116 and 122). The relative standard deviation of the procedure was less than 0.2% or 5 μmol kg^{-1} (n=10).

Samples for DIC analysis were collected in 10 mL headspace vials, left to overflow and poisoned with 10 μL of a saturated mercuric chloride ($HgCl_2$) solution. DIC analysis was performed using an AS-C3 analyser (Apollo SciTech) which consists of an acidification unit in combination with a LICOR LI-7000 CO_2/H_2O gas analyser. Quality assurance involved carrying out three replicate measurements of each sample and regular analysis of CRM. The accuracy and precision of the system are 0.15% or 3 μmol kg^{-1}.

Water for pCO_2 analysis was collected in 50 mL glass serum bottles from the Niskin bottle with Tygon tubing, left to overflow, poisoned with 50 μL of saturated $HgCl_2$ and sealed with butyl stoppers and aluminium caps. Samples were analysed within 3 weeks of collection by the headspace technique (Weiss, 1981) using gas chromatography (GC) with a methaniser and flame ionisation detection (GC-FID, SRI 8610C). The GC-FID was calibrated with pure N_2 and three CO_2:N_2 standards with a CO_2 molar fraction of 404, 1018, 3961 ppmv (Air Liquide Belgium). Headspace equilibration was done overnight in a thermostated bath, and temperature was recorded and typically within 3°C of in situ temperature. pCO_2 data were corrected to in situ temperature. Samples were collected in duplicate and the relative standard deviation of duplicate analysis averaged ±0.8% (*n*=90)

Samples for the determination of pH were collected in 100 mL glass bottles. pH measurements were done immediately after collection at in situ temperature using a glass/reference electrode cell (Metrohm 6.0259.100) following standard procedures (Dickson et al., 2007; SOP 6a). Both National Institute of Standards and Technology (NIST) and TRIS (2-amino-2-hydroxymethyl-1,3-propanediol) buffers were used for calibration. The temperature difference between buffers and samples never exceeded 2°C. pH values are expressed on the total hydrogen ion scale (pH_T).

2.2.4 Community metabolism

Net community respiration (NCP), gross primary production (GPP) and community respiration (CR) were determined using the oxygen light-dark method (Riley, 1939; Gazeau et al., 2005a). Samples were drawn from the Niskin bottle into similar BOD bottles as described in Sect. 2.2.2. Bottles were incubated on-deck in a water bath, keeping them at ambient surface-water

temperature by continuous circulation of surface water. Samples were incubated both under various light intensities and in the dark. Hard neutral density filters with varying degrees of shading capacity (Lee Filters) were used to mimic light conditions at different depths, while sample bottles incubated in the dark were covered with aluminium foil. Incubations lasted from the time of sampling (usually mid-morning) until sunset. Oxygen concentrations were determined before and after incubation using the automated Winkler titration procedure described in Sect. 2.2.2.

Samples incubated in the light were used to determine NCP by calculating the difference in oxygen concentrations between the start and end of the incubations, divided by the incubation time (5 to 13 hours). CR was determined in a similar fashion from samples incubated in the dark. GPP was subsequently calculated as NCP+CR (all rates expressed in mmol O_2 m^{-3} h^{-1}). To determine the relationship between algal biomass (represented as Chl *a* concentration) and GPP, samples from all depths were incubated in triplicate at 51.2% of surface photosynthetically active radiation (PAR). This yielded a linear relationship between [Chl *a*] and GPP for most months (data not shown). Samples from one depth (typically 3 m) were incubated at 10 different light intensities to determine the dependency of GPP on light availability (P/I curve). These data were normalised to [Chl *a*] and fitted by non-linear least squares fitting using the Eilers-Peeters function (Eilers and Peeters, 1988):

$$\text{GPP}_{\text{norm}} = p_{\text{max}} \frac{(2 + \omega)\,(I / I_{\text{opt}})}{(I / I_{\text{opt}})^2 + \omega\,(I / I_{\text{opt}}) + 1}\,, \tag{2}$$

where GPP$_{\text{norm}}$ is the measured GPP normalised to [Chl *a*] (mmol O_2 mg Chl a^{-1} h^{-1}), p_{max} is the maximum GPP$_{\text{norm}}$ (mmol O_2 mg Chl a^{-1} h^{-1}), I and I$_{\text{opt}}$ are the measured and optimum irradiance, respectively (both in µmol photons m^{-2} s^{-1}) and ω is a dimensionless indicator of the relative magnitude of photoinhibition.

Downwelling light as a function of water depth was measured using a LI-COR LI-193SA spherical quantum sensor connected to a LI-COR LI-1000 data logger. A separate LICOR LI-190 quantum sensor on the roof of the research vessel connected to this data logger was used to correct for changes in incident irradiance. Light penetration depth (LPD; 1% of surface irradiance) was quantified by calculating the light attenuation coefficient using the Lambert-Beer extinction model. To additionally assess water-column transparency, Secchi disc depth was measured and corrected for solar altitude (Verschuur, 1997). In contrast to the measurements of downwelling irradiance, which were only taken mid-morning, Secchi depths were also determined in the afternoon. Although Secchi depths cannot directly be translated into LPD estimates, they do give an indication of the seasonal and diurnal variability in subsurface light climate.

Hourly averaged measurements of incident irradiance were obtained with a LI-COR LI-190SA quantum sensor from the roof of NIOZ-Yerseke, located about 31 km from the sampling site (41.489°N, 4.057°E). These measurements, together with the light attenuation coefficient, were used to calculate the irradiance in the water column at each hour over the sampling day in 10 cm intervals until the LPD. Measured [Chl *a*] was linearly interpolated between sampling depths and combined with the fitted P/I curve (Eq. (2)) to calculate GPP (mmol O_2 m^{-3} h^{-1}) at 10 cm intervals:

$$GPP = [Chl\ a]\ p_{max}\ \frac{(2 + \omega)\,(I / I_{opt})}{(I / I_{opt})^2 + \omega\,(I / I_{opt}) + 1}\ . \tag{3}$$

These GPP values were integrated over time to determine volumetric GPP on the day of sampling (mmol O_2 m^{-3} d^{-1}). A similar procedure using measured hourly incident irradiance was followed to calculate volumetric GPP on the days in between sampling days. Parameters of the Eilers-Peeters fit were kept constant in the monthly time interval around the day of sampling, while [Chl a] depth profiles and the light attenuation coefficient were linearly interpolated between time points. These daily GPP values were integrated over time to estimate annual GPP (mmol O_2 m^{-3} yr^{-1}).

Rates of volumetric CR (mmol O_2 m^{-3} h^{-1}) were converted to daily values (mmol O_2 m^{-3} d^{-1}) by multiplying them by 24 h. An annual estimate for CR (mmol O_2 m^{-3} yr^{-1}) was calculated through linear interpolation of the daily CR values obtained on each sampling day. Finally, CR and GPP were converted from O_2 to carbon (C) units. For CR, a respiratory quotient (RQ) of 1 was used. For GPP, the photosynthetic quotient (PQ) was based on the use of ammonium (NH_4^+) or nitrate (NO_3^-) during primary production. Assuming Redfield ratios, when NH_4^+ is taken up, this results in an O_2:C ratio of 1:1, hence a PQ of 1. Alternatively, when the algae use NO_3^-, this leads to an O_2:C ratio of 138:106 and a PQ of 1.3. Since the utilisation of NH_4^+ is energetically more favourable than that of NO_3^-, the former is the preferred form of dissolved inorganic nitrogen taken up during primary production (e.g. MacIsaac and Dugdale, 1972). If $[NH_4^+] < 0.3$ µmol L^{-1}, we supposed that GPP was solely fuelled by NO_3^- uptake, while above this threshold only NH_4^+ was assumed to be taken up during GPP. Although we are aware that this is a simplification of reality, as NO_3^- uptake is not completely inhibited at $[NH_4^+] > 0.3$ µmol L^{-1} (Dortch, 1990), we have no data to further distinguish between the two pathways. Concentrations of NH_4^+ and NO_3^- were determined in conjunction with concentrations of phosphate (PO_4^{3-}), silicate ($Si(OH)_4$) and nitrite (NO_2^-) by automated colorimetric techniques (Middelburg and Nieuwenhuize, 2000) after filtration through 0.2 µm filters. Water for DOC analysis was collected in 10 mL glass vials and filtered over pre-combusted Whatman GF/F filters (0.7 µm). Samples were analysed using a Formacs Skalar-04 by automated UV-wet oxidation to CO_2, which concentration is subsequently measured with a non-dispersive infrared detector (Middelburg and Herman, 2007). Nutrient and DOC data can be found in the supplementary information.

2.2.5   Sediment fluxes

To determine DIC and TA fluxes across the sediment-water interface, we used shipboard closed-chamber incubations. Upon sediment core retrieval, the water level was adjusted to ca. 18-20 cm above the sediment surface. To mimic in situ conditions, the overlying water was replaced with ambient bottom water prior to the start of the incubations, using a gas-tight tube and ensuring minimal disturbance of the sediment-water interface. Immediately thereafter, the cores were sealed with gas-tight polyoxymethylene lids and transferred to a temperature-controlled container set at in situ temperature. The core lids contained two sampling ports on opposite sides and a central stirrer to ensure that the overlying water remained well mixed. Incubations were done in triplicate and the incubation time was determined in such a way that during incubation the concentration change of

DIC would remain linear. As a result, incubation times varied from 6 (at S1 during summer) to 65 hours (at S3 during winter).

Throughout the incubation, water samples (~7 mL) for DIC analysis were collected from each core five times at regular time intervals in glass syringes via one of the sampling ports. Concurrently, an equal amount of ambient bottom water was added through a replacement tube attached to the other sampling port. About 5 mL of the sample was transferred to a headspace vial, poisoned with 5 µL of a saturated $HgCl_2$ solution and stored submerged at 4°C. These samples were analysed as described in Sect. 2.2.3. The subsampling volume of 7 mL was less than 5% of the water mass, so no correction factor was applied to account for dilution. DIC fluxes (mmol m^{-2} d^{-1}) were calculated from the change in concentration, taking into account the enclosed sediment area and overlying water volume:

$$J = \left(\frac{\Delta C_{ow}}{\Delta t}\right)\frac{V_{ow}}{A} ,$$ (4)

where $\frac{\Delta C_{ow}}{\Delta t}$ is the change in DIC in the overlying water versus time (mmol m^{-3} d^{-1}), which was calculated from the five data points by linear regression, V_{ow} is the volume of the overlying water (m^3) and A is the sediment surface area (m^2). To determine TA fluxes, no subsampling was performed. Instead, the fluxes were calculated from the difference in TA between the beginning and end of the incubation, accounting for enclosed sediment area and overlying water volume. TA samples were collected and analysed as described in Sect. 2.2.3.

2.2.6 Carbonate system calculations

The measurement of four carbonate system parameters implies that we can check the internal consistency of the carbonate system (see Appendix 2.A). For the rest of this paper, we use DIC and pH_T for the carbonate system calculations. This has been suggested to be the best choice when systems other than the open ocean are studied and measurements of TA may be difficult to interpret (Dickson, 2010; see also Appendix 2.A). All calculations were performed using the R package *AquaEnv*. The main advantage of *AquaEnv* is that it has the possibility to include acid-base systems other than the carbonate and borate system, which is especially important in highly productive and hypoxic waters. Furthermore, it provides a suite of output parameters necessary to compute the individual impact of a process on pH, such as the acid-base buffering capacity. As equilibrium constants for the carbonate system we used those of Mehrbach et al. (1973) as refitted by Dickson and Millero (1987), which were calculated from CTD-derived T, S and p using CO2SYS (Pierrot et al., 2006). For the other equilibrium constants (borate, phosphate, ammonia, silicate, nitrite, nitrate and the auto-dissociation of water) we chose the default settings of *AquaEnv*.

CO_2 air-sea exchange (mmol C m^{-2} d^{-1}) on the day of sampling was estimated using the gradient between atmospheric pCO_2 ($pCO_{2,atm}$) and the calculated seawater pCO_2 at 1 m depth (both in atm):

$$F = k\alpha(pCO_2 - pCO_{2,atm}),$$ (5)

where k (m d^{-1}) is the gas transfer velocity, which was calculated from wind speed according to Wanninkhof (1992), normalised to a Schmidt number of 660. Daily-averaged wind speed at Wilhelminadorp (51.527°N, 3.884°E, measured at 10 m above the surface) was obtained from the Royal Netherlands Meteorological Institute (http://www.knmi.nl). The quantity α is the solubility of CO_2 in seawater (Henry's constant; mmol m^{-3} atm^{-1}) and was calculated according to Weiss (1974). For $pCO_{2,atm}$ we used monthly mean values measured at Mace Head (53.326°N, 9.899°W) as obtained from the National Oceanic and Atmospheric Administration Climate Monitoring and Diagnostics Laboratory air sampling network (http://www.cmdl.noaa.gov/). To calculate CO_2 air-sea exchange on the days between sampling days, we used daily-averaged wind speed and linear interpolation of the other parameters.

2.2.7 Acid-base buffering capacity and proton cycling

The acid-base buffering capacity plays a crucial role in the pH dynamics of natural waters. Many different formulations of this buffering capacity exist (Frankignoulle, 1994; Egleston et al., 2010). However, a recent theoretical analysis (Hofmann et al., 2008) has shown that, for natural waters, it is most adequately defined as the change in TA associated with a certain change in [H$^+$], thereby keeping all other total concentrations (e.g. DIC, total borate) constant:

$$\beta = -\left(\frac{\partial TA}{\partial [H^+]}\right). \tag{6}$$

Hence, when the acid-base buffering capacity of the water is high, one will observe only a small change in [H$^+$] for a given change in TA. It should be noted that β is intrinsically different from the well-known Revelle factor (Revelle and Suess, 1957; Sundquist et al., 1979) that quantifies the CO_2 buffering capacity of seawater, i.e. the resilience of the coupled ocean-atmosphere system towards a perturbation in atmospheric CO_2.

In this study, β was calculated according to Hofmann et al. (2008) and subsequently used to quantify the effect of several processes on pH individually as described in Hofmann et al. (2010a). Traditionally, the carbonate system is quantified using DIC and TA. Although this approach has many advantages, it can only determine the combined effect of several concomitantly acting processes on pH. In the method proposed by Hofmann et al. (2010a) pH is calculated explicitly in conjunction with DIC. As a result, the individual contribution of each individual process on pH can be extracted, even though several processes are acting simultaneously (Hagens et al., 2014). Therefore, this method is ideally suited for the analysis of proton cycling and constructing proton budgets. Briefly, each chemical reaction takes place at a certain rate and with a certain stoichiometry; for example, aerobic respiration can be described as

$$CH_2O(NH_3)_{\gamma_N}(H_3PO_4)_{\gamma_P} + O_2 \longrightarrow CO_2 + H_2O + \gamma_N NH_3 + \gamma_P H_3PO_4 \tag{7}$$
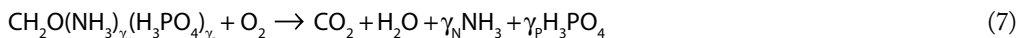
where γ_N and γ_P are the ratios of nitrogen (N) and phosphorus (P) to carbon (C) in organic matter, respectively. At first sight, this reaction equation does not seem to produce any protons. However, the CO_2 (as carbonic acid, H_2CO_3), ammonia (NH_3) and phosphoric acid (H_3PO_4) formed will immediately dissociate into other forms at a ratio similar to their occurrence at ambient pH. As

Table 2.1 Stoichiometric coefficients for the proton ($v_{H^+}^x$) for each reaction considered in the proton budget. c_2 and c_3 are the ratios of HCO_3^- and CO_3^{2-} to DIC, na_1 and na_2 are the ratios of HNO_3 and NO_3^- to total nitrate, n_1 is the ratio of NH_4^+ to total ammonia, and p_2, p_3 and p_4 are the ratios of $H_2PO_4^-$, HPO_4^{2-} and PO_4^{3-} to total phosphate, respectively.

Process x	$v_{H^+}^x$	Range in 2012
GPP (N-source = NH_4^+)	$-c_2 - 2c_3 + \gamma_N n_1 - \gamma_P (p_2 + 2p_3 + 3p_4)$	-1.01 to -0.88
GPP (N-source = NO_3^-)	$-c_2 - 2c_3 - \gamma_N na_2 - \gamma_P (p_2 + 2p_3 + 3p_4)$	-1.31 to -1.18
CR	$c_2 + 2c_3 - \gamma_N n_1 + \gamma_P (p_2 + 2p_3 + 3p_4)$	0.88 to 1.01
Nitrification	$2 - n_2 - na_1$	1.93 to 1.99
CO_2 air-sea exchange	$c_2 + 2c_3$	1.01 to 1.13
Transport/sediment efflux of TA	-1	–
Transport/sediment efflux of DIC	$\dfrac{\partial TA}{\partial DIC}$	1.01 to 1.13

a result, protons are produced during aerobic respiration, despite the fact they are absent in Eq. (7). The amount of protons produced is termed the stoichiometric coefficient for the proton ($v_{H^+}^x$) or proton release rate. This coefficient is process-specific and, for aerobic respiration, equals $c_2 + 2c_3 - \gamma_N NH_3 + \gamma_P H_3PO_4$ (Hofmann et al., 2010a; Table 2.1). Here, c_2 and c_3 are the ratios of bicarbonate (HCO_3^-) and carbonate (CO_3^{2-}) to DIC, n_1 is the ratio of NH_4^+ to total ammonia, and p_2, p_3 and p_4 are the ratios of dihydrogen phosphate ($H_2PO_4^-$), monohydrogen phosphate (HPO_4^{2-}) and PO_4^{3-} to total phosphate, respectively. As these ratios depend on the ambient pH, so does the value of $v_{H^+}^x$.

In natural systems, the vast majority of protons produced during a biogeochemical process according to $v_{H^+}^x$ are consumed through immediate acid-base reactions, thereby neutralising their acidifying effect. The extent to which this attenuation occurs is controlled by the acid-base buffering capacity of the system. Hence, the net change in $[H^+]$ due to a certain process x ($\mu mol\ kg^{-1}\ d^{-1}$) is the product of the process rate (R_x; $\mu mol\ kg^{-1}\ d^{-1}$) and the stoichiometric coefficient for the proton of that reaction ($v_{H^+}^x$), divided by β:

$$\frac{d[H^+]_x}{dt} = \frac{v_{H^+}^x}{\beta} R_x. \tag{8}$$

The total net change in $[H^+]$ over time is simply the sum of the effects of all relevant processes, as they occur simultaneously:

$$\frac{d[H^+]_{tot}}{dt} = \frac{1}{\beta} \sum_{x=1}^{n} v_{H^+}^x R_x. \tag{9}$$

A straightforward way to express the vulnerability of a system to changes in pH is to look at the proton turnover time (Hofmann et al., 2010a). For this we first need to define the proton cycling intensity, which is the sum of all proton-producing (or consuming) processes. When dividing the ambient $[H^+]$ by the proton cycling intensity, the proton turnover time (τ_{H^+}) can be estimated. The smaller the proton turnover time, the more susceptible the system is to changes in pH. In a system that is in steady state, i.e. the final change in $[H^+]$ is zero, the proton cycling intensity is the same irrespective of whether the sum of the proton producing or consuming processes is used for its calculation. In a natural system like the Den Osse basin this is not the case, meaning that total H^+ production and total H^+ consumption are not equal. Here, we use the smaller of the two for the calculation of the proton cycling intensity. As a result, the calculated turnover times should be regarded as maximal values.

2.2.8 Proton budget calculations

Figure 2.2 shows a schematic overview of the major processes affecting proton cycling in the Den Osse basin. For each of the four seasons (March, May, August and November), we estimated a proton budget for the basin by calculating the net production of protons ($\frac{d[H^+]_x}{dt}$) for GPP, CR, nitrification, CO_2 air-sea exchange, sediment-water exchange of DIC and TA and vertical water column mixing, taking account of the effects of S and T changes (Hofmann et al., 2008, 2009). These budgets thus represent the processes influencing the cycling of protons on the day of sampling. We divided the vertical of the basin into eight depth layers, whereby the eight sampling depths represented the midpoint of each layer. Using the bathymetry of the lake, for each box we calculated the total volume of water in the layer, the area at the upper and lower boundary (planar area) and the sediment area interfacing each box. The stoichiometric coefficients for the proton ($v_{H^+}^x$) were calculated with *AquaEnv* using the measured concentrations of DIC, total phosphate, total ammonia, and total nitrate (Table 2.1). Rates of nitrification (mmol N m^{-3} d^{-1}) were estimated from the measured T, $[NH_4^+]$ and $[O_2]$ (in mmol m^{-3}) using (Regnier et al., 1997):

$$R_{nitr} = 86\,400\,k_{max}\exp\left(\frac{T-20}{10}\ln\left(q_{10}\right)\right)\frac{[NH_4^+]}{[NH_4^+]+250}\frac{[O_2]}{[O_2]+15}\,, \tag{10}$$

where k_{max} is the maximum nitrification rate constant ($3\cdot10^{-4}$ mmol m^{-3} s^{-1}) and q_{10}, which is set at 2, is the factor of change in rate for a change in temperature of 10°C. CO_2 air-sea exchange rates were converted to mmol m^{-3} d^{-1} by first multiplying them with the total surface area of the Den Osse basin (m^2) and then dividing them by the volume of the uppermost box (m^3), assuming that CO_2 air-sea exchange only directly affects the proton budget of this box. Similarly, DIC and TA sediment fluxes (mmol m^{-2} d^{-1}) were multiplied by the corresponding sediment area of the basin (m^2) and then divided by the volume of the box corresponding to their measurement depth (m^3). To ensure mass conservation, vertical TA and DIC transport rates (mmol d^{-1}) were computed by multiplying the difference in mass between two consecutive boxes (mmol), i.e. the product of concentration and volume, with a mixing coefficient ζ (d^{-1}) that was calculated based on the entrainment function by Pieters et al. (1985), multiplied by the volume of water below the pycnocline. Then the transport rates were converted to mmol m^{-3} d^{-1} by dividing them by the volume of the corresponding box. Finally, all rates (expressed in mmol m^{-3} d^{-1}) were divided by $10^{-3}\cdot\rho_w$ (kg L^{-1}) to convert them to µmol kg^{-1} d^{-1}.

The sum of $\frac{d[H^+]_x}{dt}$ of all processes considered ($\frac{d[H^+]_{tot}}{dt}$; Eq. (9)) was compared with $\frac{\Delta[H^+]_{obs}}{\Delta t}$, which was calculated from the measured pH_T as the weighted average of the observed change in $[H^+]$ between the previous month and the current month, and between the current month and the next month. The difference between $\frac{\Delta[H^+]_{obs}}{\Delta t}$ and $\frac{d[H^+]_{tot}}{dt}$ is represented as the closure term of the budget, which is needed because some of the proton producing and consuming processes are unknown or have not been measured. This budget closure term includes the effect of lateral transport induced by wind and/or water entering Lake Grevelingen through the seaward sluice, which could not be quantified due to a lack of hydrodynamic data.

2.3 Results

2.3.1 Environmental settings

Over the year 2012, the surface-water temperature at Den Osse ranged from 1.99 to 21.03°C, while bottom-water temperature showed a substantially smaller variation (1.47 – 16.86°C; Fig. 2.3a). The surface water was colder than the bottom water in January, while the reverse was true between February and April. However, the temperature difference between surface and bottom water of Den Osse remained within 1°C. Warming of the surface water in late spring rapidly increased the difference between surface and bottom water to 9.3°C in May. This surface-to-bottom difference in temperature decreased but persisted until August. The thermocline, which was located between 10 and 15 m in May, deepened to 15-20 m in June. In July and August, on the contrary, temperature continuously decreased with depth. In September, the temperature depth profile was almost homogeneous, while in November and December surface waters were again cooler than bottom waters.

Salinity (Fig. 2.3b) increased with water depth at all months, but the depth of the halocline and the magnitude of the salinity gradient varied considerably over the year. This salinity gradient resulted from denser, more saline North Sea water that sank when entering Lake Grevelingen. Variations in the sluice operation, and resulting changes in North Sea exchange volumes, could therefore explain the observed month-to-month variability in salinity depth profiles. Halocline depth varied between ca. 6 m (March and from August to October) to ca. 17 m (November). The largest difference between surface (30.08) and bottom (32.21) water salinity was found in March. Lower inflow and outflow volumes, resulting from strict water level regulations in spring and early summer (Wetsteyn, 2011), led to a lower salinity throughout the water column between April and June. In July and August, a small (~0.2) but noticeable decrease in salinity was recorded from 15-20 m onwards, suggesting the intrusion of a different water mass. Precipitation did not appear to exert a major control on the salinity distribution, as there was no correlation between mean water-column salinity and monthly rainfall as calculated from daily-integrated rainfall data obtained from the Royal Netherlands Meteorological Institute (http://www.knmi.nl) measured at Wilhelminadorp.

Similar to temperature, the difference in density anomaly (σ_T; Fig. 2.3c) between surface and deep water was highest in May. This density gradient was sustained until August, indicating strong water-column stratification during this period. The depth of the pycnocline decreased from

ca. 15 m in May and June to ca. 10 m in July and August. This corresponded to a weakening of the stratification as indicated by the stratification parameter ϕ, which dropped from 3.34 J m^{-3} in May to 2.09 J m^{-3} in August (Fig. 2.3e). This weakening in stratification was presumably due to the delayed warming of bottom water compared to surface water. A week before sampling in September, weather conditions were stormy (maximum daily-averaged wind speed of 7.0 m s^{-1}), which most likely disrupted stratification and led to ventilation of the bottom water. The resemblance in the spatio-temporal patterns of T, S and σ_T indicates that the water-column

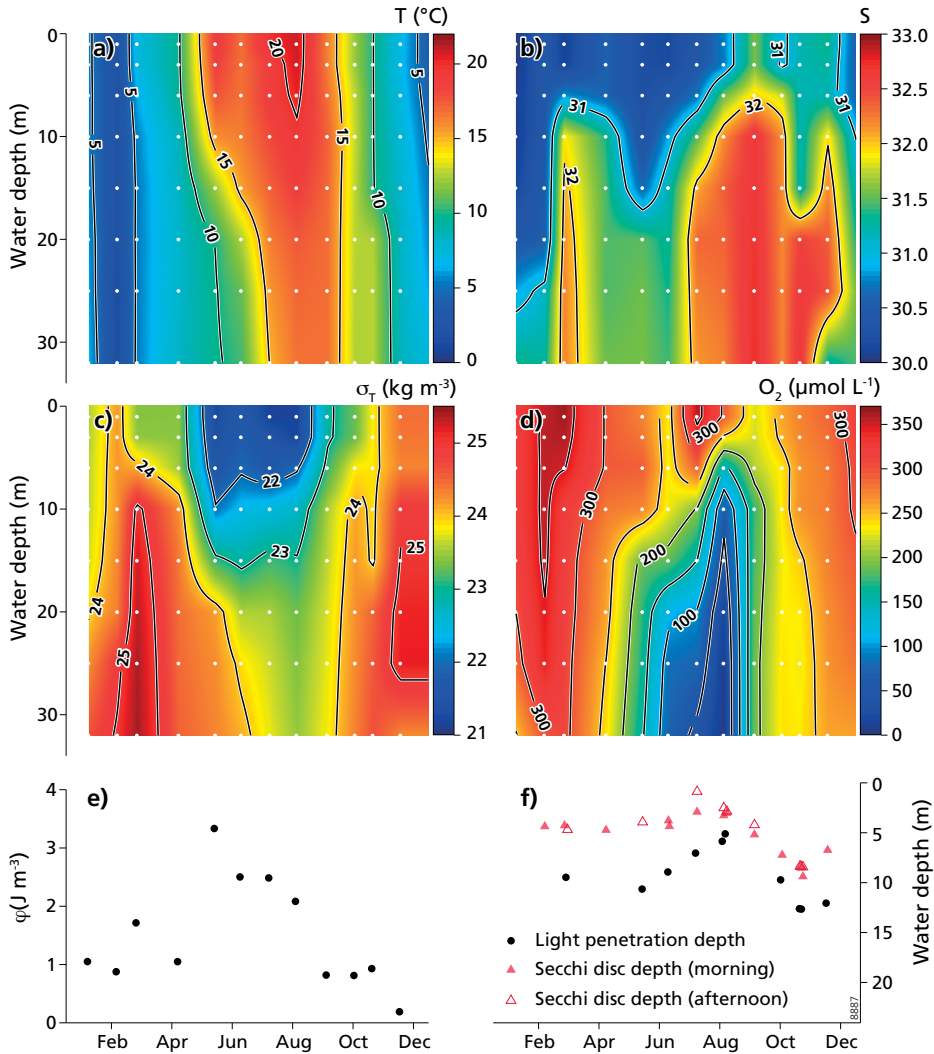**Figure 2.3** (a) Temperature (°C), (b) salinity, (c) density anomaly (kg m^{-3}), (d) O$_2$ (µmol L^{-1}), (e) stratification parameter ϕ (J m^{-3}), and (f) light penetration and Secchi disc depths at the Den Osse basin in 2012. Black dots in (a) – (d) indicate measurements. Data from (a) – (d) were linearly interpolated in space and time.

stratification was controlled by both temperature and salinity, where salinity was important in winter (ϕ values of ca. 1 J m^{-3}) and temperature gradients intensified stratification in late spring and summer.

Oxygen concentrations (Fig. 2.3d) were highest in February as a result of the low water temperatures, increasing O_2 solubility. A second peak in $[O_2]$ occurred in the surface water in July, during a period of high primary production (see Sect. 2.3.3.1), and led to O_2 oversaturation in the upper metres. From late spring onwards, water-column stratification led to a steady decline in $[O_2]$ below the mixed-layer depth, resulting in hypoxic conditions (< 62.5 μmol L^{-1}) below the pycnocline in July and August. Although in August the bottom water was fully depleted of O_2, $[H_2S]$ remained below the detection limit (5 μM), indicating the absence of euxinia. From September onwards, water-column mixing restored high O_2 concentrations throughout the water column.

Lake Grevelingen surface water is generally characterised by high water transparency and deep light penetration (Fig. 2.3e). LPD was 9.4 m in March and slightly increased to 10.6 m in May. Between June and August, during a period of high primary production (see Sect. 2.3.3.1), LPD decreased until 5.8 m. From September onwards, the surface water turned more transparent again. Accordingly, LPD increased up to 12.6 m in November, after which it stabilised at a value of 12.0 m in December. The Secchi disc data generally confirm the observed temporal pattern in the LPD, as is shown by the significant correlation between morning Secchi depths and LPD (r^2 = 0.86; P < 0.001). Secchi disc depth was on average ~80% of LPD and, similar to LPD, was highest in November and lowest in July. Additionally, the Secchi depths indicate that diurnal variations in light penetration may exist. Especially in July, during an intense dinoflagellate bloom (see Sect. 2.3.3.1), light penetrated much deeper into the water column in the morning than in the afternoon (Secchi disc depths of 2.9 and 0.9 m, respectively). The difference between morning and afternoon Secchi disc depth was much smaller in August (3.3 and 2.5 m) and virtually absent in November (8.5 and 8.4 m).

2.3.2   Carbonate system variability

2.3.2.1 pH_T, DIC, TA, pCO_2

In January, pH_T showed little variation with depth, with an average value of 8.04 (Fig. 2.4a). From February to April, pH_T increased throughout the water column, though the increase was faster at the surface than at depth, up to a maximum of 8.36 in the surface water in April. From June onwards, stratification augmented the difference between surface and bottom water pH_T. In August, this difference had increased to 0.69 units. The sharp decrease in pH_T with depth during this month coincided with the declining trend seen for $[O_2]$ (Fig. 2.3d), highlighting the connection between bottom-water pH and low $[O_2]$ in seasonally stratified waters. Additionally, elevated surface water pH_T in summer co-occurred with high $[O_2]$, concurrent with an intense dinoflagellate bloom (see Sect. 2.3.3.1). Similar to the depth profiles of $[O_2]$, the termination of stratification diminished the gradient between surface and bottom-water pH_T. However, pH_T at the end of 2012 was significantly lower (average value of 7.98) than at the beginning of 2012. Over the year, surface-water pH_T varied 0.46 units, while bottom-water pH_T variation was higher (0.60 units).

DIC (Fig. 2.4b) showed little variation with depth in January and February (average value 2257 µmol kg^{-1}), with the exception of the bottom water, where DIC was slightly (40-50 µmol kg^{-1})
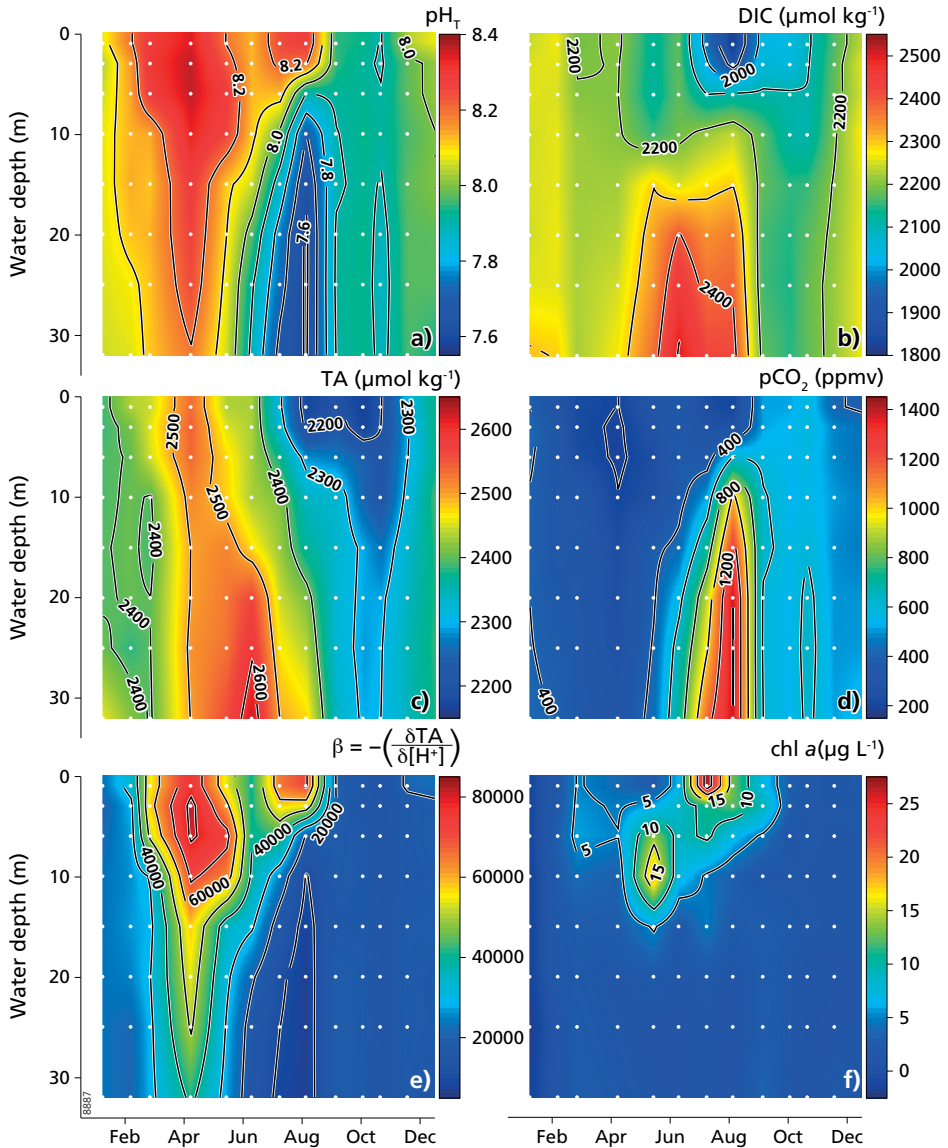
Figure 2.4 (a) pH$_T$ (at in situ temperature), (b) DIC (µmol kg^{-1}), (c) TA (µmol kg^{-1}), (d) pCO$_2$ (ppmv), (e) buffering capacity (β), and (f) concentration of Chl *a* (µg L^{-1}) at Den Osse in 2012. Black dots indicate sampling intervals. TA and pCO$_2$ were calculated from measured pH$_T$ and DIC using the equilibrium constants of Mehrbach et al. (1973) as refitted by Dickson and Millero (1987), while β was calculated from measured pH$_T$ and calculated TA. All data were linearly interpolated in space and time.

elevated. In March, DIC decreased slightly throughout the water column, with a stronger drawdown in the upper 6-10 m, and the higher bottom-water concentrations diminished. The difference between surface and deeper water increased until ca. 70 µmol kg^{-1} in April, due to an increase in bottom-water DIC. In May, a concurrent drawdown in DIC above 15 m and increase in DIC below this depth resulted in a surface-to-bottom DIC difference of 250 µmol kg^{-1}. The depth of this sharp transition coincided with the pycnocline depth. In June, DIC increased strongly (by 100-200 µmol kg^{-1}) below the pycnocline, while in July and August, a strong drawdown in DIC occurred above the pycnocline, concurrent with an intense dinoflagellate bloom (see Sect. 2.3.3.1). In combination with the persisting stratification, this resulted in a surface-to-bottom difference in DIC of 600 µmol kg^{-1}. After the disruption of the stratification, the difference between surface and bottom water DIC was greatly reduced, and decreased further from 144 to 47 µmol kg^{-1} between September and December. Concomitantly, the average DIC increased from 2146 to 2201 µmol kg^{-1}, although the month October was characterised by overall slightly lower DIC (average value of 2123 µmol kg^{-1}). Surface-water DIC variation over the year (453 µmol kg^{-1}) was somewhat higher than in the bottom water (361 µmol kg^{-1}).

TA (Fig. 2.4c) generally showed more temporal than spatial variability. Therefore, variations in TA with depth were usually much smaller compared to DIC. In January and February, TA was fairly constant with depth (average value of 2404 µmol kg^{-1}), with the exception of bottom-water). TA in January (2460 µmol kg^{-1}). In March and April, TA in the upper 6 m was 40-50 µmol kg^{-1} higher than in the underlying water. Overall, TA in April had increased by on average 105 µmol kg^{-1} compared to March. The period of water-column stratification was characterised by a positive surface-to-bottom-water TA difference correlating with pycnocline depth. This difference was highest in June (195 µmol kg^{-1}), as a result of high bottom-water TA, and in August (306 µmol kg^{-1}), mainly due to the strong drawdown in surface-water TA. Because of this, average water-column TA in June was much higher (2520 µmol kg^{-1}) than in August (2366 µmol kg^{-1}). The low surface-water TA persisted until November, while TA below 10 m depth was much less variable. Similar to DIC, the month of October was characterised by overall lower TA. There was little difference between surface- and bottom-water variation in TA over the entire year (372 and 337 µmol kg^{-1}, respectively

The pattern of pCO$_2$ (Fig. 2.4d) was inversely proportional to that of pH$_T$. January was characterised by little variation with depth and an average pCO$_2$ (404 ppmv) close to pCO$_{2,atm}$ (396 ppmv). In February, low T throughout the water column led to a drawdown of pCO$_2$ which continued until April, albeit with larger magnitude in the surface compared to the bottom water. The onset of stratification in May led to a build-up of CO$_2$ resulting from organic matter degradation in the bottom water. Maximum bottom-water pCO$_2$ (1399 ppmv) was found in August and, as expected, co-occurred with the period of most intense hypoxia (Fig. 2.3d). While in May and June, pCO$_2$ increased throughout the water column, in July and August a substantial drawdown in surface-water pCO$_2$ was observed coinciding with an increase in [O$_2$], which is indicative of high autotrophic activity. Water-column ventilation disrupted the surface-to-bottom pCO$_2$ difference from September onwards. Mean water-column pCO$_2$ decreased from 584 to 490 ppmv between September and December, although pCO$_2$ values were slightly higher in November,

especially in the bottom water (601 ppmv on average). Note that, in contrast to January, the average water-column pCO_2 in December was much higher than $pCO_{2,atm}$ (398 ppmv). Similar to pH_T, pCO_2 variation over the year was higher in the bottom water (1099 ppmv) than in the surface water (375 ppmv).

We investigated the correlation between the different carbonate system parameters and O_2 by calculating coefficients of determination and testing their significance using the package *Stats* in R (R Core Team, 2015). In line with our visual observations, we found a strong correlation between pH_T and pCO_2 ($r^2 = 0.89$, P < 0.001) and weak to moderate correlations between pH_T and O_2 ($r^2 = 0.68$, P < 0.001), pCO_2 and O_2 ($r^2 = 0.70$, P < 0.001), and DIC and TA ($r^2 = 0.56$, P < 0.001). DIC does not appear to be correlated with pH_T ($r^2 = 0.18$, P < 0.001), pCO_2 ($r^2 = 0.17$, P < 0.001) or O_2 ($r^2 = 0.21$, P < 0.001). Finally, as expected TA could not statistically significantly be correlated to pH_T ($r^2 = 0.01$, P = 0.278), pCO_2 ($r^2 = 0.01$, P = 0.384) or O_2 ($r^2 = 0.04$, P = 0.066).

2.3.2.2 Acid-base buffering capacity

The acid-base buffering capacity generally showed a similar spatio-temporal pattern to pH_T and the inverse of the pCO_2 pattern (Fig. 2.4e). In January, β had an average value of 22967 and hardly varied with depth. From February to April, the buffering capacity increased throughout the water column, with a faster increase in the surface compared to the bottom water and a maximum of 82557 in the surface water in April. In May and June, the acid-base buffering capacity showed an overall decline. In contrast to pH_T, the onset of stratification did not lead to a direct amplification of the difference between surface and bottom water β. July was characterised by a sharp increase in surface-water β, coinciding with the decrease in DIC, and a decrease in bottom-water β, a trend that was intensified in August. During this period of strongest hypoxia, surface-water β (71454) was an order of magnitude higher than bottom-water β (6802). Between September and December, i.e. after bottom-water ventilation, the buffering capacity did not show any substantial variations with depth. Over the course of the year, surface-water β varied by a factor of 2 more than bottom-water β.

To assess the effect of temperature on the acid-base buffering capacity, we calculated β for each month and depth using the annual average temperature at Den Osse, which was 10.8°C for 2012. From this, we calculated the anomaly in β as the difference between the actual and isothermally calculated values for β. This analysis shows that the β anomaly is negatively correlated with the T anomaly, i.e. an increase in temperature leads to a decrease in the acid-base buffering capacity. However, β changed by at most ~30000 as a result of the range of temperatures the Den Osse Basin experienced in 2012, while the actual seasonal variation in the acid-base buffering capacity exceeds 60000. Temperature thus only partly explains the variation in β over the year. To further elucidate what controls the acid-base buffering capacity, we calculated the contribution of various acid-base systems to β for the surface and bottom water in August (Table 2.2). This calculation shows that in the oxic surface water, where β is high, the relative contribution of the borate system to the total buffering capacity was higher than in the anoxic, poorly buffered bottom water (24 and 17%, respectively), while the reverse holds for the carbonate system (73 versus 81%). Acid-base systems other than the carbonate and borate system contributed most to the buffering capacity in the

Table 2.2 Contributions of various acid-base systems to the acid-base buffering capacity β in August at 1 and 32 m depth.

Acid-base system	Oxic surface water (pH$_T$ = 8.28)	Anoxic bottom water (pH$_T$ = 7.52)
Carbonate	72.99 %	81.14 %
Borate	24.41 %	17.44 %
Water (auto-dissociation)	2.42 %	0.72 %
Phosphate	0.09 %	0.30 %
Silicate	0.08 %	0.29 %
Ammonium	0.00 %	0.08 %
Other	0.00 %	0.03 %

anoxic bottom water, due to the accumulation of NH_4^+, PO_4^{3-} and $Si(OH)_4$. However, their total contribution never exceeded 1%.

2.3.3 Rate calculations

2.3.3.1 *Gross primary production and community respiration*

Chl *a*, which was used as an indicator for algal biomass, showed three periods of elevated concentrations (Fig. 2.4f). In March, surface-water [Chl *a*] showed a slight increase up to 5.2 µg L^{-1}. In May, elevated [Chl *a*] could be found between 6 and 15 m, with a subsurface maximum of 19.0 µg L^{-1} at 10 m depth. Finally, the most prominent peak in [Chl *a*] (27.3 µg L^{-1}) was found in the surface water in July. Together with elevated [O$_2$] and pH$_T$ and a drawdown of DIC and pCO$_2$, this indicated the presence of a major phytoplankton bloom. Microscopic observations of phytoplankton samples from this bloom showed that it consisted mainly of the dinoflagellate *Prorocentrum micans*.
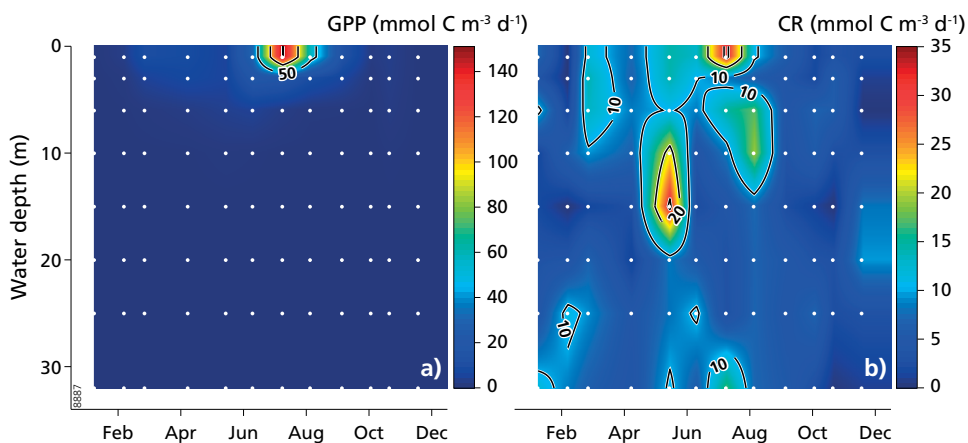

Figure 2.5 Volumetric rates of (a) GPP (mmol C m^{-3} d^{-1}), and (b) CR (mmol C m^{-3} d^{-1}) at Den Osse in 2012. Black dots indicate sampling intervals. Rates were calculated as described in Sect. 2.2.4.

Measured volumetric rates of GPP ranged from 0.0 to 150.7 mmol C m^{-3} d^{-1} (Fig. 2.5a), while volumetric CR ranged from 0.0 – 31.5 mmol C m^{-3} d^{-1} (Fig. 2.5b). To a large extent, their spatio-temporal patterns confirm the trends in [Chl a]. GPP showed a distinct seasonal pattern, with one major peak in July 2012 (151 mmol C m^{-3} d^{-1} at 1 m depth) coinciding with high surface water [Chl a] and CR (31 mmol C m^{-3} d^{-1}). Elevated CR in August between 6 and 10 m depth (19 mmol C m^{-3} d^{-1}) may reflect degrading algal material from this bloom. Although surface water [Chl a] showed a slight increase in March, this was not reflected in the GPP during this month (maximum 9.4 mmol C m^{-3} d^{-1}). The peak in [Chl a] in May correlated with a major peak in CR (maximum 31 mmol C m^{-3} d^{-1}) but not in GPP. Since this Chl a subsurface maximum was close to the LPD of 10.6 m, this indicates that this algal biomass could not substantially contribute to GPP, as confirmed by the rate measurements. Hence, it presumably represented sinking algal biomass that was being degraded. The fact that the Chl a peak at ca. 10 m depth in May was not preceded by a surface water Chl a peak of equal magnitude could mean that part of the algal biomass may not have formed in situ, but was imported with North Sea water. As an alternative explanation, there was a relatively long period between sampling in March and April (42 days) and between sampling in April and May (37 days). This means that in either of those periods an algal bloom could have formed and led to the increase in CR in May. Between March and May, [NH$_4^+$] declined from 0.76 to 0.00 μmol kg^{-1} and [NO$_3^-$] from 20.6 to 0.08 μmol kg^{-1} (see supplementary information), supporting the idea of a bloom between sampling dates.

To assess the metabolic balance in the surface water, we averaged the volumetric GPP and CR in the photic zone. This analysis reveals that in summer, from June to September, volumetric GPP was higher than CR above the light penetration depth. Before and after this period, average photic zone CR was higher than GPP. This is another indication that a significant part of the organic carbon respired within the surface water layer was not produced in situ, emphasising the potential importance of lateral input of detrital matter at the field site. Yearly integrated GPP averaged over the photic zone was estimated to be 2494 mmol C m^{-3} yr^{-1}, which amounts to an average of 6.8 mmol C m^{-3} d^{-1}. Annual depth-weighted photic zone CR was slightly higher than GPP, i.e. 2852 mmol C m^{-3} yr^{-1} or 7.8 mmol C m^{-3} d^{-1}. Depth-weighted volumetric CR below the photic zone, the annual rate of which was approximated at 2232 mmol C m^{-3} yr^{-1} or 6.1 mmol C m^{-3} d^{-1}, was lower than average photic zone CR except for February and December.

2.3.3.2 CO$_2$ air-sea exchange

For most of 2012, the surface water (1 m) of the Den Osse basin was undersaturated with respect to pCO$_{2,atm}$, which led to CO$_2$ uptake from the atmosphere (Fig. 2.6a). In January, surface-water pCO$_2$ was very close to pCO$_{2,atm}$, resulting in a very small influx. From February to April, surface-water pCO$_2$ steadily declined to a value of 199 ppmv in April. This brought about an increasingly larger gradient and a CO$_2$ uptake that was highest in April (21.4 mmol C m^{-2} d^{-1}). Surface-water pCO$_2$ increased in late spring until a value of 350 ppmv in June, after which it declined to 202 ppmv in August. Water-column ventilation from September onwards brought CO$_2$-rich bottom water to the surface, leading to a surface-water pCO$_2$ value exceeding that of the atmosphere and inducing strong outgassing of CO$_2$ towards the atmosphere. Outgassing continued until the end of 2012, albeit with a smaller magnitude due to a decrease in surface water pCO$_2$ to 411 ppmv in December.

Although the direction of the CO_2 air-sea flux is solely determined by the saturation state of surface water with respect to $pCO_{2,atm}$, its magnitude is also influenced by the gas transfer velocity k, which is parameterised as a function of wind speed. Daily-averaged wind speed over 2012 varied between 1.5 and 14.5 m s^{-1}, with an average of 4.6 m s^{-1}. With the exception of January, February, April and December, our samples were taken on days with wind speeds below average (see supplementary information). We interpolated the CO_2 air-sea flux as described in Sect. 2.2.6 (red dotted line in Fig. 2.6a). When integrated over the year, this leads to a value of -0.98 mol C m^{-2} yr^{-1}, or an average flux of -2.66 mmol C m^{-2} d^{-1}, indicating that the Den Osse basin was a weak sink for CO_2.

2.3.3.3 Sediment fluxes

In all months, sediment DIC fluxes were highest at S1 (Fig. 2.6b). Since S1 is located at the deepest point of the Den Osse basin, it receives the highest input of organic matter through both sinking
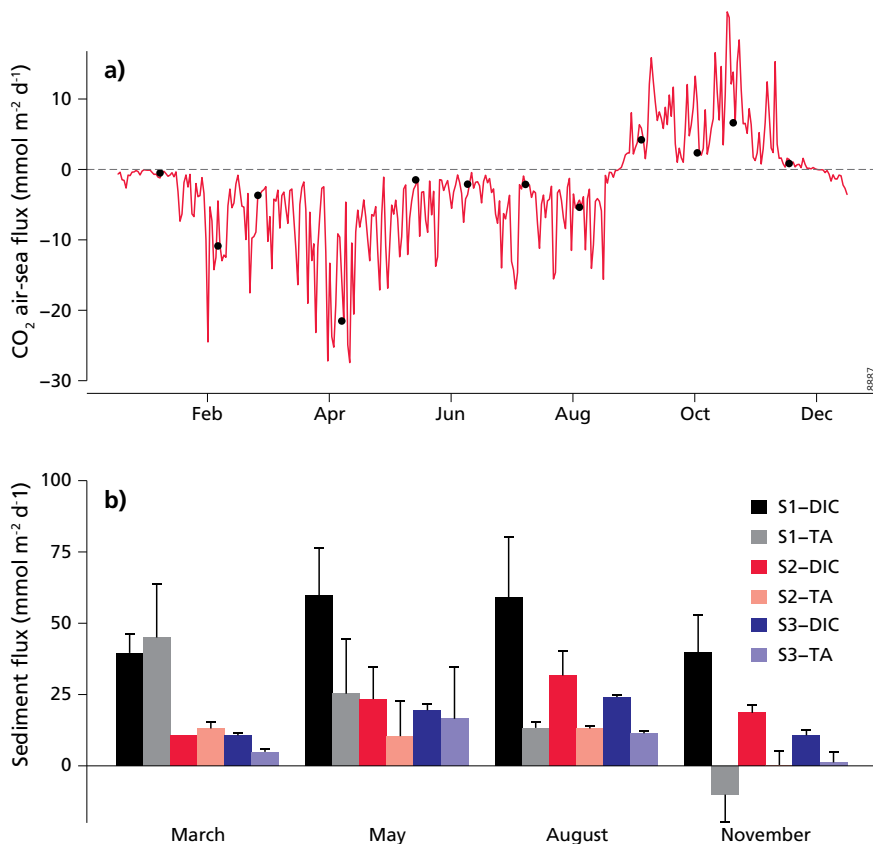
Figure 2.6 (a) CO_2 air-sea flux (mmol C m^{-2} d^{-1}), and (b) total sediment DIC and TA fluxes (mmol m^{-2} d^{-1}) at three different depths (S1 = 34 m, S2 = 23 m, S3 = 17 m) in the Den Osse basin. CO_2 air-sea flux was interpolated using linear interpolation of the CO_2 sea-air gradient and daily averaged wind speed data measured at Wilheminadorp (51.527°N, 3.884°E). Sediment fluxes were obtained from core incubations executed in triplicate (see Sect. 2.2.5).

and lateral transport. S2 and S3 showed similar DIC fluxes throughout the year, with the exception of November, when the flux at S2 (18.6 ± 2.9 mmol m^{-2} d^{-1}) exceeded that of S3 (10.7 ± 2.3 mmol m^{-2} d^{-1}). In August, DIC fluxes at S2 and S3 were substantially higher than in the other months. During this month, the amount of organic matter sinking through the water column may have been high as a result of a peak in primary production in the preceding month.

The sediment TA fluxes generally showed much more site-specific variability, making it difficult to identify any spatial or temporal patterns. TA fluxes in March showed a clear spatial variability, with the highest flux at S1 (45.0 ± 19.0 mmol m^{-2} d^{-1}), followed by S2 (13.1 ± 2.7 mmol m^{-2} d^{-1}) and S3 (4.9 ± 1.3 mmol m^{-2} d^{-1}). May and August did not display any difference between stations or months, with fluxes varying from 10.4 ± 12.7 to 25.3 ± 19.3 mmol m^{-2} d^{-1}. In November, TA fluxes at S2 (0.3 ± 5.2 mmol m^{-2} d^{-1}) and S3 (1.2 ± 3.9 mmol m^{-2} d^{-1}) were similar and very small, while S1 showed an uptake rather than release of TA (-10.1 ± 9.9 mmol m^{-2} d^{-1}), likely because of reoxidation processes that consume TA. *Beggiatoa* spp. were abundant in these sediments in November (Seitaj et al., 2015a) and their activity may generate a decrease in surface-sediment TA (Sayama et al., 2005).

For most of the year, the ratio of sediment DIC to TA flux was higher than 1, meaning that more DIC than TA was released from the sediments. Only in March at S1 and S2, the efflux of TA was higher than that of DIC. Because of the sedimentary uptake of TA at S1 in November, the corresponding DIC:TA was negative.

2.4   Discussion

2.4.1   Community metabolism

In 2012, Lake Grevelingen experienced a major phytoplankton bloom in summer (July), a minor bloom with completely different dynamics in early spring (March), and a potential third bloom in late spring (April). The minor March bloom is reflected in a slightly elevated surface water [Chl *a*] and pH$_T$, no obvious peak in GPP, but a small peak in CR. The major peak in CR in May, accompanied by a Chl *a* peak at 10 m depth, could result from the early spring bloom, as we might not have captured its full extent, or the potential late spring bloom (see Sect. 2.3.3.1). However, it most likely represents laterally transported degrading *Phaeocystis globosa*, the haptophyte that makes up the spring bloom in the southern part of the North Sea (Cadée and Hegeman, 1991). Highest *P. globosa* cell counts have been found between mid-April and mid-May, corresponding to the timing of the CR peak, at the mouth of the Eastern Scheldt (51.602°N, 3.721°E) between 1990 and 2010 (Wetsteyn, 2011), and off the Belgian coast between 1989 and 1999 (Lancelot et al., 2007). Moreover, the years with high *P. globosa* cell counts at the mouth of the Eastern Scheldt coincided with a large area of low-oxygen water in the entire Lake Grevelingen (Peperzak and Poelman, 2008; Wetsteyn, 2011), highlighting the connection between *P. globosa* blooms and O$_2$ consumption in the lake. The high CR in May combined with the onset of stratification led to a rapid decline in bottom water [O$_2$]. The major dinoflagellate bloom in July was short but very intense in terms of GPP and [Chl *a*] and appeared to contribute to the sharp increase in hypoxic

water volume between June and August. Sinking *P. micans* from this bloom was degraded, which is reflected in higher CR in July and August compared to June, and the products of this degradation were trapped in the water below the pycnocline, as is indicated by elevated DIC levels. However, the higher CR in July and August and subsequent decline in $[O_2]$ may also result from higher water temperatures (Fig. 2.3a), resulting in faster degradation of allochthonous organic matter. The drawdown of bottom-water O_2 is, however, not due to CR alone. The fact that $[O_2]$ declines with depth at all months indicates that sediment oxygen uptake may be an important process affecting water-column $[O_2]$. Indeed, substantial sediment O_2 uptake was found to take place year-round with rates up to 61 mmol m^{-2} d^{-1} at S1 (Seitaj et al., 2015b).

Our depth-weighted, annually averaged CR of 7.8 mmol C m^{-3} d^{-1} in the photic zone and 6.1 mmol C m^{-3} d^{-1} below the LPD are similar to estimates from the nearby located Western Scheldt, where annually averaged CR ranged from 4.7 − 19.1 mmol C m^{-3} d^{-1}, with a mean value of 6.6 mmol C m^{-3} d^{-1} (Gazeau et al., 2005b). In the mesohaline part of the seasonally hypoxic Chesapeake Bay, summertime surface-water CR was found to vary between 9.8 − 53.0 mmol C m^{-3} d^{-1}, while bottom-water CR varied between 0 − 45.6 mmol C m^{-3} d^{-1} (Lee et al., 2015). Thus, our measurements of CR are well within the range of published values, both for the Dutch coastal zone and for other seasonally hypoxic basins.

Recent modelling studies and previous measurement campaigns have presented lake-wide estimates of GPP ranging from 100 g C m^{-2} yr^{-1} (Nienhuis and Huis in 't Veld, 1984) to 572 g C m^{-2} yr^{-1} (Meijers and Groot, 2007). When integrating annual volumetric GPP over the depth of the photic zone, we arrive at an estimate of GPP for the Den Osse basin of 225 g C m^{-2} yr^{-1} in 2012. Given the different methods used and time periods considered, our estimate of GPP is consistent with these previous studies. In comparison with other coastal systems in the Netherlands, GPP in the Den Osse basin is somewhat lower than that in the adjacent Eastern Scheldt (200 − 550 g C m^{-2} yr^{-1}; Wetsteyn and Kromkamp, 1994) and of similar magnitude to that in the western Wadden Sea between 1988 and 2003 (185±13 g C m^{-2} yr^{-1}; Philippart et al., 2007) and in the Western Scheldt in 2003 (150 g C m^{-2} yr^{-1}; Gazeau et al., 2005b).

2.4.2   Proton cycling due to GPP and CR

The fluctuations in pH$_T$ as shown in Fig. 2.4a result from the balance between rates and stoichiometry of proton-producing and -consuming processes, mediated by the acid-base buffering capacity of the water. Taking into account that variations in the stoichiometric coefficient for the proton are relatively minor (Table 2.1) compared to changes in process rates (Figs. 2.5 and 2.6) and acid-base buffering capacity (Fig. 2.4e), we will focus our discussion mainly on the latter two.

Any biogeochemical process will either consume or produce protons based on its stoichiometry, as the reaction always proceeds in the forward direction. The signs of $v_{H^+}^x$ in Table 2.1 indicate whether a process produces (positive) or consumes (negative) protons. Thus, CR and nitrification increase $[H^+]$, while GPP leads to an increase in pH. For transport processes, the direction of the flux determines whether protons are produced or consumed. For example, CO_2 uptake from the atmosphere leads to an increase in $[H^+]$, while outgassing of CO_2 to the atmosphere consumes

protons. For vertical transport and sediment-water exchange, the direction of the net change in [H^+] depends on the ratio of TA to DIC flux entering the water mass. When the flux of TA exceeds that of DIC, protons are consumed. On the contrary, when DIC fluxes are higher than TA fluxes, the net effect is an increase in [H^+]. Considering the magnitude of the seasonal variability in the various process rates measured at Den Osse, they must significantly impact H^+ dynamics.

Aside from this, the spatio-temporal variations in buffering capacity (Fig. 2.4e) also exert a major control on the proton cycling in this basin. Taking the month of August as an example, β decreases by one order of magnitude when going from surface to bottom water. When the rate of a certain process does not change with depth, the number of protons produced or consumed by this process per kg of water is 1 order of magnitude higher in the bottom water than in the surface water (see Eq. (8)). This indicates that, in August, the bottom water is much more prone to changes in pH than the surface water. In line with previous studies focussing on the CO_2 buffering capacity (e.g. Thomas et al., 2007; Shadwick et al., 2013), temperature was found to exert an important control on the seasonal variability of the acid-base buffering capacity in the Den Osse Basin. The fact that the contribution of acid-base systems other than the carbonate and borate system to β is highest in the anoxic bottom water is in line with previous work (e.g. Ben-Yaakov, 1973; Soetaert et al., 2007). However, their small contribution in the Den Osse basin contrasts with results from the Eastern Gotland basin in the Baltic Sea. Here, generation of TA during remineralisation under anoxic conditions by denitrification, sulphate reduction and the release of NH_4^+ and PO_4^{3-}, and the resultant increase in buffering capacity were found to contribute significantly to the observed changes in pH (Edman and Omstedt, 2013).

To understand how variations in both process rates and acid-base buffering capacity control proton cycling in the Den Osse basin, we used Eq. (8) to calculate the change in [H^+] (µmol kg^{-1} d^{-1}) due to GPP at 1 m depth and CR at 1 and 25 m depth. This analysis reveals that it is the interplay between GPP (Fig. 2.7d) and β (Fig. 2.7b) that drives temporal variations in $\frac{d[H^+]_{GPP}}{dt}$ (Fig. 2.7e). The seasonal pattern of $\frac{d[H^+]_{GPP}}{dt}$ resembles that of GPP, but its magnitude is significantly modulated by β, especially in late summer. For example, GPP in August was 4.6 times higher than that of September (57.9 and 12.6 µmol kg^{-1} d^{-1}, respectively), but $\frac{d[H^+]_{GPP}}{dt}$ in August was only 1.8 times higher. This difference cannot be explained by $v_{H^+}^{GPP}$ (Fig. 2.7c), which had a higher magnitude in August (-1.31) in comparison with September (-0.92), due to a switch from NO_3^- to NH_4^+ uptake (Sect. 2.2.4). Thus, the relatively high proton consumption in September was driven by the lower surface-water buffering capacity, which is a factor of 3.7 smaller in September compared to August (71454 versus 19474). When comparing $\frac{d[H^+]_{GPP}}{dt}$ and $\frac{d[H^+]_{CR}}{dt}$ in the surface layer (Fig. 2.7e), we see that when GPP was higher than CR, the decrease in [H^+] due to GPP was also higher than the increase in [H^+] due to CR. This can simply be explained by the fact that β was the same for both processes Fig. 2.7b), and the effect of $v_{H^+}^{GPP}$ was only minor (Fig. 2.7c), so that the difference between $\frac{d[H^+]_{GPP}}{dt}$ and $\frac{d[H^+]_{CR}}{dt}$ can directly be linked to the difference between GPP and CR (Fig. 2.7d). Some clear differences between the patterns of $\frac{d[H^+]_{CR}}{dt}$ at 1 and 25 m depth can be identified (Fig. 2.7e). With the exception of February, October and December, volumetric CR was higher at 1 m depth than at 25 m depth (Fig. 2.7d). Thus, the higher $\frac{d[H^+]_{CR}}{dt}$ in June and August at 25 m compared to 1 m depth was solely driven by the lower acid-base buffering capacity of the bottom water (Fig. 2.7b). In July,
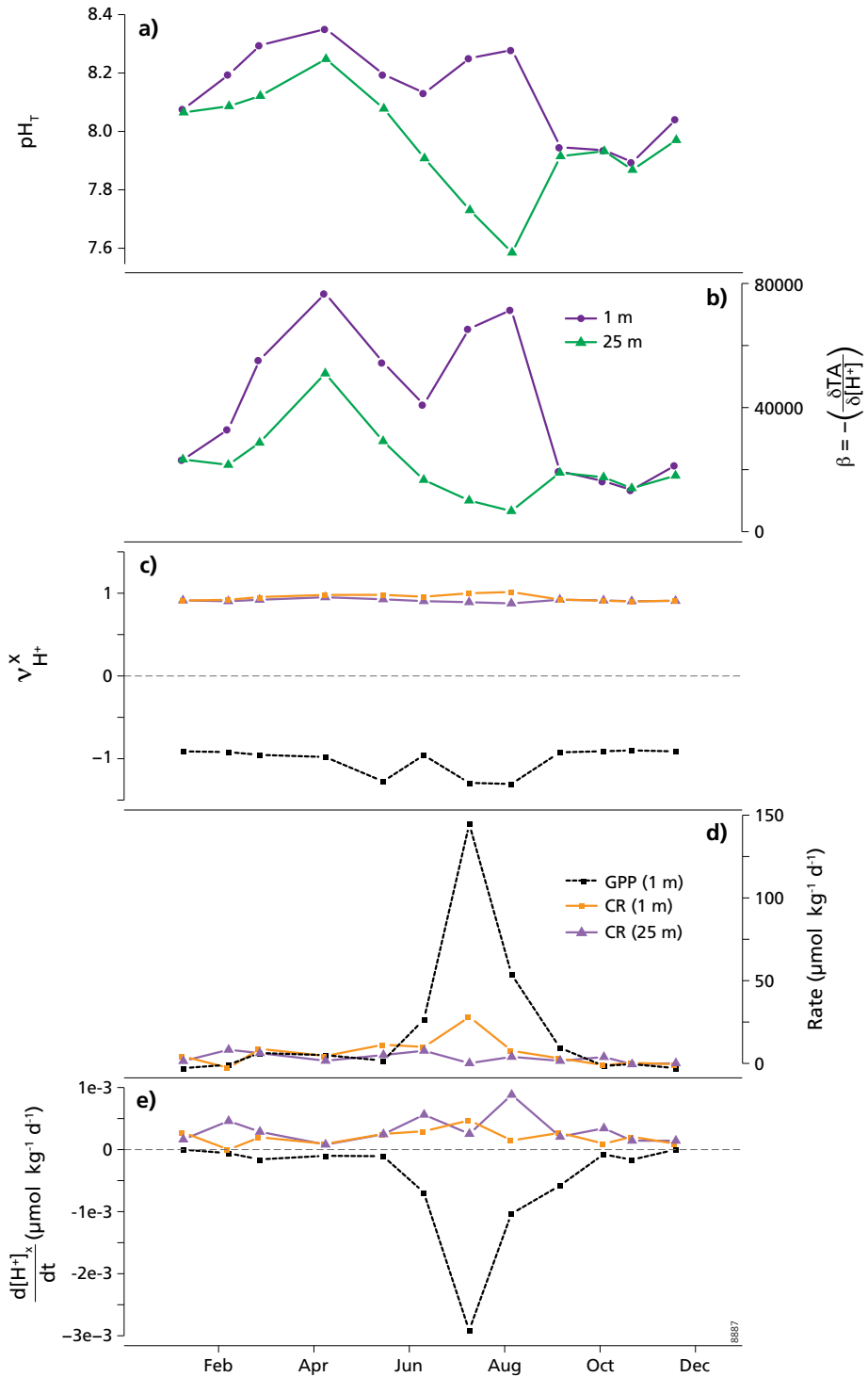
on the contrary, CR at 1 m depth was so much higher than at 25 m depth (30.8 versus 2.9 µmol kg^{-1} d^{-1}) that this compensated for the lower buffering capacity at depth (65373 versus 10025) and led to a higher surface-water $\frac{d[H^+]_{CR}}{dt}$. Again, this highlights that the magnitudes of both CR and β play a role in determining the actual change in pH.

In summary, in the Den Osse surface water we observe relatively small pH fluctuations (Fig. 2.7a), despite high variability in the balance between GPP and CR. In the bottom water, CR is much more constant, yet pH variability is much higher. Assuming these processes are the main biogeochemical processes producing or consuming H$^+$ on a seasonal scale, this shows that seasonal changes in the acid-base buffering capacity play a major role in pH dynamics. Thus, our calculations clearly demonstrate that we cannot use only measured process rates to estimate the effect of a certain process on pH. Rather, it is the combined effect of variability in process rates and buffering capacity, combined with minor fluctuations in $\nu_{H^+}^x$, that determines the change in pH induced by a certain process.

2.4.3 Proton budget for the Den Osse basin

To further elucidate the driving mechanisms of pH fluctuations, we calculated a full proton budget for each of the four seasons in 2012. One should realise that these proton budgets are among the first of their kind based on measured data and contain many uncertainties. Figure 2.8 shows these budgets for 1 and 25 m depth; the budgets for the other depths can be found in the supplementary information. This calculation illustrates that of all the measured processes, GPP and CR generally had the highest contribution to proton cycling intensity in 2012. CR always dominated the total proton production between 4.5 and 17.5 m and was usually a major contributing process above and below this interval. In the surface water GPP accounted for 34.8 – 99.2% of H$^+$ consumption, but deeper in the photic zone GPP still accounted for a significant part of the proton removal (2.7 – 30.3 % between 4.5 and 8 m depth). CO_2 air-sea exchange usually played a minor role in the surface-water proton cycling, apart from November when outgassing of CO_2 was high, and 56.6% of the total proton consumption in the surface water was due to this process. In March, CO_2 air-sea exchange contributed 14.2% to the budget, while in May and August, its influence was less than 6%. Nitrification accounted for 0.00 – 34.4% of the total proton production and was mostly a significant proton cycling process in November and in May below 17.5 m depth. The change in temperature from one day to the next contributed 0.2 – 30.7% to the proton cycling intensity and was generally a more important factor in the proton budget in March and November than in May and August. The effect of vertical mixing was even less pronounced, as it accounted for only 0.04 – 12.7% of the proton cycling intensity throughout the water column.

(previous page) **Figure 2.7** (a) pH$_T$ (at in situ temperature), and (b) acid-base buffering capacity β at 1 and 25 m depth; (c) Stoichiometric coefficient for the proton $\nu_{H^+}^x$, (d) process rate (µmol kg^{-1} d^{-1}), and (e) $\frac{d[H^+]_x}{dt}$ (µmol kg^{-1} d^{-1}) for gross primary production (GPP; at 1 m depth) and community respiration (CR; at 1 and 25 m depth) at Den Osse in 2012.

With the exception of March, the net result of the TA and DIC fluxes from the sediment was the dominant contributor to the total H⁺ production in the bottom layer (62.3 – 99.4%). Higher up in the basin, its contribution ranged from 2.6 to 49.2%. In March, the net result of the sediment flux at S1 was a contribution of 24.0% to the total proton consumption, while at S2 and S3 its effect on the budget was less than 10%. During all months and at all depths, the absolute value of $\frac{d[H^+]_{CR}}{dt}$ was larger than that of $\frac{\Delta[H^+]_{obs}}{\Delta t}$. This was also usually the case for $\frac{d[H^+]_{GPP}}{dt}$, $\frac{d[H^+]_{exch}}{dt}$ and $\frac{d[H^+]_{sed}}{dt}$, and in March and November for $\frac{d[H^+]_{nitr}}{dt}$ and $\frac{d[H^+]_{temp}}{dt}$, at the depths where these processes took place. Thus, as was the case for another coastal system (Hofmann et al., 2009), the final change in [H⁺] resulting from all proton-producing and -consuming processes was much smaller than the change in [H⁺] induced by each of the separate processes.

The sum of $\frac{d[H^+]_x}{dt}$ of all measured processes ($\frac{d[H^+]_{tot}}{dt}$; Eq. (9)) was 1-2 orders of magnitude higher than $\frac{\Delta[H^+]_{obs}}{\Delta t}$. As a result, the budget closure term dominated the proton cycling intensity, with the exception of the surface water in March and November. Its contribution ranged from 34.8 to 100% of the total H⁺ production or consumption, the latter depending on the sign of the budget closure term. The dominance of the closure term highlights the uncertainties underlying the current proton cycling budget. These uncertainties arise from spatial and temporal variability, measurement error and incomplete coverage of all processes affecting proton cycling. Taking the sediment fluxes (Fig. 2.6b) as an example, we see that the standard deviation of both the TA and DIC fluxes, which mostly results from small-scale spatial variability, ranges up to ~100% of the measured flux. This imposes a large uncertainty on the corresponding proton flux, which may severely impact the bottom-water proton budget. Similarly, by using an empirical nitrification rate expression based on
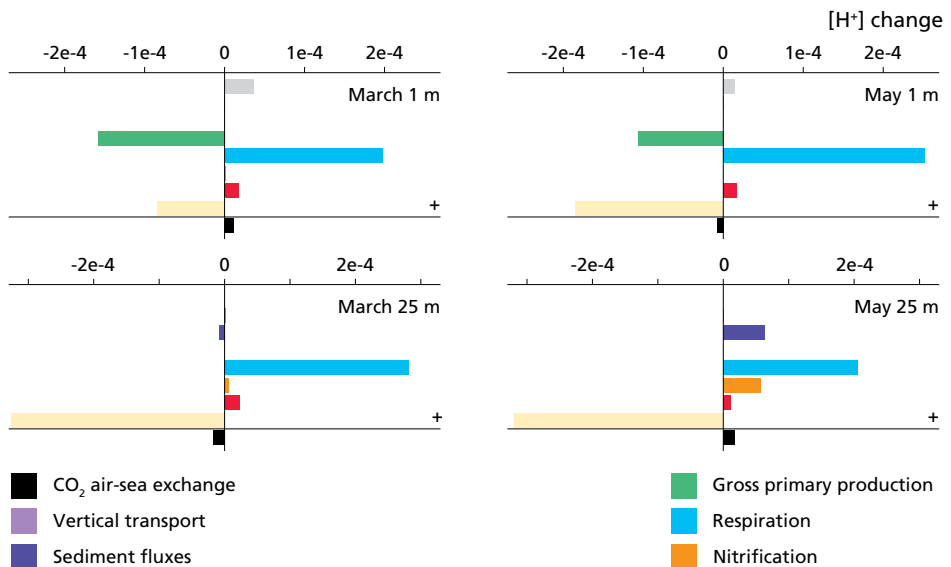

Figure 2.8 Proton budget for the Den Osse basin at 1 and 25 m depth for the months of March, May, August change in [H⁺].

[NH$_4^+$] and [O$_2$], we ignore temporal variability caused by, for example, changes in the microbial community. As the nitrification rate, like the other process rates, linearly correlates with the amount of protons produced, changes therein may especially impact the proton budget in November.

Since $\frac{d[H^+]_{tot}}{dt}$ was mostly positive, the processes making up the closure term generally had to decrease [H$^+$], i.e. remove protons from the basin. Taking account of both its order of magnitude and direction of change, we calculated that lateral transport may have accounted for the budget closure term. The average inflow in Lake Grevelingen through the seaward sluice in 2012 was 221 m^3 s^{-1} and took place for 9.9 h per day (calculated based on sluice water levels measured at 10-minute intervals; P. Lievense, personal communication, 2013). Meijers and Groot (2007) showed that 30.2% of the water entering Lake Grevelingen through the sluice remains in the lake for a longer period of time and is not directly transported back during the consecutive period of outflow. This means that, per day, 24·10^5 m^3 of North Sea water enters Lake Grevelingen. Assuming that all of this water eventually reaches the Den Osse basin and taking account of the total volume of this basin (655·10^5 m^3), this means that the inflow of the seaward sluice can fully replenish the Den Osse basin in 30 days. The average density of the water in the basin in 2012 was 1023.7 kg m^{-3}. If we assume that the pH of the inflowing water was 8.2, or [H$^+$] was 6.31·10^{-3} µmol kg^{-1}, then the proton flux entering the Den Osse basin was 1.55·10^7 µmol d^{-1}. Dividing this by the total volume of the Den Osse basin, which may be a valid assumption if stratification is absent, and correcting for density led to a proton flux of 2.11·10^{-4} µmol kg^{-1} d^{-1} into the entire basin. This is in the same order of magnitude as the closure term, which, for example, for the surface water in May was -1.85·10^{-4} µmol kg^{-1} d^{-1}. Note, however, that the net proton flux will be smaller as protons are also leaving

(µmol kg^{-1} d^{-1})

Temperature change

Closure term (lateral transport)

Net [H$^+$] change
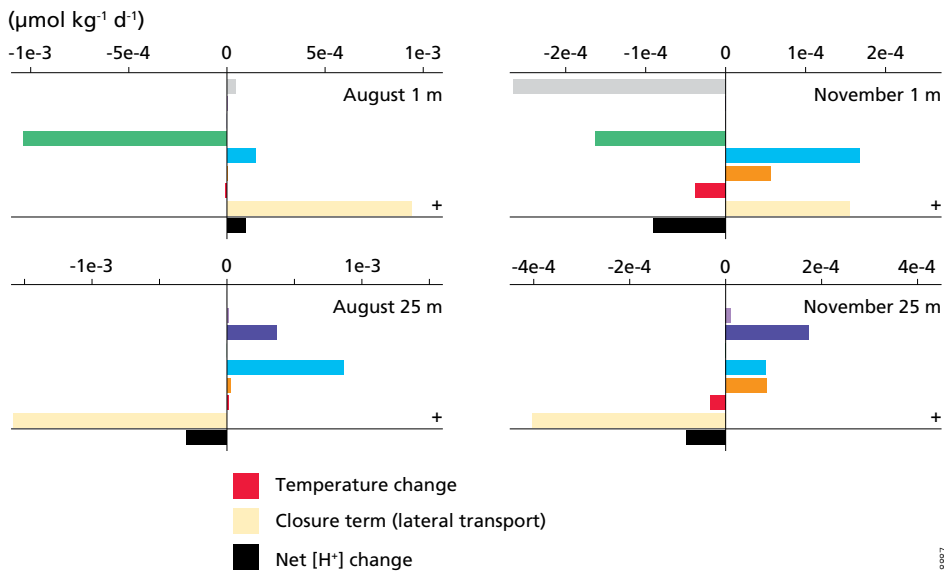
and November. The closure term is calculated as the difference between the calculated and measured net

the basin with outflowing water. Additionally, on both the seaward and landward sides, Den Osse is surrounded by shallower waters, which are supposed to have a pH similar to that of the surface water at Den Osse. Depending on the depths at which water is entering and leaving the Den Osse basin, most likely more protons will be removed from the basin than it will receive from the adjacent water during horizontal water exchange, thus leading to a negative $\frac{d[H^+]_{closure}}{dt}$. This is in line with the negative sign of the budget closure term for most months.

Over the course of the year, proton turnover time (τ_{H^+}) varied substantially. In March (32.8 days) and November (35.9 days), the linearly interpolated and depth-averaged τ_{H^+} in the basin was much higher than in May (17.7 days) and August (14.4 days). For each month, different driving factors explain these patterns. The proton turnover time is linearly correlated with both ambient [H$^+$] and β, and inversely correlated to the process rates. The high average value of τ_{H^+} in March is mostly explained by a high buffering capacity in combination with low biogeochemical activity. The decrease in May resulted from a significant increase in biogeochemical and physical process rates, since both the average [H$^+$] and β were higher compared to March. In August, on the contrary, average β decreased a factor of 2.6 while average [H$^+$] increased a factor of 2.7, thereby almost cancelling out each other's effect on τ_{H^+}. The higher turnover time in November, finally, was mostly driven by low process rates in combination with a relatively high average [H$^+$]. To summarise, the proton turnover time in the Den Osse basin is a complex combination of variability in process rates and buffering capacity, but also depends on the ambient pH.

When the proton turnover time is divided by β, one calculates the gross proton turnover time, i.e. the turnover time without buffering (Hofmann et al., 2010a). Given that the average β in the Den Osse basin is ~30000 and τ_{H^+} varies between 14.4 and 35.9 days in the 4 months studied, the gross proton turnover time is in the order of minutes. This demonstrates that buffering reactions in active natural systems are extremely important in modulating the net change in [H$^+$], and again highlights the fact that pH dynamics in these settings cannot be studied by measuring process rates alone.

2.5 Conclusions

The Den Osse basin experiences temperature-induced seasonal stratification that, combined with high oxygen consumption, results in the development of hypoxic bottom water with higher DIC and pCO$_2$ and lower pH$_T$. The strong correlation between pH$_T$ and pCO$_2$ in 2012 and their moderate correlations with O$_2$ suggest a link between GPP, CR and pH$_T$, which was further investigated in a detailed proton study. Volumetric GPP showed a major peak in July, while CR was highest in late spring. Although atmospheric CO$_2$ was taken up for most of the year, the relatively strong outgassing after the termination of stratification resulted in the Den Osse basin being only a weak sink for CO$_2$. Sediment DIC fluxes were highest at the deepest point of the basin and were generally higher than TA fluxes.

The calculated proton budgets clearly show that it is the combination of changes in process rates and changes in buffering capacity that determines the net proton change of the system. Which of

these two dominates depends on the season, depth and the process considered. However, it appears that variations in the process rates control the general pattern of proton cycling, while the buffering capacity dampens its signal with varying intensity. In 2012, this became especially apparent during the period of summer hypoxia, when the decrease in buffering capacity with depth led to a much shorter proton turnover time at depth compared with the surface. Of the process rates considered, the balance between primary production and respiration had the biggest impact on proton cycling. The influence of CO_2 air-sea exchange was most apparent during outgassing in autumn, while sedimentary TA and DIC fluxes impinged the proton balance in the deepest part of the basin. While the effect of vertical mixing on the proton balance was mostly negligible, horizontal exchange appeared to exert a major control on the proton budget of the basin.

This work highlights that process rates, buffering capacity and ambient pH are all essential compartments when determining the vulnerability of a system to changes in pH. By constructing one of the first proton budgets originating from in situ measurements, this study shows the associated uncertainties and challenges for future studies.

Appendix 2.A: Overdetermination of carbonate system

2.A1   Contribution of particles and organic alkalinity to TA

In oceanic research, samples for the determination of TA are typically not filtered before measurements (e.g. Dickson et al., 2007). In an open ocean setting concentrations of suspended matter are usually low and its effect on TA may therefore be neglected. However, in highly productive regions, such as coastal regions, high concentrations of particulate organic matter and calcium carbonate ($CaCO_3$) particles are often found. In an incubation experiment, Kim et al. (2006) showed that the titration of surface sites on phytoplankton and bacterial cells can add significantly to the measured TA. By filtering seawater upon collection, particulates are removed and the contribution of particulate organic matter (POM) and $CaCO_3$ particles to TA can be ignored.

We assessed the contribution of suspended particulate matter (SPM) to TA by calculating the difference between TA measured on unfiltered and filtered (0.45 μm) seawater. This difference ΔTA, which could indicate the contribution of SPM to TA, is not significantly different from zero (t = 0.1281, df = 190, P = 0.898; two-sided Student's t-test calculated using the package *Stats* in R), nor does it not show a clear pattern with TA (Fig. 2.A1; blue triangles), pH_T or SPM (results not shown). Additionally, the outliers in this data set could not unequivocally be correlated to events such as the phytoplankton bloom in July or high CR in May.

Additionally, dissolved organic matter (DOM) may contribute to TA, as DOM is composed of several compounds that have acid-base groups attached to them. The bulk of terrestrial-derived DOM consists of humic and fulvic acids and their contribution to estuarine TA and acid-base properties were described by Cai et al. (1998). In general, the contribution of DOM-associated acid-base groups to TA can be assessed using a chemical model set up by Oliver et al. (1983), which

was calibrated for natural waters by Driscoll et al. (1989). However, the calibration performed by these authors was done on freshwater lakes with maximum pH < 7.5. Thus, their parameterisation might not be directly applicable to saline waters including Lake Grevelingen, where most DOM is derived from phytoplankton. Both in incubation experiments (Hernández-Ayon et al., 2007; Kim and Lee, 2009; Koeve and Oschlies, 2012) and in biologically active natural waters (Hernández-Ayon et al., 2007; Muller and Bleie, 2008) it has been shown that DOM resulting from phytoplankton may contribute significantly to seawater TA. The contribution of DOM to TA relies on two factors: the density of acid-base functional groups within the organic matter compounds and their associated pK_a values. Both of these factors depend on DOM quality and source material, and neither of them is well known for marine DOM. To highlight this complexity, the increase in TA per unit increase of DOM in phytoplankton culture experiments appears to be species-specific (Kim and Lee, 2009).

In theory, one would expect that TA calculated from DIC (and total concentrations of borate, ammonia, phosphate and other inorganic species contributing to TA) represents the inorganic, aqueous fraction of TA. When TA is measured directly using a filtered seawater sample, one implicitly includes TA derived from dissolved organic acids and bases. We evaluated the contribution of DOM to the total alkalinity by: 1) comparing TA calculated from pH and DIC with TA determined from filtered (0.45 μm) seawater; and 2) applying the formulation of Driscoll et al. (1989) using concentrations of DOC.
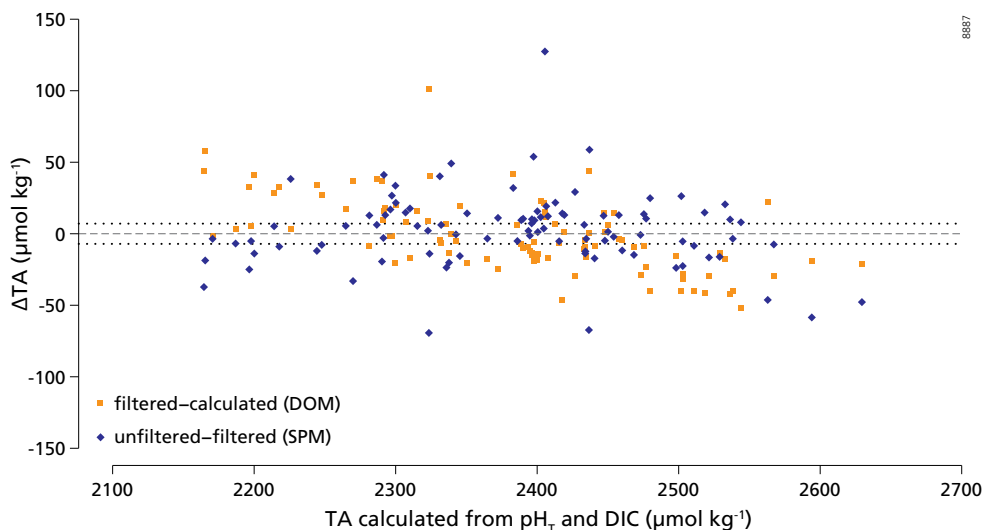
Figure 2.A1 Differences in total alkalinity (ΔTA; μmol kg^{-1}) measured on unfiltered and filtered (0.45 μm) samples (blue triangles; representing the effect of particles) and between TA measured on filtered seawater and TA calculated from DIC and pH_T (red squares; representing potential organic alkalinity), plotted as a function of TA calculated from DIC and pH_T. The dotted lines indicate the typical standard deviation of the difference between two measurements.

A two-sided Student's t-test revealed that there was no significant difference between TA measured on filtered samples and TA calculated from DIC and pH_T (t = -0.044, df = 187, P = 0.965). However, Fig. 2.A1 shows that, in general, the difference between TA measured on filtered samples and TA calculated from DIC and pH (red squares) is positive in the lower range of TA values. A positive difference might indicate that DOM-associated acid-base groups increase TA. On the contrary, a negative difference was found in the higher range of TA values, indicating that DOM-associated groups decrease the acid neutralisation capacity of the water. When these data were plotted as a function of pH_T or DOC, no pattern was observed (results not shown). Similar to the difference between TA measured on unfiltered and filtered seawater, we found no correlation between the outliers in this data set and biogeochemical process rates.

The contribution of organic alkalinity to TA as calculated with the model calibrated by Driscoll et al. (1989) did not show any systematic variability and ranged between 16 and 32 μmol kg^{-1}, with DOC ranging between 119 and 237 μmol kg^{-1} (see supplementary information). Its pattern did not resemble the difference between TA measured from filtered samples and calculated TA, indicating that the model could not explain the current results. In the range of pH values observed at Den Osse, the operational pK value derived from the Driscoll et al. (1989) model, which is an average representative of various DOM-associated acid-base groups, ranged between 5.91 and 6.06, indicating that the majority of these groups were present in their basic form. However, this operational pK value is significantly lower than the pK_a of organic acids associated with phytoplankton, which was found to be above 7 (Hernández-Ayon et al., 2007), indicating that the fraction of organic acid-base groups present in their basic form may be smaller. This would thus decrease the calculated contribution of DOC to TA. Additionally, the fraction of DOC that is releasing bases during phytoplankton blooms is unknown but may be higher than the 14% calibrated by Driscoll et al. (1989), which would mean that their model underestimates organic alkalinity in coastal systems.

2.A2   Comparison of measured and calculated pCO_2 values

During this study, we measured four parameters of the carbonate system (DIC, TA, pCO_2, pH_T), while, theoretically, only two parameters are necessary for a full determination. Which two parameters can best be measured to describe the carbonate system is subject of an ongoing debate. Dickson et al. (2007) suggest that, if possible, it is always better to measure a parameter rather than calculate it from other parameters, since there are limitations to the accuracy of the carbonate system prediction when certain combinations of parameters are used. For instance, in a compilation of incubation studies it was found that calculating pCO_2 from DIC and TA tends to underestimate pCO_2 at high levels (i.e. ~1000 ppmv) by up to 30%, for, as yet, unknown reasons (Hoppe et al., 2012).

In 2012, pCO_2 calculated from DIC and pH_T ranged between 189 and 1407 ppmv in the Den Osse basin. To check whether this natural system also showed internal inconsistencies, and to further highlight the complexity of an overdetermined system, we compared pCO_2 values calculated with different combinations of TA, DIC and pH_T with measured pCO_2 values (Fig. 2.A2). For each combination of parameters, we assessed their agreement with measured pCO_2 by calculating the

sum of squared differences. This calculation showed that using pH_T and DIC provides the best agreement between measured and calculated pCO_2. The highest sum of squares was found when using DIC with either filtered or unfiltered TA, which is another indication of the uncertainties introduced when using this combination of carbonate system parameters in non-open-ocean settings. Another feature in Fig. 2.A2 is that calculated pCO_2 values are generally lower than measured values, as indicated by a positive ΔpCO_2. Only in the higher range of measured pCO_2 (> ca. 1000 ppmv) and when TA is used as a starting parameter is the calculated pCO_2 mostly higher than the measured pCO_2. A closer look at these data reveals that all samples below the pycnocline in August show higher calculated than measured pCO_2 when DIC and either of the TA measurements are used as the parameter combination. These differences range between 3 and 299 ppmv (0 – 21.4%) and are generally higher when unfiltered TA samples are used. Furthermore, the two points where TA calculated from pH and DIC is highest (2593 and 2629 µmol kg^{-1}; Fig. 2.A1), which are the samples taken at 25 and 32 m depth in July, also show a higher calculated than measured pCO_2 when DIC and unfiltered TA are used as parameter combination (differences of 185 and 169 ppmv or 20.6 and 17.6%, respectively).
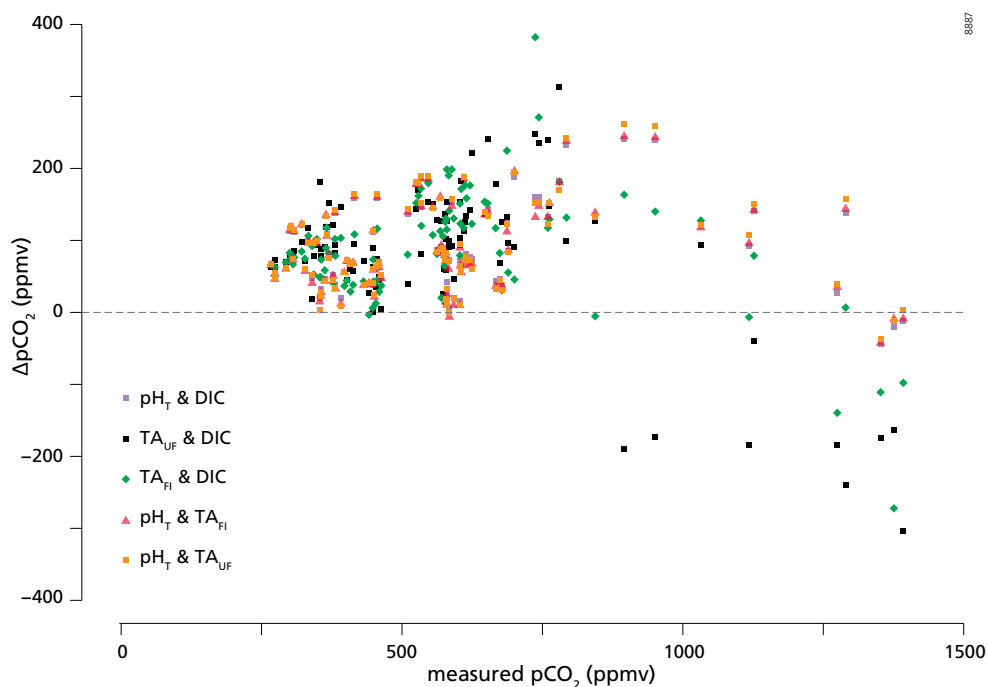
Figure 2.A2 Differences in partial pressure of CO_2 (ΔpCO_2; ppmv) measured by the headspace technique using gas chromatography and calculated using a suite of parameter combinations (pH_T and DIC, TA and DIC, pH_T and TA). TA_{Fl} and TA_{UF} indicate TA measured on filtered and unfiltered samples, respectively.

2.A3   Concluding remarks

To summarise, these results suggest that, especially in hypoxic natural waters, TA cannot unequivocally be chosen as one of the two parameters necessary to quantify the carbonate system. Additionally, the Den Osse data set cannot be used to draw any clear conclusions on the effect of DOM and SPM on TA. This conclusion supports our choice of using pH_T and DIC for the carbonate system calculations.

Acknowledgements

Figure 2.S1 Proton budget for the Den Osse basin at 3, 6, 10, 15, 20 and 32 m depth for the months of and measured net change in [H⁺]

(μmol kg^{-1} d^{-1})

Temperature change
Closure term (lateral transport)
Net [H$^+$] change

8887

March, May, August and November. The closure term is calculated as the difference between the calculated

Table 2.S1 Measurements during the 2012 Den Osse sampling campaign. Wind speed refers to the Meteorological Institute. The time of sampling is approximate within 15 minutes. For the other variables,
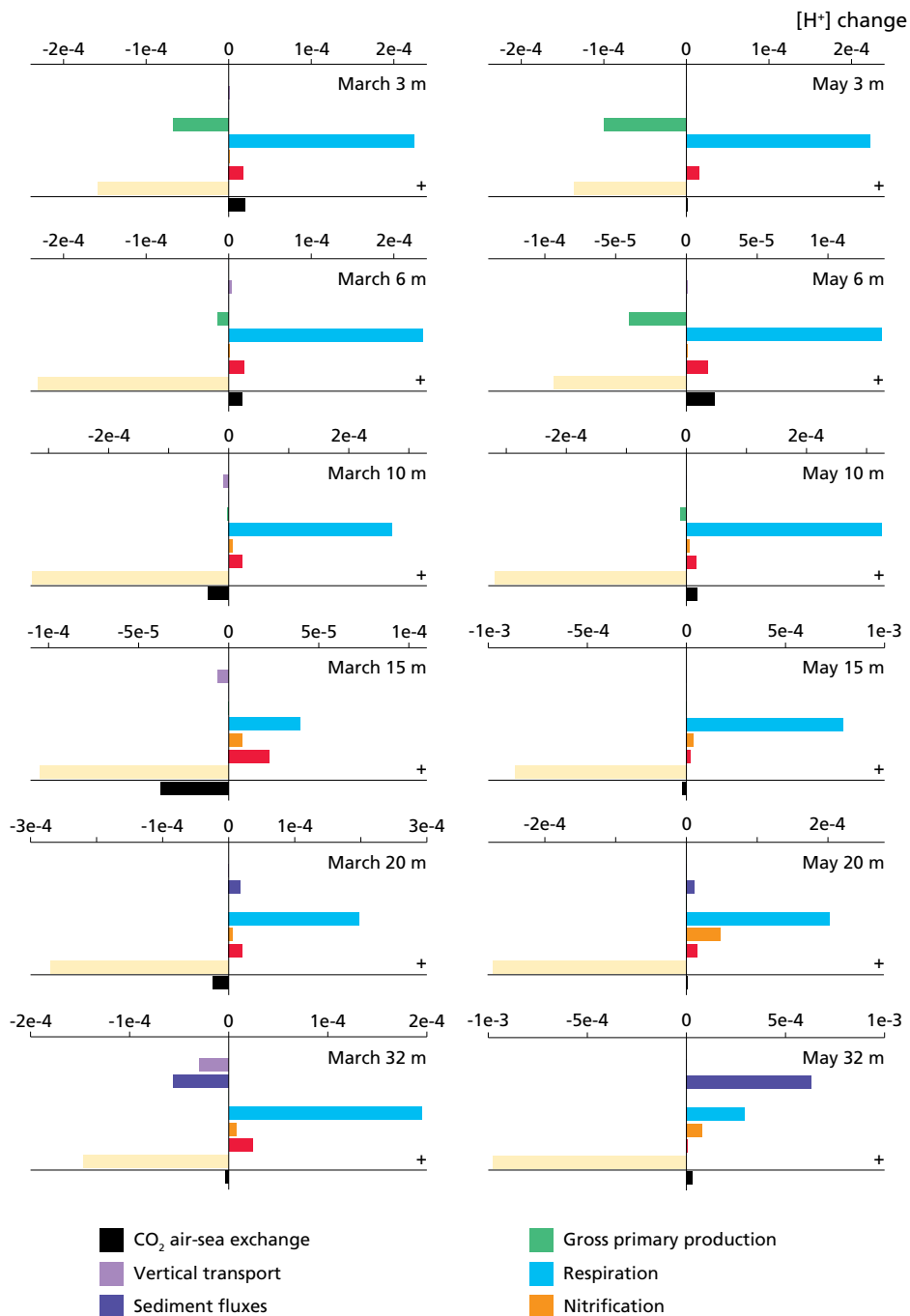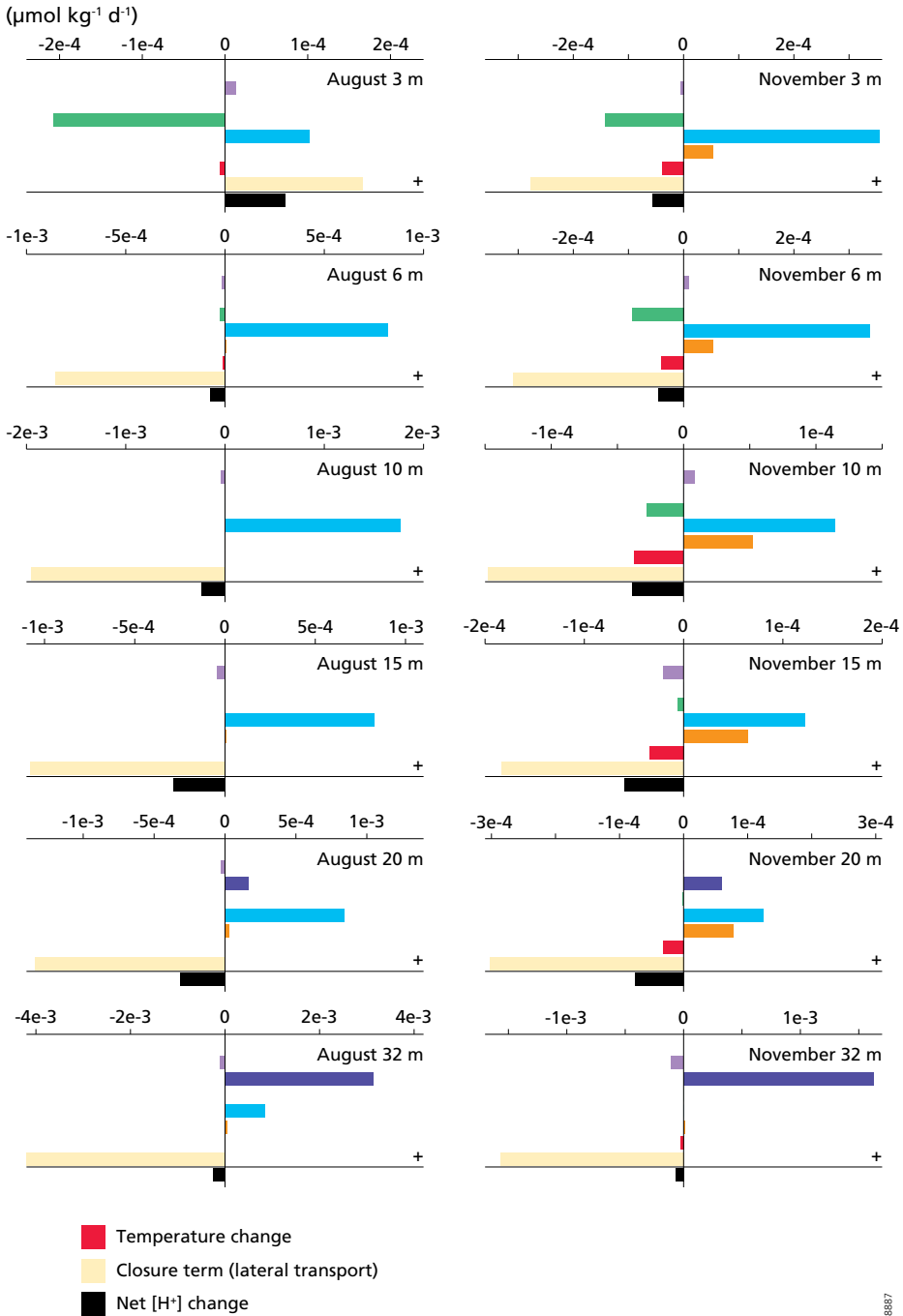
Date (dd-mm-yyyy)	Time of sampling (hh:mm, UTC+1)	Wind speed (m s^{-1})	Depth (m)	Temperature (°C)	Salinity (-)	Density anomaly (kg m^{-3})	Chl a (µg L^{-1})	O$_2$ (µmol L^{-1})
23–01–2012	12:25	5.6	1	5.36	30.01	23.58	-1.44	318.45
23–01–2012	12:12		3	5.36	30.00	23.58	-1.38	316.26
23–01–2012	12:00		6	5.42	30.05	23.63	-1.38	316.26
23–01–2012	11:47		10	5.40	30.04	23.64	-1.76	314.70
23–01–2012	11:30		15	5.56	30.14	23.72	-1.57	310.32
23–01–2012	11:15		20	5.86	30.45	23.95	-1.77	300.32
23–01–2012	11:00		25	6.11	30.85	24.26	-2.18	287.20
23–01–2012	10:50		32	6.46	31.37	24.66	-1.61	247.82
21–02–2012	09:20	6.1	1	1.99	30.43	24.20	2.01	355.95
21–02–2012	09:29		3	1.99	30.43	24.21	1.91	358.45
21–02–2012	09:37		6	1.98	30.43	24.23	2.84	357.20
21–02–2012	09:48		10	1.97	30.43	24.25	2.40	358.45
21–02–2012	09:59		15	1.93	30.49	24.32	1.92	356.26
21–02–2012	10:10		20	1.94	30.52	24.37	1.92	347.51
21–02–2012	10:21		25	1.29	31.10	24.90	1.11	343.45
21–02–2012	10:38		32	1.47	31.27	25.06	1.12	300.64
12–03–2012	09:15	2.8	1	7.18	30.08	23.42	5.23	365.95
12–03–2012	09:40		3	7.08	30.10	23.46	5.56	361.89
12–03–2012	09:50		6	6.31	30.80	24.12	5.85	351.26
12–03–2012	10:00		10	5.61	31.92	25.10	4.04	320.32
12–03–2012	10:15		15	5.36	32.07	25.27	2.46	315.01
12–03–2012	10:30		20	5.41	32.16	25.36	2.16	313.76
12–03–2012	10:45		25	5.42	32.22	25.42	2.44	310.95
12–03–2012	11:00		32	5.46	32.21	25.45	2.73	309.07
23–04–2012	08:40	6.4	1	9.78	30.57	23.43	3.79	296.26
23–04–2012	08:55		3	9.76	30.57	23.44	4.70	296.57
23–04–2012	09:05		6	9.55	30.59	23.50	5.09	296.26
23–04–2012	09:17		10	8.60	31.37	24.27	2.99	279.70
23–04–2012	09:27		15	8.30	31.45	24.40	2.68	264.70
23–04–2012	09:35		20	8.08	31.47	24.47	1.44	260.32
23–04–2012	09:45		25	8.04	31.47	24.50	1.74	249.07
23–04–2012	09:57		32	8.30	31.54	24.55	2.20	239.07

daily-averaged wind speed at 10 m above the surface, which was obtained from the Royal Netherlands see the chapter.

DIC (μmol kg^{-1})	pH$_T$ (in situ)	TA$_{FI}$ (μmol kg^{-1})	TA$_{UF}$ (μmol kg^{-1})	pCO$_2$ (ppmv)	DOC (μmol L^{-1})	NH$_4^+$ (μmol L^{-1})	NO$_3^-$ (μmol L^{-1})	Si(OH)$_4$ (μmol L^{-1})	PO$_4^{3-}$ (μmol L^{-1})
2246	8.077	2382	2390	452	180.66	8.89	30.08	18.94	0.84
2257	8.041	2392	2386	454	179.28	8.87	29.93	18.95	0.83
2258	8.058	2383	2381	451	176.56	8.80	29.87	18.94	0.82
2250	8.076	2385	2386	461	164.63	8.77	29.94	19.45	0.86
2253	8.074	2379	2388	457	166.30	8.81	30.24	19.95	0.90
2250	8.069	2383	2389	463	162.61	8.87	30.29	19.96	0.88
2259	8.065	2391	2402	444	149.69	9.92	29.19	21.70	1.02
2306	8.060	2455	2443	466	147.67	13.42	23.18	22.43	1.12
2266	8.195	2437	2495	373	164.30	3.64	32.05	9.41	0.52
2259	8.157	2419	2440	366	156.94	3.58	31.10	9.42	0.51
2254	8.146	2426	2436	359	155.78	3.47	30.96	9.32	0.48
2261	8.134	2421	2547	357	171.20	3.51	30.94	9.33	0.49
2260	8.139	2418	2437	359	162.55	3.44	30.91	9.36	0.49
2264	8.121	2426	2429	385	155.99	4.17	31.70	11.25	0.70
2260	8.086	2425	2456	394	141.80	4.57	32.85	12.90	0.75
2297	8.069	2420	2433	435	134.13	7.82	33.00	17.20	0.95
2190	8.295	2461	2473	277	170.21	0.76	20.61	0.00	0.02
2196	8.306	2454	2466	277	170.21	0.71	20.68	0.00	0.03
2205	8.285	2457	2457	296	166.62	0.91	21.91	0.21	0.03
2219	8.142	2391	2444	381	132.78	2.51	27.26	5.26	0.33
2220	8.121	2380	2390	401	121.00	3.10	27.66	5.90	0.46
2223	8.135	2386	2387	405	118.91	2.81	27.70	6.14	0.47
2228	8.122	2382	2396	411	119.36	2.97	27.94	6.53	0.48
2226	8.117	2381	2391	416	118.62	3.19	28.15	6.92	0.49
2208	8.351	2495	2504	311	160.83	0.66	7.06	2.36	0.00
2202	8.371	2492	2499	306	152.92	0.68	7.15	2.35	0.00
2200	8.369	2499	2494	303	167.29	0.54	7.07	2.38	0.00
2206	8.340	2477	2491	325	143.52	2.80	11.36	3.10	0.05
2222	8.284	2462	2487	368	130.90	5.52	14.89	4.12	0.18
2234	8.267	2471	2465	384	124.42	6.99	15.53	5.14	0.18
2252	8.248	2471	2462	419	140.02	9.14	16.83	6.67	0.31
2271	8.192	2475	2451	459	126.76	10.61	17.39	8.19	0.44

Table 2.S1 (continued)

Date (dd-mm-yyyy)	Time of sampling (hh:mm, UTC+1)	Wind speed (m s^{-1})	Depth (m)	Temperature (°C)	Salinity (-)	Density anomaly (kg m^{-3})	Chl a (µg L^{-1})	O$_2$ (µmol L^{-1})
30–05–2012	08:55	2.3	1	19.10	30.20	21.23	2.45	274.39
30–05–2012	09:05		3	18.65	30.20	21.35	5.95	280.01
30–05–2012	09:19		6	17.81	30.22	21.59	13.90	293.45
30–05–2012	09:31		10	16.05	30.28	22.05	19.03	273.45
30–05–2012	09:44		15	12.28	30.63	23.10	5.36	189.69
30–05–2012	09:56		20	10.07	31.50	24.18	2.31	171.57
30–05–2012	10:11		25	9.90	31.55	24.27	1.08	165.63
30–05–2012	10:25		32	9.79	31.56	24.34	1.26	153.13
25–06–2012	08:25	4.2	1	16.97	30.16	21.71	6.30	236.57
25–06–2012	08:35		3	16.87	30.17	21.75	8.62	235.32
25–06–2012	08:50		6	16.85	30.38	21.93	8.83	235.01
25–06–2012	09:00		10	16.50	30.86	22.39	7.29	231.26
25–06–2012	09:15		15	15.57	31.21	22.89	2.10	187.19
25–06–2012	09:28		20	12.61	31.29	23.58	1.28	110.63
25–06–2012	09:40		25	11.18	31.36	23.91	1.16	82.50
25–06–2012	09:57		32	10.55	31.43	24.11	1.20	72.50
24–07–2012	08:55	2.3	1	20.01	30.36	21.13	27.33	361.58
24–07–2012	09:10		3	18.90	30.41	21.46	10.93	332.51
24–07–2012	09:18		6	18.98	30.70	21.66	10.68	292.51
24–07–2012	09:25		10	18.21	31.49	22.47	4.58	197.51
24–07–2012	09:35		15	17.40	32.09	23.15	4.72	149.38
24–07–2012	09:47		20	16.53	32.34	23.56	2.07	96.88
24–07–2012	10:05		25	15.79	32.24	23.67	1.41	74.07
24–07–2012	10:20		32	15.13	32.15	23.78	1.60	40.63
20–08–2012	08:50	3.4	1	21.03	30.74	21.15	12.86	294.07
20–08–2012	09:10		3	20.95	30.73	21.17	12.48	245.95
20–08–2012	09:15		6	20.44	31.54	21.93	6.82	139.69
20–08–2012	09:25		10	19.63	32.19	22.65	3.13	64.06
20–08–2012	09:47		15	18.77	32.38	23.03	2.32	39.06
20–08–2012	10:00		20	17.64	32.36	23.31	1.13	16.25
20–08–2012	10:20		25	17.19	32.31	23.41	0.85	5.31
20–08–2012	10:45		32	16.81	32.24	23.47	1.02	3.44

DIC ($\mu mol\ kg^{-1}$)	pH_T (in situ)	TA_{FI} ($\mu mol\ kg^{-1}$)	TA_{UF} ($\mu mol\ kg^{-1}$)	pCO_2 (ppmv)	DOC ($\mu mol\ L^{-1}$)	NH_4^+ ($\mu mol\ L^{-1}$)	NO_3^- ($\mu mol\ L^{-1}$)	$Si(OH)_4$ ($\mu mol\ L^{-1}$)	PO_4^{3-} ($\mu mol\ L^{-1}$)
2126	8.195	2481	2412	343	218.16	0.00	0.08	0.03	0.18
2125	8.230	2468	2465	330	236.88	0.00	0.10	0.00	0.14
2119	8.281	2467	2480	309	191.90	0.37	2.00	0.14	0.12
2154	8.260	2440	2464	346	163.91	2.51	4.83	0.61	0.13
2298	8.115	2492	2475	513	138.33	12.43	11.36	10.38	0.68
2327	8.098	2516	2499	538	139.11	17.31	11.60	15.44	0.92
2340	8.078	2515	2535	558	146.38	19.69	11.44	17.22	1.00
2377	8.059	2585	2538	592	141.73	26.51	10.61	24.20	1.67
2176	8.132	2425	2412	537	201.07	1.15	0.91	5.66	0.83
2177	8.132	2418	2414	529	195.95	1.05	0.64	5.64	0.84
2178	8.128	2423	2428	532	195.14	1.12	0.65	5.71	0.84
2187	8.118	2430	2415	550	190.14	1.54	0.72	6.00	0.84
2255	8.059	2444	2442	613	169.90	7.86	1.62	10.48	1.17
2404	7.967	2537	2529	796	147.12	22.80	4.55	25.66	2.59
2461	7.908	2575	2516	899	139.91	34.28	7.46	38.38	3.91
2509	7.879	2608	2560	954	137.57	40.04	8.30	45.22	4.51
1966	8.251	2315	2329	337	217.66	0.14	0.21	2.21	1.18
2007	8.221	2332	2333	369	216.70	0.19	0.00	2.77	1.11
2100	8.131	2348	2358	452	199.78	0.19	0.08	4.57	0.93
2218	7.981	2371	2385	703	170.00	1.76	2.87	12.18	1.42
2283	7.855	2397	2426	847	155.59	5.72	8.04	17.71	2.37
2343	7.760	2449	2443	1035	144.37	4.54	18.50	24.09	3.76
2376	7.730	2459	2444	1130	151.49	4.28	22.09	27.25	4.38
2428	7.672	2483	2458	1293	148.59	6.35	24.81	33.07	5.83
1813	8.279	2169	2165	270	230.33	0.17	0.07	4.33	1.70
1872	8.205	2190	2183	352	236.67	0.24	0.08	6.82	1.87
2109	7.897	2273	2284	692	186.00	0.89	0.08	13.44	1.95
2243	7.699	2324	2303	1121	159.12	0.21	0.10	19.29	2.36
2298	7.623	2347	2343	1278	154.64	0.38	0.07	22.06	3.11
2364	7.584	2409	2403	1355	153.18	2.48	10.55	28.39	4.94
2390	7.585	2432	2414	1396	153.25	4.31	11.58	31.35	5.55
2424	7.592	2453	2463	1379	163.40	11.46	1.70	38.37	6.82

Table 2.S1 (continued)

Date (dd-mm-yyyy)	Time of sampling (hh:mm, UTC+1)	Wind speed (m s^{-1})	Depth (m)	Temperature (°C)	Salinity (-)	Density anomaly (kg m^{-3})	Chl a (µg L^{-1})	O$_2$ (µmol L^{-1})
20–09–2012	08:15	3.7	1	16.41	31.57	22.91	7.10	224.35
20–09–2012	08:25		3	16.41	31.57	22.92	9.42	222.75
20–09–2012	08:40		6	16.87	31.98	23.14	4.56	214.70
20–09–2012	08:50		10	17.38	32.67	23.57	1.47	177.37
20–09–2012	09:00		15	17.14	32.67	23.65	2.78	181.87
20–09–2012	09:15		20	16.97	32.70	23.73	2.59	187.43
20–09–2012	09:30		25	16.93	32.73	23.79	2.69	191.24
20–09–2012	09:50		32	16.86	32.74	23.84	3.38	190.56
18–10–2012	08:29	2.8	1	12.10	30.92	23.30	2.99	260.01
18–10–2012	08:40		3	12.08	30.93	23.32	2.56	256.26
18–10–2012	08:55		6	12.76	31.79	23.87	1.46	238.76
18–10–2012	09:07		10	12.91	32.17	24.15	1.74	238.76
18–10–2012	09:15		15	12.78	32.19	24.21	2.05	232.82
18–10–2012	09:30		20	12.72	32.21	24.26	1.69	235.95
18–10–2012	09:45		25	12.67	32.22	24.30	1.75	238.45
18–10–2012	10:00		32	12.58	32.23	24.36	1.73	239.07
05–11–2012	08:55	3.8	1	10.04	31.21	23.88	1.71	275.37
05–11–2012	09:10		3	10.04	31.20	23.88	1.78	272.71
05–11–2012	09:22		6	10.05	31.20	23.90	1.94	266.70
05–11–2012	09:35		10	10.05	31.20	23.91	1.62	268.33
05–11–2012	09:50		15	10.09	31.22	23.94	1.82	245.76
05–11–2012	10:03		20	12.61	32.54	24.54	0.55	236.62
05–11–2012	10:18		25	12.73	32.64	24.62	0.93	232.13
05–11–2012	10:35		32	12.72	32.68	24.68	0.49	237.54
03–12–2012	09:28	5.2	1	6.75	31.33	24.45	1.94	289.59
03–12–2012	09:42		3	6.71	31.28	24.42	1.89	284.94
03–12–2012	09:57		6	6.97	31.19	24.34	1.42	279.36
03–12–2012	10:10		10	7.55	31.96	24.88	1.49	278.03
03–12–2012	10:23		15	7.94	32.21	25.04	1.55	276.36
03–12–2012	10:35		20	8.21	32.39	25.17	1.02	269.65
03–12–2012	10:48		25	8.34	32.44	25.21	1.23	266.69
03–12–2012	11:05		32	8.48	31.26	24.30	2.24	259.98

Acidification in a seasonally hypoxic coastal basin

DIC (μmol kg^{-1})	pH$_T$ (in situ)	TA$_{FI}$ (μmol kg^{-1})	TA$_{UF}$ (μmol kg^{-1})	pCO$_2$ (ppmv)	DOC (μmol L^{-1})	NH$_4^+$ (μmol L^{-1})	NO$_3^-$ (μmol L^{-1})	Si(OH)$_4$ (μmol L^{-1})	PO$_4^{3-}$ (μmol L^{-1})
2035	7.946	2203	2197	650	208.52	1.83	0.60	7.29	2.57
2059	7.949	2229	2266	655	190.52	2.45	0.67	7.90	2.48
2110	7.918	2307	2273	690	174.61	4.37	0.84	9.53	2.29
2172	7.896	2326	2331	766	152.44	8.65	0.88	13.86	1.95
2177	7.886	2327	2366	763	145.31	8.66	0.93	13.50	1.86
2160	7.911	2365	2350	747	149.64	8.52	0.99	13.12	1.79
2158	7.915	2425	2355	741	142.59	8.19	0.98	12.77	1.75
2179	7.904	2339	2387	783	149.37	8.52	0.98	12.82	1.77
2034	7.935	2208	2170	586	205.97	5.10	3.42	9.65	1.87
2042	7.915	2223	2203	583	198.49	5.16	3.51	9.13	1.78
2109	7.924	2279	2266	624	176.34	7.74	4.78	9.46	1.76
2109	7.932	2275	2266	618	170.16	7.20	4.61	9.21	1.75
2151	7.925	2308	2348	628	160.16	8.80	6.11	9.82	1.63
2146	7.935	2327	2307	616	215.76	8.39	6.37	9.84	1.56
2144	7.932	2325	2330	609	155.80	8.03	6.46	9.85	1.55
2148	7.937	2311	2323	607	149.04	8.07	6.46	9.78	1.54
2091	7.895	2229	2203	595	196.79	8.27	7.33	12.48	1.89
2096	7.891	2241	2226	587	195.82	7.58	6.67	12.88	1.65
2104	7.905	2243	2247	583	191.55	8.03	7.03	13.11	1.63
2106	7.911	2251	2241	582	189.81	8.10	7.12	13.29	1.64
2154	7.894	2282	2287	606	158.27	9.88	8.12	14.57	1.60
2172	7.875	2301	2297	677	147.97	10.10	8.52	14.97	1.48
2179	7.868	2295	2321	681	154.63	10.90	8.30	15.51	1.59
2178	7.879	2320	2341	670	140.10	10.36	8.56	15.04	1.51
2168	8.042	2293	2310	571	183.34	8.32	12.94	15.13	1.30
2177	7.980	2295	2311	566	174.36	8.23	13.06	15.16	1.30
2179	7.977	2280	2312	573	176.12	8.20	13.13	15.40	1.31
2194	7.963	2332	2336	580	147.39	7.67	15.87	17.22	1.31
2206	7.977	2343	2318	576	136.32	7.44	18.19	18.55	1.29
2212	7.971	2338	2336	579	135.16	7.71	17.76	18.42	1.31
2218	7.970	2330	2344	581	138.03	7.64	17.15	18.41	1.32
2215	7.961	2365	2348	606	138.77	8.73	16.28	19.06	1.32

Chapter 3:

Phytoplankton primary production in a coastal marine lake: a comparison of methods

"The sea is everything. It covers seven tenths of the terrestrial globe. Its breath is pure and healthy. It is an immense desert, where man is never lonely, for he feels life stirring on all sides."

Jules Verne

Abstract

Coastal zone primary production is of high importance for the global carbon cycle, but difficult to quantify due to spatial and temporal variation and differences in methodology. Here we compare three different methods of quantifying gross primary production (GPP) and discuss their differences in the context of phytoplankton group dynamics. We used the oxygen light-dark method, high-resolution oxygen sensor deployment and the assimilation of labelled carbon into particulate matter to measure GPP in a nutrient-rich dynamic coastal marine basin. Furthermore, we use labelling of phospholipid-derived fatty acids (PLFA) to identify the active fraction of the phytoplankton population and compare these results with algal biomass estimated with both pigments and PLFA composition.

Similar estimates of GPP were obtained with all three methods, with the in situ sensor deployment generating overall highest estimates of GPP. The in vitro GPP methods differed with higher carbon assimilation relative to oxygen production as GPP increases. GPP based on PLFA assimilation was significantly lower than using the oxygen light-dark method but showed the same unimodal seasonal pattern. GPP was high in both July and August, but biomass biomarkers showed a marked transition in species composition between these months, with dinoflagellates being dominant in July and Cryptophyceae and diatoms taking over in August. Group-specific growth rates revealed that while green algae had the fastest turnover, the contribution of dinoflagellates and the haptophyte *Phaeocystis globosa* to GPP was highest because of their higher biomass. Our results reveal that, despite the uncertainties and assumptions associated with each method, they are all suitable for determining GPP in the eutrophic coastal zone. However, their differences cannot unequivocally be linked to species dynamics.

CHAPTER 3

3.1 Introduction

About half of the global net primary production (NPP) is of oceanic origin (Field et al., 1998), highlighting the importance of the marine realm in the global carbon (C) cycle. Within the oceanic domain, the coastal zone is generally acknowledged as being among the most productive regions, comprising ca. 7% of the surface area but accounting for 14-30% of total oceanic primary production (PP; Gattuso et al., 1998). It is therefore essential to accurately quantify PP in the coastal zone, but this is challenging due to various reasons.

First, there is large natural variability in PP, both temporally and spatially. PP varies not only between different ecosystems, but also among similar ecosystems, and even within the same ecosystem at various locations (Cloern et al., 2014). Temporal variability in PP occurs on diurnal, seasonal and interannual time scales (e.g. Bates, 2001; Sarma et al., 2005). Both types of variability may result from many factors, including but not limited to temperature (Eppley, 1972), nutrient availability (Dugdale, 1967), grazing (Calbet, 2001), and light climate (Kirk, 1994), which, in turn, may be driven by physical forcing such as eddy formation (Mahadevan et al., 2012) and tidal forcing (Blauw et al., 2012).

Another source of uncertainty in PP may result from the different methods currently used for its quantification. Each of these methods has its advantages, limitations and difficulties (Robinson and Williams, 2005; Duarte et al., 2013b) and neither of them has been shown to unequivocally measure PP (Laws et al., 2000).

Aside from estimating PP based on proxies for biomass (e.g. satellite-derived measurements of chlorophyll *a* (Chl *a*; Behrenfeld et al., 2001)) and empirical relationships between biomass, light availability and PP (Cole and Cloern, 1987), methods for quantifying PP can be classified as either in vitro or in situ. In vitro or incubation methods are prone to bottle effects resulting from contamination during sampling (Williams and Robertson, 1989) and the containment of water samples. The latter may alter trophic interactions (Pomeroy et al., 1994), not in the least since zooplankton is partially absent in incubation bottles, and result in a change in the ratio between new and regenerated production (Collos et al., 1993). In addition, it can be challenging to undertake in vitro methods at the ambient temperature, which is a principal factor controlling microbial respiration rates (Rivkin and Legendre, 2001). Light climate may also be altered during in vitro determination of PP. For instance, incubation bottles made from borosilicate or plastic have been shown to filter out UV-B radiation and, as a result, significantly alter measured net community production (NCP) rates (Agustí et al., 2014). In situ or incubation-free methods rely on assumptions with respect to mixed layer dynamics and the exchange of gases with the atmosphere and surrounding waters (Luz and Barkan, 2000; Duarte et al., 2013b). Additionally, most in situ methods can only resolve time- and depth-integrated estimates of PP, whereby the integration depth typically equals mixed layer depth, and the investigation period is in the order of weeks (Robinson and Williams, 2005).

Besides this major difference, methods for quantifying PP also differ in their currency. Although in principle changes in every constituent consumed or produced during PP could be quantified to assess phytoplankton growth rates, in most studies the evolution of either C or oxygen (O_2) over time is tracked (Howarth and Michaels, 2000). During photosynthesis, inorganic C is converted to organic C in a chain of reactions, thereby utilising nutrients and producing O_2 (Falkowski and Raven, 2013). One could argue that the uptake of C represents actual phytoplankton growth, while the change in O_2 is rather the net result of several processes, including algal respiration and the possible conversion from oxidised to reduced nitrogen (N) species (Sarmiento and Gruber, 2006). Because of this difference, properly converting rates from O_2 to C units is of utmost importance but can be ambiguous. Conversion is normally done using the photosynthetic quotient (PQ), which is defined as the ratio of O_2 change versus incorporated CO_2 The value of PQ is, however, variable and depends not only on the N source that is used for growth, but also on the C:N ratio of phytoplankton and the type of organic compound produced (Williams et al., 1979; Sarmiento and Gruber, 2006).

Moreover, for certain methods the incubation time exerts a major control on what process is represented by the measurement (Falkowski and Raven, 2013, and references therein). Taking the ^{14}C assimilation method as example, it has been subject of debate for decades whether this method represents gross PP (GPP) or NPP (Underwood and Kromkamp, 1999). Consensus has, however, been reached that this depends on the ratio of photosynthesis to respiration and that the shorter the incubation period, the closer the estimate is to GPP (Weger et al., 1989; Williams and Lefevre, 1996; Marra, 2002).

Finally, uncertainty in PP estimates may be due to variations in experimental protocols and the upscaling procedures adopted. A recent data compilation of coastal ecosystems has shown that distinct protocols of the same method can provide up to 3-fold different estimates of annual phytoplankton primary production, depending on how incubation took place and rates were integrated over depth and time (Cloern et al., 2014).

The vast majority of in vitro PP measurements has been done with the ^{14}C method as originally described by Steemann Nielsen (1952). As a result, it is often seen as a benchmark against which other methods are compared. Its basic principle is that it quantifies the assimilation of ^{14}C-labeled dissolved inorganic carbon (DIC), which is added to the incubation bottle, into organic C. Aside from the uncertainty in process representation related to incubation time, additional ambiguity may arise form the fraction of the organic C pool that is measured. In most studies incubations are terminated by filtration, after which the particulate organic carbon (POC) pool is measured. However, it is also possible to measure total organic carbon (TOC) production and thus also quantify transfer of assimilated C to dissolved organic substances, which may comprise a substantial fraction of the total C assimilation (Karl et al., 1998; Van den Meersche et al., 2004).

The O_2 light-dark method, which is based on tracking the evolution in [O_2], has a long history of applications in natural waters (Gaarder and Gran, 1927; Riley, 1939). Dark bottles are used to quantify community respiration (CR), while bottles incubated in the light represent NCP. Their

sum is then used as a measure for GPP. One major assumption in using this method is that respiration in the dark is not different from that in the light. There is conflicting evidence related to the validity of this assumption (Harris and Lott, 1973; Grande et al., 1989).

One increasingly used method for measuring GPP in situ is high-resolution O_2 monitoring from buoys (Emerson et al., 2008) or gliders (Nicholson et al., 2008). Using this method, initiated by Odum (1956) and often referred to as the diel oxygen method, the observed O_2 signal is decomposed into individual signals induced by the various processes influencing O_2, including GPP. This method therefore requires an accurate estimation of physical processes such as air-sea O_2 gas exchange (Tobias et al., 2009) and may be challenging to apply in systems where many processes impact O_2 concurrently, e.g. where transport processes are complex (Swaney et al., 1999). In recent work, these issues have been addressed using various statistical modelling techniques (Hanson et al., 2008; Holtgrieve et al., 2010; Batt and Carpenter, 2012). Similar to the in vitro O_2 light-dark method, this in situ method assumes no difference between light and dark respiration.

Conversion between different methods measuring PP is not unambiguous, but may be aided by concomitantly measuring PP using at least two independent techniques (Marra, 2002). In coastal regions, comparison studies have been performed in a suite of ecosystems, such as an Arctic fjord (Tanaka et al., 2013), an oligotrophic coastal bay (González et al., 2008) and two temperate estuaries (Gazeau et al., 2005a, 2007a). Recently, Regaudie-de-Gioux et al. (2014) compiled concurrent open-ocean PP estimates and subsequently used these to construct conversion equations between some of the most commonly used techniques for estimating volumetric PP. These equations have, however, not been tested on or applied to coastal ecosystems.

In addition, it remains uncertain how species composition affects differences in PP based on various techniques. All methods discussed so far only quantify total PP, without providing information on the species involved. Various eukaryotic algae and cyanobacteria can concurrently contribute to PP, all having different intrinsic properties such as maximum specific growth rate (Zubkov, 2014), light tolerance levels (Harris and Lott, 1973) and nutrient acquisition efficiency (Sunda and Hardison, 2010). In addition, each species may have a different sensitivity to external threats such as grazing (Roberts et al., 2011), viral attacks (Brussaard, 2004) and interactions with other phytoplankton species (Barber and Hiscock, 2006). As a result of one or more of these factors, phytoplankton composition varies both spatially and temporally (Cloern et al., 2014).

Algal species can be identified and quantified using a variety of techniques, among which microscopy has traditionally been used. Microscopy is a precise but time-consuming technique and, for better comparisons in time and space, requires conversion to either carbon units (Menden-Deuer and Lessard, 2000) or biovolume (Hillebrand et al., 1999). Algal biomass can also be quantified by means of chlorophyll, carotenoid and biliprotein pigments, which are normally measured by high-performance liquid chromatography (HPLC; Roy, 1987). While Chl a is a generally abundant pigment often used as a proxy for total phytoplankton biomass, many pigments are class or even species-specific, making them very useful tools for determining phytoplankton community composition (Wright and Jeffrey, 2006) which is aided with computational composition

estimators (Mackey et al., 1996; Van den Meersche et al., 2008). Furthermore, species-specific biomass can be measured using phospholipid-derived fatty acids (PLFA), which are abundant in all algal species and bacteria. Phospholipids are the principal lipids in cell membranes and degrade rapidly after cell death (Boschker and Middelburg, 2002), indicating that PLFA represent viable organisms (Pinkart et al., 2002). PLFA characteristic of specific algal groups have been described previously (Reuss and Poulsen, 2002; Dijkman and Kromkamp, 2006). Similar to pigment data analysis, the composition of PLFA in a sample can be used in composition estimators to infer algal community composition, thereby including bacteria.

Total algal biomass, however, is not necessarily equal to the biomass of the active population and is thus not by definition proportional to GPP (Dijkman et al., 2009). Recently, the incorporation of ^{13}C into PLFA has been developed as a method for not only identifying active groups of algae (Shin et al., 2000), but also quantifying group-specific GPP (Dijkman et al., 2009). This is based on the premise that synthesis of polar lipids is closely linked to microorganism growth (Boschker and Middelburg, 2002). The use of ^{13}C for determining PP is not restricted by radionuclide legislation or health concerns, making it also an ideal tracer for in situ measurements in, e.g. mesocosms (de Kluijver et al., 2013).

Here we compare three different methods (O_2 light-dark method, assimilation of ^{14}C-labeling into POC, and diel oxygen method) to measure GPP in a nutrient-rich, dynamic coastal marine lake. Furthermore, we use ^{13}C-labeling of PLFA to identify the dynamics of phytoplankton growth and compare these results with algal biomass based on both pigment and PLFA concentrations. The aims of this study are to compare these three GPP methods, and to discuss their differences in the context of phytoplankton group dynamics.

3.2   Methods

3.2.1   Study site

Lake Grevelingen, a coastal marine basin (salinity 29-32), is located in the south-western delta area of the Netherlands and has an area and average depth of ~108 km^2 and 5.3 m, respectively (Nienhuis, 1978). Characteristic of the lake bathymetry is that several deep gullies intersect extensive shallow (i.e. < 5 m) areas. Within the main gully, various deep basins are present which are spatially separated by sills and extend down to max. 45 m depth. The hydrodynamics of the lake are dominated by regulated in- and outflow through a sluice on the seaward side. The main gully of Lake Grevelingen has been known to experience seasonal stratification and hypoxia for at least 35 years, which differ in extent and severity interannually (Wetsteyn, 2011). Previous studies have estimated a range of ~200 – 500 g C m^{-2} yr^{-1} for GPP in Lake Grevelingen, which, according to Nixon (1995), classifies it as a eutrophic system.

Monthly sampling campaigns on board the R/V *Luctor* were performed in 2012 to survey water-column chemistry and process rates. Samples were collected mid-morning at the deepest point of the Den Osse basin (51.747°N, 3.897°E), a 34-m deep basin located in the main gully of the lake.

Sills extending up to 10 and 20 m below the water level, respectively, confine the basin on both the landward and seaward side. For further details, see the extensive site description in Hagens et al. (2015). Depth profiles of temperature (T), salinity (S) and Chl *a* were recorded with a YSI6600 CTD probe. We obtained discrete water-column samples from eight different depths (1, 3, 6, 10, 15, 20, 25, and 32 m) using a 12 L Niskin bottle with gas-tight tubing. From the Niskin bottle, samples were drawn for the assessment of concentrations of pigments, dissolved organic carbon (DOC), POC and its isotopic composition ($\delta^{13}C_{POC}$), and DIC and its isotopic composition ($\delta^{13}C_{DIC}$). The dates and times of sampling, along with information on additionally measured parameters, can be found in the supplementary material of Hagens et al. (2015).

3.2.2 Discrete water sample handling

Water for the determination of DOC was collected in 10 mL glass vials, filtered over pre-combusted Whatman GF/F filters (0.7 μm) and stored at -20°C. Analysis took place on a Formacs Skalar-04 via automated UV-wet oxidation to CO_2, which concentration was subsequently determined using a non-dispersive infrared technique (Middelburg and Herman, 2007).

Samples for $\delta^{13}C_{DIC}$ analysis were collected in 30 mL glass serum bottles, which were allowed to overflow and promptly closed with a gas-tight rubber stopper and screw cap. Samples were poisoned with 60 μL of saturated mercuric chloride ($HgCl_2$) solution, which was injected through the rubber stopper into the sample using a glass syringe and needle. A second needle was inserted simultaneously through the rubber stopper to release the overpressure. The bottle was stored upside down at 4°C. For the analysis, 0.7 mL of sample was injected into He-flushed 10 mL scintillation vials containing 3 drops of 100% H_3PO_4 and vigorously shaken. Samples were analysed using continuous flow – isotope ratio mass spectrometry (CF-IRMS) on a Thermo Finnigan MAT 253 gas mass spectrometer coupled to a Thermo Electron Gas Bench II via a Thermo Electron Conflo IV split interface. For calibration towards the V-PDB scale 2 mM solutions of both in-house (Na_2CO_3) and international (LSVEC; Li_2CO_3) standards were used. Replicate measurements of the standards indicated that the reproducibility was ±0.1‰.

To determine POC and $\delta^{13}C_{POC}$, ca. 2500 mL water was filtered over pre-weighed, pre-combusted Whatman GF/F filters (0.7 μm), which were stored at -20°C. For the analysis, the filters were oven-dried overnight at 60°C and placed in a desiccator containing 37% HCl for at least 72 hours to remove the inorganic carbon fraction. POC was analysed using a Fisons NA-1500 NCS elemental analyser using dry combustion at 1030°C. Calibration occurred against atropine and acetanilide standards, showing that the precision and accuracy of the method were <2%. This was independently verified with a nicotinamide standard. For the determination of $\delta^{13}C_{POC}$, the elemental analyser was coupled to a Finnigan Delta Plus isotope ratio mass spectrometer. Results for $\delta^{13}C_{POC}$ were normalised using nicotinamide and NAXOS graphite quartzite standards. Duplicate measurements on a selection of samples indicated that the reproducibility was better than ±0.15‰.

To determine concentrations of pigments, 500-1500 mL water was filtered over pre-combusted Whatman GF/C filters (1.2 μm), which were stored at -80°C. Samples were extracted and

analysed using high-performance liquid chromatography (HPLC) as described in Barranguet et al. (1997). In order to estimate pigment-based phytoplankton composition, we used the Bayesian Composition Estimator (BCE; Van den Meersche et al., 2008) with the input ratios of Dijkman and Kromkamp (2006).

3.2.3 ^{14}C assimilation rate incubations

Sampling for ^{14}C assimilation rate incubations occurred mid-morning on March 15, May 31, August 23 and November 8, which was 1-3 days after the water-column chemistry measurements of that month. Water was collected from three different depths: 1, 3 and 6 m in March and August, and 3, 6 and 10 m in May and November, when the CTD probe recorded a peak in Chl *a* around 10 m. Particulate C-fixation rates were determined as described by Kromkamp et al. (1995). Following sampling, duplicate 50 mL samples were promptly spiked with 100 μL of 1186 kBq mL^{-1} NaH^{14}CO$_3$ (Amersham) and put in a rotating incubator for 2 h at in situ surface-water temperature and a gradient of 11 different irradiances ranging from 0 to 732 μmol photons m^{-2} s^{-1}. Incubations were terminated by low-pressure filtration over 0.45 μm nitrocellulose filters, which were placed in HCl fumes for ca. 30 min to remove inorganic ^{14}C, air-dried, and analysed using standard counting techniques. From this, the particulate C-fixation rate was determined according to Steemann Nielsen (1952). This rate, which may be assumed to represent GPP due to the short incubation time (Falkowski and Raven, 2013), was normalised to CTD-derived Chl *a* and quantified as a function of light (P/I curve) according to Eilers and Peeters (1988):

$$GPP_{norm} = p_{max} \frac{(2 + \omega)\,(I / I_{opt})}{(I / I_{opt})^2 + \omega\,(I / I_{opt}) + 1} \tag{1}$$

Here, GPP_{norm} is the measured GPP normalised to CTD-derived Chl *a* (mmol C mg Chl a^{-1} h^{-1}), I and I_{opt} are the measured and optimum irradiance, respectively (both in μmol photons m^{-2} s^{-1}), p_{max} is the maximum GPP_{norm} (mmol C mg Chl a^{-1} h^{-1}), which occurs at I_{opt}, and ω is a dimensionless indicator of the relative magnitude of photoinhibition.

Downwelling light as a function of water depth was determined at the time of sampling, corrected for fluctuations in incident irradiance, and used to calculate the light attenuation coefficient and light penetration depth (LPD; 1% of incident irradiance) by applying the Lambert-Beer extinction model. Together with hourly averaged incident irradiance measurements collected ~31 km from the sampling site (41.489°N, 4.057°E), the light attenuation coefficient was used to calculate hourly averaged water column irradiance at 10 cm intervals until the LPD. Water column irradiance was combined with linearly interpolated CTD-derived Chl *a* and the fitted P/I curve (Eq. (1)) to calculate GPP_{14C} (mmol C m^{-3} h^{-1}) at 10 cm intervals. These values were integrated over the photoperiod to determine volumetric GPP_{14C} on the day of sampling (mmol C m^{-3} d^{-1}) and subsequently depth-integrated over the photic zone to derive areal GPP_{14C} (mmol C m^{-2} d^{-1}).

3.2.4 Oxygen light-dark incubations

Oxygen light-dark incubations were used to determine NCP, GPP and CR as described in Hagens et al. (2015). Briefly, samples were drawn into biochemical oxygen demand (BOD) bottles of ca. 120 mL and incubated on-deck at ambient surface-water temperature from the time of sampling

until sunset. Aluminium foil and Lee hard neutral density filters were used to mimic dark and a gradient of light conditions, respectively. Before and after incubation, [O_2] was determined using an automated Winkler titration routine with potentiometric end-point identification (Mettler Toledo DL50 titrator and a platinum redox electrode). Reagents were prepared and standardisations executed according to Knap et al. (1994).

The difference in [O_2] between the end and start of the samples incubated in the light and dark was used to determine NCP and CR, respectively, while GPP was resolved by summation (all rates in mmol O_2 m^{-3} h^{-1}). Samples from each depth were incubated in triplicate at 51.2% of photosynthetically active radiation (PAR) to determine the relationship between GPP and algal biomass (represented as CTD-derived Chl *a*), typically yielding a linear trend. To determine the dependency of GPP on light conditions, samples from one depth (usually 3 m) were incubated at 10 different fractions of incident irradiance, normalised to algal biomass concentration and fitted according to Eilers and Peeters (1988). CTD-derived Chl *a* was linearly interpolated between sampling depths and combined with hourly averaged water column irradiance and the Eilers-Peeters function to calculate GPP_{O_2} (mmol O_2 m^{-3} h^{-1}) at 10 cm intervals. Similar to GPP_{14C}, these values were integrated over depth and time to arrive at daily volumetric and areal GPP_{O_2} rates. Finally, GPP_{O_2} was converted from O_2 to C units using a photosynthetic quotient (PQ) that depended on the ammonium (NH_4^+) concentration. If [NH_4^+] exceeded 0.3 μmol L^{-1}, it was assumed to be the sole N source for GPP, resulting in a PQ of 1. Else, a PQ of 1.3 was used, in line with nitrate (NO_3^-) assimilation. Concentrations of NH_4^+ and NO_3^- were determined by automated colorimetric techniques (Middelburg and Nieuwenhuize, 2000) after filtration through 0.2 μm filters and can be found in the supplementary material of Hagens et al. (2015).

3.2.5 High-resolution in situ oxygen measurements

In March and August 2012, O_2 was measured at 10-minute intervals using an optode (Aanderaa 4835 used in conjunction with a Seaguard) attached to a buoy close to the main water-column sampling station (51.742°N, 3.872°E) and fixed at ca. 1 m depth. Deployment time was 6 days in March and 7 days in August, and measurements were terminated at the day of the ^{14}C assimilation rate incubations. From these high-resolution in situ O_2 measurements, GPP was determined using the Fourier method described by Cox et al. (2014). Briefly, the central concept of this method is that every process influencing O_2 acts on a different time scale, so that the O_2 time-series can be decomposed into several frequencies using a Fourier transformation. By assuming that the signal with a 24 h period is dominantly resulting from GPP, its impact on O_2 can be disentangled from other processes. Time-averaged GPP, or $\overline{GPP(t)}$ (in mmol O_2 m^{-2} d^{-1}), can subsequently be calculated by fitting the result from this specific Fourier transform to a truncated sinusoidal function, thereby assuming that during the day GPP smoothly follows the incident irradiance curve, while during the night its value equals zero:

$$\overline{GPP(t)} \approx 2\omega_1 \frac{\sin \theta - \theta \cos \theta}{-\frac{1}{2}\sin 2\theta} A_{O_2} \tag{2}$$

Here, $\theta = \pi f_{DL}$, where f_{DL} is the fraction of daylight relative to a complete 24 h cycle. The quantity ω_1 is the diurnal frequency, defined as 2π rad d^{-1}, and A_{O_2} is the amplitude of the Fourier-

transformed O_2 signal at this frequency. Following photic zone-averaged $[NH_4^+]$, $\overline{GPP(t)}$ was converted to C units using a PQ of 1 in March and 1.3 in August.

3.2.6 Group-specific primary production using ^{13}C uptake in PLFA

Group-specific primary production was estimated using the method of Dijkman et al. (2009) as adapted by de Kluijver et al. (2010). Incubations were carried out monthly between March and November 2012 on the same dates as either ^{14}C fixation rate incubations (March, May, August, November) or oxygen light-dark incubations (other months). We used water from 1, 3 and 6 m depth, with the exception of May, November (see ^{14}C uptake) and June when 3, 6 and 10 m were chosen as sampling depths. Water was collected into 2.5 L HDPE jerry cans and spiked with 99% $NaH^{13}CO_3$ (Cambridge Isotopes) at 0.6-0.9% of the ambient DIC concentration. Jerry cans were incubated on-deck at ambient surface-water temperature and ~50% of incident irradiance, and were shaken regularly during the incubation to prevent settling of particulate matter. Incubations were terminated after 4 hours by filtering over pre-combusted GF/F filters, from which PLFA were extracted as described in Boschker (2004). Briefly, filters were put in a mixture of chloroform, methanol and ultrapure water (1:2:0.8 by volume) immediately after filtration and stored frozen until further analysis. Total lipids were extracted using a modified Bligh-Dyer method by adding chloroform and ultrapure water until a volumetric chloroform:methanol:water ratio of 1:1:0.9. Following density separation the chloroform fraction was collected. Separation of the total lipid fraction into different polarity classes occurred through sequential elution with chloroform, acetone and methanol over a heat-activated silicic acid column. The methanol fraction, containing PLFA, was derivatised to fatty acid methyl esters (FAME) using mild alkaline methanolysis. As internal FAME standards 12:0 and 19:0 were used.

Concentrations of FAME were determined by gas chromatography – flame ionisation detection using a special large-volume injection technique (LV-GC-FID) on a Thermo Scientific TRACE GC Ultra with a polar analytical column (Scientific Glass Engineering BPX-70). The isotopic composition of every individual FAME was measured using gas chromatography – combustion – isotope ratio mass spectrometry (GC-C-IRMS) and corrected for the C atom added during derivatisation to obtain the δ^{13}C of PLFA (Middelburg et al., 2000). Identification of FAME and corresponding PLFA was done using a custom-made script in the open-source programming framework R based on the comparison of retention time data with known standards. To check the robustness of this method, peaks were additionally identified on a subset of samples using gas chromatography – mass spectrometry (GC-MS). Shorthand PLFA nomenclature is according to Guckert et al. (1985).

Concentrations of PLFA (μg C L^{-1}) were calculated from the FAME peak area relative to the area of the internal 19:0 FAME standard (Boschker, 2004). To characterise total phytoplankton dynamics, the sum of PLFA 18:3ω3, 18:4ω3, 18:5ω3(12-15), 18:5ω3(12-16), 20:5ω3 and 22:6ω3 was used (Boschker and Middelburg, 2002; Dijkman et al., 2009; De Kluijver et al., 2010). The phytoplankton community was separated into diatoms (PLFA 16:2ω4, 16:4ω1, 20:4ω6 and 20:5ω3), dinoflagellates (PLFA 18:5ω3(12-15) and 22:6ω3), the haptophyte *Phaeocystis globosa* (PLFA 18:5ω3(12-16)) and green algae (PLFA 16:3ω3, 16:4ω3 and 18:3ω3) according to Dijkman

and Kromkamp (2006) and Dijkman et al. (2009). Similar to the pigment data, BCE was used with the input ratios of Dijkman and Kromkamp (2006) to estimate PLFA-based phytoplankton composition. PLFA concentrations (in µg C-PLFA L^{-1}) were converted to biomass (mg C L^{-1}) using the PLFA-to-organic C ratios determined by Dijkman and Kromkamp (2006). From this, group-specific and total phytoplankton growth rates (GPP_{PLFA}; mmol C m^{-3} h^{-1}) were calculated according to de Kluijver et al. (2010). Additionally, we calculated specific growth rates (µ; h^{-1}) from the fraction of ^{13}C before and after incubation:

$$\mu = \frac{1}{\Delta t} \ln \left(\frac{\left(^{13}C \ / \left(^{13}C + {}^{12}C \right) \right)_{t_0 + \Delta t}}{\left(^{13}C \ / \left(^{13}C + {}^{12}C \right) \right)_{t_0}} \right) \tag{3}$$

Here, t_0 represent the initial time, Δt is the incubation time and ^{13}C and ^{12}C are the concentrations of both C isotopes.

Finally, GPP_{PLFA} was integrated in both space and time to arrive at rates of mmol C m^{-2} d^{-1} necessary for method comparison. In contrast to GPP_{14C} and GPP_{O2}, where the influence of light availability on growth was specifically quantified, this was not done for GPP_{PLFA} and so a fairly simple approach was used. First, to test if biomass and growth rates of different depths were significantly different ($p < 0.05$), we applied a two-sided homoscedastic t-test using the R-package *Stats* (R Core Team, 2015). For most months and groups, this analysis revealed no significant differences between depths, meaning that we present all PLFA-derived data as depth-averaged values ± standard deviation. Then, we multiplied the depth-averaged GPP_{PLFA} with the daylight duration to arrive at a daily estimate for both GPP_{PLFA} (mmol C m^{-3} d^{-1}) and µ (d^{-1}). This was followed by a multiplication with the LPD to arrive at a depth-integrated estimate for GPP_{PLFA} (mmol C m^{-2} d^{-1}).

3.3   Results

3.3.1   Carbon dynamics

Spatial and temporal variability of the C system in the Den Osse basin in 2012 is shown in Fig. 3.1. From January until April, when the basin was well-mixed (Hagens et al., 2015), both DIC (Fig. 3.1a) and DOC (Fig. 3.1e) did not show much variation with time and depth, suggesting little biological activity. In May, photic-zone DIC started to decrease to an average of 2123 µmol kg^{-1}, which was 105 µmol kg^{-1} lower than the average in the first four months of 2012. This decrease was accompanied by an increase in average photic-zone DOC of 49 µmol L^{-1} to 216 µmol L^{-1} and elevated POC (Fig. 3.1c; max. 0.74 mg C L^{-1}), $\delta^{13}C_{POC}$ (Fig. 3.1d; max. -20.8‰) and $\delta^{13}C_{DIC}$

(next page) **Figure 3.1** (a) DIC (µmol kg^{-1}), (b) $\delta^{13}C_{DIC}$ (‰ VPDB), (c) POC (mg C L^{-1}), (d) $\delta^{13}C_{POC}$ (‰ VPDB), and (e) DOC (µmol L^{-1}). Data for POC, $\delta^{13}C_{POC}$ and $\delta^{13}C_{DIC}$ before May are lacking. Black dots indicate sampling depths and data were linearly interpolated in space and time.
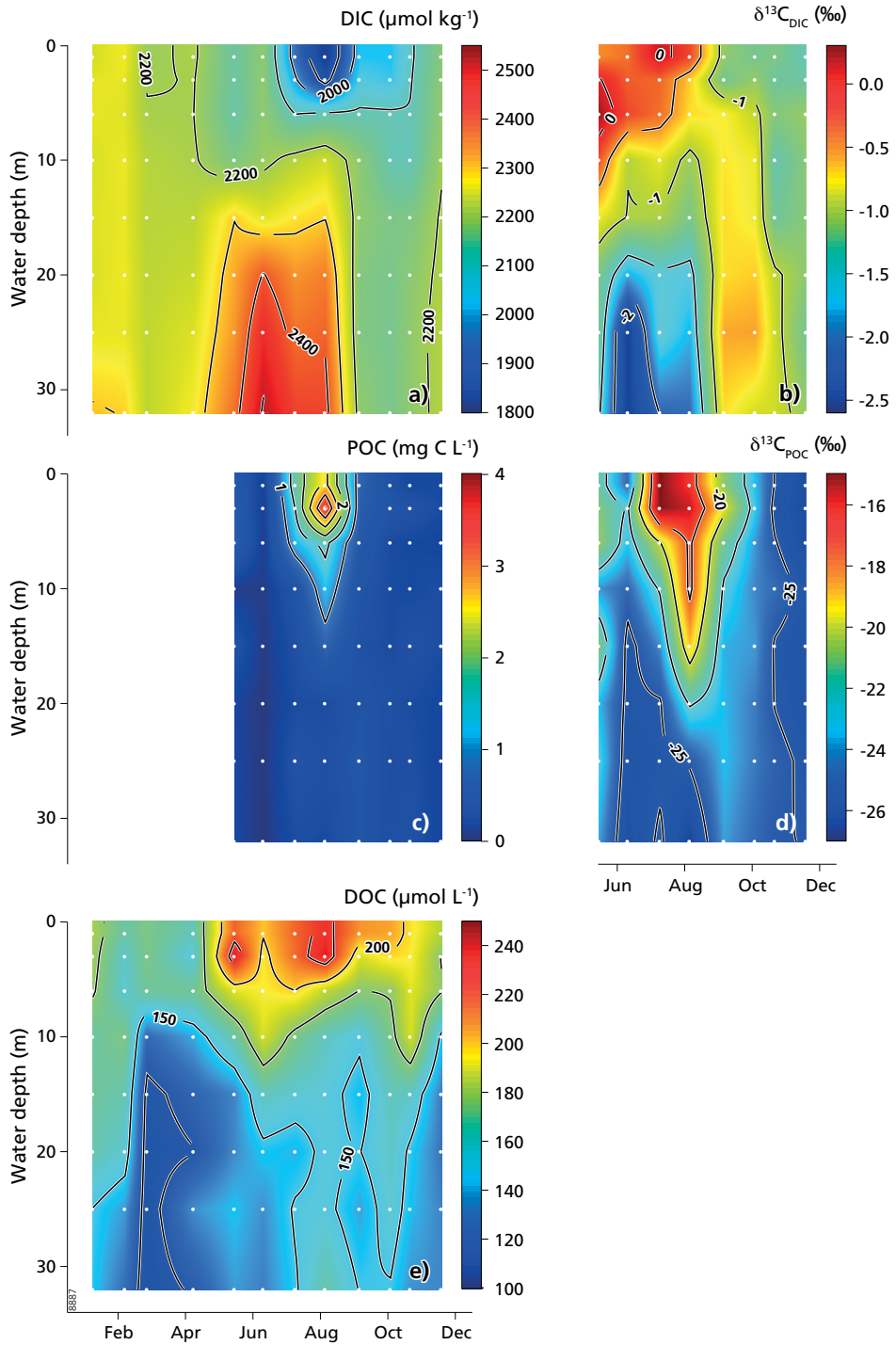
(Fig. 3.1b; max. 0.2‰), all indicative of phytoplankton activity. This trend in photic-zone C dynamics continued until August, with reduced surface-water DIC values especially in July and August (min. 1813 μmol kg^{-1}) and a concurrent increase in $\delta^{13}C_{DIC}$ up to 0.1‰. DOC showed two distinct surface-water peaks during this period: in May and in July-August, both with concentrations ranging up to 237 μmol L^{-1}. Values of $\delta^{13}C_{POC}$ went up to -15.1‰ in August, also the month of highest POC accumulation (max. 3.55 mg C L^{-1}), which is more than 10‰ higher than the surface-water value in December (-26.2‰) and well above the range for average North Sea POC of ca. -23 to -18‰ (Dauby et al., 1994). Concomitantly, a drawdown in the level of carbon dioxide (CO_2) and elevated [O_2] were observed (Hagens et al., 2015). All these observations point to high autotrophic activity, especially in July and August. At the same time, as a result of strongest water-column stratification, a build-up of bottom-water DIC enriched in $\delta^{13}C$ was observed between May and August. Lowest bottom-water $\delta^{13}C_{DIC}$ (-2.5‰) was found in June, concomitant with highest DIC concentration, indicating high respiratory activity. Stratification was disrupted before sampling in September, leading to less pronounced variations with depth, although both surface-water DOC and $\delta^{13}C_{DIC}$ were consistently higher than in the bottom water. Highest bottom-water $\delta^{13}C_{POC}$ values (-23.3‰) in 2012 were observed in September, reflecting vertical transport and subsequent degradation of the POC produced in the surface water in summer. Surface-water DIC remained lower than bottom-water DIC in early autumn. In concurrence with slightly elevated DOC (192 μmol L^{-1} on average), this suggests phytoplankton activity, although lower than during the period May-August.

3.3.2 Pigment-based phytoplankton composition

One way of characterising seasonality in phytoplankton composition is through specific pigment distributions, which are shown in Fig. 3.2. Fucoxanthin presence in the Den Osse Basin in 2012 (Fig. 3.2a) showed a marked seasonality, with a main peak in the subsurface water in May (3.35 – 3.66 μg L^{-1}). Additionally, fucoxanthin displayed elevated concentrations throughout the first 15 m in March (1.60 – 2.10 μg L^{-1}) and June (1.43 – 2.14 μg L^{-1}), in July at ~6 m depth (2.27 μg L^{-1}), and in the surface water in August (1.97 μg L^{-1}). Both fucoxanthin and Chl c (Fig. 3.2b) are ubiquitous in diatoms, but can also be derived from other phytoplankton groups, including *P. globosa* (Dijkman and Kromkamp, 2006). A comparison of their distribution indeed revealed many similarities in their spatiotemporal patterns, especially in spring, when a similar subsurface peak in May (1.72 – 2.01 μg L^{-1}) and slightly elevated surface water values in March (0.86 – 1.01 μg L^{-1}) were observed. The summer surface water Chl c peak, however, was more prominent (3.24 – 4.12 μg L^{-1}) and showed a clear decrease with depth, implying that these pigments had at least partly different origins. Both alloxanthin (Fig. 3.2c), which is specific for the class Cryptophyceae, and peridinin (Fig. 3.2d), characteristic of certain dinoflagellates (Wright and Jeffrey, 2006), showed increased surface water contents in summer. However, while alloxanthin concentrations were only elevated in the surface water in August (up to 2.14 μg L^{-1}), surface-water peridinin content was high in both July and

(next page) **Figure 3.2** Concentrations (in μg L^{-1}) of (a) fucoxanthin, (b) Chl c, (c) alloxantin, (d) peridinin, (e) diadinoxanthin, (f) Chl b, (g) Chl c_3, and (h) CTD-derived Chl a in the Den Osse basin in 2012. Black dots in (a) – (g) indicate sampling depths. All data were linearly interpolated in space and time.
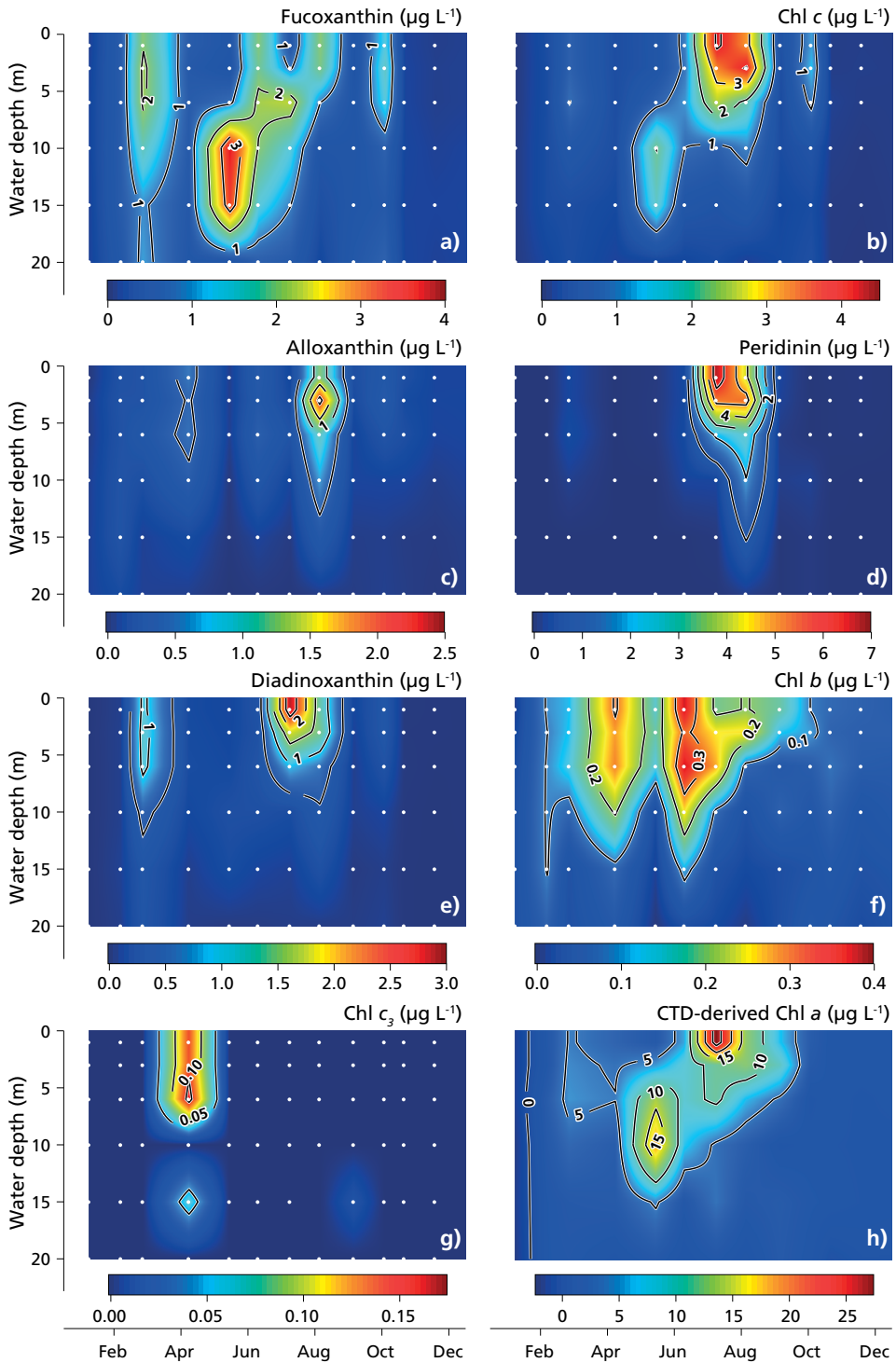
August, extending up to 6.62 µg L^{-1}. Diadinoxanthin (Fig. 3.2e), indicative of dinoflagellates but also the class Haptophyta I to which *P. globosa* belongs (Dijkman and Kromkamp, 2006), displayed two marked peaks in 2012, both in the surface water: in March (1.14 µg L^{-1}) and during summer (max. 2.83 µg L^{-1}). The seasonal pattern of Chl *b* (Fig. 3.2f), which occurs in all green algae, was quite different from the previously discussed pigments; however, its concentration never exceeded 0.37 µg L^{-1}. Peaks of Chl *b* were found in April (up to 0.31 µg L^{-1}) and particularly June, with the
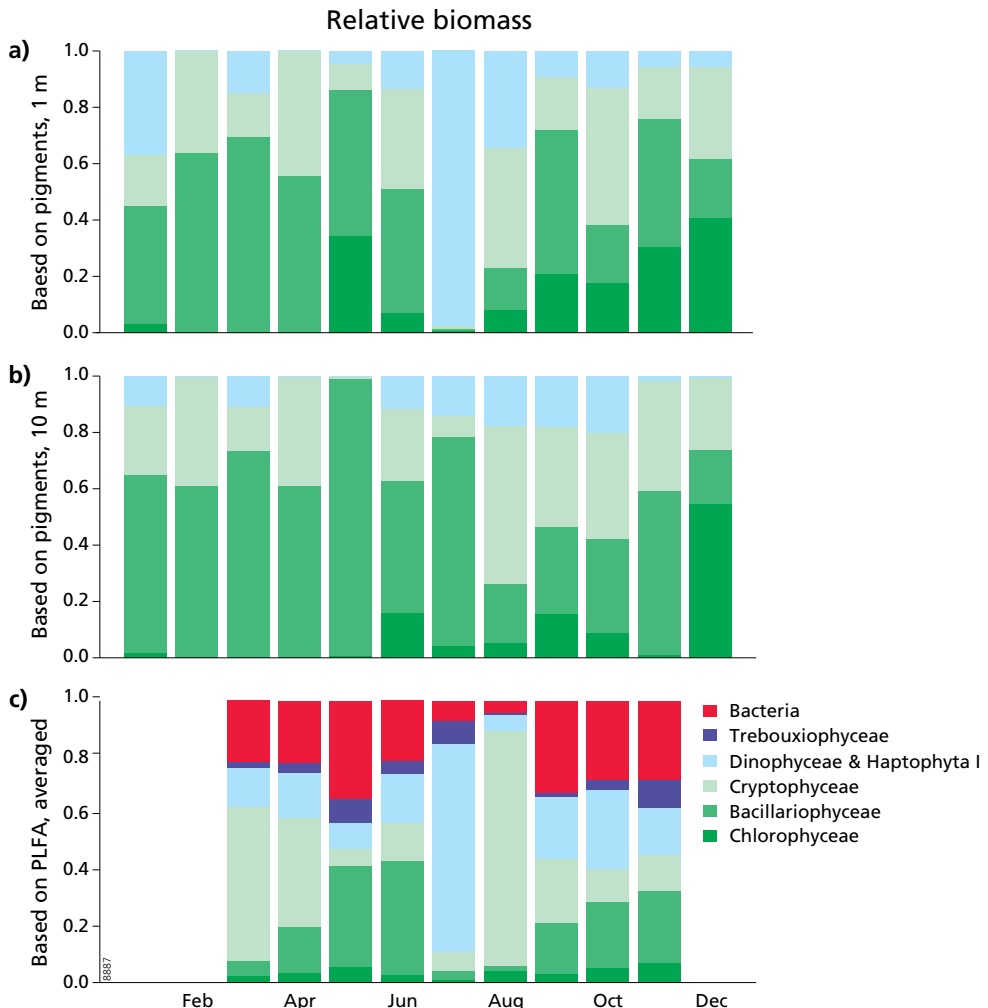
Figure 3.3 Relative biomass of specific algal classes and bacteria as determined by a Bayesian Composition Estimator based on (a) pigment composition at 1 m depth, (b) pigment composition at 10 m depth, and (c) depth-averaged PLFA composition, presented as the average of the initial and final composition. Fewer compounds and algal groups were included for the pigment data analysis than for the PLFA data analysis. No samples for PLFA analysis were taken in January, February and December.

latter one extending until July. Concentrations of Chl c_3 (Fig. 3.2g), present in haptophytes such as *P. globosa*, were only elevated in April but did not reach high values (max. 0.16 µg L⁻¹). Finally, concentrations of the generic Chl *a* as derived from the CTD probing (Fig. 3.2h) showed two main features: elevated subsurface-water concentrations in May, peaking at 19.0 µg L⁻¹ at 10 m depth, and highest surface-water concentration in July (27.3 µg L⁻¹). In conjunction with the drawdown of DIC and elevated $\delta^{13}C_{DIC}$ and DOC concentrations, this latter peak indicated the presence of a substantial phytoplankton bloom. Microscopic observations revealed that the main bloom-forming species during this month was the dinoflagellate *Prorocentrum micans*. The surface-water July peak was part of a longer period of elevated concentrations in the top 6 m, ranging from June until September. In addition, CTD-derived Chl *a* was slightly elevated in March throughout the mixed layer (4.04 – 5.85 µg L⁻¹).

Community composition was estimated using the BCE for each depth separately to account for observed spatial and temporal variations in pigments, such as the subsurface May and surface-water July peaks of CTD-derived Chl *a*. Here we present the data for 1 and 10 m depth (Figs. 3.3a-b). The combined class Dinophyceae & Haptophyta I comprises both *P. globosa* and dinoflagellates, while Trebouxiophyceae and Chlorophyceae both belong to the green algae. Diatoms are part of the Bacillariophyceae, while Cryptophyceae are a class of algae including *Rhodomonas* spp. and *Hemiselmis* spp. In line with what would be expected, substantial variations in pigment-based phytoplankton composition with depth were only observed between May and August, when water-column mixing was poor. From January until April, the most important class in the pigment-based phytoplankton community was Bacillariophyceae, comprising 42 – 73% of the total biomass. Furthermore, both Cryptophyceae and Dinophyceae & Haptophyta I were present. May was characterised by an increase in Chlorophyceae in the surface water, while the subsurface-water community was almost entirely comprised by Bacillariophyceae. In June, phytoplankton communities in the surface and subsurface water did not display a clear difference. Although the Bacillariophyceae contributed most to the total biomass, all classes made up a substantial fraction of the community. In July, the surface water was entirely dominated by Dinophyceae & Haptophyta I, in agreement with the visual observation of the *P. micans* bloom. In the subsurface water, however, Bacillariophyceae still dominated the community. August was characterised by a big community shift in both the surface and subsurface water. While Dinophyceae & Haptophyta I still made up 34% of the surface-water community, the biggest contribution (42%) to the total biomass came from the Cryptophyceae, which was also the most dominant fraction (56%) in the subsurface water. From September onwards, when stratification had been terminated, differences between the surface and subsurface phytoplankton community were again relatively minor, although Chlorophyceae generally comprised a larger part of the biomass in the surface than in the subsurface water, with the exception of December. Dinophyceae & Haptophyta I comprised at most 20% of the algal biomass, and both Cryptophyceae and Bacillariophyceae were substantially present.

3.3.3 PLFA-based phytoplankton biomass and composition

PLFA-based biomass estimates were used to investigate phytoplankton composition (Fig. 3.4a). Overall, dinoflagellate biomass was the highest of all species, with a value of 0.45±0.04 mg C L⁻¹ in March, after which it decreased until June. In line with the microscopic observations, dinoflagellate

biomass substantially increased afterwards, reaching peak values of 1.91±0.41 and 1.75±0.22 mg C L^{-1} in July and August, respectively. September displayed again a much lower dinoflagellate biomass (0.31±0.05 mg C L^{-1}), while in October and November it was virtually absent. The seasonal pattern of *P. globosa* biomass followed that of the dinoflagellates, with a minor peak in March (0.34±0.04 mg C L^{-1}), highest concentrations in July and August, followed by a decrease in September and very low levels afterwards. The summer peak concentrations were, however, much lower than the dinoflagellate biomass (0.89±0.15 and 0.77±0.10 mg C L^{-1} in July and August). In contrast, the seasonal pattern of diatoms as revealed by PLFA showed some marked differences. Biomass showed a small peak in March (0.25±0.02 mg C L^{-1}) and decreased in April (0.13±0.02 mg C L^{-1}), after which it remained relatively constant until July. Diatoms topped out in August (0.44±0.05 mg C L^{-1}), after which they declined again in September (0.19±0.02 mg C L^{-1}) and were virtually absent afterwards. Thus, diatom biomass peaked in late summer only, while dinoflagellate and *P. globosa* biomass was high throughout most of the summer period. Green algal biomass, finally, was low throughout the year and displayed its highest value (0.08±0.01 mg C L^{-1}) in August.
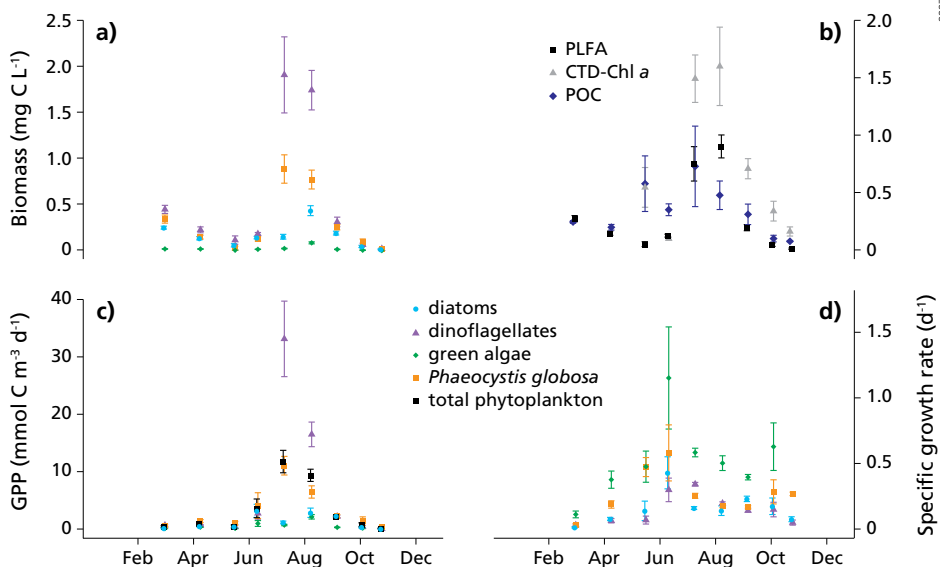
Figure 3.4 (a) Depth-averaged biomass (mg C L^{-1}) of diatoms, dinoflagellates, green algae and *P. globosa* as determined from PLFA; (b) Depth-averaged POC concentration and total biomass as derived from PLFA and CTD-derived Chl *a* (mg C L^{-1}). PLFA-derived values are presented as the average of the initial and final biomass, while POC and CTD-derived Chl *a* were measured at t_0 only. (c) GPP$_{PLFA}$ (mmol C m^{-3} d^{-1}), and (d) specific growth rates (μ; d^{-1}) as determined from PLFA. Values are presented as depth-averaged ± standard deviation, whereby only the depths of the ^{13}C-incubations were included.

PLFA-based community composition estimated using the BCE (Fig. 3.3c) shows a slightly different pattern than the pigment-based composition, which is partly due to the fact that, following Dijkman and Kromkamp (2006), bacteria were additionally included for PLFA analysis and fewer compounds and algal classes were used for pigment than PLFA analysis. Although bacterial biomass is presented in this figure, contributing at most 35% to the total PLFA-based biomass, the discussion and percentages mentioned below do not take into account the bacterial fraction, for a better comparison with the pigment-based composition that is limited to phytoplankton. March and April showed fairly similar patterns, with the Cryptophyceae being dominant, contributing 49 – 70% to the total algal biomass, and only minor contributions of the Dinophyceae & Haptophyta I (17 – 20%) and the Bacillariophyceae (7 – 21 %). This latter observation clearly contrasts with the pigment-based data. The contribution of Bacillariophyceae to the total biomass substantially increased in May (55%) and June (52%), mostly at the expense of Cryptophyceae. The importance of Chlorophyceae, Trebouxiophyceae and Dinophyceae & Haptophyta I remained relatively constant with time, although the first two groups showed an increase in relative biomass in May (9 and 14%, respectively), in line with the pigment-based surface-water data. In July, Dinophyceae & Haptophyta I dominated the PLFA-based phytoplankton biomass (79%), agreeing with both the pigment data and microscopic observations. Similar to the surface-water pigment data, a big shift in community composition occurred in August, with the Cryptophyceae contributing most (87%) to the total biomass. From September onwards, community composition is relatively stable, with Bacillariophyceae (27 – 36%) and Dinophyceae & Haptophyta (23 – 39%) comprising most of the algal biomass, closely followed by Cryptophyceae (16 – 34%). However, if we combined Chlorophyceae and Trebouxiophyceae biomass, the green algal biomass would be of similar magnitude to the other three groups.

3.3.4   Total phytoplankton biomass

Total phytoplankton biomass was revealed by means of PLFA, CTD-derived Chl a as well as POC concentrations (Fig. 3.4b). To this end, CTD-derived Chl a (μg L^{-1}) was converted to biomass (mg C L^{-1}) using a C:Chl a ratio of 45 (de Kluijver et al., 2010). These biomasses are all presented as depth-averaged values ± standard deviation, whereby only the depths of the ^{13}C-incubations were included. In line with their dominance, the seasonal pattern of PLFA-derived total phytoplankton biomass followed that of the dinoflagellates. Biomass was 0.28±0.03 mg C L^{-1} in March, displayed low values between April and June, peaked in July (0.76±0.15 mg C L^{-1}) and August (0.91±0.10 mg C L^{-1}), decreased again in September (0.20±0.03 mg C L^{-1}) and did not show significant values afterwards. Note that these values are lower than the maximum dinoflagellate biomass; the reasons for this will be discussed later. The seasonal pattern of Chl a-derived biomass somewhat deviates from that of the PLFA-derived biomass. The main difference is the relative higher concentration in May (0.58±0.24 mg C L^{-1}), caused by the subsurface Chl a peak (see Fig. 3.2h). Furthermore, Chl a-derived biomass was substantially higher in July (0.73±0.35 mg C L^{-1}) compared to August (0.48±0.12 mg C L^{-1}). The seasonal dynamics of POC had features of both the PLFA-derived and Chl a-derived total biomass, but generally displayed higher values. POC peaked in May (0.55±0.17 mg C L^{-1}), was low in June (0.10±0.01 mg C L^{-1}), showed highest levels in July and August (1.50±0.21 and 1.61±0.34 mg C L^{-1}, respectively), declined in September (0.71±0.09 mg C L^{-1}) and had even lower concentrations afterwards.

3.3.5 Total phytoplankton primary production

Depth-integrated measurements of gross primary productivity in 2012 are presented in Fig. 3.5. All methods found a clear unimodal distribution of GPP over the year, with highest rates in summer. GPP_{O2}, the only method that was applied year-round, showed highest rates in July (324 mmol C m^{-2} d^{-1}), followed by August (131 mmol C m^{-2} d^{-1}) and June (115 mmol C m^{-2} d^{-1}). In winter and late autumn (January-February and October-December) GPP_{O2} did not exceed 17.3 mmol C m^{-2} d^{-1}. When comparing the in vitro and in situ oxygen-based GPP estimates, it becomes clear that the in situ estimates were substantially higher and in fact displayed the highest GPP values of all methods. $\overline{GPP(t)}$ was 176 mmol C m^{-2} d^{-1} in March and 347 mmol C m^{-2} d^{-1} in August, which is 5.8 and 2.7 times higher than in vitro GPP_{O2}, respectively. A similar discrepancy was found between $\overline{GPP(t)}$ and the in vitro carbon-based GPP estimate: while $\overline{GPP(t)}$ in August was relatively close to GPP_{14C} (274 mmol C m^{-2} d^{-1}), GPP_{14C} in March was 1 order of magnitude lower (15.8 mmol C m^{-2} d^{-1}). GPP_{14C} was higher than GPP_{O2} in May and August and lower in March and November.

The three methods determining changes in O_2 or the total C pool were compared with depth-integrated rates of total phytoplankton GPP_{PLFA}. The annual pattern of GPP_{PLFA} closely resembled that of GPP_{O2}, with highest rates in July (82.1 mmol C m^{-2} d^{-1}), followed by August (55.8 mmol C m^{-2} d^{-1}) and June (32.0 mmol C m^{-2} d^{-1}). Furthermore, with the exception of October where GPP_{O2} was lowest, GPP_{PLFA} consistently displayed lowest values. In the four months where these three methods were concomitantly used, GPP_{PLFA} was on average 20.0% of GPP_{O2} and 22.5%
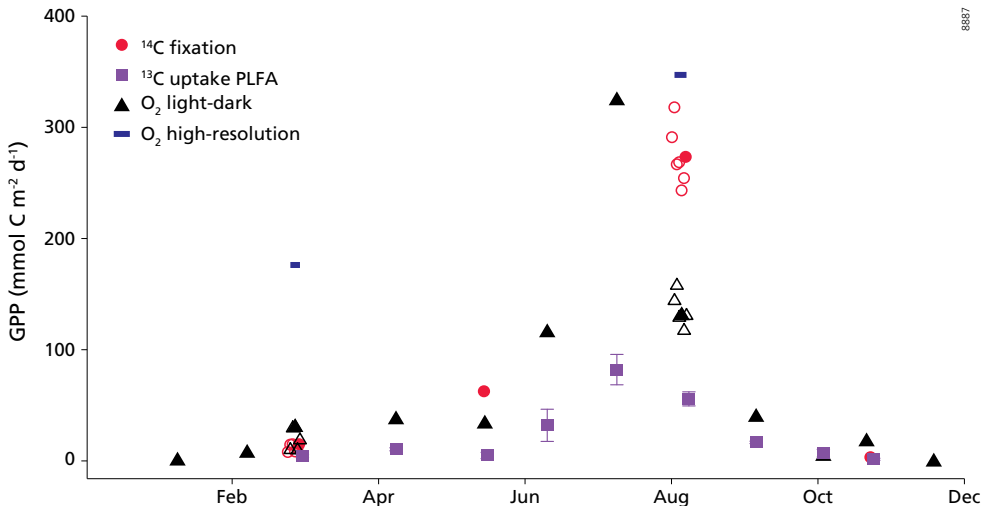
Figure 3.5 Comparison of GPP derived from the 4 different methods. Results for GPP_{PLFA} are presented as average values ± standard deviation. For March and August, the results for GPP_{14C} and GPP_{O2} were interpolated for the duration of O_2 sensor deployment using the hourly-averaged measurements of incident irradiance, constant interpolation of the parameters from the Eilers-Peeters fit and linearly interpolated Chl *a* and light attenuation coefficients (open symbols).

of the measured GPP_{14C}. For GPP_{O2}, this value would change to 22.6% if we took the linearly interpolated values from the same days as the PLFA sampling, and to 26.7% if we included all months except October.

Volumetric rates of total phytoplankton GPP_{PLFA} (Fig. 3.4c) displayed a similar annual pattern to the depth-integrated rates, although the difference between August (9.36±1.06 mmol C m^{-3} d^{-1}) and June (3.61±1.63 mmol C m^{-3} d^{-1}) was more pronounced. This is due to the deeper light penetration in June (8.9 m) compared to August (5.8 m; Hagens et al., 2015), which diminishes the difference in volumetric rates during depth-integration. Volumetric total phytoplankton GPP_{PLFA} was highest in July (11.8±1.96 mmol C m^{-3} d^{-1}). This value is substantially lower than the average of volumetric GPP_{O2} at 1, 3 and 6 m depth as presented in Hagens et al. (2015), which was 56.1 mmol C m^{-3} d^{-1}. To test how GPP_{O2} and GPP_{PLFA} were correlated, we followed the procedure of Regaudie-de-Gioux et al. (2014) and performed a reduced or standard major axis (SMA) regression using the R package *lmodel2* (Legendre, 2014) on log-transformed volumetric GPP_{O2} and GPP_{PLFA}, whereby the former was not converted to C units. This analysis showed that over the year, GPP_{O2} and GPP_{PLFA} could be correlated according to $GPP_{PLFA} = 0.204\ GPP_{O2}^{1.07}$. Due to the small number of samples (n=9), the estimates for both the slope (0.669 to 1.711) and intercept (-2.724 to -0.884) of the log-transformed data show a broad range in their 95% confidence interval. An F-test performed using the R package *Stats* indicates that the slope of the log-transformed data is not significantly different from 1 (P=0.8734), indicating that the ratio of GPP_{PLFA} to GPP_{O2} does not significantly change when GPP_{O2} increases. However, since the intercept of the log-transformed data is always negative in the 95% confidence interval, it can be concluded that volumetric GPP_{PLFA} is always significantly lower than GPP_{O2}.

3.3.6 Group-specific phytoplankton growth rates

In addition to total phytoplankton GPP_{PLFA}, we also determined group-specific GPP_{PLFA} for diatoms, dinoflagellates, green algae, and the haptophyte *P. globosa*. Considering data from all species, volumetric GPP_{PLFA} (Fig. 3.4c) varied between 0.03±0.01 and 33.1±6.58 mmol C m^{-3} d^{-1}. Dinoflagellate GPP_{PLFA} showed a clear summer peak in line with its biomass: it started to increase in June (2.74±1.14 mmol C m^{-3} d^{-1}), was highest in July (33.1±6.58 mmol C m^{-3} d^{-1}), remained high in August (16.5±2.14 mmol C m^{-3} d^{-1}), decreased again in September (2.20±0.19 mmol C m^{-3} d^{-1}) and was low afterwards. GPP_{PLFA} of *P. globosa* followed a similar summer trend to the dinoflagellates, but with significant lower peak values (11.0±1.62 mmol C m^{-3} d^{-1} in July). The relatively high biomass of both *P. globosa* and dinoflagellates in early spring was, however, not reflected in their group-specific GPP_{PLFA}. In line with their low biomass, green algal GPP_{PLFA} was low throughout the year, reaching a maximum value of 2.13±0.39 mmol C m^{-3} d^{-1} in August. Diatom GPP_{PLFA} showed two periods of high rates: in June (3.17±1.13 mmol C m^{-3} d^{-1}) and in late summer (2.83±0.81 and 2.27±0.12 mmol C m^{-3} d^{-1} in August and September, respectively). This latter peak was accompanied by an increase in biomass, while this was not the case in June. Similar to the biomass results, total phytoplankton GPP_{PLFA} generally displayed lower values than dinoflagellate and, in some months, *P. globosa* GPP_{PLFA}.

Finally, turnover rates for the different groups of algae are shown in Fig. 3.4d. Despite their low biomass and GPP_{PLFA} throughout the year, the green algae predominantly showed the highest specific growth rates. Generally growth rates peaked 1-2 months preceding highest biomass. Both green algae (1.15±0.39 d^{-1}) and diatoms grew fastest in June (0.43±0.12 d^{-1}) but only displayed highest biomass in August. *P. globosa* grew fastest in July (0.58±0.21 d^{-1}), when biomass was highest. Dinoflagellate specific growth rates were generally lower than those of *P. globosa* and the diatoms and were highest in June (0.30±0.090 d^{-1}) and July (0.34±0.014 d^{-1}), while biomass peaked in July and August.

3.4   Discussion

3.4.1   Gross primary production in the Den Osse basin

We extrapolated GPP_{O2} to an annual estimate by using hourly averaged incident irradiance measurements, interpolation of the parameters from the Eilers-Peeters fit, and linear interpolation of CTD-derived Chl *a* and the light attenuation coefficient. After conversion from moles to grams C, this yielded a value of 225 g C m^{-2} yr^{-1} for the Den Osse basin in 2012, which can be compared with previous estimates. Using a 1D model, Meijers and Groot (2007) calculated a lake-wide GPP of 572 g C m^{-2} yr^{-1} as average for the years 2000-2005. By coupling a 3D hydrodynamic model to a generic ecological model, Nolte et al. (2008) found a value of 243 g C m^{-2} yr^{-1} for their reference year 2000. Previous measurements of GPP in Lake Grevelingen are only available until ca. 1980. Using ^{14}C fixation rate incubations, GPP was estimated at 225 g C m^2 yr^{-1} for the entire lake and 385 g C m^2 yr^{-1} for the 22 m deep Dreischor basin (51.715°N, 4.000°E), another basin located in the main gully of Lake Grevelingen (Vegter and De Visscher, 1984). It would be unrealistic to directly compare these early estimates with our current measurements because of significant changes in the sluice regime, which have influenced factors like nutrient and light availability. However, given the different methods used and time periods considered, we may conclude that our estimate of GPP is consistent with previous estimates for Lake Grevelingen.

3.4.2   Short-term temporal variability in GPP

The high-resolution O_2 monitoring provides a time-averaged estimate of GPP for the duration of sensor deployment, which was 6-7 days in our study. To get an indication of the daily variability of GPP in relation to the estimate of $\overline{GPP(t)}$, we interpolated the results for GPP_{14C} and GPP_{O2} for the duration of sensor deployment using the hourly-averaged measurements of incident irradiance, interpolation of the parameters from the Eilers-Peeters fit and linearly interpolated CTD-derived Chl *a* and light attenuation coefficients. This analysis revealed substantial daily variation: GPP_{14C} varied by about a factor 2 during the sensor deployment period in March (8.63 – 15.6 mmol C m^{-2} d^{-1}, average 12.1 mmol C m^{-2} d^{-1}), and ~30% in August (244 – 319 mmol C m^{-2} d^{-1}, average 274 mmol C m^{-2} d^{-1}). In the same period, GPP_{O2} varied by varied a factor 3 in March (9.91 – 30.2 mmol C m^{-2} d^{-1}, average 19.6 mmol C m^{-2} d^{-1}) and by ~ 35% in August (117 – 158 mmol C m^{-2} d^{-1}, average 135 mmol C m^{-2} d^{-1}). In August, our measured values of GPP_{14C} and GPP_{O2} agree well with the average of the interpolated values. In March, this is the case for GPP_{14C} but not for GPP_{O2}, which was measured on the day of highest GPP. Based on this analysis we can conclude

that a monthly sampling resolution may be too low for a dynamic, eutrophic basin like the Den Osse basin.

3.4.3 In situ versus in vitro oxygen-based methods

The results from our study suggest that in situ measured oxygen-based rates of GPP in the Den Osse basin are substantially higher than in vitro measured rates. To understand this difference, it is important to realise which factors might bias both methods. As mentioned before, in vitro methods suffer from bottle effects, changing trophic interactions (Pomeroy et al., 1994), turbulence, temperature, nutrient availability (Collos et al., 1993) and light climate (Agustí et al., 2014). In May and November, we measured nutrient concentrations after 4 h incubations in 1 L Schott bottles to estimate possible nutrient limitation during incubation. These results show that both dissolved inorganic nitrogen and phosphorus did not substantially alter during the incubation period, indicating that nutrient limitation did not differ between in situ and in vitro incubations. Despite continuous circulation of surface water to keep the BOD bottles at ambient surface-water temperature during incubation, this may have been challenging during summer when air temperatures considerably exceeded surface-water temperatures. Temperature was reasonably constant in the photic zone (max. ~2°C difference between the top and bottom of the photic zone), indicating that keeping all incubations at surface-water temperature is not likely to have substantially affected our estimate of GPP_{O_2}. Furthermore, we acknowledge that light climate during incubations may not have reflected in situ conditions properly, as neighbouring bottles may have influenced each other, thereby decreasing the amount of incoming light. This may have affected our fit of the Eilers-Peeters parameters and, as a result, led to an underestimation of GPP_{O_2}. Finally, the estimate of GPP_{O_2} is dependent on the rate of nitrification, the oxidation of NH_4^+ to NO_3^-. In this method, CR is assumed to equal total oxygen consumption, while part of the O_2 may also be consumed via nitrification. In the nearby Western Scheldt estuary, nitrification was found to comprise up to ~70% of total oxygen consumption, thus significantly decreasing estimates of CR and, as a consequence, GPP_{O_2} (Gazeau et al., 2007a). In the Den Osse basin, nitrification was modelled based on $[NH_4^+]$ and $[O_2]$ rather than measured, and it was found to comprise 0.00-44.1% of total oxygen consumption in the upper 10 m of the water column between March and November (Hagens et al., 2015). However, nitrification never exceeded 6% of photic-zone total oxygen consumption between March and August. Thus, we may conclude that ignoring the contribution of nitrification to the change in $[O_2]$ may have led to a substantial overestimation of GPP_{O_2} only in autumn.

Since the in situ method resolves a depth-integrated estimate of PP, an accurate depth integration of the in vitro method is required for a proper comparison between both oxygen-based methods. Each month, samples for estimating GPP_{O_2} were taken from 8 different depths and 10 light regimes were simulated corresponding to these depths. This is in line with the range suggested by Cloern et al. (2014) necessary for an accurate depth integration of GPP, indicating that this procedure most likely does not contribute to the uncertainty associated with the in vitro method.

In situ oxygen-based methods rely on accurate estimations of (variability in) LPD, mixed layer depth (Duarte et al., 2013b), air-sea O_2 gas exchange (Tobias et al., 2009) and transport processes

(Swaney et al., 1999). In the Den Osse basin in 2012, the water column was well mixed except from May – August. Within this period, the mixed layer seemed to shallow over time to ~10 m in August (Hagens et al., 2015). Since mixed layer depth exceeded LPD throughout the year, this did not seem to influence the estimate of $\overline{GPP(t)}$. However, mixed layer depth might have varied during the period of sensor deployment, thereby affecting $\overline{GPP(t)}$. The Den Osse basin was not found to be very turbulent; hence, we do not expect that uncertainty in quantifying turbulence may have impacted $\overline{GPP(t)}$. What could have severely affected $\overline{GPP(t)}$, however, are lateral transport processes. A previous estimate has shown that the water of the Den Osse basin could be fully renewed by inflowing sluice water in ca. 30 days (Hagens et al., 2015), which is 4-5 times longer than sensor deployment time. Since most of Lake Grevelingen is much shallower than the Den Osse basin, implying both smaller depth-integrated respiration rates and the possible presence of benthic primary production, the oxygen signal measured in the Den Osse basin might be influenced by one or both of these ex situ processes. Moreover, uncertainty may be added as the period of sensor deployment was relatively short compared to what is considered necessary for an accurate estimate of $\overline{GPP(t)}$ (Robinson and Williams, 2005; Cox et al., 2014), although other studies have used a similar deployment time (Hanson et al., 2008).

Finally, another major assumption of both in situ and in vitro O_2-based methods is that they assume no difference between light and dark respiration. While some studies have found no significant difference between CR in the light and in the dark (González et al., 2008; Marra and Barber, 2004), others have found either higher (Harris and Lott, 1973) or lower (Grande et al., 1989) light than dark respiration. If respiration were enhanced in the light, this would mean that the rates of both GPP_{O_2} and $\overline{GPP(t)}$ would be underestimated.

3.4.4 Carbon versus oxygen-based methods

Since rates of GPP are commonly expressed in C units, both in situ and in vitro O_2-based methods require that the oxygen is converted to carbon units. The value of PQ has, however, been subject of debate. For rapidly growing phytoplankton it has been estimated at ~1.25 when NH_4^+ is used as N source and $1.5 - 1.8$ if NO_3^- fuels GPP (Williams et al., 1979). These values are higher than the values used by Gazeau et al. (2007) and in this study, which were calculated from stoichiometric reaction equations using the Redfield ratio. A higher PQ during NO_3^- uptake may indicate a C:N ratio lower than Redfield. Furthermore, PQ will be reduced if dissolved organic nitrogen, which importance as N source for growth has been demonstrated before (Veuger et al., 2004), fuels primary production, or if oxidised organic compounds such as acids are produced. To indicate the importance of PQ, we take the high-resolution in situ O_2 measurements as an example. If we were to use a PQ of 1.25 for March and 1.8 for August, i.e. the range of Williams et al. (1979), we would end up with values for $\overline{GPP(t)}$ of 141 and 251 mmol C m^{-2} d^{-1}, respectively. While the March estimate would still be much higher than the estimates of the other methods, the August estimate now well overlaps with GPP_{14C}.

Moreover, for the calculations of GPP_{O_2} and GPP_{14C} it is more important to get a higher precision in the Chl *a* depth profiles than more accurate values of Chl *a*, since in both procedures measured values were always normalised to Chl *a* before performing the Eilers-Peeters fit. In the subsequent

depth interpolation at 10 cm intervals, values were multiplied with the Chl *a* concentration, highlighting the need for precise depth profiles as obtained with CTD probing. This is the main reason why we deliberately chose to use Chl *a* derived from the CTD probing rather than Chl *a* determined using HPLC for the biomass and GPP calculations. Despite its well-known lower accuracy and the fact that CTD-derived Chl *a* is usually regarded as total chlorophyll, i.e. comprising not only Chl *a* but also other chlorophyll pigments and their precursors and breakdown products, we felt it better reflected both the spatial and temporal biomass patterns.

Our estimate of GPP_{14C} might underestimate total C assimilation since we only investigated assimilation into particulate matter, while production of dissolved organic compounds may also comprise a substantial fraction of the TOC production, in particular in oligotrophic systems (Karl et al., 1998; González et al., 2008). For the nearby-located Western Scheldt estuary, Gazeau et al. (2007) found that DOC production was < 10% of the total C assimilation except for the most upstream station, suggesting it might also not be of importance in the Den Osse basin. However, given the noticeable increase in surface-water DOC in the Den Osse basin from May – September (Fig. 3.1e), we cannot assume that DOC production is insignificant. We therefore conclude that during this period, GPP_{14C} may have underestimated total C assimilation.

Furthermore, incubation periods between the GPP_{14C} and GPP_{O2} varied substantially, i.e. 2 h and 5-13 h, the latter depending on the time of sampling and the photoperiod. Short incubation periods for carbon-based methods are generally acknowledged to represent GPP, based on the premise that photosynthesis far exceeds respiration (Marra, 2002; Williams and Lefevre, 1996; Weger et al., 1989). In a population with a high specific growth rate, implying fast turnover of the C pool, substantial respiration of the added ^{14}C may already take place within 2 hours. In this case, the method may underestimate GPP and rather represent NPP. The oxygen light-dark method is less sensitive to the incubation period, although it should be long enough to measure a significant difference in $[O_2]$.

To further test the relation between GPP_{O2} and GPP_{14C}, we applied the conversion equation of Regaudie-de-Gioux et al. (2014) to test if our GPP_{O2} measurements can be readily predicted from our GPP_{14C} estimates. Although this equation, which is $GPP_{O2} = 8.585\,GPP_{14C}^{0.76}$, is based on volumetric GPP rates, we applied it on the depth-integrated rates. Since both rates were depth-integrated in exactly the same way, we believe this is a valid approach. This conversion leads to predicted values for GPP_{O2} of 70.0, 201, 612 and 25.1 mmol O_2 m^{-2} d^{-1}. In contrast, the measured rates were 30.9, 17.3, 175.5 and 14.4 mmol O_2 m^{-2} d^{-1}, which is 8.6 – 57.3% of the predicted values. The equations of Regaudie-de-Gioux et al. (2014) were fitted on open-ocean estimates, with GPP mostly below 10 mmol C m^{-3} d^{-1} and never exceeding 100 mmol C m^{-3} d^{-1}. In the Den Osse basin, however, GPP went up to 150.7 mmol C m^{-3} d^{-1}, indicating that it falls outside the range of GPP values used to construct the conversion equations, thereby questioning their validity for a coastal, highly productive setting. On the contrary, their slope of the log-transformed data was significantly different from 1 (P < 0.0001) and smaller than 1. This indicates that the ratio of GPP_{O2} to GPP_{14C} significantly decreases when GPP_{14C} increases, which is in line with our results. Thus, although the relation proposed by Regaudie-de-Gioux et al. (2014) shows the same general trend between

GPP$_{14C}$ and GPP$_{O2}$ as observed in this work, we cannot use their open ocean-based equation for a direct conversion.

3.4.5 GPP linked to species dynamics

One question we would like to address is how estimates of total GPP are linked to species activity. To this end, we assessed not only species biomass but also quantified growth, both as turnover rates (μ) and as C assimilation rates (GPP$_{PLFA}$). Both of these quantifications have two major uncertainties associated with them.

First, we assigned specific PLFA to specific algal classes, while in fact most PLFA are not species- or even class-specific. For example, Cryptophyceae lack unique PLFA biomarkers (Dijkman and Kromkamp, 2006), which is the main reason why we did not include them as a separate group in our analysis of PLFA-based biomass, μ and GPP$_{PLFA}$. PLFA-based phytoplankton biomass using BCE (Fig. 3.3c), which includes all PLFA abundant in a certain group, revealed however that Cryptophyceae were the most dominant group in terms of biomass in August. The most important PLFA in Cryptophyceae are 18:3ω3, 18:4ω3, 20:5ω3 and 22:6ω3 (Dijkman and Kromkamp, 2006). It is therefore well possible that part of what we quantified as diatoms or green algae may in fact be Cryptophyceae. From this it also follows that the PLFA assigned as characteristic to a specific group appear in other groups as well, thereby posing an uncertainty to our distinction between groups. The most general explanation for this is that certain PLFA act as intermediates in metabolic pathways synthesising other PLFA (Dijkman et al., 2009). For example, 16:3ω3 may act as an intermediate towards 16:4ω3 (Bergé and Barnathan, 2005). Since we used both PLFA as biomarkers for green algae, this will not affect our group attribution. The formation of the diatom-specific 20:5ω3, on the contrary, was found to involve many intermediates (Arao and Yamada, 1994), such as 20:4ω6 which we also treated as diatom-specific, but also 18:3w3 which we attributed to green algae. Another reason is that certain groups share PLFA because of a common evolutionary history. This has been suggested as the reason why the PLFA 18:5ω3(12-15), which we attributed to dinoflagellates, was characterised as specific not only for photosynthetic dinoflagellates but also for certain haptophytes (Okuyama et al., 1993).

Second, we assume that the incubation period is long enough to represent growth, but, similar to the GPP$_{14C}$ method, short enough not to take into account respiration of labelled C. A study by Dijkman et al. (2009) showed that the increase in δ^{13}C of PLFA was linearly correlated with time for incubation periods of up to 8 hours, suggesting that this is the upper limit of incubation time. Moreover, this study showed that, even though it takes > 24 hours before PLFA and POC are equally labelled, the ratio between labelling of PLFA 16:0 and POC within this period is constant, implying that we can compare GPP$_{PLFA}$ and GPP$_{14C}$. Finally, it was shown that the slope of the increase in δ^{13}C varies per PLFA and per species, with shorter PLFA generally showing a faster labelling than longer PLFA. The authors attributed this to fast-labelled PLFA being first intermediates in pathways, which not only affect group attribution as discussed above, but also our estimate of growth rates.

Turnover or specific growth rates are regarded as a measure for phytoplankton dynamics. They do not, however, include the contribution of that phytoplankton group to the total C assimilation. For example, in the Den Osse basin we found that green algae have high specific growth rates, in line with previous work (de Kluijver et al., 2010). However, because of their low biomass (Fig. 3.4a), their contribution to GPP_{PLFA} is low. In addition, the PLFA on which green algal biomass is based ($16:3\omega3$, $16:4\omega3$ and $18:3\omega3$) are among the first to be synthesised in marine algae (Bergé and Barnathan, 2005) and may be transformed into other PLFA as discussed above.

While the specific growth rate μ is independent of conversion factors, this does not apply for the estimates of PLFA-based biomass and GPP_{PLFA}, which rely on the conversion from PLFA (μg C L^{-1}) to biomass (mg C L^{-1}). The importance of this conversion can most clearly be observed in the dinoflagellate (and in some cases *P. globosa*) biomass and GPP_{PLFA}. These values were generally higher than the numbers for total phytoplankton biomass, while this is obviously not possible. The PLFA-to-organic C ratios derived by Dijkman and Kromkamp (2006) are based on cultured organisms, which were partly obtained from culture collections and partly from the Western Scheldt estuary. They may therefore not be fully representative for the Lake Grevelingen field population, but they are the best numbers available. Rather than tweaking the ratios based on our field data, we have chosen to present the PLFA-derived biomass and GPP_{PLFA} data as they are, thereby taking into account their uncertainties.

Given all issues and uncertainties discussed above, thereby including the relatively simple approach we used for the depth integration of GPP_{PLFA}, we may conclude that total phytoplankton GPP_{PLFA} is comparable with the estimates of the three other methods used for quantifying GPP and well captures the seasonal trend. While GPP_{O2} may be expected to deviate from both GPP_{14C} and GPP_{PLFA} due to differences in currency and associated uncertainties, it is more surprising that GPP_{14C} and GPP_{PLFA} differ even more from each other. This can at least partly be explained by recalling that the PLFA-derived total biomass (Fig. 3.3b) is lower than the dinoflagellate biomass (Fig. 3.3a), indicating again that the conversion from PLFA to organic C might need better constraints. The finding that GPP_{O2} is significantly higher than GPP_{PLFA} is consistent with a previous study (Tanaka et al., 2013); however, during that study GPP_{14C} measured on TOC was always higher than both GPP_{O2} and GPP_{PLFA} (Tanaka et al., 2013; Engel et al., 2013). In our study this is not found, but we have only considered GPP_{14C} measured on POC.

3.4.6 Species biomass and dynamics

In case of the biomass calculations, such as the conversion from Chl *a* to C biomass, using CTD-Chl *a* adds to the uncertainty in, e.g. the applicability of a fixed C:Chl *a* ratio. Furthermore, the use of both Chl *a* and POC as a proxy for biomass has often been subject of debate (e.g. Le Floc'h et al., 2002; Sobczak et al., 2002). There is, however, always uncertainty associated with the use of any kind of conversion factors, as discussed above in the conversion from μg C L^{-1} PLFA to mg C L^{-1} biomass. As long as these uncertainties are kept in mind, the current study provides very valuable data on biomass dynamics in the Den Osse basin in 2012.

Long-term monitoring in the surface water of the Dreischor basin indicated that from 1990 – 2008 Chl *a* concentrations usually varied between 0.1 and 20 µg L^{-1}, with some years having peaks around 30 – 40 µg L^{-1} (Wetsteyn, 2011), and annual averages varying between 2.5 and 9.0 µg L^{-1}. These values are in line with our observations, which showed an annually averaged CTD-derived Chl *a* of 6.0 µg L^{-1}. Microscopic observations of phytoplankton presented in this study indicated that during these two decades high cell counts of both diatoms and dinoflagellates could occur both in spring and summer. This lack of a clear seasonal succession of species is in line with our PLFA-based biomass observations (Fig. 3.4a), although we did observe that diatoms peaked later in the summer than dinoflagellates. The BCE runs (Fig. 3.3) revealed a dynamic phytoplankton community over the summer. However, both the pigment and PLFA-based community composition indicated that the Cryptophyceae, rather than the Bacillariophyceae to which diatoms belong, peaked in August. Differences in group abundances between the PLFA-based biomass estimates and the BCE runs stem partly from the fact that in the BCE, PLFA are not added as unique biomarkers, while they are used as such in the group-specific estimates of biomass and GPP$_{PLFA}$. Moreover, phytoplankton compositions estimated using BCE, or a matrix factorisation program like CHEMTAX, are very dependent on the input ratio matrices and should be regionally adapted, as has been extensively discussed before (Mackey et al., 1996; Dijkman and Kromkamp, 2006). We used the input ratios based on data from the mouth of the nearby-located Western Scheldt estuary (Table 3 of Dijkman and Kromkamp (2006), salinity 28). However, due to its distinct flow patterns and nutrient regime, Lake Grevelingen might have a somewhat different community. Additionally, since Cryptophyceae lack unique PLFA biomarkers, this group is particularly sensitive to changes in the fitting algorithm, such as analysing the data as depth-averaged values rather than separated per depth or per incubation (Dijkman and Kromkamp, 2006). In this study we ran the BCE on both the pigment and PLFA data for each month separately, thus allowing for temporal variation in the input ratio matrix. Since the high abundance of Cryptophyceae in August is not only observed in the PLFA but also in the pigment data, which have alloxanthin as diagnostic biomarker, we believe this trend is real.

A striking difference between the data presented in Fig. 3.4 and the data in Wetsteyn (2011) is that he found that peaks in diatom cell counts were substantially higher than dinoflagellate peaks. Their findings are in line with our pigment-based phytoplankton composition as determined from the BCE (Figs. 3.3a-b). Moreover, using pigment data this diatom dominance has also been observed in 9 European estuaries, among which was the nearby-located Western Scheldt estuary (Lemaire et al., 2002). One possible explanation for this discrepancy between PLFA-based data and the other methods is the uncertainty in the conversion from PLFA (µg L^{-1}) to biomass (mg C L^{-1}) as discussed before. The fact that also the PLFA-based phytoplankton composition (Fig. 3.4c) does not display a dominance of the Bacillariophyceae may be due to the previously discussed uncertainties in the input ratio matrix, or may be a result of the fact that we averaged the data with depth to be consistent with the other PLFA-based estimates.

Among the other species described by Wetsteyn (2011) in the Dreischor basin are Cryptophyceae and green algae, which presence has also been indicated in this study by both pigment and PLFA observations. The presence of *P. globosa* is not specifically mentioned. However, their blooms develop

in spring in the coastal zone of the North Sea (Peperzak and Poelman, 2008; Wetsteyn, 2011) and reach Lake Grevelingen through lateral transport. The Den Osse basin is located more closely to the seaward sluice than the Dreischor basin, indicating that it is likely to be affected more severely by lateral transport processes. As mentioned before, the residence time of water in the Den Osse basin is ~30 days, while Lake Grevelingen water residence time has been estimated at 229 days (Meijers and Groot, 2007). This indicates the potential importance of lateral transport on the Den Osse basin.

3.5   Summary and conclusions

We showed that consistent estimates of GPP in a eutrophic coastal marine basin can be obtained with the in situ high-resolution O_2 sensor deployment, the in vitro oxygen light-dark method and the assimilation of ^{14}C into POC. In the two periods of sensor deployment, this in situ method displayed the highest estimates of GPP, while the ratio of GPP_{14C}:GPP_{O2} increased with higher productivity. GPP_{PLFA} was significantly lower than GPP_{O2} but showed the same unimodal seasonal pattern, with highest productivity in summer. Biomarkers for algal biomass (pigments and PLFA) showed a marked transition in species composition between the two months of highest GPP. While dinoflagellates were dominant in July, as also observed by microscopy, diatoms and Cryptophyceae made up most of the algal biomass in August. Group-specific growth rates showed that, despite green algae having the highest specific growth rate, dinoflagellates and *P. globosa* contribute most to GPP because of their higher biomass. The absence of a clear link between variations in species composition and activity and differences between the various methods quantifying GPP indicates that other factors may be more important in driving these differences.

Acknowledgements

Chapter 4:

Biogeochemical context impacts seawater pH changes resulting from atmospheric sulphur and nitrogen deposition

"For most of history, man has had to fight nature to survive; in this century he is beginning to realise that, in order to survive, he must protect it."

Jacques-Yves Cousteau

Abstract

Seawater acidification can be induced both by absorption of atmospheric carbon dioxide (CO_2) and by atmospheric deposition of sulphur and nitrogen oxides and ammonia. Their relative significance, interplay, and dependency on water-column biogeochemistry are not well understood. Using a simple biogeochemical model we show that the initial conditions of coastal systems are not only relevant for CO_2-induced acidification but also for additional acidification due to atmospheric acid deposition. Coastal areas undersaturated with respect to CO_2 are most vulnerable to CO_2-induced acidification but are relatively least affected by additional atmospheric deposition-induced acidification. In contrast, the pH of CO_2-supersaturated systems is most sensitive to atmospheric deposition. The projected increment in atmospheric CO_2 by 2100 will increase the sensitivity of coastal systems to atmospheric deposition-induced acidification by up to a factor 4, but the additional annual change in proton concentration is at most 28%.

4.1 Introduction

Combustion of biomass and fossil fuels releases SO_x and NO_x to the atmosphere. Due to the short (i.e. ~1 week) residence time of atmospheric sulphur (S) and nitrogen (N) oxides, their deposition in the marine realm occurs mainly in coastal areas downwind of the principal terrestrial source regions (Rodhe et al., 2002) and in waters with intensive shipping (Tsyro and Berge, 1997). In marine systems, atmospheric S and N oxides eventually end up as H_2SO_4 and HNO_3, either through chemical alterations in the atmosphere and wet deposition of H_2SO_4 and HNO_3, or through dry deposition of SO_x and NO_x and subsequent fast hydration in the seawater (Doney et al., 2007). Absorption of S and N oxides by seawater thus causes a decrease in total alkalinity (TA) and hence a lowering in pH, whereby the effect of S oxide deposition on TA is twice as high as the effect of N oxide deposition (Doney et al., 2007; Hunter et al., 2011).

Ammonia (NH_3) emissions originate mostly from animal husbandry, as well as fertiliser use, and its deposition to marine systems causes an increase in TA and hence a rise in pH. However, in the atmosphere NH_3 can be transformed to acidic N through various processes (Dentener and Crutzen, 1994) and when any of the deposited NH_3 is nitrified, the alkaline flux effectively changes to an acidity flux with the same stoichiometry as N oxide deposition (Doney et al., 2007; Hunter et al., 2011).

While acidification of terrestrial and freshwater systems due to atmospheric deposition has been investigated for decades (Schindler, 1988), there are very few studies explicitly dealing with the effects of atmospheric deposition on seawater pH. Seawater acidification induced by absorption of CO_2 and by atmospheric deposition co-occur, but their relative importance and interactions (synergistic or antagonistic) have been poorly documented. Using time series of rainfall and seawater CO_2 parameters in the North Atlantic Ocean near Bermuda, Bates and Peters (2007) showed that wet deposition of acids contributes at most 2-5% to surface water acidification. By coupling a biogeochemical model to a global circulation model, Doney et al. (2007) found a similar magnitude of the contribution of anthropogenic S and N deposition to surface water acidification, but they calculated changes in carbonate chemistry as high as 10-50% of the CO_2-induced changes close to source regions and in shallow seas. Hunter et al. (2011) focused on three coastal seas and reported that atmospheric inputs of strong acids compensate the CO_2-induced acidification. This implies that ocean acidification trajectories based on CO_2 absorption alone provide an incomplete, biased picture. Hassellöv et al. (2013) focused on global acidification due to shipping activities and found that in certain coastal hot spots shipping-based acidification can be of the same order of magnitude as CO_2-induced acidification.

Although the three modelling studies (Doney et al., 2007; Hunter et al., 2011; Hassellöv et al., 2013) used a similar approach, their estimated contribution of atmospheric deposition to ocean acidification varies from negligible to substantial. This is due to differences in the systems and processes considered and in the way the effects of atmospheric S and N deposition on seawater pH are quantified. Here we use a simple model to identify key factors and to explain the effect of different initial conditions on the additive pH change due to atmospheric acid deposition.

4.2 Methodological considerations

4.2.1 The fraction of atmospheric NH₃ deposition that will be nitrified

The fraction of deposited NH_3 that is nitrified is highly relevant for the calculated changes in TA and pH (Doney et al., 2007; Hunter et al., 2011). As this fraction is poorly known, likely variable, and time scale dependent, these studies considered the two extreme cases (i.e. zero and complete nitrification of the deposited NH_3). Including biological feedbacks resulting from enhanced N availability, which may especially be of importance in N-limited coastal marine ecosystems, Doney et al. (2007) found that globally approximately 98% of the deposited NH_3 will be nitrified over a time span of 10 years.

For studies focussing on the seasonal to interannual scales, we propose to use the parameterisation by Yool et al. (2007) who, based on a compilation of a global data set, suggested a mean specific nitrification rate of 0.2 d^{-1}. If we include their lower (0.02 d^{-1}) and upper (2 d^{-1}) limits and convert to percentages of ammonia being used for nitrification, this leads to values of 43, 16, and 81%, respectively, of which the lower estimate is close to the 15% suggested by Middelburg and Soetaert (2004) for the North Sea.

4.2.2 Open versus closed system calculations

So far, modelling studies have adopted different strategies to calculate the effect of atmospheric deposition on seawater pCO_2 ($pCO_{2,sw}$) and thus acidification:

1. Hunter et al. (2011), in four of their scenarios ("CO_2+SO_x", "$CO_2+SO_x+NO_x$", "$CO_2+SO_x+NO_x+NH_3$" and "after nitrification"), and Hassellöv et al. (2013) did not allow re-equilibration of $pCO_{2,sw}$ with the atmosphere (closed system).
2. In their "after buffering" scenarios, Hunter et al. (2011) restored $pCO_{2,sw}$ values to their original values, i.e. full re-equilibration of $pCO_{2,sw}$ with the atmosphere (open system).
3. Doney et al. (2007) dynamically calculated $pCO_{2,sw}$ values at each time step taking CO_2 equilibration and atmospheric deposition into account.

The first approach, which neglects air-sea exchange of CO_2, is limited to the additive effect of atmospheric CO_2 uptake and acid deposition and results in too much acidification. The second approach restores $pCO_{2,sw}$ values and in this way numerically generates CO_2 effluxes that modulate the decrease in pH. The third approach, in contrast, allows for simultaneous calculation of all processes, thus producing the most accurate $pCO_{2,sw}$ values. However, the choice for a specific approach highly depends on the time scale of the study. Doney et al. (2007) looked at annual changes in a time span of 10 years using small time steps, highlighting the need for an iteratively determined $pCO_{2,sw}$. Hunter et al. (2011) considered 1 year, an interval in which $pCO_{2,sw}$ may be assumed to be in equilibrium with atmospheric pCO_2 ($pCO_{2,atm}$). However, Hassellöv et al. (2013) used monthly intervals over a 1 year period where $pCO_{2,sw}$ was updated using measured rather than calculated data. This approach led to an overestimation of the calculated total surface water acidification in CO_2-supersaturated systems.

4.2.3 Supersaturated versus undersaturated systems

In natural systems, $pCO_{2,sw}$ can be out of equilibrium with $pCO_{2,atm}$ (Takahashi et al., 2009), either seasonally due to biological activity and/or temperature effects, or more permanently as a result of their hydrodynamic setting. The time scale on which $pCO_{2,sw}$ equilibrates with the atmosphere (approximately weeks) is long compared to the residence time of atmospheric S and N oxides (approximately days), indicating the potential for atmospheric deposition to influence the equilibration process. The decrease in TA caused by atmospheric S and N deposition and associated increase in $pCO_{2,sw}$ will have different effects on CO_2-supersaturated and undersaturated systems. The direction and rate of CO_2 air-sea exchange are thus key to accurate projection of seawater acidification. We illustrate this with a simple case study.

A comparison is made of three systems which have the same TA, salinity, and temperature but differ in their initial $pCO_{2,sw}$. System one is initially in equilibrium with $pCO_{2,atm}$. In the second, undersaturated system 11.5 µmol kg^{-1} yr^{-1} of dissolved inorganic carbon (DIC) is removed by biological processes, resulting in an initial $pCO_{2,sw}$ of 250 ppmv. The third, supersaturated system has an initial $pCO_{2,sw}$ of 600 ppmv, corresponding to a net DIC production of 17.4 µmol kg^{-1} yr^{-1}. Using a time step of 1 year, we calculated the net effect on $pCO_{2,sw}$ and pH of (1) a constant acid deposition flux where either zero or complete nitrification of the deposited NH_3 results in a TA decrease of 1.34 and 3.94 µmol kg^{-1} yr^{-1}, respectively, and (2) increasing $pCO_{2,atm}$ to 936 ppmv in 2100 according to the output of the highest Representative Concentration Pathway, RCP8.5 (Meinshausen et al., 2011). Air-sea exchange of CO_2 was calculated using a simple kinetic rate law

$$R = k\,(CO_2^{sat} - [CO_2]) \tag{1}$$

with a rate constant k of 2 yr^{-1}, so that there was incomplete equilibration with the atmosphere.

All three systems show an increase in $pCO_{2,sw}$ and a decrease in pH (Fig. 4.1). Atmospheric deposition causes further decreases in pH, because the additional lowering in TA reduces the capacity of the system to buffer changes. Consistent with Doney et al. (2007) and Hunter et al. (2011), nitrification of atmospheric NH_3 leads to lower pH values.

The sensitivity toward ocean acidification and the interaction with atmospheric deposition depend on the biogeochemical context, i.e. the biological (or physical) processes adding or removing DIC, moderated by CO_2 air-sea exchange. The undersaturated system is most sensitive to CO_2-induced acidification (ΔpH is -0.431), as the enhanced gradient between $pCO_{2,atm}$ and $pCO_{2,sw}$ increases the CO_2 influx. Atmospheric deposition, however, lowers this CO_2 gradient, resulting in a reduced influx. As a result, this system is relatively least vulnerable to atmospheric deposition (additional decrease in proton concentration ($[H^+]$) of 11.5% and 38.0% excluding and including nitrification, respectively). The reverse holds for the supersaturated system, where the CO_2-induced ΔpH is -0.255. Here a higher $pCO_{2,sw}$ resulting from atmospheric deposition increases the gradient between $pCO_{2,sw}$ and $pCO_{2,atm}$ and thus leads to a higher CO_2 efflux, i.e. it is more perturbed. This results in a relatively higher additive $[H^+]$ decrease of 14.4% and 47.8% excluding and including nitrification, respectively.

4.2.4 Model description

Based on the discussion above, we extended the model of Hunter et al. (2011). Rather than assuming two extreme scenarios for nitrification and outgassing of CO_2 to the atmosphere (zero versus complete), we implemented kinetic descriptions for both processes: the Yool et al. (2007) parameterisation for nitrification (Sect. 4.2.1) and a simple air-sea exchange expression

$$R_{exch} = k_d (CO_2^{sat} - [CO_2]) \tag{2}$$

with a transfer velocity k_d of 2.7 m d^{-1}, which corresponds to a wind speed of 7.6 m s^{-1} (Liss and Merlivat, 1986), within the range of median wind speeds for the European coastal zone (Gazeau et al., 2004). The model was run until the end of the 21st century assuming that atmospheric deposition fluxes remain constant within this time period and the increase in $pCO_{2,atm}$ follows the RCP8.5 scenario. Horizontal advection and exchanges with the deep water were not taken into account. Finally, in addition to the southern North Sea, Baltic Sea and South China Sea case studies presented by Hunter et al. (2011), we included the north-western (NW) Mediterranean Sea as a fourth case study (for parameterisation see Table 4.S1 in the supporting information).

We calculated the evolution of pH using the explicit pH modelling approach of Hofmann et al. (2010a) (see supporting information for extensive explanation). Briefly, the main advantage of this approach is that changes in pH can be directly attributed to the different processes affecting pH:

$$\frac{d[H^+]_p}{dt} = S_p R_p \tag{3}$$
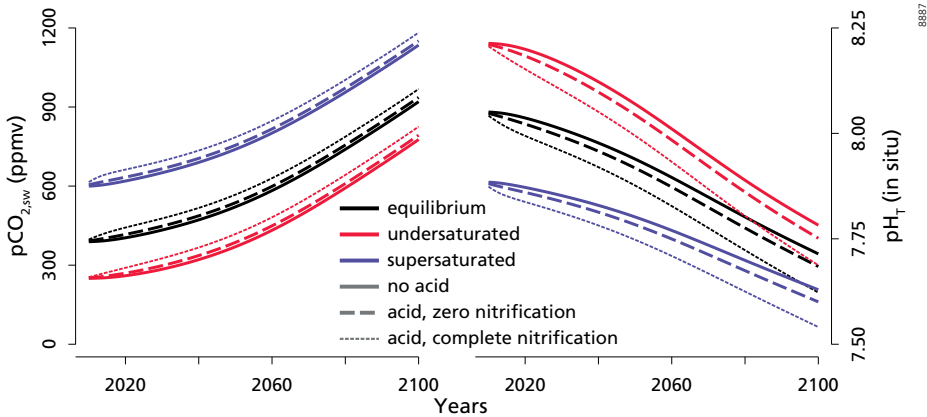
Figure 4.1 Different effects of atmospheric deposition and $pCO_{2,atm}$ increase on a supersaturated and an undersaturated system. Initial conditions: TA = 2260 µmol kg^{-1}, S = 34, T = 12°C, and $pCO_{2,sw}$ = 389 ppmv (equilibrated system), 250 ppmv (undersaturated system), or 600 ppmv (supersaturated system). The increase in $pCO_{2,atm}$ was taken from the RCP8.5 scenario. Acid deposition leads to a decrease in TA of 1.34 (no nitrification) or 3.94 µmol kg^{-1} yr^{-1} (complete nitrification). pH on total scale, equilibrium constants of Mehrbach et al. (1973) as refitted by Dickson and Millero (1987).

Here, R_p is the rate of a process p (mol kg^{-1} yr^{-1}) and sensitivity (S_p) is defined as the ratio of a stoichiometric coefficient for the proton in the reaction ($v_{H^+}^p$) and a buffer factor (β):

$$S_p = \frac{v_{H^+}^p}{\beta} \qquad (4)$$

The buffer factor is defined as:

$$\beta = -\left(\frac{\partial TA}{\partial [H^+]}\right) \qquad (5)$$

This way, all processes affecting pH can be included simultaneously while their individual contribution can still be extracted. All calculations were performed on the total pH scale using the R packages *AquaEnv* (Hofmann et al., 2010b) and *deSolve* (Soetaert et al., 2010) with a time step of 1 year, using the equilibrium constants of Mehrbach et al. (1973) as refitted by Dickson and Millero [1987] for the carbonate system and of Dickson (1990) for sulphate.

4.3 Results

With 43% of the atmospheric NH_3 being nitrified ΔpH is smallest (-0.336) in the NW Mediterranean Sea and largest (-0.386) in the southern North Sea (Fig. 4.2a). The latter coastal system is also most sensitive to changes in the fraction of atmospheric NH_3 deposition that is nitrified. With 16% nitrification the total pH decrease for the North Sea is 0.0128 smaller, while pH decreases by an additional 0.0187 with a fraction of 81%. For the South China Sea these numbers are slightly lower, while for the other two seas varying the degree of nitrification leads to a negligible change in the total acidification (data not shown). Comparing our results with model runs with CO_2-induced acidification only (Fig. 4.2b), we see that the additive ΔpH due to atmospheric acid deposition is also highest (0.0430 until 2100) in the southern North Sea. The contribution of acid deposition is smallest in the NW Mediterranean Sea (0.0006 additional pH decrease until 2100), probably due to its deep mixed layer and high buffering capacity (Fig. 4.2f).

The contribution of the processes involved in proton cycling to the net change in [H$^+$] is shown for the southern North Sea in Fig. 4.2c. The net change (grey line) increases with time until 2071, after which it slows down. The magnitude of [H$^+$] change induced by each process increases with time. Atmospheric acid deposition rates are constant, so the increase in $\frac{d[H^+]}{dt}$ with time can be attributed directly to increased sensitivity (S_p). Air-sea exchange of CO_2 (R_{exch}), however, does not remain constant (Fig. 4.2e) since both atmospheric and seawater CO_2 change with time. This explains why the relative contribution of CO_2 air-sea exchange to acid deposition first decreases and then increases with time (Fig. 4.2c), following the trend in R_{exch} (Fig. 4.2e). However, the absolute value of [H$^+$] change is primarily controlled by the increase of S_{exch} (Fig. 4.2d) rather than changes in R_{exch}.

Using CO_2 air-sea exchange as an example, we show that changes in sensitivity predominantly result from changes in the buffering capacity. The stoichiometric coefficient for the proton $v_{H^+}^{exch}$

decreases slightly until 2100, ranging from 3.9% in the Baltic Sea to 5.8% in the South China Sea (Fig. 4.2d). Changes in the stoichiometric coefficient for the proton of nitrification ($\nu_{H^+}^{nitr}$) are even
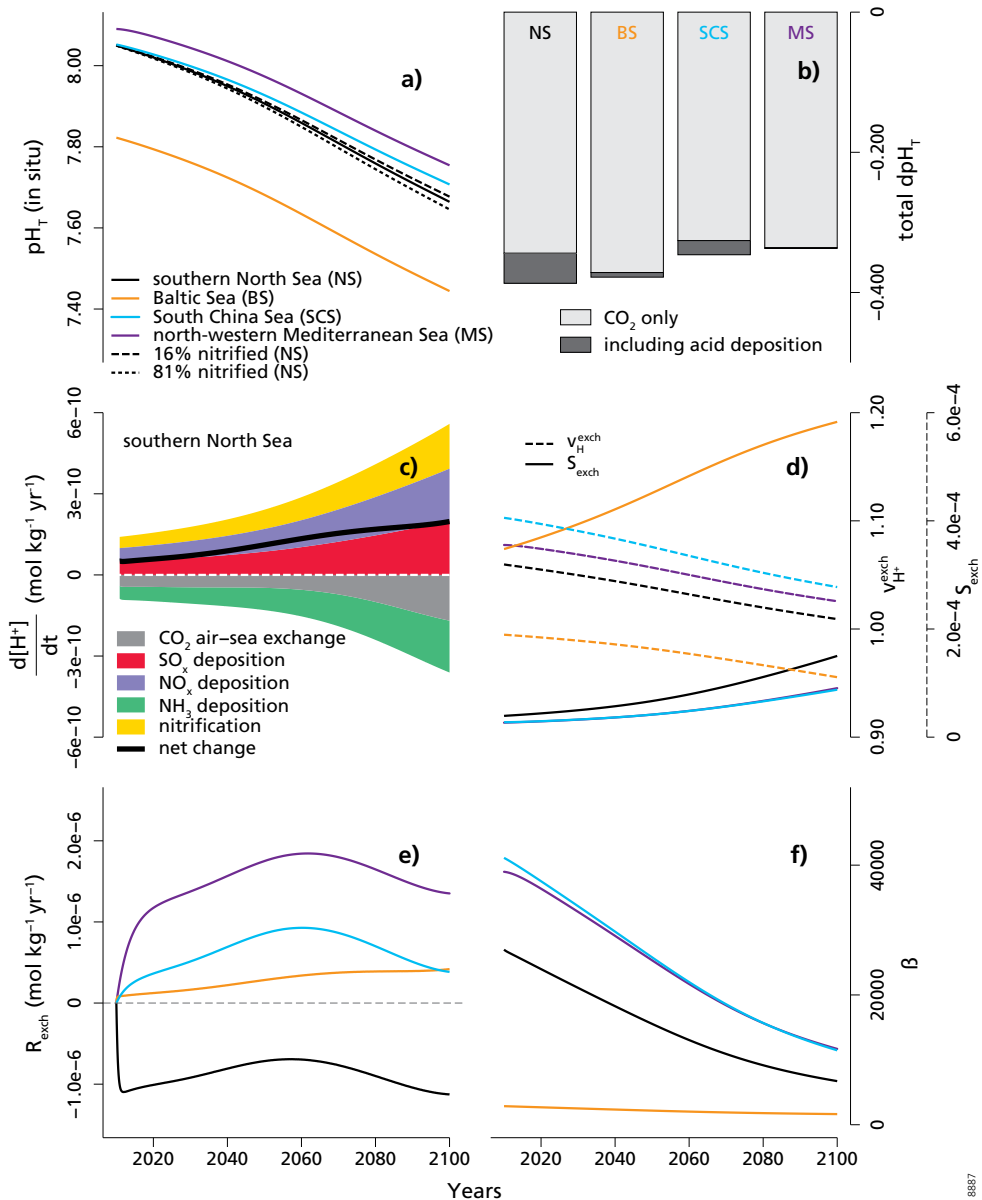

Figure 4.2 Model output for the four different coastal seas using a constant acid deposition flux, 43% nitrification of NH_3 input and the RCP8.5 scenario for $pCO_{2,atm}$. (a) pH_T at in situ temperature, (b) total ΔpH_T without and with acid deposition, (c) contribution of separate processes to net $[H^+]$ change in southern North Sea, (d) sensitivity (S_{exch}) and stoichiometric proton coefficient ($\nu_{H^+}^{exch}$) of CO_2 air-sea exchange, (e) uncorrected contribution of CO_2 air-sea exchange to proton balance (R_{exch}), and (f) buffering capacity (β).

smaller because the equilibrium constant of the NH_4^+ / NH_3 acid-base pair is far from the range of pH considered here. The buffer factor β decreases by 57% in the Baltic Sea and roughly fourfold in the southern North Sea (Fig. 4.2f). The fourfold decrease in buffering (β) by the end of the 21st century combined with minor changes in stoichiometric coefficients for the proton ($v_{H^+}^p$) means that the southern North Sea becomes about 4 times more sensitive to any process involving proton transfer. Differences in buffering capacity also explain why the Baltic Sea is the most sensitive and the South China Sea and NW Mediterranean Sea least sensitive to processes consuming or producing protons, as β is inversely related to S_p (Eq. (5)).

Increasing $pCO_{2,atm}$ is by far the most important process contributing to the total change in pH (Fig. 4.2b), but this does not imply that CO_2 air-sea exchange dominates proton cycling (Fig. 4.2c). The cumulative effect of atmospheric deposition is a production of protons (Fig. 4.2c), inducing an increase of $pCO_{2,sw}$. However, at the same time the increment in $pCO_{2,atm}$ lowers the air-sea gradient of CO_2. The balance between both processes determines whether the net CO_2 flux is in or out. In the southern North Sea, the increase of $pCO_{2,sw}$ by acid deposition is stronger than the increase of $pCO_{2,atm}$, resulting in an efflux and implying proton consumption due to CO_2 air-sea exchange (negative R_{exch}, Fig. 4.2e). Thus, the acidifying effect of a growing $pCO_{2,atm}$ is here masked in the proton balance. In the other three seas, the increment of $pCO_{2,atm}$ dominates, resulting in net proton production (positive R_{exch}, Fig. 4.2e).

4.4 Discussion

4.4.1 Comparison with previous studies

The global annual mean (0.00037) and median (0.00018) decrease in pH due to total atmospheric acid inputs as calculated by Hassellöv et al. (2013) are an order of magnitude smaller than the measured annual open-ocean acidification (Santana-Casiano et al., 2007; Midorikawa et al., 2012). With the RCP8.5 scenario for $pCO_{2,atm}$, pH at our four coastal sites is expected to decrease at a magnitude roughly similar to global estimates (Bopp et al., 2013). The inclusion of atmospheric acid deposition leads to an additional change in [H^+] of at most 28%, which appears to be higher than the average global contribution. However, annual acidification at two distinct coastal sites, i.e. the southern North Sea (Provoost et al., 2010) and Tatoosh Island, Washington state, USA (Wootton and Pfister, 2012), currently occurs at a rate 1 order of magnitude higher than in the open ocean. This is an indication that some important processes that affect pH in coastal areas are not included in our model. Possible mechanisms are site-specific and may include alkalinity inputs from shelf sediments (Thomas et al., 2009), increased upwelling (Feely et al., 2008), increased inputs of riverine dissolved organic carbon (Wootton and Pfister, 2012), and changes in the production-respiration balance (Borges and Gypens, 2010; Provoost et al., 2010).

4.4.2 Regional and saturation state-related differences

Regionally distinct initial conditions are known to influence the response of a system to increasing $pCO_{2,atm}$. For example, the Arctic Ocean is widely recognised to be one of the systems most vulnerable to increasing $pCO_{2,atm}$, because of its naturally low pH, buffering capacity, and

temperature (Orr et al., 2005), while low-latitudinal regions are generally less susceptible to CO_2 invasion (Egleston et al., 2010). This is the first study showing that initial conditions also play a role in the effect of atmospheric acid deposition on pH.

Systems supersaturated with respect to $pCO_{2,atm}$, such as heterotrophic ecosystems where respiration exceeds gross production, are most sensitive to additive acidification by acid deposition, whereas CO_2 undersaturated systems, in particular autotrophic ecosystems, are least sensitive. The metabolic balance and CO_2 saturation conditions of coastal ecosystems are spatially and temporally heterogeneous and their role as a source or sink of atmospheric CO_2 is debated (Cai et al., 2006; Chen and Borges, 2009). The southern North Sea and northern part of the South China Sea are reported to be sources of CO_2 to the atmosphere (Thomas et al., 2004; Zhai et al., 2005). Thus, atmospheric acid deposition strengthens the outgassing fluxes from these seas. In contrast, both the north-western Mediterranean Sea (Durrieu de Madron et al., 2003) and the Baltic Sea (Thomas et al., 2010) are generally sinks of atmospheric CO_2 and atmospheric acid deposition leads to a weakened CO_2 uptake in these seas.

The spatial and temporal variability in coastal air-sea CO_2 gradients, which ranges, e.g. from approximately -100 to 100 ppmv in the southern North Sea (Thomas et al., 2004), introduces uncertainty to our calculated annual CO_2 air-sea gas exchange rates. Additionally, selecting one from the several parameterisations that exist for k_d adds a factor of 2 uncertainty (Garbe et al., 2014).

4.4.3   Future projections

Globally, atmospheric S and N emissions are expected to decline within the next century due to air-quality regulations and reduced fertiliser and fossil fuel use. However, emissions tend to become relatively more concentrated in economic growth regions such as China, India, and Brazil (Van Vuuren et al., 2011). Generally speaking, low-latitudinal shelf seas and near-shore coastal areas are CO_2-supersaturated, while CO_2-undersaturated shelf seas are mostly found at middle to high latitudes (Chen and Borges, 2009). Since most economic growth regions are present at low latitudes, their CO_2-supersaturated coastal systems are especially vulnerable to future acid deposition.

Acknowledgements

Table 4.S1 Input parameters used for the north-western Mediterranean Sea. Parameters are taken from the DYFAMED (CNRS-INSU) site (Observatoire Océanologique de Villefranche-sur-mer, http://www.obs-vlfr. fr/dyfBase/) unless stated otherwise. Input parameters of other case studies are taken from Hunter et al. (2011).

Parameter	North-western Mediterranean Sea	
Mixed layer depth (m)	220	
Salinity	38.4	
Temperature (°C)	13.2	
TA (μmol kg^{-1})	2575	
H_2SO_4 flux (mmol m^{-2} yr^{-1})	15	(Derwent et al., 2005)
HNO_3 flux (mmol m^{-2} yr^{-1})	32.85	(Guerzoni et al., 1999)
$NH_3 + NH_4^+$ flux (mmol m^{-2} yr^{-1})	21.9	(Guerzoni et al., 1999)

Supplementary material. Explicit pH modelling approach

The approach adopted follows that of Hofmann et al. (2010a) and the interested reader is referred to this communication for more information.

Derivation of the stoichiometric coefficient for the proton (ν_{H^+})

Each chemical reaction involving acid-base species can always be described in several ways. Taking calcite precipitation as an example, the following reaction equations have been used to describe this process:

$$Ca^{2+} + CO_3^{2-} \longrightarrow CaCO_3 \tag{S1}$$

$$Ca^{2+} + 2\,HCO_3^- \longrightarrow CaCO_3 + CO_2 + H_2O \tag{S2}$$

$$Ca^{2+} + HCO_3^- \longrightarrow CaCO_3 + H^+ \tag{S3}$$

$$Ca^{2+} + CO_2 + H_2O \longrightarrow CaCO_3 + 2\,H^+ \tag{S4}$$
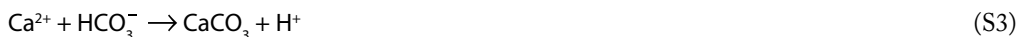
Here, Ca^{2+} is the calcium ion, CO_3^{2-} is the carbonate ion, $CaCO_3$ is calcite, HCO_3^- is the bicarbonate ion, CO_2 is dissolved carbon dioxide, H_2O is water, and H^+ is the proton. Each of these reactions is a stoichiometrically correct description of the same process, but neither provides a complete picture of the acid-base cycling involved with calcite precipitation.

Calcite precipitation occurs at a rate R_{precip}. Using Eq. (S1) as an example, most of the CO_3^{2-} consumed by this process will be replaced by immediate acid-base reactions, i.e. the dissociation of HCO_3^- and $CO_2 + H_2O$:

$$CO_2 + H_2O \rightarrow CO_3^{2-} + 2\,H^+ \tag{S5}$$

$$HCO_3^- \rightarrow CO_3^{2-} + H^+ \tag{S6}$$

As the speed of these acid-base reactions exceeds R_{precip} by orders of magnitude, CO_3^{2-} in Eq. (S1) can technically be replaced by HCO_3^- and CO_2+H_2O by making use of Eqs. (S5-S6):

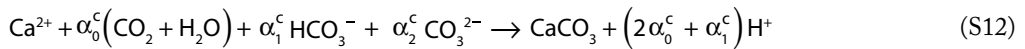$$Ca^{2+} + (CO_2 + H_2O - 2\,H^+) \rightarrow CaCO_3 \tag{S7}$$

$$Ca^{2+} + (HCO_3^- - H^+) \rightarrow CaCO_3 \tag{S8}$$

Together the species CO_2, HCO_3^- and CO_3^{2-} make up the total dissolved inorganic carbon (DIC). In a system where DIC remains constant, the relative distribution of these three species varies as a result of changes in proton concentration, $[H^+]$. This relative distribution is often described in terms of ionisation fractions:

$$\alpha_0^c = \frac{[CO_2]}{DIC} \tag{S9}$$

$$\alpha_1^c = \frac{[HCO_3^-]}{DIC} \tag{S10}$$

$$\alpha_2^c = \frac{[CO_3^{2-}]}{DIC} \tag{S11}$$

where the squared brackets represent concentrations and, by definition, the sum of α_0^c, α_1^c and α_2^c equals 1. As a result, a general expression for calcite precipitation can be generated by combining Eqs. (S1), (S7) and (S8) and taking into account the relative distribution of the three inorganic carbon species:

$$Ca^{2+} + \alpha_0^c\left(CO_2 + H_2O\right) + \alpha_1^c\,HCO_3^- + \alpha_2^c\,CO_3^{2-} \rightarrow CaCO_3 + \left(2\alpha_0^c + \alpha_1^c\right)H^+ \tag{S12}$$

The quantity $2\alpha_0^c + \alpha_1^c$ determines how many protons are produced during this reaction. Hence, it is termed the stoichiometric coefficient for the proton ($\nu_{H^+}^{precip}$). Note that the values of the ionisation fractions depend on $[H^+]$, and so does the value of $\nu_{H^+}^{precip}$. Thus, the amount of protons produced during calcite precipitation, or any other biogeochemical process, depends on $[H^+]$.

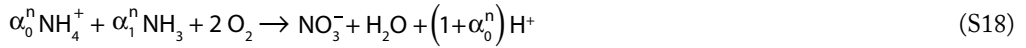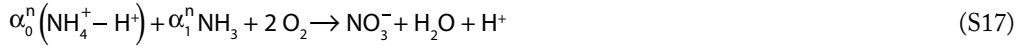Similarly to calcite precipitation, we can deduce the stoichiometric coefficients for the proton for CO_2 air-sea exchange ($\nu_{H^+}^{exch}$) and nitrification ($\nu_{H^+}^{nitr}$), the two pH-dependent processes producing protons in our study. For CO_2 air-sea exchange:

$$CO_2\,(g) + H_2O \rightarrow CO_2 + H_2O \tag{S13}$$

$$CO_2\,(g) + H_2O \rightarrow \alpha_0^c\left(CO_2 + H_2O\right) + \alpha_1^c\left(HCO_3^- + H^+\right) + \alpha_2^c\left(CO_3^{2-} + 2\,H^+\right) \tag{S14}$$

$$CO_2 \text{ (g)} + H_2O \rightarrow \alpha_0^c \left(CO_2 + H_2O\right) + \alpha_1^c \, HCO_3^- + \alpha_2^c \, CO_3^{2-} + \left(\alpha_1^c + 2\,\alpha_2^c\right) H^+ \tag{S15}$$
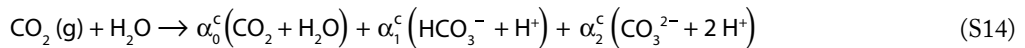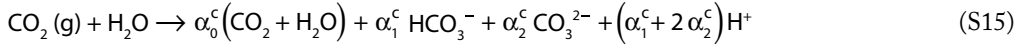
So, $\nu_{H^+}^{exch}$ equals $\alpha_1^c + 2\alpha_2^c$.

For nitrification:

$$NH_3 + 2\,O_2 \rightarrow NO_3^- + H_2O + H^+ \tag{S16}$$

$$\alpha_0^n \left(NH_4^+ - H^+\right) + \alpha_1^n \, NH_3 + 2\,O_2 \rightarrow NO_3^- + H_2O + H^+ \tag{S17}$$

$$\alpha_0^n \, NH_4^+ + \alpha_1^n \, NH_3 + 2\,O_2 \rightarrow NO_3^- + H_2O + \left(1 + \alpha_0^n\right) H^+ \tag{S18}$$

In Eqs. (S16-S18), NH_3 is dissolved ammonia, NH_4^+ is the ammonium ion, O_2 is oxygen, and α_0^n and α_1^n are the ionisation fractions of NH_4^+ and NH_3 with respect to total dissolved ammonium, respectively. The value of $\nu_{H^+}^{nitr}$ is thus $1 + \alpha_0^n$.

Quantification of the change in proton concentration

Generally, the rate of change in proton concentration due to a certain process p (mol kg^{-1} yr^{-1}) can be described as the product of the reaction rate of that process (R_p; mol kg^{-1} yr^{-1}) and a dimensionless quantity that determines how many protons are produced or consumed by that reaction, termed sensitivity (S_p):

$$\frac{d[H^+]_p}{dt} = S_p R_p \tag{S19}$$

In an infinitely dilute solution, S_p will be equal to the stoichiometric coefficient for the proton, $\nu_{H^+}^p$. In natural systems, however, the vast majority of protons produced during a certain process are consumed by immediate acid-base reactions, thereby neutralising their acidifying effect. The extent to which this attenuation occurs is controlled by the buffering capacity (β) of the system; a system with a high β will be more efficient in attenuating changes in [H$^+$] and thus display a lower net pH change. Hence, S_p should be defined as the quotient of $\nu_{H^+}^p$ and β:

$$S_p = \frac{\nu_{H^+}^p}{\beta} \tag{S20}$$

The remaining question is how the buffering capacity is defined. To arrive at this definition, we will return to the example of calcite precipitation. In an aqueous system only containing DIC the total alkalinity (TA) of the system is defined as:

$$TA = [HCO_3^-] + 2[CO_3^{2-}] + [OH^-] - [H^+] \tag{S21}$$

The carbonate system species in Eq. (S21) can also be expressed in terms of ionisation fractions:

$$TA = \left(\alpha_1^c + 2\alpha_2^c\right) DIC + [OH^-] - [H^+] \tag{S22}$$

Irrespective of which reaction equation is used to describe calcite precipitation, the changes in DIC and TA resulting from this process can be described as follows:

$$\frac{dTA}{dt} = -2\,R_{precip} \tag{S23}$$

$$\frac{dDIC}{dt} = -R_{precip} \tag{S24}$$

Since the changes in TA and DIC are independent of the reaction equation chosen, they are termed reaction invariants and because of this, they are often used as state variables when calculating the carbonate system. As changes in $[H^+]$ are derived from changes in DIC and TA, we call this the implicit pH modelling approach, In contrast, the explicit pH modelling approach applied in this study uses DIC and $[H^+]$ as state variables and changes in TA are derived from this. Hence, we can express changes in TA as the partial derivatives of TA with respect to $[H^+]$ and DIC:

$$\frac{dTA}{dt} = \left(\frac{\partial TA}{\partial [H^+]}\right)\frac{d[H^+]}{dt} + \left(\frac{\partial TA}{\partial DIC}\right)\frac{dDIC}{dt} \tag{S25}$$

Equation (S25) can be rearranged to arrive at an expression for $\frac{d[H^+]}{dt}$:

$$\frac{d[H^+]}{dt} = \frac{1}{\left(\frac{\partial TA}{\partial [H^+]}\right)}\left(\frac{dTA}{dt} - \left(\frac{\partial TA}{\partial DIC}\right)\frac{dDIC}{dt}\right) \tag{S26}$$

Substituting $\frac{dTA}{dt}$ and $\frac{dDIC}{dt}$ with Eqs. (S23) and (S24) leads to

$$\frac{d[H^+]}{dt} = \frac{1}{\left(\frac{\partial TA}{\partial [H^+]}\right)}\left(-2\,R_{precip} + \left(\frac{\partial TA}{\partial DIC}\right)R_{precip}\right) \tag{S27}$$

which, in turn, can be rearranged to

$$\frac{d[H^+]}{dt} = \frac{1}{-\left(\frac{\partial TA}{\partial [H^+]}\right)}\left(2 - \left(\frac{\partial TA}{\partial DIC}\right)\right)R_{precip} \tag{S28}$$

Comparing Eqs. (S19-S20) with Eq. (S28), it becomes clear that

$$\frac{v_{H^+}^{precip}}{\beta} = \frac{2 - \left(\frac{\partial TA}{\partial DIC}\right)}{-\left(\frac{\partial TA}{\partial [H^+]}\right)} \tag{S29}$$

The partial derivative of TA with respect to DIC can be found using Eq. (S22):

$$\left(\frac{\partial TA}{\partial DIC}\right) = \alpha_1^c + 2\,\alpha_2^c \tag{S30}$$

Plugging Eq. (S30) into Eq. (S29) gives us

$$\frac{\nu_{H^+}^{precip}}{\beta} = \frac{2 - \left(\alpha_1^c + 2\alpha_2^c\right)}{-\left(\frac{\partial TA}{\partial [H^+]}\right)} \tag{S31}$$

By remembering that, by definition, the sum of α_0^c, α_1^c and α_2^c equals 1, Eq. (S31) can be rewritten into

$$\frac{\nu_{H^+}^{precip}}{\beta} = \frac{2\alpha_0^c + \alpha_1^c}{-\left(\frac{\partial TA}{\partial [H^+]}\right)} \tag{S32}$$

Since the numerator of Eq. (S32) is equal to the earlier derived value of $\nu_{H^+}^{precip}$ as shown in Eq. (S12), it follows that:

$$\beta = -\left(\frac{\partial TA}{\partial [H^+]}\right) \tag{S33}$$

Thus, we have now arrived at the final expression that can be used to quantify the change in proton concentration induced by a process p in natural systems:

$$\frac{d[H^+]_p}{dt} = \frac{\nu_{H^+}^p}{-\left(\frac{\partial TA}{\partial [H^+]}\right)} R_p \tag{S34}$$

The total change in proton concentration in a system is then simply equal to the sum of all these processes, as they occur simultaneously:

$$\frac{d[H^+]_{tot}}{dt} = \frac{1}{-\left(\frac{\partial TA}{\partial [H^+]}\right)} \sum_p \nu_{H^+}^p R_p \tag{S35}$$

Chapter 5:

Generalised expressions for the response of pH to changes in ocean chemistry

"Everything must be made as simple as possible. But not simpler."

Albert Einstein

Abstract

The extent to which oceans are capable of buffering changes in pH resulting from the uptake of carbon dioxide (CO_2) or other acidifying processes can be quantified using buffer factors. Here we present general expressions describing the sensitivity of pH to a change in ocean chemistry. These expressions can include as many acid-base systems as desirable, making them suitable for application to, e.g. upwelling regions or nutrient-rich coastal waters. We show that these expressions are fully consistent with previously derived expressions for the Revelle factor and other buffer factors, which only included the carbonate and borate acid-base systems, and provide more accurate values. A comparison of our analytically derived sensitivities with numerical approximations indicates that a small (~0.1%) disturbance is required to accurately estimate all sensitivities.

We apply our general expressions to contemporary global ocean surface water and possible changes therein by the end of the 21st century. These results show that most sensitivities describing a change in pH are of greater magnitude in a warmer, high-CO_2 ocean, indicating a decreased seawater buffering capacity. This trend is driven by the increase in CO_2 and slightly moderated by the warming. On the contrary, by the end of the 21st century global ocean pH becomes less sensitive to changes in temperature. Our work highlights that, to gain further insight into current and future pH dynamics, it is crucial to properly quantify the various concurrently acting buffering mechanisms.

CHAPTER 5

5.1   Introduction

The ocean provides an important ecosystem service to mankind by absorbing ~26% of the anthropogenic carbon dioxide released (Le Quéré et al., 2009). This ocean carbon uptake not only limits global warming, but also causes changes in ocean chemistry, collectively referred to as ocean acidification. These changes include increases in carbon dioxide, dissolved inorganic carbon (DIC) and proton (H^+) concentrations and decreases in carbonate ion concentration, calcium carbonate saturation states and the efficiency of ocean carbon dioxide uptake. The latter results from a decrease in the ocean CO_2 buffer capacity due to diminished dissolved carbonate ions (Sundquist et al., 1979; Frankignoulle, 1994).

Long-term observations on the inorganic carbon system and pH at a number of sites revealed systematic decreases in pH and increases in DIC (Dore et al., 2009; Bates et al., 2014), consistent with model simulations showing declining open-ocean surface water pH since the industrial revolution (Orr et al., 2005). Moreover, model projections indicate that the pH in the future ocean will be more sensitive to changes in ocean chemistry (Caldeira and Wickett, 2003; Egleston et al., 2010; Hofmann et al., 2010a). The response of pH to biogeochemical processes or external forcing depends on the magnitude of the forcing or process rate, the number of protons involved (reaction stoichiometry) and the sensitivity of seawater (Hagens et al., 2014; Hofmann et al., 2010a). The latter depends primarily on carbonate system parameters of seawater and will thus change with the steady increasing concentrations of atmospheric carbon dioxide. Moreover, carbonate system parameters vary with different magnitudes at diurnal, seasonal and interannual time scales (Wootton and Pfister, 2012; Midorikawa et al., 2010; Hofmann et al., 2011) and spatially. Polar regions, for example, are known to be relatively vulnerable due to their naturally low pH, and the temperature dependency of CO_2 solubility and acid-base dissociation constants, while the reverse holds for warmer tropical regions (Fabry et al., 2009; Orr et al., 2005). This temporal and regional variability in the sensitivity of pH to changes in atmospheric carbon dioxide implies that we need to advance our understanding of the factors governing pH in the ocean.

The sensitivity of pH to a change in driving factors is usually expressed in terms of buffering capacity or buffer factors. Traditionally, the buffering capacity of a solution is defined as its ability to neutralise changes in pH or $[H^+]$ upon the addition of a strong acid or base (Van Slyke, 1922) and is calculated from the inverse slope of a titration curve (Stumm and Morgan, 1996; Morel and Hering, 1993):

$$\beta = \left(\frac{\partial pH}{\partial ANC}\right)^{-1} \tag{1}$$

where ANC, or acid neutralisation capacity, represents the difference between base and acid concentration of a solution relative to a predefined zero level of protons (Stumm and Morgan, 1996). For natural waters, ANC is usually replaced by total alkalinity (TA), which is defined as the ANC with a zero level of protons at a pH of 4.5, a temperature of 25ºC, standard atmospheric pressure, and zero ionic strength (Dickson, 1981):

$$\beta = \left(\frac{\partial pH}{\partial TA}\right)^{-1} \tag{2}$$

The increasing awareness that ocean chemistry is changing has stimulated theoretical work on pH buffering and two related buffer factors have been introduced. Egleston et al. (2010) presented and derived an explicit equation for β_{TA}:

$$\beta_{TA} = \left(\frac{\partial \ln[H^+]}{\partial TA}\right)^{-1} \tag{3}$$

and Hofmann et al. (2010a) introduced a proton concentration buffer factor β_H:

$$\beta_H = \left(\frac{\partial [H^+]}{\partial TA}\right) \tag{4}$$

The explicit links among these three buffer factors will be presented below. Note that the partial derivatives in Eq. (1-4) indicate that other chemical water properties, e.g. DIC and other total concentrations of acid-base species, are kept constant when determining this buffering capacity (Morel and Hering, 1993). Equations (2-4) represent the most general way of describing the resistance of natural waters to changes in pH. Depending on the context, however, one may be interested in the way a particular biogeochemical process (Soetaert et al., 2007; Zhang, 2000) or a specific acid-base system, rather than TA, influences the change in pH.

Here we present explicit equations for calculating the sensitivity of protons to changes in ocean chemistry. This information is required if we are to better understand pH dynamics in a changing world or the impact of biogeochemical processes on pH. The sensitivity $\frac{\partial[H^+]}{\partial TA}$ as presented in this paper is identical to the inverse of the buffer factor (Eq. (4)) of Hofmann et al. (2010a), and conceptually equivalent to the inverse of the buffer capacity (Morel and Hering, 1993) and the buffer factor β_{TA} of Egleston et al. (2010), but differs with the latter two in that it is defined as a derivative with respect to $[H^+]$ rather than pH or $\ln[H^+]$. We will first derive general explicit equations for the sensitivity of protons to changes in ocean chemistry. Secondly, we will show how the derived relationships relate to previous studies that were limited to homogeneous reactions or that excluded acid-base systems other than borate (Frankignoulle, 1994; Egleston et al., 2010) and we will show that a similar approach applies to the well-known Revelle factor. Thirdly, we use our analytical approach to establish the range within which numerical estimates of sensitivities are valid. Finally, we show how much more sensitive the pH will be in the year 2100 given projected atmospheric carbon dioxide levels.

5.2   Methods

5.2.1   Analytical derivations of buffer factors

To arrive at a general, complete set of buffer factors, we combined and extended several earlier outlined approaches (Frankignoulle, 1994; Egleston et al., 2010; Soetaert et al., 2007). If examples

are used for clarification, they will be given for the carbonate system, but similar derivations can be made for any other acid-base system.

Generally speaking, any given change in pH can be split into multiple parts representing multiple processes:

$$dpH = \left(\frac{\partial pH}{\partial T}\right) dT + \left(\frac{\partial pH}{\partial S}\right) dS + \left(\frac{\partial pH}{\partial DIC}\right) dDIC + \left(\frac{\partial pH}{\partial TA}\right) dTA + \ldots \tag{5}$$

where T is temperature and S is salinity. The partial derivatives in Eq. (5) indicate that they are only valid if other variables are kept constant within their derivation. The dots indicate that more acid-base systems may be included, depending on the system of interest and the processes taking place. Usually, only carbonate and borate systems are used in the calculations, but in coastal systems, in pore-waters and in ocean oxygen minimum zones, other acid-base systems such as sulphide may impact pH. Following Soetaert et al. (2007), we decided to include the ammonium, phosphate, nitrate, nitrite, sulphide, silicate, fluoride and sulphate acid-base systems in our derivation, and ignore the contribution of other minor acid-base species and organic acids. These acid-base systems should thus be included in the definition of TA, which then becomes (Dickson, 1981; Wolf-Gladrow et al., 2007):

$$TA = [HCO_3^-] + 2[CO_3^{2-}] + [B(OH)_4^-] + [NH_3] + [HPO_4^{2-}] + 2[PO_4^{3-}] - [H_3PO_4] - [HNO_3] - [HNO_2] +$$
$$[HS^-] + 2[S^{2-}] + [SiO(OH)_3^-] + 2[SiO_2(OH)_2^{2-}] - [HF] - 2[H_2SO_4] - [HSO_4^-] + [OH^-] - [H^+] \tag{6}$$

This definition can be rewritten by grouping each acid-base system together:

$$TA = TA_{DIC} + TA_{TotB} + TA_{TotNH_4} + TA_{TotPO_4} + TA_{TotNO_3} + \tag{7}$$
$$TA_{TotNO_2} + TA_{TotS} + TA_{TotSi} + TA_{TotF} + TA_{TotSO_4} + TA_{H_2O}$$

Taking the carbonate system as an example, we can see that $TA_{DIC} = [HCO_3^-] + 2[CO_3^{2-}]$. Equation (7) can be differentiated with respect to $[H^+]$:

$$\frac{\partial TA}{\partial[H^+]} = \frac{\partial TA_{DIC}}{\partial[H^+]} + \frac{\partial TA_{TotB}}{\partial[H^+]} + \frac{\partial TA_{TotNH_4}}{\partial[H^+]} + \frac{\partial TA_{TotPO_4}}{\partial[H^+]} + \frac{\partial TA_{TotNO_3}}{\partial[H^+]} +$$
$$\frac{\partial TA_{TotNO_2}}{\partial[H^+]} + \frac{\partial TA_{TotS}}{\partial[H^+]} + \frac{\partial TA_{TotSi}}{\partial[H^+]} + \frac{\partial TA_{TotF}}{\partial[H^+]} + \frac{\partial TA_{TotSO_4}}{\partial[H^+]} + \frac{\partial TA_{H_2O}}{\partial[H^+]} \tag{8}$$

It is important to realise that the subscripts in Eq. (8) simply represent terms belonging together being grouped (similar to Eq. (7)) and do not imply that total concentrations of all acid-base species remain constant. However, if we do make this additional assumption, i.e. TA changes only due to changes in $[H^+]$, then Eq. (8) is directly linked to the inverse of the well-known acid-base buffering capacity (Eq. (2)) sensu Morel and Hering (1993) and identical to the inverse of proton concentration buffer factor (Eq. (4)) of Hofmann et al. (2010a):

$$\beta_H = \sum_{i=1}^{k} \left(\frac{\partial TA_i}{\partial[H^+]}\right)_i \tag{9}$$

Here, i represents the total concentration of an acid-base system, TA_i represents the contribution of that acid-base system to TA, and k represents the total number of acid-base systems present in the system.

Since we are interested in the effect of the change in the total concentration of a certain acid-base species (TotX) on $[H^+]$, we differentiate both TotX and TA with respect to changes in proton concentration and the concentration of an acid-base species X that makes up part of TotX:

$$dTotX = \left(\frac{\partial TotX}{\partial [X]}\right)_{H^+} d[X] + \left(\frac{\partial TotX}{\partial [H^+]}\right)_{X} d[H^+] \tag{10a}$$

$$dTA = \left(\frac{\partial TA}{\partial [X]}\right)_{H^+} d[X] + \left(\frac{\partial TA}{\partial [H^+]}\right)_{X} d[H^+] \tag{10b}$$

We can convert these expressions to describe the sensitivity of $[H^+]$ to a change in TotX by making use of the matrix inversion method (Egleston et al., 2010).

$$\begin{pmatrix} dTotX \\ dTA \end{pmatrix} = J \begin{pmatrix} d[X] \\ d[H^+] \end{pmatrix} \tag{11}$$

The Jacobian J is defined as:

$$J = \begin{pmatrix} a & b \\ c & d \end{pmatrix} = \begin{pmatrix} \left(\frac{\partial TotX}{\partial [X]}\right)_{H^+} & \left(\frac{\partial TotX}{\partial [H^+]}\right)_{X} \\ \left(\frac{\partial TA}{\partial [X]}\right)_{H^+} & \left(\frac{\partial TA}{\partial [H^+]}\right)_{X} \end{pmatrix} \tag{12}$$

From matrix algebra, we know that

$$\begin{pmatrix} d[X] \\ d[H^+] \end{pmatrix} = J^{-1} \begin{pmatrix} dTotX \\ dTA \end{pmatrix} \tag{13}$$

The inverse Jacobian J^{-1} can then be defined as

$$J^{-1} = \begin{pmatrix} \dfrac{\partial [X]}{\partial TotX} & \dfrac{\partial [X]}{\partial TA} \\ \dfrac{\partial [H^+]}{\partial TotX} & \dfrac{\partial [H^+]}{\partial TA} \end{pmatrix} = \begin{pmatrix} \dfrac{-d}{bc-ad} & \dfrac{b}{bc-ad} \\ \dfrac{c}{bc-ad} & \dfrac{-a}{bc-ad} \end{pmatrix} \tag{14}$$

where a, b, c and d refer to the corresponding partial derivatives of Eq. (12).

The sensitivities $\left(\frac{\partial TA}{\partial [X]}\right)_{H^+}$, $\left(\frac{\partial TotX}{\partial [X]}\right)_{H^+}$ and $\left(\frac{\partial TotX}{\partial [H^+]}\right)_{X}$ (Eq. (12)) can be analytically derived in a relatively easy manner. Combined with the sensitivity $\left(\frac{\partial TA}{\partial [H^+]}\right)_{X}$ one obtains the analytical expression for $\frac{\partial [X]}{\partial TA}$, $\frac{\partial [X]}{\partial TotX}$, and the two sensitivities which are of most interest to this study, $\frac{\partial [H^+]}{\partial TotX}$ and $\frac{\partial [H^+]}{\partial TA}$ (Eq. (14)).

Table 5.1a Expressions for TA_{TotX} for the major acid-base systems present in marine waters expressed in terms of the reference species (X_{ref}), $[H^+]$ and the dissociation constants. The reference species, or the zero level of protons, is that species of an acid-base system that does not contribute to TA, i.e. the stoichiometric contribution to TA (n) equals 0. These expressions are applicable when the total concentration of the acid-base system TotX, of either of its species X, is the state variable. Expressions are taken from Park (1969) and (Stumm and Morgan, 1996).

Acid-base system (TotX)	Reference species (X_{ref})	Contribution to TA (TA_{TotX})	TA_{TotX} (TotX or X is state variable)
Ammonium (TotNH$_4$)	NH_4^+	$[NH_3]$	$\left(\dfrac{K_{NH_4^+}}{[H^+]}\right)[NH_4^+]$
Borate (TotB)	$B(OH)_3$	$[B(OH)_4^-]$	$\left(\dfrac{K_{B(OH)_3}}{[H^+]}\right)[B(OH)_3]$
Carbonate (DIC)	H_2CO_3	$[HCO_3^-]+2[CO_3^{2-}]$	$\left(\dfrac{K_{H_2CO_3}}{[H^+]}+\dfrac{2\,K_{H_2CO_3}K_{HCO_3^-}}{[H^+]^2}\right)[H_2CO_3]$
Phosphate (TotPO$_4$)	$H_2PO_4^-$	$[HPO_4^{2-}]+2[PO_4^{3-}]-[H_3PO_4]$	$\left(\dfrac{K_{H_2PO_4^-}}{[H^+]}+\dfrac{2\,K_{H_2PO_4^-}K_{HPO_4^{2-}}}{[H^+]^2}-\dfrac{[H^+]}{K_{H_3PO_4}}\right)[H_2PO_4^-]$
Nitrate (TotNO$_3$)	NO_3^-	$-[HNO_3]$	$\left(\dfrac{-[H^+]}{K_{HNO_3}}\right)[NO_3^-]$
Nitrite (TotNO$_2$)	NO_2^-	$-[HNO_2]$	$\left(\dfrac{-[H^+]}{K_{HNO_2}}\right)[NO_2^-]$
Sulphide (TotS)	H_2S	$[HS^-]+2[S^{2-}]$	$\left(\dfrac{K_{H_2S}}{[H^+]}+\dfrac{2\,K_{H_2S}K_{HS^-}}{[H^+]^2}\right)[H_2S]$
Silicate (TotSi)	$Si(OH)_4$	$[SiO(OH)_3^-]+2[SiO_2(OH)_2^{2-}]$	$\left(\dfrac{K_{Si(OH)_4}}{[H^+]}+\dfrac{2\,K_{Si(OH)_4}K_{SiO(OH)_3^-}}{[H^+]^2}\right)[Si(OH)_4]$
Fluoride (TotF)	F^-	$-[HF]$	$\left(\dfrac{-[H^+]}{K_{HF}}\right)[F^-]$
Sulphate (TotSO$_4$)	SO_4^{2-}	$-2[H_2SO_4]-[HSO_4^-]$	$\left(\dfrac{-[H^+]}{K_{HSO_4^-}}-\dfrac{[H^+]^2}{K_{H_2SO_4}K_{HSO_4^-}}\right)[SO_4^{2-}]$
Water (auto-dissociation)	H_2O	$[OH^-]-[H^+]$	-

The remaining challenge is thus to obtain a general expression for the term $\left(\frac{\partial TA}{\partial [H^+]}\right)_X$, which is the change in TA due to the change in $[H^+]$ under the assumption that species X is kept constant. It is therefore not equal to β_H, which implies that all total concentrations are constant, but it is tightly linked to it. Specifically:

Table 5.1b Expressions for TA_{TotX} for the major acid-base systems present in marine waters expressed in terms of the total concentration (TotX), $[H^+]$ and the dissociation constants. These expressions are applicable when the total concentration of the acid-base system is a reaction invariant. The final expression for TA (Eq. (6)) for the specific situation is arrived at by summing the appropriate term (a or b) for each acid-base system involved.

Acid-base system (TotX)	Contribution to TA (TA_{TotX})	TA_{TotX} (TotX or X is reaction invariant)
Ammonium ($TotNH_4$)	$[NH_3]$	$\dfrac{K_{NH_4^+}}{[H^+] + K_{NH_4^+}} TotNH_4$
Borate (TotB)	$[B(OH)_4^-]$	$\dfrac{K_{B(OH)_3}}{[H^+] + K_{B(OH)_3}} TotB$
Carbonate (DIC)	$[HCO_3^-] + 2[CO_3^{2-}]$	$\dfrac{K_{H_2CO_3}[H^+] + 2\, K_{H_2CO_3} K_{HCO_3^-}}{[H^+]^2 + K_{H_2CO_3}[H^+] + K_{H_2CO_3} K_{HCO_3^-}} DIC$
Phosphate ($TotPO_4$)	$[HPO_4^{2-}] + 2[PO_4^{3-}] - [H_3PO_4]$	$\dfrac{K_{H_3PO_4} K_{H_2PO_4^-}[H^+] + 2\, K_{H_3PO_4} K_{H_2PO_4^-} K_{HPO_4^{2-}} - [H^+]^3}{[H^+]^3 + K_{H_3PO_4}[H^+]^2 + K_{H_3PO_4} K_{H_2PO_4^-}[H^+] + K_{H_3PO_4} K_{H_2PO_4^-} K_{HPO_4^{2-}}} TotPO_4$
Nitrate ($TotNO_3$)	$-[HNO_3]$	$\dfrac{-[H^+]}{[H^+] + K_{HNO_3}} TotNO_3$
Nitrite ($TotNO_2$)	$-[HNO_2]$	$\dfrac{-[H^+]}{[H^+] + K_{HNO_2}} TotNO_2$
Sulphide (TotS)	$[HS^-] + 2[S^{2-}]$	$\dfrac{K_{H_2S}[H^+] + 2\, K_{H_2S} K_{HS^-}}{[H^+]^2 + K_{H_2S}[H^+] + K_{H_2S} K_{HS^-}} TotS$
Silicate (TotSi)	$[SiO(OH)_3^-] + 2[SiO_2(OH)_2^{2-}]$	$\dfrac{K_{Si(OH)_4}[H^+] + 2\, K_{Si(OH)_4} K_{Si(OH)_3^-}}{[H^+]^2 + K_{Si(OH)_4}[H^+] + K_{Si(OH)_4} K_{Si(OH)_3^-}} TotSi$
Fluoride (TotF)	$-[HF]$	$\dfrac{-[H^+]}{[H^+] + K_{HF}} TotF$
Sulphate ($TotSO_4$)	$-2[H_2SO_4] - [HSO_4^-]$	$\dfrac{-K_{H_2SO_4}[H^+] - 2\,[H^+]^2}{[H^+]^2 + K_{H_2SO_4}[H^+] + K_{H_2SO_4} K_{HSO_4^-}} TotSO_4$
Water (auto-dissociation)	$[OH^-] - [H^+]$	$\dfrac{K_W}{[H^+]} - [H^+]$

$$\left(\frac{\partial TA}{\partial [H^+]}\right)_X = \beta_H - \left(\frac{\partial TA_{TotX}}{\partial [H^+]}\right)_{TotX} + \left(\frac{\partial TA_{TotX}}{\partial [H^+]}\right)_X \tag{15}$$

To illustrate the procedure we select the carbonate system as the system of interest. As an example we take the addition of CO_2, meaning that DIC changes while the total concentrations of the

Table 5.2a Expressions for $\left(\frac{\partial TA_{TotX}}{\partial[H^+]}\right)_X$ for the major acid-base systems present in marine waters. These are used when the total concentration of the acid-base system (TotX), or either of its species, is the state variable. The factor n corresponds to the stoichiometric factor in the contribution of X to TA, which is by default 0 for the reference species. The reference species (X_{ref}) is that species of an acid-base system that does not contribute to TA.

Acid-base system (TotX)	Reference species (X_{ref})	$\left(\frac{\partial TA_{TotX}}{\partial[H^+]}\right)_X$
Ammonium (TotNH$_4$)	NH_4^+	$\frac{-1}{[H^+]}\left(-n\,TA_{TotNH_4} + [NH_3]\right)$
Borate (TotB)	$B(OH)_3$	$\frac{-1}{[H^+]}\left(-n\,TA_{TotB} + [B(OH)_4^-]\right)$
Carbonate (DIC)	H_2CO_3	$\frac{-1}{[H^+]}\left(-n\,TA_{DIC} + [HCO_3^-] + 4[CO_3^{2-}]\right)$
Phosphate (TotPO$_4$)	$H_2PO_4^-$	$\frac{-1}{[H^+]}\left(-n\,TA_{TotPO_4} + [H_3PO_4] + [H_2PO_4^-] + 4[PO_4^{3-}]\right)$
Nitrate (TotNO$_3$)	NO_3^-	$\frac{-1}{[H^+]}\left(-n\,TA_{TotNO_3} + [HNO_3]\right)$
Nitrite (TotNO$_2$)	NO_2^-	$\frac{-1}{[H^+]}\left(-n\,TA_{TotNO_2} + [HNO_2]\right)$
Sulphide (TotS)	H_2S	$\frac{-1}{[H^+]}\left(-n\,TA_{TotS} + [HS^-] + 4[S^{2-}]\right)$
Silicate (TotSi)	$Si(OH)_4$	$\frac{-1}{[H^+]}\left(-n\,TA_{TotSi} + [SiO(OH)_3^-] + 4[SiO_2(OH)_2^{2-}]\right)$
Fluoride (TotF)	F^-	$\frac{-1}{[H^+]}\left(-n\,TA_{TotF} + [HF]\right)$
Sulphate (TotSO$_4$)	SO_4^{2-}	$\frac{-1}{[H^+]}\left(-n\,TA_{TotSO_4} + 4[H_2SO_4] + [HSO_4^-]\right)$
Water (auto-dissociation)	H_2O	-

other acid-base systems and TA remain constant. To this purpose, we assume that [CO$_2$] equals [H$_2$CO$_3$]. In this case, H$_2$CO$_3$ is our species of interest X and DIC is our independent state variable TotX, while the other total concentrations are reaction invariants, i.e. they are not affected by the

Table 5.2b Expressions for $\left(\frac{\partial TA_{TotX}}{\partial [H^+]}\right)_{TotX}$ for the major acid-base systems present in marine waters. These are valid when the total concentration of the acid-base system (TotX) is the reaction invariant. The final expression for $\left(\frac{\partial TA}{\partial [H^+]}\right)_X$ for the specific situation (Eq. (15)), is arrived at by summing the appropriate term (a or b) for each acid-base system involved.

Acid-base system (TotX)	$\left(\frac{\partial TA_{TotX}}{\partial [H^+]}\right)_{TotX}$
Ammonium (TotNH$_4$)	$\frac{-1}{[H^+]}\left([NH_3]\frac{[NH_4^+]}{TotNH_4}\right)$
Borate (TotB)	$\frac{-1}{[H^+]}\left([B(OH)_4^-]\frac{[B(OH)_3]}{TotB}\right)$
Carbonate (DIC)	$\frac{-1}{[H^+]}\left([HCO_3^-]\left(\frac{[H_2CO_3]-[CO_3^{2-}]}{DIC}\right)+2\,[CO_3^{2-}]\left(\frac{2\,[H_2CO_3]+[HCO_3^-]}{DIC}\right)\right)$
Phosphate (TotPO$_4$)	$\frac{-1}{[H^+]}\left(\begin{array}{l}-[H_3PO_4]\left(\frac{-[H_2PO_4^-]-2[HPO_4^{2-}]-3[PO_4^{3-}]}{TotPO_4}\right)+[HPO_4^{2-}]\left(\frac{2\,[H_3PO_4]+[H_2PO_4^-]-[PO_4^{3-}]}{TotPO_4}\right)\\ +2\,[PO_4^{3-}]\left(\frac{3\,[H_3PO_4]+2\,[H_2PO_4^-]+[HPO_4^{2-}]}{TotPO_4}\right)\end{array}\right)$
Nitrate (TotNO$_3$)	$\frac{-1}{[H^+]}\left(-[HNO_3]\frac{[NO_3^-]}{TotNO_3}\right)$
Nitrite (TotNO$_2$)	$\frac{-1}{[H^+]}\left(-[HNO_2]\frac{[NO_2^-]}{TotNO_2}\right)$
Sulphide (TotS)	$\frac{-1}{[H^+]}\left([HS^-]\left(\frac{[H_2S]-[S^{2-}]}{TotS}\right)+2\,[S^{2-}]\left(\frac{2\,[H_2S]+[HS^-]}{TotS}\right)\right)$
Silicate (TotSi)	$\frac{-1}{[H^+]}\left([SiO(OH)_3^-]\left(\frac{[Si(OH)_4]-[SiO_2(OH)_2^{2-}]}{TotSi}\right)+2\,[SiO_2(OH)_2^{2-}]\left(\frac{2\,[Si(OH)_4]+[SiO(OH)_3^-]}{TotSi}\right)\right)$
Fluoride (TotF)	$\frac{-1}{[H^+]}\left(-[HF]\frac{[F^-]}{TotF}\right)$
Sulphate (TotSO$_4$)	$\frac{-1}{[H^+]}\left(-2\,[H_2SO_4]\left(\frac{-[HSO_4^-]-2\,[SO_4^{2-}]}{TotSO_4}\right)-[HSO_4^-]\left(\frac{[H_2SO_4]-[SO_4^{2-}]}{TotSO_4}\right)\right)$
Water (auto-dissociation)	$\frac{-1}{[H^+]}\left([OH^-]+[H^+]\right)$

chemical transformations in the systems (Waller and Makila, 1981). However, the addition of H_2CO_3 affects $[H^+]$ and thus will change the speciation of these acid-base systems. Therefore, to analytically derive the partial derivatives of Eq. (8) that belong to the reaction invariants, it is

necessary to express the corresponding species of Eq. (6) in terms of their total concentration, $[H^+]$ and equilibrium constants only (Park, 1969; Soetaert et al., 2007; Table 5.1b). The corresponding analytical expressions for the partial derivatives can be found in Table 5.2b. In our example, DIC is not invariant, and $\left(\frac{\partial TA}{\partial [H^+]}\right)_{H_2CO_3}$ cannot be equal to β_H. Therefore, to analytically represent $\left(\frac{\partial TA}{\partial [H^+]}\right)_{H_2CO_3}$ the term $\left(\frac{\partial TA_{DIC}}{\partial [H^+]}\right)_{DIC}$ has to be removed from the definition of β_H. However, we can recall that the addition of CO_2 does not affect TA. Thus, if DIC is the state variable, $[H_2CO_3]$ may be regarded as invariant when one is interested in the change in TA as a function of $[H^+]$ as described in Eq. (8). Therefore, we can express TA_{DIC}, as well as its partial derivative $\frac{\partial TA_{DIC}}{\partial [H^+]}$, in terms of equilibrium constants, $[H^+]$ and $[H_2CO_3]$ (Tables 5.1a – 5.2a) and add this to the analytical representation of $\left(\frac{\partial TA}{\partial [H^+]}\right)_{H_2CO_3}$. We will refer to this expression as $\left(\frac{\partial TA_{DIC}}{\partial [H^+]}\right)_{H_2CO_3}$ or, in more general terms, $\left(\frac{\partial TA_{TotX}}{\partial [H^+]}\right)_X$. Since β_H is explicitly defined under the assumption that TA changes only due to changes in $[H^+]$, i.e. all total concentrations are reaction invariants, we can find the analytical expression for β_H by summing all the terms from Table 5.1b. Then, taking again the addition of CO_2 as example, we can find the analytical expression for $\left(\frac{\partial TA}{\partial [H^+]}\right)_{H_2CO_3}$ by subtracting $\left(\frac{\partial TA_{DIC}}{\partial [H^+]}\right)_{DIC}$ (Table 5.2b) from β_H and adding $\left(\frac{\partial TA_{DIC}}{\partial [H^+]}\right)_{H_2CO_3}$ (Table 5.2a). This yields:

$$\left(\frac{\partial TA}{\partial [H^+]}\right)_{H_2CO_3} = \beta_H - \left(\frac{\partial TA_{DIC}}{\partial [H^+]}\right)_{DIC} + \left(\frac{\partial TA_{DIC}}{\partial [H^+]}\right)_{H_2CO_3} \tag{16}$$

where:

$$\left(\frac{\partial TA_{DIC}}{\partial [H^+]}\right)_{DIC} = \frac{-1}{[H^+]}\left([HCO_3^-]\left(\frac{[H_2CO_3]-[CO_3^{2-}]}{DIC}\right) + 2\,[CO_3^{2-}]\left(\frac{2\,[H_2CO_3]+[HCO_3^-]}{DIC}\right)\right) \tag{17; Table 5.2b}$$

and

$$\left(\frac{\partial TA_{DIC}}{\partial [H^+]}\right)_{H_2CO_3} = \frac{-1}{[H^+]}\left(-n\,TA_{DIC} + \left([HCO_3^-]+4\,[CO_3^{2-}]\right)\right) \tag{18; Table 5.2a}$$

where n stands for the charge contribution to alkalinity (Soetaert et al., 2007). In the case of the carbonate system, adding or removing CO_2 changes DIC but not TA, i.e. n equals 0, such that Eq. (18) simplifies. However, addition or removal of HCO_3^- or CO_3^{2-} changes TA and n is 1 and 2, respectively. As a result, Eq. (16) can also be applied to the addition or removal of HCO_3^- or CO_3^{2-}, with the same expression but a different result for Eq. (18). The relation between $\left(\frac{\partial TA_{DIC}}{\partial [H^+]}\right)_{H_2CO_3}$ and either of the terms $\left(\frac{\partial TA_{DIC}}{\partial [H^+]}\right)_{HCO_3^-}$ or $\left(\frac{\partial TA_{DIC}}{\partial [H^+]}\right)_{CO_3^{2-}}$ can be generalised into:

$$\left(\frac{\partial TA_{TotX}}{\partial [H^+]}\right)_X = \left(\frac{\partial TA_{TotX}}{\partial [H^+]}\right)_{X_{ref}} + \frac{n\,TA_{TotX}}{[H^+]} \tag{19}$$

Here, X_{ref} is the reference species of the acid-base system TotX for the total alkalinity expression. This reference species is also referred to as the zero level of protons (Wolf-Gladrow et al., 2007). Moreover, since adding or removing CO_2 changes DIC but not TA, this means that a change in $[CO_2]$ is equivalent to a change in DIC when other properties are held constant (MacIntyre, 1978). These principles are applicable to any of the reference species for TA.

Generally, using the appropriate combination of terms expressing TA from Tables 5.1a – b for the state variable of interest, we can write the analytical expression for Eq. (7) that is applicable to the

Table 5.3 Expressions for some sensitivities of interest in studying global change. The sensitivities in Table 5.3a are generally applicable to any combination of acid-base systems, any number of state variables, and for any total concentration or any of species contributing to the total concentration as independent state variable. The sensitivities in Table 5.3b are applicable to any combination of acid-base systems, two state variables (one of which is TA), and for any total concentration or any of species contributing to the total concentration as independent state variable. TotX refers to the total concentration of the acid-base system of interest (one of the state variables), X to the species of interest of that acid-base system (which equals the reference species for TA (X_{ref}) in the case a change in TotX is specified), n to the stoichiometric factor in the contribution of X to TA (which equals 0 in the case a change in TotX is specified), and TA_{TotX} to the contribution of all species of TotX to TA

Table 5.3a		Table 5.3b	
Sensitivity	**Expression**	**Sensitivity**	**Expression**
$\left(\dfrac{\partial TA}{\partial [H^+]}\right)_X$	$\beta_H - \left(\dfrac{\partial TA_{TotX}}{\partial [H^+]}\right)_{TotX} + \left(\dfrac{\partial TA_{TotX}}{\partial [H^+]}\right)_X$	$\dfrac{\partial [H^+]}{\partial TA}$	$\dfrac{TotX\,[H^+]}{TA_{TotX}^2 + \left([H^+]\left(\dfrac{\partial TA}{\partial [H^+]}\right)_X - n\,TA_{TotX}\right)TotX}$
$\left(\dfrac{\partial TotX}{\partial [H^+]}\right)_X$	$\dfrac{n\,TotX - TA_{TotX}}{[H^+]}$	$\dfrac{\partial [H^+]}{\partial TotX}$	$\dfrac{-TA_{TotX}\,[H^+]}{TA_{TotX}^2 + \left([H^+]\left(\dfrac{\partial TA}{\partial [H^+]}\right)_X - n\,TA_{TotX}\right)TotX}$
$\left(\dfrac{\partial TA}{\partial [X]}\right)_{H^+}$	$\dfrac{TA_{TotX}}{[X]}$	$\dfrac{\partial [X]}{\partial TA}$	$\dfrac{-[X]\,(-TA_{TotX} + n\,TotX)}{TA_{TotX}^2 + \left([H^+]\left(\dfrac{\partial TA}{\partial [H^+]}\right)_X - n\,TA_{TotX}\right)TotX}$
$\left(\dfrac{\partial TotX}{\partial [X]}\right)_{H^+}$	$\dfrac{TotX}{[X]}$	$\dfrac{\partial [X]}{\partial TotX}$	$\dfrac{[X]\,[H^+]\left(\dfrac{\partial TA}{\partial [H^+]}\right)_X}{TA_{TotX}^2 + \left([H^+]\left(\dfrac{\partial TA}{\partial [H^+]}\right)_X - n\,TA_{TotX}\right)TotX}$
$\left(\dfrac{\partial TA}{\partial pH}\right)_X$	$-\ln(10)\left(\beta_H - \left(\dfrac{\partial TA_{TotX}}{\partial [H^+]}\right)_{TotX} + \left(\dfrac{\partial TA_{TotX}}{\partial [H^+]}\right)_X\right)$	$\dfrac{\partial pH}{\partial TA}$	$\dfrac{-TotX}{\ln(10)\left(TA_{TotX}^2 + \left([H^+]\left(\dfrac{\partial TA}{\partial [H^+]}\right)_X - n\,TA_{TotX}\right)TotX\right)}$
$\left(\dfrac{\partial TotX}{\partial pH}\right)_X$	$-\ln(10)\,(n\,TotX - TA_{TotX})$	$\dfrac{\partial pH}{\partial TotX}$	$\dfrac{TA_{TotX}}{\ln(10)\left(TA_{TotX}^2 + \left([H^+]\left(\dfrac{\partial TA}{\partial [H^+]}\right)_X - n\,TA_{TotX}\right)TotX\right)}$

situation. Thus, with the carbonate system as the acid-base system of interest, one would take TA_{DIC} from Table 5.1a and the other terms of Eq. (7) from Table 5.1b. For each of the terms in Tables 5.1a – b, the derivatives are given in Table 5.2. The derivatives of Table 5.2a, which are valid in case of an independent state variable TotX, are written in such a general way that they can also be applied in case a change in any of the species contributing to TotX is specified.

5.2.2 Linking generalised expressions to prior work limited to the carbonate and borate acid-base systems

The expressions we derived in Tables 5.1 and 5.2 are generally applicable to any combination of acid-base systems, any number of state variables, and for any total concentration or any of species contributing to the total concentration as independent state variable. The expressions in Table 5.3a are also generally applicable, as long as the conditions under which $\left(\frac{\partial TA}{\partial [H^+]}\right)_X$ is valid are correctly taken into account for the specific situation. As Egleston et al. (2010) pointed out, more than one acid-base system can be added as an independent state variable, yielding an m by m Jacobian matrix (Eq. (12)) where m equals the number of acid-base systems of interest plus 1 (due to the inclusion of TA). In such cases, $\left(\frac{\partial TA}{\partial [H^+]}\right)_{X_1, X_2, \dots, X_m}$ (Eq. (15)) is built up from (m-1) parts of Table 5.2a.

The resulting expressions in Table 5.3b are valid for any combination of acid-base systems and any total concentration, or any of species contributing to the total concentration, as independent state variable. The main difference with the expressions in Tables 5.2 and 5.3a is that these are only valid in the case of two independent state variables: TA and the total concentration, or either of its species, of the acid-base system of interest. That is simply because the matrix inversion given in Eq. (13) is only valid for a 2 x 2 matrix. As the number of state variables increases, the inverse of the Jacobian matrix becomes significantly more complex, meaning that it is difficult to analytically derive the sensitivities $\left(\frac{\partial [H^+]}{\partial TA}\right)_{X_1, X_2, \dots, X_m}$, $\left(\frac{\partial [H^+]}{\partial TotX_m}\right)_{X_1, X_2, \dots, X_{m-1}, X_m}$, $\left(\frac{\partial [X_m]}{\partial TotX_m}\right)_{H^+, X_1, X_2, \dots, X_{m-1}}$ and $\left(\frac{\partial [X_m]}{\partial TA}\right)_{H^+, X_1, X_2, \dots, X_{m-1}}$. In such cases it is recommended to numerically perform the matrix inversion. For the purpose of this work, however, it is not necessary to add more than one acid-base system simultaneously as our aim is rather the opposite, i.e. to partition the contributions of separate processes to a change in pH.

The implicit assumption that the partial derivatives in Table 5.3b are homogeneous, i.e. they are only valid when all other properties are kept constant, has another consequence. A careful look at our factors derived in Table 5.3b with Eq. (19) in mind shows that, in the case of a change in DIC, the factor $\frac{\partial [H^+]}{\partial DIC}$ will be the same irrespective of whether $\left(\frac{\partial TA}{\partial [H^+]}\right)_X$ is defined with X being H_2CO_3, HCO_3^- or CO_3^{2-}. Conceptually this makes sense, as this is implied in the definition of $\frac{\partial [H^+]}{\partial DIC}$. In other words, for the analytical derivation of $\frac{\partial [H^+]}{\partial TotX}$ it is only of importance to specify TotX; the choice for X is free and will not affect the outcome of $\frac{\partial [H^+]}{\partial TotX}$. Since a change in TotX is equivalent to a change in X_{ref}, $\frac{\partial [H^+]}{\partial TotX}$ in fact describes the response of $[H^+]$ to a change in either TotX or X_{ref}. In a similar fashion, the factor $\frac{\partial [H^+]}{\partial TA}$ will produce the same value irrespective of which total concentration, or even which species, is used in its calculation. So as long as X is defined as a species contributing to TotX, $\frac{\partial [H^+]}{\partial TA}$ can be calculated. These generalisations can, for obvious reasons, not be made for the sensitivities describing a change in [X]. As a result, the subscripts presented in Table 5.3a have been dropped in Table 5.3b.

Finally, all buffer factors presented so far consider the change in $[H^+]$. Since we usually work with pH, rather than $[H^+]$, it is convenient to convert them to factors describing the change in pH. To convert the factors in Table 5.3a from $[H^+]$ to pH, we used Eq. (20) (Stumm and Morgan, 1996; Frankignoulle, 1994):

$$\left(\frac{\partial A}{\partial pH}\right)_X = \frac{\partial[H^+]}{\partial pH}\left(\frac{\partial A}{\partial[H^+]}\right)_X = -\ln(10)\,[H^+]\left(\frac{\partial A}{\partial[H^+]}\right)_X \tag{20}$$

where A may refer to either TotX or TA. Similarly, for the factors in Table 5.3b,

$$\frac{\partial pH}{\partial A} = \frac{\partial pH}{\partial[H^+]}\,\frac{\partial[H^+]}{\partial A} = \frac{-1}{\ln(10)\,[H^+]}\,\frac{\partial[H^+]}{\partial A} \tag{21}$$

The generalised expressions for the buffer factors presented in this paper are fully consistent with those presented by Frankignoulle (1994) and Egleston et al. (2010), where $\frac{\partial[H^+]}{\partial TA}$ was determined with DIC as state variable, while assuming that total borate was invariant and neglecting the contribution of other acid-base systems except the auto-dissociation of water. For example, the equation given by Egleston et al. (2010) for β_{TA} is as follows:

$$\beta_{TA} = \left(\frac{\partial \ln[H^+]}{\partial TA}\right)^{-1} = \frac{TA_{DIC}^2}{DIC} - S \tag{22}$$

with:

$$S = [HCO_3^-] + 4[CO_3^{2-}] + \frac{[B(OH)_4^-]\,[H^+]}{K_{B(OH)_3} + [H^+]} + [OH^-] + [H^+] \tag{23}$$

This equation is equivalent to our expression for $\frac{\partial[H^+]}{\partial TA}$ under the conditions defined in their paper. Egleston et al. (2010) only included the carbonate and borate acid-base systems and auto-dissociation of water in their definition of TA. The proton concentration buffer factor β_H is thus also only built up from these three components:

$$\beta_H = \left(\frac{\partial TA_{DIC}}{\partial[H^+]}\right)_{DIC} + \left(\frac{\partial TA_{TotB}}{\partial[H^+]}\right)_{TotB} + \left(\frac{\partial TA_{H_2O}}{\partial[H^+]}\right)_{H_2O} \tag{24}$$

Since a change in DIC is equivalent to a change in H_2CO_3, we define DIC as the independent state variable TotX, so that the contribution of the independent state variable to TA is TA_{DIC} and the species of interest is H_2CO_3. The expression for $\left(\frac{\partial TA}{\partial[H^+]}\right)_{H_2CO_3}$ (Eq. (16)) then becomes:

$$\left(\frac{\partial TA}{\partial[H^+]}\right)_{H_2CO_3} = \left(\frac{\partial TA_{DIC}}{\partial[H^+]}\right)_{H_2CO_3} + \left(\frac{\partial TA_{TotB}}{\partial[H^+]}\right)_{TotB} + \left(\frac{\partial TA_{H_2O}}{\partial[H^+]}\right)_{H_2O} \tag{25}$$

Taking the relevant factors of Tables 5.2a – b, and recalling that n equals 0 in the case of a DIC addition, with some rearranging we define

$$\left(\frac{\partial TA}{\partial[H^+]}\right)_{H_2CO_3} = \frac{-1}{[H^+]}\left([HCO_3^-] + 4[CO_3^{2-}] + [B(OH)_4^-]\,\frac{[B(OH)_3]}{TotB} + [OH^-] + [H^+]\right) \tag{26}$$

It can mathematically be shown that $\frac{[B(OH)_4^-]\,[H^+]}{K_{B(OH)_3}+[H^+]}$ is equal to $[B(OH)_4^-]\frac{[B(OH)_3]}{TotB}$, from which it follows that:

$$\left(\frac{\partial TA}{\partial[H^+]}\right)_{H_2CO_3} = \frac{-1}{[H^+]}\,S \tag{27}$$

Now we insert this definition into our expression for $\frac{\partial[H^+]}{\partial TA}$ (Table 5.3b) and adapt it to include our previously defined parameters X = H_2CO_3, n = 0, TotX = DIC and TA_{TotX} = TA_{DIC}:

$$\frac{\partial[H^+]}{\partial TA} = \frac{DIC\,[H^+]}{TA_{DIC}^2 + \left([H^+]\left(\dfrac{-1}{[H^+]}\,S\right)\right)DIC} \tag{28}$$

This can be rearranged to yield

$$\frac{\partial[H^+]}{\partial TA} = \frac{DIC\,[H^+]}{TA_{DIC} - SDIC} \tag{29}$$

Dividing both numerator and denominator on the right hand side by DIC and dividing the left and right hand sides by $[H^+]$ gives:

$$\frac{1}{[H^+]}\frac{\partial[H^+]}{\partial TA} = \frac{DIC\,[H^+]}{\dfrac{TA_{DIC}^2}{DIC} - S} \tag{30}$$

from which it can easily be seen that:

$$\left(\frac{1}{[H^+]}\frac{\partial[H^+]}{\partial TA}\right)^{-1} = \left(\frac{\partial \ln[H^+]}{\partial TA}\right)^{-1} = \frac{TA_{DIC}^2}{DIC} - S \tag{31}$$

The factors that Egleston et al. (2010) derived are valid for a change in DIC without taking into account which species of DIC is changed, although they are also applicable in case of a change in the reference species CO_2. Thus, their factors β_{TA} and β_{DIC} are equivalent to our factors $\frac{\partial[H^+]}{\partial TA}$ and $\frac{\partial[H^+]}{\partial TotX}$, respectively, as presented in Table 5.3b. Their factors γ_{TA} and γ_{DIC} are equivalent to our $\frac{\partial[X]}{\partial TA}$ and $\frac{\partial[X]}{\partial TotX}$, but only in the cases where X equals X_{ref}, since both γ_{TA} and γ_{DIC} are defined for the addition of CO_2 (which is X_{ref} for the carbonate system) and lack a term describing the charge contribution to alkalinity. Interestingly though, their factors ω_{TA} and ω_{DIC} are also similar to our factors $\frac{\partial[X]}{\partial TA}$ and $\frac{\partial[X]}{\partial TotX}$, but with X = CO_3^{2-}. This is further detailed in Appendix 5.A.

The factors β_{TA} and β_{DIC} of Egleston et al. (2010) are also equivalent to the factors Φ_D and Φ_H derived by Frankignoulle (1994), which describe the change in pH due to change in dissolved CO_2 and TA, respectively. Frankignoulle (1994), however, additionally derived chemical, heterogeneous buffer factors that describe the change in pH resulting from changes in HCO_3^- and CO_3^{2-}. By specifically inducing a change in either of these species, both DIC and TA are affected. After converting from pH to $[H^+]$, his results can be summarised as: (see Appendix 5.B for the derivation)

$$\frac{\partial[H^+]}{\partial X} = \frac{\partial[H^+]}{\partial TotX} + n\,\frac{\partial[H^+]}{\partial TA} \tag{32}$$

Thus, if H_2CO_3 is added or removed, $\frac{\partial[H^+]}{\partial X}$ equals $\frac{\partial[H^+]}{\partial TotX}$, in line with what has been discussed above.

The generalised expression for the buffer factors can in principle also be used to elucidate and quantify the salinity, temperature and pressure (p) dependencies of pH (Hofmann et al., 2009). However, the resulting expressions are rather complex and it is therefore recommended to calculate the sensitivities numerically (see Appendix 5.C).

The acid-base buffer factor (β_H) and underlying terms are also linked to the well-known Revelle factor (RF) expressing the sensitivity of pCO_2 to changes in DIC (Revelle and Suess, 1957; Bolin and Eriksson, 1959; Sundquist et al., 1979):

$$RF = \frac{\partial \ln[CO_2]}{\partial \ln DIC} = \frac{DIC}{[CO_2]}\left(\frac{\partial[CO_2]}{\partial DIC}\right) \tag{33}$$

From the expression for $\frac{\partial[X]}{\partial TotX}$ in Table 5.3b, and defining that TotX = DIC, X = CO_2 (from now on denoted H_2CO_3 for consistency) and, as a result, n equals 0, we can define $\frac{\partial[H_2CO_3]}{\partial DIC}$:

$$\frac{\partial[H_2CO_3]}{\partial DIC} = \frac{[H_2CO_3][H^+]\left(\dfrac{\partial TA}{\partial[H^+]}\right)_{H_2CO_3}}{TA_{DIC}^2 + [H^+]\left(\dfrac{\partial TA}{\partial[H^+]}\right)_{H_2CO_3} DIC} \tag{34}$$

The factor $\left(\frac{\partial TA}{\partial[H^+]}\right)_{H_2CO_3}$ is defined as in Eq. (16). From Eq. (34) it easily follows that:

$$RF = \frac{[H^+]\left(\dfrac{\partial TA}{\partial[H^+]}\right)_{H_2CO_3} DIC}{TA_{DIC}^2 + [H^+]\left(\dfrac{\partial TA}{\partial[H^+]}\right)_{H_2CO_3} DIC} \tag{35}$$

This generalised Revelle factor includes all acid-base systems relevant for the system of interest and it can easily be shown that it is fully consistent with the homogeneous RF derived by Sundquist et al. (1979) and Zeebe and Wolf-Gladrow (2001). The work done by Sundquist et al. (1979) only includes the carbonate and borate acid-base systems and neglects the auto-dissociation of water. In this specific case, $\left(\frac{\partial TA}{\partial[H^+]}\right)_{H_2CO_3}$ is defined as:

$$\left(\frac{\partial TA}{\partial[H^+]}\right)_{H_2CO_3} = \left(\frac{\partial TA_{DIC}}{\partial[H^+]}\right)_{H_2CO_3} + \left(\frac{\partial TA_{TotB}}{\partial[H^+]}\right)_{TotB} \tag{36}$$

Assuming for this purpose that proton activity and concentration are equal, the expression given by Sundquist et al. (1979) reads:

$$RF = DIC\left([H_2CO_3] + [CO_3^{2-}] + \frac{\gamma[HCO_3^-] - 4[CO_3^{2-}]^2}{[HCO_3^-] + 4[CO_3^{2-}] + \gamma}\right)^{-1} \tag{37}$$

with:

$$\gamma = \frac{TotB\, K_{B(OH)_3}[H^+]}{K_{B(OH)_3} + [H^+]} \tag{38}$$

The work by Zeebe and Wolf-Gladrow (2001) also includes the auto-dissociation of water. In this case, $\left(\frac{\partial TA}{\partial[H^+]}\right)_{H_2CO_3}$ is defined as in Eq. (25). Their expression for RF reads:

$$RF = \frac{DIC}{[H_2CO_3]}\left(\frac{\partial DIC}{\partial[H_2CO_3]}\right)^{-1} \tag{39}$$

with:

Table 5.4 Initial conditions for our globally averaged model system for the surface ocean for the year 2000. For TotS we took the global average of dimethylsulphide (DMS), which is the most important reduced sulphur form in the surface ocean.

Parameter	Value		Reference
T	18.252	°C	Locarnini et al. (2013); average of 1°x1° climatological mean surface-water data for all decades
S	34.617		Zweng et al. (2013); average of 1°x1° climatological mean surface-water data for all decades
p	1.008	dbar	Pressure at a latitude of 45° and 1 m depth calculated according to (Fofonoff and Millard, 1983)
TA	2304.91	µmol kg^{-1}	Key et al. (2004); average of 1°x1° gridded data
TotNH$_4$	0.3	µmol L^{-1}	Gruber (2008); average concentration of euphotic zone; uncertainty ca. ±20%
TotB	428.4	µmol kg^{-1}	calculated from salinity using the relationship of Lee et al. (2010)
DIC	2017.14	µmol kg^{-1}	Key et al. (2004); average of 1°x1° gridded data
TotPO$_4$	0.530	µmol L^{-1}	Garcia et al. (2013); average of 1°x1° climatological mean surface-water data for all decades
TotNO$_3$	5.207	µmol L^{-1}	Garcia et al. (2013); average of 1°x1° climatological mean surface-water data for all decades
TotNO$_2$	0.1	µmol L^{-1}	Gruber (2008); average concentration of euphotic zone; uncertainty ca. ±20%
TotS (DMS)	2.35·10^{-3}	µmol L^{-1}	Lana et al. (2011); average of 1°x1° climatological annual mean surface-water data
TotSi	7.466	µmol L^{-1}	Garcia et al. (2013); average of 1°x1° climatological mean surface-water data for all decades
TotF	67.579	µmol kg^{-1}	calculated from salinity using the relationship of Riley (1965)
TotSO$_4$	2.793·10^4	µmol kg^{-1}	calculated from salinity using the relationship of Morris and Riley (1966)

$$\frac{\partial DIC}{\partial [H_2CO_3]} = \frac{\left(\begin{array}{l} \dfrac{4\,K_{H_2CO_3}K_{HCO_3^-}}{[H^+]^2} + \dfrac{K_{H_2CO_3}}{[H^+]} + \dfrac{(K_{H_2CO_3})^2\,K_{HCO_3^-}}{[H^+]^3} + \\[2mm] \dfrac{[H^+]}{[H_2CO_3]}\left(1 + \dfrac{K_{H_2CO_3}K_{HCO_3^-}}{[H^+]^2} + \dfrac{K_{H_2CO_3}}{[H^+]}\right)\left(1 + \dfrac{K_W}{[H^+]^2} + \dfrac{TotB K_{B(OH)_3}}{(K_{B(OH)_3} + [H^+])^2}\right) \end{array} \right)}{\dfrac{4\,K_{H_2CO_3}K_{HCO_3^-}}{[H^+]^2} + \dfrac{K_{H_2CO_3}}{[H^+]} + \dfrac{[H^+]}{[H_2CO_3]}\left(1 + \dfrac{K_W}{[H^+]^2} + \dfrac{TotB\,K_{B(OH)_3}}{(K_{B(OH)_3} + [H^+])^2}\right)} \tag{40}$$

Appendix 5.D shows that Eqs. (37) and (39) are both equivalent to Eq. (35).

5.2.3 Implementation of the buffer factors

We have now derived all partial derivatives of Eq. (5) and are thus able to attribute changes in pH to different factors. To make these buffer factors more tangible, and to get a feeling for the importance of each of the factors, we will take the global ocean surface water as a model system and apply changes in each of the factors discussed in Sect. 5.2.1 and 5.2.2. Since $\frac{\partial pH}{\partial TotX}$ and $\frac{\partial pH}{\partial TA}$ are independent of the species of the acid-base system that is added or removed (Table 5.3b), we will only consider changes in TotX, rather than the individual species. All calculations were performed on the free pH scale using the R package *AquaEnv* (Hofmann et al., 2010b). To highlight that the free scale is used in this paper, from now on we will denote pH as pH_F. As carbonate dissociation constants we used those of Mehrbach et al. (1973) as refitted by Dickson and Millero (1987). This is done as Takahashi et al. (1993), when determining the effect of changes in T on pCO_2, got the best fit between the experimental and computed data when using these constants in combination with the CO_2 solubility expression of Weiss (1974). In addition, these dissociation constants were used in the construction of the GLODAP database (Key et al., 2004) that we use for estimating the initial conditions of the carbonate system. Since these dissociation constants are not included in *AquaEnv*, they were calculated using CO2SYS (Lewis and Wallace, 1998). For the other acid-base dissociation constants, we chose the default settings of *AquaEnv*.

Table 5.4 shows the initial conditions of our model system, which is assumed to represent the global open-ocean surface water mean of the year 2000. We calculated the sensitivities of pH_F to changes in TotX, TA, T and S for 2000 and 2100, assuming that temperature and atmospheric pCO_2 ($pCO_{2,atm}$) change according to the highest Representative Concentration Pathway, RCP8.5. The increase in $pCO_{2,atm}$ until 2100 was taken from (Meinshausen et al., 2011), thereby assuming that seawater pCO_2 increases by the same magnitude. The increase in global average SST from the 1990s to the 2090s has been estimated at 2.73±0.72°C (Bopp et al., 2013). All other parameters were kept constant. If necessary, nutrient concentrations were converted from μmol L^{-1} to μmol kg^{-1}.

5.3   Results and discussion

5.3.1   Sensitivities in contemporary global ocean surface water

Table 5.5 shows the sensitivities describing a change in pH_F calculated for the contemporary global open ocean surface water and how these may change by the end of the 21st century. We first discuss their general meaning, thereby keeping Eq. (5) in mind. A negative sensitivity indicates that adding this species to the system leads to a decrease in pH_F. This is e.g. the case for DIC, which is consistent with our general knowledge of the carbonate system. The reverse holds for the positive sensitivities, such as $\frac{\partial pH}{\partial TA}$, where an increase in TA leads to an increase in pH_F. The signs of the sensitivities do not change in the range of conditions we consider here and, in fact, do not change over the whole range of pH_F values in oceanic and coastal waters. This is due to the way the sensitivities with respect to changes in the total concentrations are defined; the denominator in the sensitivities of Table 5.3b always has a negative sign, i.e. the term $\left([H^+]\left(\frac{\partial TA}{\partial [H^+]} \right)_X - nTA_{TotX} \right) TotX$

is always negative and exceeds TA_{TotX}^2. Therefore, the sign of $\frac{\partial pH}{\partial TotX}$ depends on the sign of TA_{TotX}; if the contribution of an acid-base system to TA is positive, then $\frac{\partial pH}{\partial TotX}$ is by definition negative. As this is the case for most of the acid-base systems, most of the sensitivities are negative and thus lead to a decrease in pH_F when their total concentration increases.

The magnitude of a sensitivity with respect to a total concentration of an acid-base species mainly depends on two factors: (1) TA_{TotX}, which controls the numerator in $\frac{\partial pH}{\partial TotX}$, and (2) TotX, which linearly correlates with the absolute value of the denominator ($R^2 = 1$, $P < 0.001$). This can be explained by the fact that TotX is much more variable than $\left[[H^+]\left(\frac{\partial TA}{\partial[H^+]}\right)_X - nTA_{TotX}\right] TotX$ and much larger than TA_{TotX}^2, the other two terms in the denominator. The factor $\left(\frac{\partial TA}{\partial[H^+]}\right)_X$ only deviates substantially from β_H when TA_{TotX} contributes substantially to TA; in these cases, $\left(\frac{\partial TA}{\partial[H^+]}\right)_X$ exceeds β_H by up to 1 order of magnitude (in the case of TA_{DIC}). It varies per species whether TotX or TA_{TotX} mainly controls the magnitude of $\frac{\partial pH}{\partial TotX}$. For example, the denominators of $\frac{\partial pH}{\partial DIC}$ and $\frac{\partial pH}{\partial TotB}$ have a similar order of magnitude, but since TA_{TotB} is 1 order of magnitude smaller than TA_{DIC}, the absolute value of $\frac{\partial pH}{\partial DIC}$ is much higher than that of $\frac{\partial pH}{\partial TotB}$. On the contrary, TA_{TotB} is 1 order of magnitude higher than TA_{TotSi}, but due to the much smaller total concentration of silicate in comparison to borate, the absolute value of $\frac{\partial pH}{\partial TotSi}$ is higher.

Table 5.5 shows that $\frac{\partial pH}{\partial TotPO_4}$ has the highest absolute value. So, if one were to add a fixed increment of the total concentration of each acid-base system to our model system separately, then the addition of $TotPO_4$ would lead to the biggest change in pH_F, followed by DIC and then TotS. This sensitivity of pH_F to $TotPO_4$ is the reason this nutrient, together with TotSi, is by default included in the most common programs for calculating the carbonate chemistry, such as CO2SYS (Lewis and Wallace, 1998), SWCO2 (Hunter, 2007) and the R-package *seacarb* (Gattuso et al., 2015). The units of the sensitivities with respect to changes in the total concentrations are in $(mol\ kg^{-1})^{-1}$. This means that adding 1 μmol kg^{-1} $TotPO_4$ to this system leads to a decrease in pH_F of 0.00180, while the addition of 1 μmol kg^{-1} DIC lowers pH_F by 0.00175. However, in natural systems DIC, $TotPO_4$ and other nutrients do not change by the same amounts over diurnal, seasonal or interannual timescales. Hence, as displayed in Eq. (5), it is ultimately the combination of the change in TotX combined with the sensitivity that determines the actual change in pH_F.

Increasing T, S and p all lead to a decrease in pH_F. A warming of 1ºC lowers pH by 0.0122, while the effect of changing pressure is much smaller; increasing p by 1 bar (which implies an increase in depth of ca. 10 m) leads to a decrease in pH of 0.000401. Our estimate of $\frac{\partial pH}{\partial T}$ is in reasonable agreement with the -0.016±0.001 estimated by Takahashi et al. (2014), who use a more extensive data set and report pH on the total scale (from now on denoted as pH_T). Note that Pilson (2014), in contrast to these results, calculated an increase in pH (displayed on the NIST scale, from now on denoted as pH_{NIST}) with an increase in T. This different result can, however, be explained by the different approaches used. In our approach we keep the total concentrations of the acid-base species and TA constant when calculating the sensitivity of pH with respect to an increase in T. This leads to an increase in pCO_2 while keeping DIC constant, and thus a lowering in pH. Pilson (2014), however, kept the atmospheric $[CO_2]$ and TA constant when increasing T. Since he corrected for the water vapour pressure, which is a function of T as

Table 5.5 Global mean values for all derived sensitivities at present and in 2100, using various scenarios. Contemporary average surface seawater conditions were obtained from Table 5.4. Using the dissociation constants as outlined in Sect 5.2.3, this corresponds to $pH_F = 8.21$ and $pCO_2 = 327$ ppmv. Changes in temperature (Bopp et al., 2013) and pCO_2 (Meinshausen et al., 2011) until 2100 ($pCO_2 = 894$ ppmv, T = 21.0°C) were considered both separately and combined.

Sensitivity	Unit	Present	2100 CO$_2$	2100 T	2100 T+CO$_2$
$\dfrac{\partial pH}{\partial TA}$	$(mol\ kg^{-1})^{-1}$	1600.86	2627.39	1517.41	2479.79
$\dfrac{\partial pH}{\partial TotNH_4}$	$(mol\ kg^{-1})^{-1}$	-64.75	-45.07	-75.05	-53.11
$\dfrac{\partial pH}{\partial TotB}$	$(mol\ kg^{-1})^{-1}$	-347.83	-270.84	-346.98	-274.94
$\dfrac{\partial pH}{\partial DIC}$	$(mol\ kg^{-1})^{-1}$	-1751.38	-2704.83	-1673.64	-2567.00
$\dfrac{\partial pH}{\partial TotPO_4}$	$(mol\ kg^{-1})^{-1}$	-1799.85	-2734.41	-1731.20	-2605.60
$\dfrac{\partial pH}{\partial TotNO_3}$	$(mol\ kg^{-1})^{-1}$	$4.23 \cdot 10^{-7}$	$1.68 \cdot 10^{-6}$	$3.97 \cdot 10^{-7}$	$1.54 \cdot 10^{-6}$
$\dfrac{\partial pH}{\partial TotNO_2}$	$(mol\ kg^{-1})^{-1}$	$6.25 \cdot 10^{-3}$	$2.48 \cdot 10^{-2}$	$5.87 \cdot 10^{-3}$	$2.28 \cdot 10^{-2}$
$\dfrac{\partial pH}{\partial TotS}$	$(mol\ kg^{-1})^{-1}$	-1552.99	-2444.48	-1475.88	-2323.52
$\dfrac{\partial pH}{\partial TotSi}$	$(mol\ kg^{-1})^{-1}$	-64.21	-44.68	-67.14	-47.36
$\dfrac{\partial pH}{\partial TotF}$	$(mol\ kg^{-1})^{-1}$	$3.73 \cdot 10^{-3}$	$1.48 \cdot 10^{-2}$	$3.68 \cdot 10^{-3}$	$1.43 \cdot 10^{-2}$
$\dfrac{\partial pH}{\partial TotSO_4}$	$(mol\ kg^{-1})^{-1}$	$7.74 \cdot 10^{-5}$	$3.07 \cdot 10^{-4}$	$8.06 \cdot 10^{-5}$	$3.13 \cdot 10^{-4}$
$\dfrac{\partial pH}{\partial T}$	$(°C)^{-1}$	$-1.22 \cdot 10^{-2}$	$-1.12 \cdot 10^{-2}$	$-1.19 \cdot 10^{-2}$	$-1.10 \cdot 10^{-2}$
$\dfrac{\partial pH}{\partial p}$	$(bar)^{-1}$	$-4.01 \cdot 10^{-4}$	$-4.14 \cdot 10^{-4}$	$-3.98 \cdot 10^{-4}$	$-4.08 \cdot 10^{-4}$
$\dfrac{\partial pH}{\partial S}$	-	$-8.50 \cdot 10^{-3}$	$-7.63 \cdot 10^{-3}$	$-8.49 \cdot 10^{-3}$	$-7.72 \cdot 10^{-3}$
$\left(\dfrac{\partial pH}{\partial TotF}\right)_{K_j^*}$	$(mol\ kg^{-1})^{-1}$	93.90	98.40	96.97	100.91
$\left(\dfrac{\partial pH}{\partial TotSO_4}\right)_{K_j^*}$	$(mol\ kg^{-1})^{-1}$	2.74	2.74	2.98	2.98

well, an increase in T led to a decrease of both DIC and the fugacity of CO_2 (fCO_2), which implied an increase in pH. Increasing S by 1 leads to a lowering in pH of 0.0085. By also including the

effect of S on TotB, Takahashi et al. (2014) estimated a value for $\frac{\partial pH_T}{\partial S}$ of -0.0125±0.0005. If we assume that an increase in S of 1 units leads to an increase in TotB of 12.358 µmol kg^{-1} (Lee et al., 2010), then we can calculate a combined sensitivity of increasing S and TotB of -0.0128. Taking into account the different pH scale, this is similar to the estimate of Takahashi et al. (2014).

5.3.2   Sensitivities in the future ocean

When comparing the sensitivities of the contemporary ocean and a warmer, high-CO_2 ocean, it becomes clear that not all sensitivities respond in a similar way to these processes (Table 5.5). The magnitude of the majority of sensitivities becomes greater when pCO_2 increases. This means that the change in pH associated with a certain increment of TotX will be higher in a high-CO_2 compared to the present-day ocean. Taking DIC as an example, an increase of 1 µmol kg^{-1} DIC in a high-CO_2 ocean lowers pH$_F$ by 0.00270, indicating that [H$^+$] increases 3.73 times more compared to the contemporary ocean. This factor is significantly higher than the ca. 1.4 found by Riebesell et al. (2009), who used a more conservative increase in $pCO_{2,atm}$. Also the sensitivity of pH to a change in TA increases; an increase of 1 µmol kg^{-1} TA raises pH by 0.00263, equivalent to a 3.96 times higher decrease in [H$^+$]. In addition, the high-CO_2 ocean is less sensitive to changes in S and T, the latter of which is consistent with Riebesell et al. (2009), who found the same trend in both cold and warm surface waters.

In contrast to a more acidified ocean, most sensitivities get a smaller magnitude in a warmer ocean. Thus, a warmer ocean is less sensitive to changes in pH due to changes in TotX, T or S. Taking DIC as an example, an increase of 1 µmol kg^{-1} DIC in a warmer ocean lowers pH$_F$ by 0.00167. This indicates that, when adding 1 µmol kg^{-1} DIC, the increase in [H$^+$] is 94.6% of the increase in the contemporary ocean. Similarly, the decrease in [H$^+$] in a warmer ocean is 93.8% of the current decrease resulting from an increase in TA of 1 µmol kg^{-1}. While most sensitivities related to TotX show an opposite response to warming and acidification, this is not the case for the sensitivities related to S and T changes. The effect of an increase in temperature on pH$_F$ is not intuitive: as Table 5.5 shows, the resulting relative increase in $\frac{\partial pH}{\partial T}$ upon warming is much smaller than that of, e.g. $\frac{\partial pH}{\partial DIC}$. The sensitivity $\frac{\partial pH}{\partial T}$ depends in a complex way on many acid-base dissociation constants. Changes therein might cancel each other out, as can be inferred from the contrasting responses of, e.g. $\frac{\partial pH}{\partial TotNH_4}$ and $\frac{\partial pH}{\partial DIC}$ to warming. The direct effect of temperature on changes in pH$_F$ might thus be relatively unimportant. However, temperature also affects pH$_F$ in an indirect way. Since $\frac{\partial pH}{\partial DIC}$ becomes smaller in a warmer ocean, temperature affects the response of the ocean to an increase in DIC. This secondary effect of warming on pH$_F$ might be much more important than the direct effect.

When acidification and warming are combined, the direction of change of all sensitivities, with the exception of the terms related to pH scale conversion, follows that of acidification only. This indicates that the projected increase in pCO_2 until 2100 has a bigger effect on these sensitivities than the projected increase in T. If the response of a sensitivity to an increase in T is in the opposite direction as the response to an increase in pCO_2, as is the case for most sensitivities, then the change in sensitivity is smaller than in the scenario where only pCO_2 increases. Taking again DIC and TA as examples, in this scenario a 1 µmol kg^{-1} increase in DIC lowers [H$^+$] 3.45 times more

Table 5.6 Initial conditions for the surface water of the Peruvian oxygen minimum zone (12.5°S, 77.5°W) for the year 2000. References are as in Table 5.4, except for $TotNH_4$ and $TotNO_2$, which were taken from Lam et al. (2009).

Parameter	Value (depth = 1 m)		Parameter	Value (depth = 1 m)	
T	18.934	°C	$TotPO_4$	1.304	$\mu mol\ L^{-1}$
S	35.043		$TotNO_3$	5.939	$\mu mol\ L^{-1}$
p	1.006	dbar	$TotNO_2$	0.5	$\mu mol\ L^{-1}$
TA	2327.03	$\mu mol\ kg^{-1}$	TotS (DMS)	$2.32 \cdot 10^{-3}$	$\mu mol\ L^{-1}$
$TotNH_4$	0.2	$\mu mol\ L^{-1}$	TotSi	7.238	$\mu mol\ L^{-1}$
TotB	433.1	$\mu mol\ kg^{-1}$	TotF	68.410	$\mu mol\ kg^{-1}$
DIC	2053.02	$\mu mol\ kg^{-1}$	$TotSO_4$	$2.827 \cdot 10^{4}$	$\mu mol\ kg^{-1}$

than in the contemporary ocean, while an equivalent increase in TA raises $[H^+]$ 3.64 times more. Both of these values are lower than the factors mentioned for an increase in pCO_2 only. Note that the values of the sensitivities for warming and acidification combined cannot be calculated by summing the separate changes of a higher T and pCO_2. The reason for this is that our assumption that pCO_2 is the same in both the high and the low T scenarios implies that DIC is slightly lower in the scenario where T is higher. If we had kept DIC, rather than pCO_2, the same in the high and low T scenarios, then this would have been possible.

When comparing the relative changes in sensitivity between the contemporary and a warmer, high-CO_2 ocean, it can be seen that the magnitude of $\frac{\partial pH}{\partial TA}$ increases more then the magnitude of $\frac{\partial pH}{\partial DIC}$. This is important when considering a process that influences both TA and DIC, such as calcite dissolution or precipitation where the TA:DIC production or consumption ratio is 2:1. In the contemporary ocean, the increase in $[H^+]$ by adding 1 $\mu mol\ kg^{-1}$ TA is 91.4% of the decrease in $[H^+]$ by adding 1 $\mu mol\ kg^{-1}$ DIC. In a warmer, high-CO_2 ocean, this fraction will increase to 96.6%. Thus, the change in TA becomes relatively more important to the observed pH_F change. If we only consider the sensitivities with respect to TotX that have a magnitude exceeding 1, which may be regarded the environmentally relevant sensitivities, then the biggest absolute change is seen with $\frac{\partial pH}{\partial TA}$. In contrast, oceanic pH becomes less sensitive to changes in T and S.

To summarise, a fixed increment in TotX will in most cases lead to a higher change in pH by the end of the 21st century compares to the present. The sensitivities that become smaller show a less pronounced change than those that get bigger. Thus, we can conclude that as the pCO_2 of the global ocean increases, it is less capable of buffering changes in the concentrations of acid-base species. However, this effect is slightly moderated by the increase in T.

5.3.3 Analytical versus numerical calculation of buffer factors

It has recently been pointed out that differences between analytical expressions for the Revelle factor that only include the carbonate system and treat the borate system as invariant (Frankignoulle, 1994; Sundquist et al., 1979; Zeebe and Wolf-Gladrow, 2001), and the

Table 5.7 Comparison between analytical and numerical calculation of sensitivities as defined for the contemporary average global surface ocean (see Table 5.5). The percentages in the headings of the numerical calculation refer to the relative in- and decrement of the state variable.

Sensitivity $(mol\ kg^{-1})^{-1}$	Analytical	Numerical (0.1%)	Numerical (1%)	Frankignoulle expression
RF (dimensionless)	9.899	9.900	9.935	9.911
$\dfrac{\partial pH}{\partial TA}$	1600.86	1600.88	1602.68	1602.97
$\dfrac{\partial pH}{\partial TotNH_4}$	-64.75	-64.75	-64.75	-
$\dfrac{\partial pH}{\partial TotB}$	-347.83	-347.83	-347.83	-
$\dfrac{\partial pH}{\partial DIC}$	-1751.38	-1751.39	-1752.63	-1753.68
$\dfrac{\partial pH}{\partial TotPO_4}$	-1799.85	-1799.85	-1799.85	-
$\dfrac{\partial pH}{\partial TotNO_3}$	$4.23\cdot10^{-7}$	0	0	-
$\dfrac{\partial pH}{\partial TotNO_2}$	$6.25\cdot10^{-3}$	0	0	-
$\dfrac{\partial pH}{\partial TotS}$	-1552.99	-1552.99	-1552.99	-
$\dfrac{\partial pH}{\partial TotSi}$	-64.21	-64.21	-64.21	-

numerical approximation of CO2SYS, which uses the full definition of TA as given by Dickson (1981), are highest when nutrients contribute significantly to TA (Munhoven, 2014). We can use the expressions from this paper to show that these differences are reduced, and in fact the analytical expression become more accurate than the numerical estimate, when the approach of Frankignoulle (1994) is expanded to include all relevant acid-base systems contributing to TA.

For this, we numerically estimated both RF and $\frac{\partial pH}{\partial A}$ (where A can refer to either TotX or TA) for two systems: (1) the contemporary ocean (Table 5.4), and (2) one grid cell of the climatological mean surface-water data (Table 5.4) representative for the Peruvian oxygen minimum zone (12.5°S, 77.5°W; Table 5.6). Small (1 and 0.1%) in- and decrements were applied to the variable of interest (TA or TotX), after which both resulting pH values (in the case of $\frac{\partial pH}{\partial A}$) or CO_2 values (in the case of RF) were taken and used to calculate the corresponding sensitivity. TotF and $TotSO_4$ were discarded from this analysis, as with this numerical estimation it is not possible to distinguish between the actual change in pH resulting from a change in concentration ($\frac{\partial pH}{\partial TotF}$ and $\frac{\partial pH}{\partial TotSO_4}$), and the effects related to scale conversion ($\left(\frac{\partial pH}{\partial TotF}\right)_{K_i^*}$ and $\left(\frac{\partial pH}{\partial TotSO_4}\right)_{K_i^*}$). In addition, we also analytically

Table 5.8 Comparison between analytical and numerical calculation of sensitivities as defined for the Peruvian oxygen minimum zone (12.5°S, 77.5°W). The percentages in the headings of the numerical calculation refer to the relative in- and decrement of the state variable.

Sensitivity $(mol\ kg^{-1})^{-1}$	Analytical	Numerical (0.1%)	Numerical (1%)	Frankignoulle expression
RF (dimensionless)	10.215	10.215	10.255	10.229
$\dfrac{\partial pH}{\partial TA}$	1648.05	1648.07	1650.03	1650.67
$\dfrac{\partial pH}{\partial TotNH_4}$	-63.51	-63.51	-63.51	-
$\dfrac{\partial pH}{\partial TotB}$	-336.42	-336.42	-336.42	-
$\dfrac{\partial pH}{\partial DIC}$	-1792.33	-1792.34	-1793.69	-1795.18
$\dfrac{\partial pH}{\partial TotPO_4}$	-1838.62	-1838.62	-1838.62	-
$\dfrac{\partial pH}{\partial TotNO_3}$	$4.80 \cdot 10^{-7}$	0	0	-
$\dfrac{\partial pH}{\partial TotNO_2}$	$7.10 \cdot 10^{-3}$	0	0	-
$\dfrac{\partial pH}{\partial TotS}$	-1594.89	-1594.89	-1594.89	-1594.89
$\dfrac{\partial pH}{\partial TotSi}$	-61.63	-61.63	-61.63	-

calculated the factors β_D, Φ_D and Φ_H of Frankignoulle (1994), which are equivalent to RF, $\frac{\partial pH}{\partial DIC}$ and $\frac{\partial pH}{\partial TA}$, respectively. The results of both calculations were compared with the analytically calculated sensitivities using the generalised expressions of this work.

Both for the contemporary ocean (Table 5.7) and the Peruvian oxygen minimum zone (Table 5.8), this comparison shows that the factors β_D, Φ_D and Φ_H deviate most from the analytically derived factors and the numerical estimates with smallest disturbance (0.1%), which may be assumed to be more accurate than the estimate using a higher disturbance. This shows that our method is indeed capable of analytically calculating sensitivities more accurately than previously. It is thus possible to analytically calculate RF and other sensitivities at high accuracy even in nutrient-rich waters.

Tables 5.7 – 5.8 also show that when the variable of interest is changed by 1%, in most cases $\frac{dpH}{dA}$ equals $\frac{\partial pH}{\partial A}$. Exceptions here are TA and DIC, the two variables with highest concentrations, where a smaller disturbance (0.1%) is required to arrive at the same value using 5 significant digits. It

is thus recommended to use at most a 0.1% disturbance for an accurate numerical estimate of all sensitivities, including $\frac{\partial \mathrm{pH}}{\partial \mathrm{DIC}}$ and $\frac{\partial \mathrm{pH}}{\partial \mathrm{TA}}$.

5.4   Conclusions and implications

We presented general expressions describing the change in $\mathrm{pH_F}$ or an acid-base species due to changes in TA or the total concentration of that particular acid-base system. These sensitivities are valid for any combination of acid-base systems and any total concentration, or any of the species contributing to the total concentration, as independent state variable, assuming that all other factors remain constant. They are therefore ideal when attributing which factors drive a change in $\mathrm{pH_F}$ or X. We tested this by applying these sensitivities to a global ocean surface water model system. Furthermore, we investigated the changes in these sensitivities in a warmer, more acidified ocean, thereby showing that most sensitivities increase under these conditions, thus decreasing the ocean's capacity to buffer changes in pH. This decrease is mostly driven by the increase in $\mathrm{pCO_2}$ and slightly tempered by the increase in T.

Previous studies have shown that seawater buffering capacity will decrease in a warmer, high-CO_2 ocean (e.g. Hofmann et al., 2010a; Egleston et al., 2010; Hagens et al., 2014). Our work supports this finding, but additionally is the first to give a comprehensive overview of all sensitivities and shows which of these factors are most affected by global change. The lower capacity of the global ocean to buffer changes in TA and most total concentrations of acid-base species by the end of the 21$^{\mathrm{st}}$ century has important implications. For example, we may expect a more pronounced diurnal (Schulz and Riebesell, 2013) and seasonal pH variability resulting from photosynthesis and subsequent organic matter remineralisation. This effect may be amplified if productivity were to increase in the future ocean (Low-Décarie et al., 2014), though whether this will happen is subject of debate (Eichner et al., 2014; Joint et al., 2011).

Both Frankignoulle (1994) and Egleston et al. (2010) discussed some useful applications of the buffer factors derived in their papers. Among these are estimating the ratio of organic matter production to calcification in, e.g. coral reefs, aiding experimental designs, and testing model parameter sensitivities. The sensitivities derived in this paper can be applied to the same questions and are particularly useful in waters where the contribution of acid-base systems other than the carbonate and borate system to TA is high. Examples of these are pore waters (Ben-Yaakov, 1973), upwelling regions (Dugdale et al., 1977) and anoxic bottom waters in stratified seas (Ulfsbo et al., 2011) or rivers (Gaines Jr and Pilson, 1972).

Acknowledgements

Appendix 5.A. Linking the factors of Egleston et al. (2010) to this work

In the main text we mentioned that the factors γ_{TA} and γ_{DIC} of Egleston et al. (2010) are equivalent to our factors $\frac{\partial [X]}{\partial TA}$ and $\frac{\partial [X]}{\partial TotX}$, but only in the cases where X equals X_{ref}. This is as both γ_{TA} and γ_{DIC} are defined for the addition of CO_2 (which is X_{ref} for the carbonate system) and lack a term describing the charge contribution to alkalinity. Interestingly though, their factors ω_{TA} and ω_{DIC} are also similar to our factors $\frac{\partial [X]}{\partial TA}$ and $\frac{\partial [X]}{\partial TotX}$, but with $X = CO_3^{2-}$. How does this work? Taking ω_{DIC} as an example, it is defined by Egleston et al. (2010) as:

$$\left(\frac{\partial \ln\Omega}{\partial DIC} \right)^{-1} = DIC - \frac{TA_{DIC}\, P}{W} \tag{A1}$$

with:

$$P = 2\,[H_2CO_3] + [HCO_3^-] \tag{A2}$$

and, taking into account the correction of Álvarez et al. (2014),

$$W = [HCO_3^-] - \frac{[B(OH)_4^-]\,[H^+]}{K_{B(OH)_3} + [H^+]} - [H^+] - [OH^-] \tag{A3}$$

A simple comparison between P and TA_{DIC} learns us that:

$$P = 2\,DIC - TA \tag{A4}$$

Similarly, comparing W and S leads us to conclude that:

$$W = 2\,TA_{DIC} - S \tag{A5}$$

Plugging these definitions into Eq. (A1) gives:

$$\left(\frac{\partial \ln\Omega}{\partial DIC} \right)^{-1} = DIC - \frac{TA_{DIC}\,(2\,DIC - TA)}{2\,TA_{DIC} - S} \tag{A6}$$

Now we compare this equation with our $\frac{\partial [X]}{\partial TotX}$ (Table 5.3b) adapted for the current situation. But first, we define Ω as $\frac{[Ca^{2+}]\,[CO_3^{2-}]}{K_{sp}}$. If we assume that K_{sp} and $[Ca^{2+}]$ are constants that do not change due to changes in DIC or TA, we can state the following:

$$\left(\frac{\partial A}{\partial \Omega} \right)_{H^+} = \frac{K_{sp}}{[Ca^{2+}]} \left(\frac{\partial A}{\partial [CO_3^{2-}]} \right)_{H^+} \tag{A7}$$

and

$$\left(\frac{\partial A}{\partial [H^+]} \right)_{\Omega} = \left(\frac{\partial A}{\partial [H^+]} \right)_{[CO_3^{2-}]} \tag{A8}$$

where A refers to either TA or DIC.

Similarly as in the derivation of β_{TA}, TotX is DIC and only the carbonate and borate acid-base systems are take into account, with the inclusion of the auto-dissociation of water. In the case of a change in Ω, being equivalent to a change in $[CO_3^{2-}]$, n equals 2. After some rearranging, the expression for $\left(\frac{\partial TA}{\partial [H^+]}\right)_{\Omega}$ (Eq. (16)) becomes:

$$\left(\frac{\partial TA}{\partial [H^+]}\right)_{\Omega} = \frac{-1}{[H^+]} \left(- 2\, TA_{DIC} + [HCO_3^-] + 4[CO_3^{2-}] + [B(OH)_4^-]\,\frac{[B(OH)_3]}{TotB} + [OH^-] + [H^+]\right) \tag{A9}$$

Recalling the definitions of W (Eq. (A3)) and S (Eq. (23)), it follows that:

$$\left(\frac{\partial TA}{\partial [H^+]}\right)_{\Omega} = \frac{-1}{[H^+]}\,(- 2\, TA_{DIC} + S) = \frac{-1}{[H^+]}\,(-W) \tag{A10}$$

Now we adapt our expression for $\frac{\partial [X]}{\partial TotX}$ (Table 5.3b) to include our previously defined parameters $X = \Omega$, n = 2, TotX = DIC and $TA_{TotX} = TA_{DIC}$. Note that because of the linear correlation between Ω and $[CO_3^{2-}]$, this approach is valid. In other words, we could replace Ω with $\frac{[Ca^{2+}]}{K_{sp}}[CO_3^{2-}]$, where $\frac{[Ca^{2+}]}{K_{sp}}$ is a constant factor, and obtain the same resulting expression.

$$\frac{\partial [\Omega]}{\partial DIC} = \frac{[\Omega][H^+]\left(\frac{\partial TA}{\partial [H^+]}\right)_{\Omega}}{TA_{DIC}^2 + \left([H^+]\left(\frac{\partial TA}{\partial [H^+]}\right)_{\Omega} - 2\, TA_{DIC}\right) DIC} \tag{A11}$$

Next, we plug in the definition of $\left(\frac{\partial TA}{\partial [H^+]}\right)_{\Omega}$:

$$\frac{\partial [\Omega]}{\partial DIC} = \frac{[\Omega][H^+]\left(\frac{-1}{[H^+]}\,(- 2\, TA_{DIC} + S)\right)}{TA_{DIC}^2 + \left([H^+]\left(\frac{-1}{[H^+]}\,(- 2\, TA_{DIC} + S)\right) - 2\, TA_{DIC}\right) DIC} \tag{A12}$$

Rearranging Eq. (A12) yields:

$$\frac{\partial [\Omega]}{\partial DIC} = \frac{[\Omega]\,(2\, TA_{DIC} - S)}{TA_{DIC}^2 + (2\, TA_{DIC} - S - 2\, TA_{DIC})\, DIC} \tag{A13}$$

And even further rearranging and diving both the left and right hand side by $[CO_3^{2-}]$ yields:

$$\frac{1}{[\Omega]}\frac{\partial [\Omega]}{\partial DIC} = \frac{2\, TA_{DIC} - S}{TA_{DIC}^2 - S\, DIC} \tag{A14}$$

Taking the inverse and remembering how S and W are related (Eq. (A5)), we end up with:

$$\left(\frac{1}{[\Omega]}\frac{\partial [\Omega]}{\partial DIC}\right)^{-1} = \frac{TA_{DIC}^2 - (2\, TA_{DIC} - W)\, DIC}{W} \tag{A15}$$

Next we work out the brackets and rearrange:

$$\left(\frac{\partial \ln\Omega}{\partial DIC}\right)^{-1} = \frac{TA_{DIC}\,(TA_{DIC} - 2\,DIC)}{W} + DIC \tag{A16}$$

Finally, we remember how P and TA_{DIC} are related (Eq. (A4)) and arrive at Eq. (A1):

$$\left(\frac{\partial \ln\Omega}{\partial DIC}\right)^{-1} = DIC - \frac{TA_{DIC}\,P}{W} \tag{A17}$$

Appendix 5.B. Linking the work of Frankignoulle (1994) to this work

As mentioned in the text, Frankignoulle (1994) derived the sensitivities $\frac{\partial pH}{\partial [HCO_3^-]}$ and $\frac{\partial pH}{\partial [CO_3^{2-}]}$ which, after converting from pH to [H$^+$], can be linked to $\frac{\partial [H^+]}{\partial DIC}$ via:

$$\frac{\partial [H^+]}{\partial X} = \frac{\partial [H^+]}{\partial TotX} + n\,\frac{\partial [H^+]}{\partial TA} \tag{B1}$$

To show that this is true, we first explain the approach of Frankignoulle (1994), which differs from the previously discussed approaches. He defined the expression:

$$\Phi_X = \frac{\partial pH}{\partial X} = -\left([H^+]\ln(10)\left(\frac{\partial [H_2CO_3]}{\partial [H^+]} + \frac{\partial [HCO_3^-]}{\partial [H^+]} + \frac{\partial [CO_3^{2-}]}{\partial [H^+]}\right)\right)^{-1} \tag{B2}$$

where X can refer to either H_2CO_3, HCO_3^- or CO_3^{2-}, as in his approach the carbonate system was the acid-base system of interest. Furthermore, only the borate acid-base system and the auto-dissociation of water were included. The three partial derivatives in Eq. (B2) were defined according to MacIntyre (1978):

$$\left(\frac{\partial [CO_3^{2-}]}{\partial [H^+]}\right)_X = \frac{-K_{HCO_3^-}\,TA_{DIC} + K_{HCO_3^-}\,([H^+] + 2\,K_{HCO_3^-})\left(\dfrac{\partial TA_{DIC}}{\partial [H^+]}\right)_X}{([H^+] + 2\,K_{HCO_3^-})^2} \tag{B3}$$

$$\left(\frac{\partial [HCO_3^-]}{\partial [H^+]}\right)_X = \frac{2\,K_{HCO_3^-}\,TA_{DIC} + [H^+]\,([H^+] + 2\,K_{HCO_3^-})\left(\dfrac{\partial TA_{DIC}}{\partial [H^+]}\right)_X}{([H^+] + 2\,K_{HCO_3^-})^2} \tag{B4}$$

$$\left(\frac{\partial [H_2CO_3]}{\partial [H^+]}\right)_X = \frac{TA_{DIC}\,[H^+]}{([H^+] + 2\,K_{HCO_3^-})\,K_{H_2CO_3}} + \frac{[H^+]}{K_{H_2CO_3}}\,\frac{\partial [HCO_3^-]}{\partial [H^+]} \tag{B5}$$

In Eqs. (B3-B5), the subscripts X were not added to either $\frac{\partial TA_{DIC}}{\partial [H^+]}$ or $\frac{\partial [X]}{\partial [H^+]}$ by Frankignoulle (1994). Rather, their presence was implied by stating that $\frac{\partial TA_{DIC}}{\partial [H^+]}$ is different for each of the carbonate system species, as equivalent to our Table 5.2a, and thus also affect Eqs. (B3-B5). For clarity, we will now add these subscripts to the definition of $\left(\frac{\partial TA_{DIC}}{\partial [H^+]}\right)_X$, which was given by Frankignoulle (1994) as:

$$\left(\frac{\partial TA_{DIC}}{\partial [H^+]}\right)_X = n\left(\frac{\partial DIC}{\partial [H^+]}\right)_X - \frac{\partial [B(OH)_4^-]}{\partial [H^+]} - \frac{\partial [OH^-]}{\partial [H^+]} \tag{B6}$$

with $\left(\frac{\partial DIC}{\partial [H^+]}\right)_X$ defined as the sum of Eqs. (B3-B5). Note that it is again implied that total borate does not change. Thus, when looking at the contributions of the borate system and the auto-dissociation of water to alkalinity, Eq. (B6) can be rewritten to:

$$\left(\frac{\partial TA_{DIC}}{\partial [H^+]}\right)_X = n\frac{\partial DIC}{\partial [H^+]} - \left(\frac{\partial TA_{TotB}}{\partial [H^+]}\right)_{TotB} - \left(\frac{\partial TA_{H_2O}}{\partial [H^+]}\right)_{H_2O} \tag{B7}$$

As a next step in his derivation, Frankignoulle (1994) plugged Eq. (B6) into Eqs. (B3-B5), yielding:

$$\left(\frac{\partial [CO_3^{2-}]}{\partial [H^+]}\right)_X = \frac{-K_{HCO_3^-} TA_{DIC} + K_{HCO_3^-} Q \left(n\frac{\partial DIC}{\partial [H^+]} + V\right)}{Q^2} \tag{B8}$$

$$\left(\frac{\partial [HCO_3^-]}{\partial [H^+]}\right)_X = \frac{2 K_{HCO_3^-} TA_{DIC} + [H^+] Q \left(n\frac{\partial DIC}{\partial [H^+]} + V\right)}{Q^2} \tag{B9}$$

$$\left(\frac{\partial [H_2CO_3]}{\partial [H^+]}\right)_X = \frac{TA_{DIC} [H^+]}{Q K_{H_2CO_3}} + \frac{[H^+]}{K_{H_2CO_3}} \frac{2 K_{HCO_3^-} TA_{DIC} + [H^+] Q \left(n\frac{\partial DIC}{\partial [H^+]} + V\right)}{Q^2} \tag{B10}$$

with:

$$Q = [H^+] + 2 K_{HCO_3^-} \tag{B11}$$

and

$$V = \frac{TotB\, K_{B(OH)_3}}{(K_{B(OH)_3} + [H^+])^2} + \frac{K_W}{[H^+]} + 1 = -\frac{\partial [B(OH)_4^-]}{\partial [H^+]} - \frac{\partial [OH^-]}{\partial [H^+]} + 1 \tag{B12}$$

Note that this factor V is linked both to the factor S of Eggleston et al. (2010) and to our derivative $\left(\frac{\partial TA}{\partial [H^+]}\right)_X$ via:

$$V = \left(\frac{\partial TA_{DIC}}{\partial [H^+]}\right)_{H_2CO_3} + \frac{1}{[H^+]} S \tag{B13}$$

$$V = \left(\frac{\partial TA_{DIC}}{\partial [H^+]}\right)_X - \left(\frac{\partial TA}{\partial [H^+]}\right)_X \tag{B14}$$

Then Frankignoulle (1994) summed Eqs. (B8-B10) to arrive at an expression that only includes the terms $\left(\frac{\partial DIC}{\partial [H^+]}\right)_X$, $[H^+]$ and reaction invariants. This yields the lengthy expression:

$$\left(\frac{\partial \text{DIC}}{\partial[\text{H}^+]}\right)_X = \left(\frac{\partial[\text{H}_2\text{CO}_3]}{\partial[\text{H}^+]}\right)_X + \left(\frac{\partial[\text{HCO}_3^-]}{\partial[\text{H}^+]}\right)_X + \left(\frac{\partial[\text{CO}_3^{2-}]}{\partial[\text{H}^+]}\right)_X \tag{B15}$$

$$= \frac{\text{TA}_{\text{DIC}}\,[\text{H}^+]}{Q\,K_{\text{H}_2\text{CO}_3}} + \frac{[\text{H}^+]}{K_{\text{H}_2\text{CO}_3}}\,\frac{2\,K_{\text{HCO}_3^-}\text{TA}_{\text{DIC}} + [\text{H}^+]\,Q\left(n\,\dfrac{\partial \text{DIC}}{\partial[\text{H}^+]} + V\right)}{Q^2}$$

$$+ \frac{2\,K_{\text{HCO}_3^-}\text{TA}_{\text{DIC}} + [\text{H}^+]\,Q\left(n\,\dfrac{\partial \text{DIC}}{\partial[\text{H}^+]} + V\right)}{Q^2} + \frac{-K_{\text{HCO}_3^-}\text{TA}_{\text{DIC}} + K_{\text{HCO}_3^-}\,Q\left(n\,\dfrac{\partial \text{DIC}}{\partial[\text{H}^+]} + V\right)}{Q^2}$$

After rearranging such that is $\left(\frac{\partial \text{DIC}}{\partial[\text{H}^+]}\right)_X$ isolated on the left hand side, we end up with Eq. (7) of Frankignoulle (1994):

$$\left(\frac{\partial \text{DIC}}{\partial[\text{H}^+]}\right)_X = \frac{\dfrac{1}{Q}\left(K_{\text{HCO}_3^-}\text{TA}_{\text{DIC}} + Q\,V\,([\text{H}^+] + K_{\text{HCO}_3^-}) + \dfrac{[\text{H}^+]}{K_{\text{H}_2\text{CO}_3}}\,(\text{TA}_{\text{DIC}}\,Q + 2\,K_{\text{HCO}_3^-}\,\text{TA}_{\text{DIC}} + [\text{H}^+]\,Q\,V)\right)}{Q - n\left([\text{H}^+] + K_{\text{HCO}_3^-} + \dfrac{[\text{H}^+]^2}{K_{\text{H}_2\text{CO}_3}}\right)} \tag{B16}$$

This can then be inverted and plugged into Eq. (B2):

$$\Phi_X = \frac{\partial \text{pH}}{\partial X} = \frac{-1}{\ln(10)\,[\text{H}^+]}\left(\left(\frac{\partial \text{DIC}}{\partial[\text{H}^+]}\right)_X\right)^{-1} \tag{B17}$$

We will now show the validity of Eq. (B1) using CO_3^{2-} as an example. In this case, Eq. (B17) becomes:

$$\Phi_{\text{CO}_3^{2-}} = \frac{\partial \text{pH}}{\partial[\text{CO}_3^{2-}]} = \frac{-1}{\ln(10)\,[\text{H}^+]}\left(\left(\frac{\partial \text{DIC}}{\partial[\text{H}^+]}\right)_{\text{CO}_3^{2-}}\right)^{-1} \tag{B18}$$

By multiplying both sides by $\frac{\partial[\text{H}^+]}{\partial \text{pH}}$, this can be rewritten to:

$$\frac{\partial[\text{H}^+]}{\partial[\text{CO}_3^{2-}]} = \left(\left(\frac{\partial \text{DIC}}{\partial[\text{H}^+]}\right)_{\text{CO}_3^{2-}}\right)^{-1} \tag{B19}$$

Filling in Eq. (B16) for $X = \text{CO}_3^{2-}$ and $n = 2$ and plugging into Eq. (B19) we arrive at:

$$\frac{\partial[\text{H}^+]}{\partial[\text{CO}_3^{2-}]} = \frac{Q - 2\left([\text{H}^+] + K_{\text{HCO}_3^-} + \dfrac{[\text{H}^+]^2}{K_{\text{H}_2\text{CO}_3}}\right)}{\dfrac{1}{Q}\left(K_{\text{HCO}_3^-}\text{TA}_{\text{DIC}} + Q\,V\,([\text{H}^+] + K_{\text{HCO}_3^-}) + \dfrac{[\text{H}^+]}{K_{\text{H}_2\text{CO}_3}}\,(\text{TA}_{\text{DIC}}\,Q + 2\,K_{\text{HCO}_3^-}\,\text{TA}_{\text{DIC}} + [\text{H}^+]\,Q\,V)\right)} \tag{B20}$$

We will now switch to our generalised expressions. Assuming that Eq. (B1) is valid, and knowing that $X = \text{CO}_3^{2-}$, TotX = DIC and $n = 2$, we fill in Eq. (B1) using our expressions from Table 5.3b. Note that since the denominators in Table 5.3b are all the same, they can easily be combined.

$$\frac{\partial[H^+]}{\partial[CO_3^{2-}]} = \frac{[H^+]\,(2\,DIC - TA_{DIC})}{TA_{DIC}^2 + \left([H^+]\left(\dfrac{\partial TA}{\partial[H^+]}\right)_{CO_3^{2-}} - 2\,TA_{DIC}\right)DIC} \tag{B21}$$

As said before, Frankignoulle (1994) only included the carbonate and borate acid-base system and the auto-dissociation of water. With this knowledge and using Eqs. (9) and (16), we define:

$$\beta_H = \left(\frac{\partial TA_{DIC}}{\partial[H^+]}\right)_{DIC} + \left(\frac{\partial TA_{TotB}}{\partial[H^+]}\right)_{TotB} + \left(\frac{\partial TA_{H_2O}}{\partial[H^+]}\right)_{H_2O} \tag{B22}$$

and:

$$\left(\frac{\partial TA}{\partial[H^+]}\right)_{CO_3^{2-}} = \left(\frac{\partial TA_{DIC}}{\partial[H^+]}\right)_{CO_3^{2-}} + \left(\frac{\partial TA_{TotB}}{\partial[H^+]}\right)_{TotB} + \left(\frac{\partial TA_{H_2O}}{\partial[H^+]}\right)_{H_2O} \tag{B23}$$

Taking the relevant factors of Tables 5.2a and 5.2b, with some rearranging we define:

$$\left(\frac{\partial TA}{\partial[H^+]}\right)_{CO_3^{2-}} = \frac{-1}{[H^+]}\left(-2\,TA_{DIC} + [HCO_3^-] + 4[CO_3^{2-}] + [B(OH)_4^-]\,\frac{[B(OH)_3]}{TotB} + [OH^-] + [H^+]\right) \tag{B24}$$

This can directly be linked to the definition of V (Eq. (B14)), yielding:

$$\left(\frac{\partial TA}{\partial[H^+]}\right)_{CO_3^{2-}} = \frac{-1}{[H^+]}\left(-2\,TA_{DIC} + ([HCO_3^-] + 4[CO_3^{2-}])\right) - V \tag{B25}$$

Furthermore, Frankignoulle (1994) defined all carbonate system parameters in terms of TA_{DIC} and equilibrium constants, so we need to define $[HCO_3^-]$, $[CO_3^{2-}]$ and DIC in terms of TA_{DIC}. For this, we need the expression for TA_{DIC} from Table 5.1b. After rearranging, this becomes:

$$DIC = \frac{[H^+]^2 + K_{H_2CO_3}[H^+] + K_{H_2CO_3}K_{HCO_3^-}}{K_{H_2CO_3}[H^+] + 2\,K_{H_2CO_3}K_{HCO_3^-}}\,TA_{DIC} \tag{B26}$$

which, using Eq. (B11), can be further linked to Frankignoulle (1994):

$$DIC = \frac{[H^+]^2 + K_{H_2CO_3}[H^+] + K_{H_2CO_3}K_{HCO_3^-}}{K_{H_2CO_3}Q}\,TA_{DIC} \tag{B27}$$

This definition can subsequently be plugged into the general expressions describing $[HCO_3^-]$ and $[CO_3^{2-}]$ in terms of DIC, $[H^+]$ and equilibrium constants:

$$[HCO_3^-] = \frac{K_{H_2CO_3}[H^+]}{[H^+]^2 + K_{H_2CO_3}[H^+] + K_{H_2CO_3}K_{HCO_3^-}}\,DIC \tag{B28}$$

$$[CO_3^{2-}] = \frac{K_{H_2CO_3}K_{HCO_3^-}}{[H^+]^2 + K_{H_2CO_3}[H^+] + K_{H_2CO_3}K_{HCO_3^-}}\,DIC \tag{B29}$$

When plugging Eqs. (B25) and (B27-B29) into our Eq. (B21) and doing some extensive rearranging, we end up with Eq. (B20), proving the validity of Eq. (B1).

Appendix 5.C. Effects of changes in temperature, salinity, and pressure

As stated in the main text, it is possible to quantify the effect of changes in T, S and p on pH by analytically deriving their sensitivities as a function of [H$^+$], total concentrations of acid-base species and acid-base dissociation constants. Using this approach, as many acid-base systems can be added as are relevant for the system of interest. The main disadvantage, however, is its relative complexity; even only including the carbonate and borate system yields lengthy expressions, because of the complicated way the dissociation constants depend on T, S and p (Hofmann et al., 2009). It is therefore recommended to calculate these sensitivities numerically. Here we follow the approach of Hofmann et al. (2009), who defined the following sensitivities:

$$\frac{\partial [\mathrm{H^+}]}{\partial T} = -\sum_{j=1}^{k}\left(\frac{\partial \mathrm{TA}}{\partial K_j^*}\frac{\partial K_j^*}{\partial T}\right)\Bigg/ \beta_{\mathrm{H}} \tag{C1}$$

$$\frac{\partial [\mathrm{H^+}]}{\partial p} = -\sum_{j=1}^{k}\left(\frac{\partial \mathrm{TA}}{\partial K_j^*}\frac{\partial K_j^*}{\partial p}\right)\Bigg/ \beta_{\mathrm{H}} \tag{C2}$$

$$\frac{\partial [\mathrm{H^+}]}{\partial S} = -\sum_{j=1}^{k}\left(\frac{\partial \mathrm{TA}}{\partial K_j^*}\frac{\partial K_j^*}{\partial S}\right)\Bigg/ \beta_{\mathrm{H}} \tag{C3}$$

$$\left(\frac{\partial [\mathrm{H^+}]}{\partial \mathrm{TotF}}\right)_{K_j^*} = -\sum_{j=1}^{k}\left(\frac{\partial \mathrm{TA}}{\partial K_j^*}\frac{\partial K_j^*}{\partial \mathrm{TotF}}\right)\Bigg/ \beta_{\mathrm{H}} \tag{C4}$$

$$\left(\frac{\partial [\mathrm{H^+}]}{\partial \mathrm{TotSO_4}}\right)_{K_j^*} = -\sum_{j=1}^{k}\left(\frac{\partial \mathrm{TA}}{\partial K_j^*}\frac{\partial K_j^*}{\partial \mathrm{TotSO_4}}\right)\Bigg/ \beta_{\mathrm{H}} \tag{C5}$$

In Eqs. (C1-C5), j refers to the acid-base species of interest and K_j^* to the stoichiometric acid-base dissociation constants corresponding to this species. The sensitivity $\sum_{j=1}^{k}\left(\frac{\partial \mathrm{TA}}{\partial K_j^*}\frac{\partial K_j^*}{\partial T}\right)$ was estimated by applying a 10% increase and decrease in T, taking both resulting TA values and calculating the slope. This was done similarly for the sensitivities related to p, S, TotF and TotSO$_4$. The expression for β_{H} was taken from Table 5.3a. Note that β_{H}, just as the other sensitivities in Tables 5.3a – b, is indirectly influenced by changes in T, p and S, as these changes induce a shift in the relative concentrations of the acid-base species and therefore a change in TA (see Sect. 5.3.2).

At first, the purpose of Eqs. (C4-C5) might seem unclear as Table 5.3b already contains expressions for $\frac{\partial [\mathrm{H^+}]}{\partial \mathrm{TotF}}$ and $\frac{\partial [\mathrm{H^+}]}{\partial \mathrm{TotSO_4}}$. However, these equations are necessary compartments when changing T, p or S because of the different pH scales on which equilibrium constants are defined. The following is a brief overview of the different pH scales; for more details, the interested reader is referred to Dickson (1984) and Zeebe and Wolf-Gladrow (2001). The free pH scale considers only H$^+$ ions, while in the total pH scale the total H$^+$ concentration is defined as the sum of protonated sulphate ions and free H$^+$ ions. The seawater pH scale additionally includes protonated fluoride ions in its definition of total H$^+$ concentration. Because of these different definitions, the value of pH may differ by ca. 0.1 units depending on the scale at which it is expressed. It is therefore always necessary to specify this scale when presenting pH data. Each experiment for defining an expression for an

acid-base dissociation constant is done in a specific seawater medium, usually containing sulphate or sulphate and fluoride. These species affect the measured total H$^+$ concentration and thus the pH scale on which the formulation is defined. In all derivations up until now, we have only worked with [H$^+$], which is the concentration of 'free' H$^+$ ions. By making use of the acid-base dissociation constants for TotSO$_4$ and (if applicable) TotF, we can convert from the total or seawater pH scale to the free pH scale. These conversion factors are functions of T, p or S, since they depend on the acid-base dissociation constants for TotSO$_4$ and TotF. Therefore, when one is interested in the effect of a change in T, p or S on pH, it is always necessary to include Eqs. (C4-C5) as well. Note that, in addition to the three scales mentioned above, a fourth pH scale exist which is often used in governmental monitoring programs. This so-called NIST pH scale is, however, calibrated based on a series of standard buffer solutions made in a freshwater medium. As a result, pH measurements made on this scale in a saline medium are less reliable and its use in seawater is therefore not recommended. In addition, conversion between the NIST scale and other pH scales is less straightforward.

In practice, TotSO$_4$ (Morris and Riley, 1966) and TotF (Riley, 1965) are often, similar to TotB, assumed to be proportional to S. So although the buffer factors related to Eqs. (C4) and (C5) can always be calculated, from Eq. (5) it can be deduced that they will only influence the change in pH with time if a change in S is considered. For clarity and to be as complete as possible, we will keep Eqs. (C4) and (C5) separate from Eq. (C3), but we will not further discuss them when presenting their results as they merely have a mathematical meaning.

Finally, by applying Eq. (21), Eqs. (C1-C5) can easily be converted from [H$^+$] to pH. Note that in Eqs. (20) and (21), pH is defined on the free scale.

Appendix 5.D. Linking the work of Sundquist et al. (1979) and Zeebe and Wolf-Gladrow (2001) to this work

Two previous studies have given explicit expressions for the Revelle factor: Sundquist et al. (1979) and Zeebe and Wolf-Gladrow (2001). Here we will explicitly link both expressions to our generalised expressions.

Under the conditions defined by Sundquist et al. (1979) and using the generalised expressions from this study, we can define RF as:

$$RF = \frac{[H^+]\left(\dfrac{\partial TA}{\partial [H^+]}\right)_{H_2CO_3} DIC}{TA_{DIC}^2 + [H^+]\left(\dfrac{\partial TA}{\partial [H^+]}\right)_{H_2CO_3} DIC} \tag{D1}$$

with:

$$\left(\frac{\partial TA}{\partial [H^+]}\right)_{H_2CO_3} = \left(\frac{\partial TA_{DIC}}{\partial [H^+]}\right)_{H_2CO_3} + \left(\frac{\partial TA_{TotB}}{\partial [H^+]}\right)_{TotB} \tag{D2}$$

Assuming for this purpose that proton activity and concentration are equal, the expression given by Sundquist et al. (1979) reads:

$$RF = DIC\left([H_2CO_3] + [CO_3^{2-}] + \frac{\gamma[HCO_3^-] - 4[CO_3^{2-}]^2}{[HCO_3^-] + 4[CO_3^{2-}] + \gamma}\right)^{-1} \tag{D3}$$

with:

$$\gamma = \frac{TotB\, K_{B(OH)_3}[H^+]}{K_{B(OH)_3} + [H^+]} \tag{D4}$$

We now show how Eq. (D3) can be rewritten in terms of our Eq. (D1). First, using our knowledge of the borate system, it can mathematically be shown that $[B(OH)_4^-] = \frac{TotB\, K_{B(OH)_3}}{K_{B(OH)_3} + [H^+]}$ and $\frac{[B(OH)_4^-][H^+]}{K_{B(OH)_3} + [H^+]} = [B(OH)_4^-]\frac{[B(OH)_3]}{TotB}$, from which it follows that:

$$\gamma = -[H^+]\left(\frac{\partial TA_{TotB}}{\partial [H^+]}\right)_{TotB} \tag{D5}$$

Furthermore, knowing that n equals 0 in the case of an addition of H_2CO_3 and TotX is DIC, we take $\left(\frac{\partial TA_{DIC}}{\partial [H^+]}\right)_{H_2CO_3}$ from Table 5.2a and rearrange it such that:

$$[HCO_3^-] + 4[CO_3^{2-}] = -[H^+]\left(\frac{\partial TA_{DIC}}{\partial [H^+]}\right)_{H_2CO_3} \tag{D6}$$

Plugging Eqs. (D5-D6) into Eq. (D3) yields:

$$RF = DIC\left([H_2CO_3] + [CO_3^{2-}] + \frac{-[H^+]\left(\frac{\partial TA_{TotB}}{\partial [H^+]}\right)_{TotB}[HCO_3^-] - 4[CO_3^{2-}]^2}{-[H^+]\left(\frac{\partial TA_{DIC}}{\partial [H^+]}\right)_{H_2CO_3} - [H^+]\left(\frac{\partial TA_{TotB}}{\partial [H^+]}\right)_{TotB}}\right)^{-1} \tag{D7}$$

Rearranging and plugging Eq. (D2) into Eq. (D7) yields:

$$RF = DIC\left([H_2CO_3] + [CO_3^{2-}] + \frac{-[H^+]\left(\frac{\partial TA_{TotB}}{\partial [H^+]}\right)_{TotB}[HCO_3^-] - 4[CO_3^{2-}]^2}{-[H^+]\left(\frac{\partial TA}{\partial [H^+]}\right)_{H_2CO_3}}\right)^{-1} \tag{D8}$$

Next, we multiply the terms $[H_2CO_3]$ and $[CO_3^{2-}]$ by $-[H^+]\left(\frac{\partial TA_{DIC}}{\partial [H^+]}\right)_{H_2CO_3}$ and make one big term of the nominator:

$$RF = DIC\left(\frac{F - 4[CO_3^{2-}]^2}{-[H^+]\left(\frac{\partial TA}{\partial [H^+]}\right)_{H_2CO_3}}\right)^{-1} \tag{D9}$$

where:

$$F = -[H^+]\left(\frac{\partial TA}{\partial[H^+]}\right)_{H_2CO_3}[H_2CO_3] - [H^+]\left(\frac{\partial TA}{\partial[H^+]}\right)_{H_2CO_3}[CO_3^{2-}] - [H^+]\left(\frac{\partial TA_{TotB}}{\partial[H^+]}\right)_{TotB}[HCO_3^-] \qquad (D10)$$

Using Eq. (D2) and the definition $DIC = [H_2CO_3] + [HCO_3^-] + [CO_3^{2-}]$, we can rewrite F:

$$F = -[H^+]\left(\frac{\partial TA}{\partial[H^+]}\right)_{H_2CO_3}DIC + [H^+]\left(\frac{\partial TA_{DIC}}{\partial[H^+]}\right)_{H_2CO_3}[HCO_3^-] \qquad (D11)$$

Furthermore, taking Eq. (D6), this can be rewritten:

$$F = -[H^+]\left(\frac{\partial TA}{\partial[H^+]}\right)_{H_2CO_3}DIC - [HCO_3^-]^2 - 4[HCO_3^-][CO_3^{2-}] \qquad (D12)$$

Then, we make use of the definition of TA_{DIC} (Table 5.1a) to rewrite $-4[CO_3^{2-}]^2$ in terms of TA_{DIC}^2:

$$RF = DIC\left(\frac{F+[HCO_3^-]^2 + 4[HCO_3^-][CO_3^{2-}] - TA_{DIC}^2}{-[H^+]\left(\frac{\partial TA}{\partial[H^+]}\right)_{H_2CO_3}}\right)^{-1} \qquad (D13)$$

Then we plug Eq. (D12) into Eq. (D13). It becomes immediately clear that some terms can be dropped:

$$RF = DIC\left(\frac{-[H^+]\left(\frac{\partial TA}{\partial[H^+]}\right)_{H_2CO_3}DIC - TA_{DIC}^2}{-[H^+]\left(\frac{\partial TA}{\partial[H^+]}\right)_{H_2CO_3}}\right)^{-1} \qquad (D14)$$

Finally, we take the inverse of the inverse term and rearrange to arrive at Eq. (D1):

$$RF = \frac{[H^+]\left(\frac{\partial TA}{\partial[H^+]}\right)_{H_2CO_3}DIC}{TA_{DIC}^2 + [H^+]\left(\frac{\partial TA}{\partial[H^+]}\right)_{H_2CO_3}DIC} \qquad (D15)$$

In contrast to the expression derived by Sundquist et al. (1979), the work of Zeebe and Wolf-Gladrow (2001) includes the auto-dissociation of water. Thus, we can define RF according to Eq. (D1), but the expression for $\left(\frac{\partial TA}{\partial[H^+]}\right)_{H_2CO_3}$ changes:

$$\left(\frac{\partial TA}{\partial[H^+]}\right)_{H_2CO_3} = \left(\frac{\partial TA_{DIC}}{\partial[H^+]}\right)_{H_2CO_3} + \left(\frac{\partial TA_{TotB}}{\partial[H^+]}\right)_{TotB} + \left(\frac{\partial TA_{H_2O}}{\partial[H^+]}\right)_{H_2O} \qquad (D16)$$

If we assume again for this purpose that $[CO_2]$ and $[H_2CO_3]$ are equal, then the expression given by Zeebe and Wolf-Gladrow (2001) for RF reads:

$$RF = \frac{DIC}{[H_2CO_3]}\left(\frac{\partial DIC}{\partial[H_2CO_3]}\right)^{-1} \qquad (D17)$$

with:

$$\frac{\partial DIC}{\partial[H_2CO_3]} = \frac{\begin{pmatrix} \dfrac{4\,K_{H_2CO_3}K_{HCO_3^-}}{[H^+]^2} + \dfrac{K_{H_2CO_3}}{[H^+]} + \dfrac{(K_{H_2CO_3})^2\,K_{HCO_3^-}}{[H^+]^3} + \\[2mm] \dfrac{[H^+]}{[H_2CO_3]}\left(1 + \dfrac{K_{H_2CO_3}K_{HCO_3^-}}{[H^+]^2} + \dfrac{K_{H_2CO_3}}{[H^+]}\right)\left(1 + \dfrac{K_W}{[H^+]^2} + \dfrac{TotB\,K_{B(OH)_3}}{(K_{B(OH)_3} + [H^+])^2}\right) \end{pmatrix}}{\dfrac{4\,K_{H_2CO_3}K_{HCO_3^-}}{[H^+]^2} + \dfrac{K_{H_2CO_3}}{[H^+]} + \dfrac{[H^+]}{[H_2CO_3]}\left(1 + \dfrac{K_W}{[H^+]^2} + \dfrac{TotB\,K_{B(OH)_3}}{(K_{B(OH)_3} + [H^+])^2}\right)} \tag{D18}$$

We now show how Eq. (D17) can be rewritten in terms of our Eq. (D1).

First, using again our knowledge of the borate system used to arrive at Eq. (D5), and looking at the definitions of the borate system and the auto-dissociation of water as given in Tables 5.1b and 5.2b, we can rewrite Eq. (D18):

$$\frac{\partial DIC}{\partial[H_2CO_3]} = \frac{\begin{pmatrix} \dfrac{4\,K_{H_2CO_3}K_{HCO_3^-}}{[H^+]^2} + \dfrac{K_{H_2CO_3}}{[H^+]} + \dfrac{(K_{H_2CO_3})^2\,K_{HCO_3^-}}{[H^+]^3} + \\[2mm] \dfrac{[H^+]}{[H_2CO_3]}\left(1 + \dfrac{K_{H_2CO_3}K_{HCO_3^-}}{[H^+]^2} + \dfrac{K_{H_2CO_3}}{[H^+]}\right)\left(-\left(\dfrac{\partial TA_{TotB}}{\partial[H^+]}\right)_{TotB} - \left(\dfrac{\partial TA_{H_2O}}{\partial[H^+]}\right)_{H_2O}\right) \end{pmatrix}}{\dfrac{4\,K_{H_2CO_3}K_{HCO_3^-}}{[H^+]^2} + \dfrac{K_{H_2CO_3}}{[H^+]} - \dfrac{[H^+]}{[H_2CO_3]}\left(\left(\dfrac{\partial TA_{TotB}}{\partial[H^+]}\right)_{TotB} + \left(\dfrac{\partial TA_{H_2O}}{\partial[H^+]}\right)_{H_2O}\right)} \tag{D19}$$

Then, we also rewrite the carbonate system species by implementing that $[HCO_3^-] = \frac{K_{H_2CO_3}}{[H^+]}[H_2CO_3]$ and $[CO_3^{2-}] = \frac{K_{H_2CO_3}K_{HCO_3^-}}{[H^+]^2}[H_2CO_3]$ (Table 5.1a):

$$\frac{\partial DIC}{\partial[H_2CO_3]} = \frac{\begin{pmatrix} \dfrac{4\,[CO_3^{2-}]}{[H_2CO_3]} + \dfrac{[HCO_3^-]}{[H_2CO_3]} + \dfrac{[HCO_3^-]\,[CO_3^{2-}]}{[H_2CO_3]^2} + \\[2mm] \dfrac{[H^+]}{[H_2CO_3]}\left(1 + \dfrac{[CO_3^{2-}]}{[H_2CO_3]} + \dfrac{[HCO_3^-]}{[H_2CO_3]}\right)\left(-\left(\dfrac{\partial TA_{TotB}}{\partial[H^+]}\right)_{TotB} - \left(\dfrac{\partial TA_{H_2O}}{\partial[H^+]}\right)_{H_2O}\right) \end{pmatrix}}{\dfrac{4\,[CO_3^{2-}]}{[H_2CO_3]} + \dfrac{[HCO_3^-]}{[H_2CO_3]} - \dfrac{[H^+]}{[H_2CO_3]}\left(\left(\dfrac{\partial TA_{TotB}}{\partial[H^+]}\right)_{TotB} + \left(\dfrac{\partial TA_{H_2O}}{\partial[H^+]}\right)_{H_2O}\right)} \tag{D20}$$

Multiplying both the numerator and denominator by $[H_2CO_3]$ and implementing $DIC = [H_2CO_3] + [HCO_3^-] + [CO_3^{2-}]$ yields:

$$\frac{\partial DIC}{\partial[H_2CO_3]} = \frac{4\,[CO_3^{2-}] + [HCO_3^-] + \dfrac{[HCO_3^-]\,[CO_3^{2-}]}{[H_2CO_3]} + \dfrac{[H^+]}{[H_2CO_3]}DIC\left(-\left(\dfrac{\partial TA_{TotB}}{\partial[H^+]}\right)_{TotB} - \left(\dfrac{\partial TA_{H_2O}}{\partial[H^+]}\right)_{H_2O}\right)}{4\,[CO_3^{2-}] + [HCO_3^-] - [H^+]\left(\left(\dfrac{\partial TA_{TotB}}{\partial[H^+]}\right)_{TotB} + \left(\dfrac{\partial TA_{H_2O}}{\partial[H^+]}\right)_{H_2O}\right)} \tag{D21}$$

Next, we implement the definition of $\left(\dfrac{\partial TA_{DIC}}{\partial[H^+]}\right)_{H_2CO_3}$ as rewritten in Eq. (D6) into the denominator:

$$\frac{\partial \text{DIC}}{\partial [\text{H}_2\text{CO}_3]} = \frac{4\,[\text{CO}_3^{2-}] + [\text{HCO}_3^-] + \dfrac{[\text{HCO}_3^-]\,[\text{CO}_3^{2-}]}{[\text{H}_2\text{CO}_3]} + \dfrac{[\text{H}^+]}{[\text{H}_2\text{CO}_3]}\,\text{DIC}\left(-\left(\dfrac{\partial \text{TA}_{\text{TotB}}}{\partial [\text{H}^+]}\right)_{\text{TotB}} - \left(\dfrac{\partial \text{TA}_{\text{H}_2\text{O}}}{\partial [\text{H}^+]}\right)_{\text{H}_2\text{O}}\right)}{-[\text{H}^+]\left(\dfrac{\partial \text{TA}_{\text{DIC}}}{\partial [\text{H}^+]}\right)_{\text{H}_2\text{CO}_3} - [\text{H}^+]\left(\left(\dfrac{\partial \text{TA}_{\text{TotB}}}{\partial [\text{H}^+]}\right)_{\text{TotB}} + \left(\dfrac{\partial \text{TA}_{\text{H}_2\text{O}}}{\partial [\text{H}^+]}\right)_{\text{H}_2\text{O}}\right)} \quad \text{(D22)}$$

Rearranging and plugging Eq. (D16) into Eq. (D22) yields:

$$\frac{\partial \text{DIC}}{\partial [\text{H}_2\text{CO}_3]} = \frac{4\,[\text{CO}_3^{2-}] + [\text{HCO}_3^-] + \dfrac{[\text{HCO}_3^-]\,[\text{CO}_3^{2-}]}{[\text{H}_2\text{CO}_3]} + \dfrac{[\text{H}^+]}{[\text{H}_2\text{CO}_3]}\,\text{DIC}\left(-\left(\dfrac{\partial \text{TA}_{\text{TotB}}}{\partial [\text{H}^+]}\right)_{\text{TotB}} - \left(\dfrac{\partial \text{TA}_{\text{H}_2\text{O}}}{\partial [\text{H}^+]}\right)_{\text{H}_2\text{O}}\right)}{-[\text{H}^+]\left(\dfrac{\partial \text{TA}}{\partial [\text{H}^+]}\right)_{\text{H}_2\text{CO}_3}} \quad \text{(D23)}$$

Again multiplying both numerator and denominator by $[\text{H}_2\text{CO}_3]$ yields:

$$\frac{\partial \text{DIC}}{\partial [\text{H}_2\text{CO}_3]} = \frac{\text{G} + [\text{H}^+]\left(-\left(\dfrac{\partial \text{TA}_{\text{TotB}}}{\partial [\text{H}^+]}\right)_{\text{TotB}} - \left(\dfrac{\partial \text{TA}_{\text{H}_2\text{O}}}{\partial [\text{H}^+]}\right)_{\text{H}_2\text{O}}\right)\text{DIC}}{-[\text{H}^+]\left(\dfrac{\partial \text{TA}}{\partial [\text{H}^+]}\right)_{\text{H}_2\text{CO}_3}[\text{H}_2\text{CO}_3]} \quad \text{(D24)}$$

with:

$$\text{G} = [\text{H}_2\text{CO}_3]\,(4\,[\text{CO}_3^{2-}] + [\text{HCO}_3^-]) + [\text{HCO}_3^-]\,[\text{CO}_3^{2-}] \quad \text{(D25)}$$

Next we replace $[\text{H}_2\text{CO}_3]$ in the term G by $\text{DIC} - [\text{HCO}_3^-] - [\text{CO}_3^{2-}]$, and partly work out the brackets to isolate the term including DIC:

$$\text{G} = \text{DIC}\,(4\,[\text{CO}_3^{2-}] + [\text{HCO}_3^-]) - ([\text{HCO}_3^-] + [\text{CO}_3^{2-}])\,(4\,[\text{CO}_3^{2-}] + [\text{HCO}_3^-]) + [\text{HCO}_3^-]\,[\text{CO}_3^{2-}] \quad \text{(D26)}$$

Then, we plug Eq. (D6) into Eq. (D26) and rearrange:

$$\text{G} = -\,([\text{HCO}_3^-] + [\text{CO}_3^{2-}])\,(4\,[\text{CO}_3^{2-}] + [\text{HCO}_3^-]) + [\text{HCO}_3^-]\,[\text{CO}_3^{2-}] - [\text{H}^+]\left(\dfrac{\partial \text{TA}_{\text{DIC}}}{\partial [\text{H}^+]}\right)_{\text{H}_2\text{CO}_3}\text{DIC} \quad \text{(D27)}$$

Working out the rest of the brackets in Eq. (D27) and rearranging yields:

$$\text{G} = -[\text{HCO}_3^-]^2 - 4[\text{HCO}_3^-]\,[\text{CO}_3^{2-}] - 4[\text{CO}_3^{2-}]^2 - [\text{H}^+]\left(\dfrac{\partial \text{TA}_{\text{DIC}}}{\partial [\text{H}^+]}\right)_{\text{H}_2\text{CO}_3}\text{DIC} \quad \text{(D28)}$$

This can be simplified and rewritten using the definition of TA_{DIC} (Table 5.1a):

$$\text{G} = -\,\text{TA}_{\text{DIC}}^2 - [\text{H}^+]\left(\dfrac{\partial \text{TA}_{\text{DIC}}}{\partial [\text{H}^+]}\right)_{\text{H}_2\text{CO}_3}\text{DIC} \quad \text{(D29)}$$

The term G can now be plugged back into Eq. (D24), which is then rearranged to arrive at:

$$\frac{\partial DIC}{\partial [H_2CO_3]} = \frac{-TA_{DIC}^2 - [H^+]\left(\left(\frac{\partial TA_{DIC}}{\partial [H^+]}\right)_{H_2CO_3} + \left(\frac{\partial TA_{TotB}}{\partial [H^+]}\right)_{TotB} + \left(\frac{\partial TA_{H_2O}}{\partial [H^+]}\right)_{H_2O}\right) DIC}{-[H^+]\left(\frac{\partial TA}{\partial [H^+]}\right)_{H_2CO_3} [H_2CO_3]}$$
(D30)

Multiplying numerator and denominator by -1 and plugging in Eq. (D16) yields:

$$\frac{\partial DIC}{\partial [H_2CO_3]} = \frac{TA_{DIC}^2 + [H^+]\left(\frac{\partial TA}{\partial [H^+]}\right)_{H_2CO_3} DIC}{[H^+]\left(\frac{\partial TA}{\partial [H^+]}\right)_{H_2CO_3} [H_2CO_3]}$$
(D31)

Finally, Eq. (D31) is plugged into Eq. (D17) to yield RF:

$$RF = \frac{DIC}{[H_2CO_3]}\left(\frac{\partial DIC}{\partial [H_2CO_3]}\right)^{-1} = \frac{[H^+]\left(\frac{\partial TA}{\partial [H^+]}\right)_{H_2CO_3} [H_2CO_3]}{TA_{DIC}^2 + [H^+]\left(\frac{\partial TA}{\partial [H^+]}\right)_{H_2CO_3} DIC}$$
(D32)

which can easily be rewritten to our Eq. (D1):

$$RF = \frac{[H^+]\left(\frac{\partial TA}{\partial [H^+]}\right)_{H_2CO_3} DIC}{TA_{DIC}^2 + [H^+]\left(\frac{\partial TA}{\partial [H^+]}\right)_{H_2CO_3} DIC}$$
(D33)

Chapter 6:

Attributing seasonal pH variability in surface ocean waters to governing factors

"Even if you never have the chance to see or touch the ocean, the ocean touches you with every breath you take, every drop of water you drink, every bite you consume. Everyone, everywhere is inextricably connected to and utterly dependent upon the existence of the sea."

Sylvia A. Earle

Abstract

Sensitivities describing the change in pH resulting from changes in total alkalinity (TA) or the total concentration of an acid-base system (TotX) can play an important role in attributing pH variability to its governing factors. Here we applied recently derived expressions for such sensitivities to three seasonal data sets of surface ocean waters spanning at least 15 years, including a wide range of measured variables, and covering a range of physical and chemical states. For each variable a long-term trend was removed if present, after which all data were merged into a composite year to which a harmonic function with several periodicities was fit. We varied all variables over the year according to this fit and calculated pH from these variations and the sensitivities. This predicted pH was compared to the observed pH of the composite year.

Our results reveal that for all three sites, pH can be accurately predicted if seasonal cycles of TA, TotX, temperature and salinity are known. The factors responsible for most of the pH variability differ however per site. Seasonality in pH at Station ALOHA (subtropical Pacific Ocean) is almost entirely driven by temperature changes. In the north-western Mediterranean Sea, changes in temperature are responsible for the majority of pH variability in summer and autumn, while variations in dissolved inorganic carbon (DIC) contribute most to the observed pH trends for the rest of the year. In the Iceland Sea, variations in DIC dominate the pH signal for most of the year, although temperature drives most pH changes in early summer and TA variability is the dominant determining factor in early winter. This work highlights the power of sensitivities in quantifying pH variability and its driving factors, and shows that they can be used to gain further insight into current and future pH dynamics in any marine system.

6.1 Introduction

Dissolved carbon dioxide (CO_2), pH and other carbonate system parameters vary at diurnal, seasonal and interannual time scales (Keeling et al., 2004; Midorikawa et al., 2010; Hofmann et al., 2011; Wootton and Pfister, 2012). These fluctuations are due to multi-scale variability in salinity, temperature, primary production, respiration and other system-specific processes (Gruber et al., 2002; Duarte et al., 2013a; Bates et al., 2014; Hagens et al., 2015). The amplitude of carbonate-system variability depends on the magnitude of the drivers and the sensitivity of the system to changes in ocean chemistry (Sarmiento and Gruber, 2006; Takahashi et al., 2014; Chapter 5). Polar regions, for example, are known to be relatively vulnerable due to their naturally low pH, ocean mixing patterns, and the temperature dependency of CO_2 solubility and acid-base dissociation constants, while the reverse holds for warmer tropical regions (Fabry et al., 2009; Orr et al., 2005). It is therefore essential to quantify carbonate system variability and its driving factors at these different time scales and with different initial conditions.

Several studies have quantified the drivers of seasonal and/or interannual variability in mixed-layer dissolved inorganic carbon (DIC) using a diagnostic box model based on time-series data (Gruber et al., 1998, 2002; Keeling et al., 2004; Shadwick et al., 2011). Others have investigated the drivers of seasonal and/or interannual changes in the partial pressure of CO_2 (pCO_2), either by separating the observed pCO_2 into isochemical (i.e. the calculated pCO_2 change at constant DIC) and isothermal terms (Keeling, 1993; Takahashi et al., 2002; Riebesell et al., 2009), or by splitting the modelled change in pCO_2 with time to changes in temperature, freshwater inputs, and salinity-normalised total alkalinity (sTA) and DIC (sDIC) (Doney et al., 2009b; Thomas et al., 2008; Lovenduski et al., 2007). Independent of the time scale of interest, each of these approaches requires that the sensitivity of the parameter studied (DIC, pCO_2, pH, Ω_{cal} or Ω_{ara}) to a change in the driving factor of interest is known.

Takahashi et al. (1993) provided a useful relationship for the temperature sensitivity of pCO_2, which allows attributing seasonality in pCO_2 to seasonal temperature changes. Sarmiento and Gruber (2006) extended this approach and presented pCO_2 sensitivities for temperature (T), salinity (S), DIC and total alkalinity (TA), which they used to partition the seasonal pCO_2 record

Table 6.1 Details on the three data sets used for this study.

Data set	Region	Period	Used variables	Reference
HOT (Hawaii Ocean Time-series), station ALOHA	Pacific Ocean (22° 45′ N, 158°00′ W)	1990 – 2013	S, t, p, DIC, TA, pH, TotP, TotNO$_3$, TotSi	(Dore et al., 2003, 2009)
DYFAMED (DYnamique des Flux Atmosphériques en MEDiterrannée)	Mediterranean Sea (43° 25′ N, 7° 52′ E)	1998 – 2000; 2003 – 2007	S, t, p, DIC, TA, TotP, TotNO$_3$, TotNO$_2$, TotSi	(Touratier and Goyet, 2009)
Iceland Sea time series (part of CARINA data collection)	Iceland Sea (68° 00′ N, 12°40′ W)	1983 – 2006	S, t, p, DIC, TA, pH, TotP, TotNO$_3$, TotSi	(Olafsson et al., 2010)

Table 6.2 Fitting coefficients for Station ALOHA (with P-value given in between brackets) for a harmonic function of the form , with t being Julian day and T being the length of 1 year, i.e. 365 days. The function was applied to the linearly detrended time series of as a three-harmonic function (m=3) with periods of 12 (k=1), 6 (k=2) and 4 (k=3) months. Bold values are significant (P < 0.05). Missing values indicate that no function could be fitted to the data.

Parameter	H_0	a_1	b_1	a_2	b_2	a_3	b_3
pH_{fit} (-)	**8.214**	**$7.768 \cdot 10^{-3}$**	**$6.497 \cdot 10^{-3}$**	$6.743 \cdot 10^{-4}$	$4.423 \cdot 10^{-4}$	$-1.403 \cdot 10^{-3}$	$4.113 \cdot 10^{-4}$
	(< 0.001)	**(< 0.001)**	**(< 0.001)**	(0.395)	(0.593)	(0.079)	(0.619)
T (°C)	**24.86**	**-1.425**	**-0.612**	**-0.135**	-0.0733	0.0745	-0.0903
	(< 0.001)	**(< 0.001)**	**(< 0.001)**	**(0.003)**	(0.123)	(0.102)	(0.057)
DIC (μmol kg^{-1})	**1957.88**	**5.582**	**2.991**	0.3387	0.2471	0.6009	-0.3879
	(< 0.001)	**(< 0.001)**	**(0.010)**	(0.762)	(0.833)	(0.593)	(0.740)
TA (μmol kg^{-1})	-	-	-	-	-	-	-
S (-)	**34.92**	$-1.761 \cdot 10^{-2}$	**$6.139 \cdot 10^{-2}$**	$-8.534 \cdot 10^{-4}$	$-3.983 \cdot 10^{-3}$	$7.417 \cdot 10^{-3}$	$-1.062 \cdot 10^{-2}$
	(< 0.001)	(0.314)	**(<0.001)**	(0.961)	(0.825)	(0.668)	(0.556)
TotP (μmol kg^{-1})	**$7.959 \cdot 10^{-2}$**	**$1.271 \cdot 10^{-2}$**	$6.663 \cdot 10^{-4}$	$-1.036 \cdot 10^{-3}$	$-1.800 \cdot 10^{-3}$	$5.620 \cdot 10^{-4}$	$3.531 \cdot 10^{-3}$
	(<0.001)	**(0.011)**	(0.893)	(0.838)	(0.708)	(0.906)	(0.488)
TotNO$_3$ (μmol kg^{-1})	**$-2.840 \cdot 10^{-3}$**	$-8.733 \cdot 10^{-4}$	$-3.388 \cdot 10^{-3}$	$9.252 \cdot 10^{-4}$	$-1.935 \cdot 10^{-3}$	$-6.833 \cdot 10^{-4}$	$-1.516 \cdot 10^{-3}$
	(<0.001)	(0.614)	(0.056)	(0.607)	(0.255)	(0.685)	(0.404)
TotSi (μmol kg^{-1})	**1.403**	**$9.706 \cdot 10^{-2}$**	**$9.807 \cdot 10^{-2}$**	$-3.842 \cdot 10^{-4}$	$-2.445 \cdot 10^{-2}$	$-1.144 \cdot 10^{-2}$	$3.808 \cdot 10^{-2}$
	(<0.001)	**(0.024)**	**(0.022)**	(0.993)	(0.552)	(0.779)	(0.391)

into temperature and DIC components. Recently, Takahashi et al. (2014) presented sensitivities for pCO_2, pH and the saturation states of calcite (Ω_{cal}) and aragonite (Ω_{ara}) and used these to calculate seasonal amplitudes of pCO_2, pH and the saturation states at five stations.

In Chapter 5, we derived a set of explicit expressions describing the sensitivity of pH to a change in ocean chemistry. In this study we use these sensitivities to calculate seasonal changes in pH resulting from changes in T, S, TA and DIC, as well as other acid-base systems, in three ocean time-series stations: DYFAMED in the Mediterranean Sea, ALOHA in the North Pacific gyre and Iceland Sea in the North Atlantic. Our aims are to show that seasonality in pH can be predicted from seasonality in TA, DIC and to quantify the driving factors of the seasonal variations in pH in these contrasting settings.

6.2 Methods

6.2.1 Time-series station data

Three time-series stations with seasonal resolution were chosen: (1) the highly saline Mediterranean Sea (DYFAMED, located in the Ligurian Sea), (2) the oligotrophic Pacific open ocean (Station

ALOHA), and (3) the high-latitude Iceland Sea. Details on these data sets can be found in Table 6.1. From all three data sets, we only used the surface data (around 5 m depth). Not all nutrients have been measured for all three time-series and if a nutrient had not been measured, we used the global climatological surface-ocean average for the year 2000 as given in Table 5.4 and assumed its concentration did not vary over the year. Additionally, we only used data from those cruises where at least two carbonate system parameters were measured. In cases where measurements of more than two carbonate system parameters were available, we used DIC and TA. Our DIC and TA have not been normalised to salinity (see Appendix 6.A).

To obtain a seasonal cycle from the DYFAMED, ALOHA and Iceland Sea data sets, we applied the method of Keeling et al. (2004) and Gruber et al. (1998, 2002). This method involves removing a statistically significant ($P < 0.05$) linear trend from the data (this step was discarded for the Mediterranean Sea data, where the time span of the data was not long enough to obtain consistent trends) followed by combining the detrended data into a composite year, thereby neglecting interannual variations. This composite year thus represents a climatological average for the period that the data spans (Gruber et al., 1998). Then, we used a least squares method to fit the following harmonic function to each parameter of the adjusted data set separately:

Table 6.3 Same as Table 6.2 but for the DYFAMED time series. This time series was not linearly detrended before the harmonic function was applied.

Parameter	H_0	a_1	b_1	a_2	b_2	a_3	b_3
pH$_{fit}$ (-)	**8.181**	$-1.930 \cdot 10^{-3}$	$2.779 \cdot 10^{-3}$	$\mathbf{-1.583 \cdot 10^{-2}}$	$-1.034 \cdot 10^{-2}$	$7.211 \cdot 10^{-3}$	$2.100 \cdot 10^{-3}$
	(< 0.001)	(0.793)	(0.696)	**(0.039)**	(0.142)	(0.299)	(0.782)
T (°C)	**17.27**	**-3.389**	**-3.632**	**0.671**	0.312	0.084	-0.204
	(< 0.001)	**(< 0.001)**	**(< 0.001)**	**(0.020)**	(0.231)	(0.746)	(0.470)
DIC (µmol kg^{-1})	**2250.03**	**22.06**	**17.86**	**7.847**	2.224	-5.566	-5.118
	(< 0.001)	**(< 0.001)**	**(< 0.001)**	**(0.044)**	(0.531)	(0.117)	(0.189)
TA (µmol kg^{-1})	**2565.22**	-1.231	-5.105	1.979	-3.358	-1.902	-5.769
	(< 0.001)	(0.714)	(0.120)	(0.563)	(0.293)	(0.546)	(0.101)
S (-)	**38.30**	$-3.015 \cdot 10^{-3}$	$-2.398 \cdot 10^{-2}$	$4.582 \cdot 10^{-2}$	$-4.230 \cdot 10^{-2}$	$-1.150 \cdot 10^{-2}$	$-4.324 \cdot 10^{-2}$
	(< 0.001)	(0.929)	(0.452)	(0.182)	(0.184)	(0.716)	(0.212)
TotP (µmol kg^{-1})	$\mathbf{6.032 \cdot 10^{-2}}$	$\mathbf{3.477 \cdot 10^{-2}}$	$2.296 \cdot 10^{-2}$	$1.013 \cdot 10^{-2}$	$2.199 \cdot 10^{-3}$	$-3.531 \cdot 10^{-3}$	$2.212 \cdot 10^{-3}$
	(<0.001)	**(0.033)**	(0.143)	(0.531)	(0.884)	(0.813)	(0.890)
TotNO$_3$ (µmol kg^{-1})	**1.021**	**0.710**	**1.241**	0.498	0.288	-0.0952	-0.245
	(<0.001)	**(0.006)**	**(<0.001)**	(0.059)	(0.211)	(0.679)	(0.342)
TotNO$_2$ (µmol kg^{-1})	$\mathbf{4.968 \cdot 10^{-2}}$	$2.743 \cdot 10^{-2}$	$2.578 \cdot 10^{-2}$	$3.498 \cdot 10^{-3}$	$-1.032 \cdot 10^{-2}$	$-2.210 \cdot 10^{-2}$	$-1.662 \cdot 10^{-2}$
	(<0.001)	(0.060)	(0.079)	(0.816)	(0.445)	(0.106)	(0.280)
TotSi (µmol kg^{-1})	**1.642**	$-8.389 \cdot 10^{-2}$	0.7930	-0.4344	0.118	-0.2491	-0.4979
	(<0.001)	(0.785)	(0.012)	(0.181)	(0.681)	(0.391)	(0.125)

Table 6.4 Same as Table 6.2 but for the Iceland Sea time series

Parameter	H_0	a_1	b_1	a_2	b_2	a_3	b_3
pH_{fit} (-)	**8.128**	**-2.545·10⁻²**	**-2.677·10⁻²**	2.234·10⁻⁴	5.783·10⁻³	1.201·10⁻²	4.511·10⁻³
	(< 0.001)	(< 0.001)	(< 0.001)	(0.960)	(0.443)	(0.033)	(0.506)
T (°C)	**2.201**	**-2.940**	**-1.554**	**0.996**	0.0696	0.0697	**0.477**
	(< 0.001)	(< 0.001)	(< 0.001)	(< 0.001)	(0.722)	(0.629)	(0.008)
DIC (µmol kg⁻¹)	**2091.92**	**30.56**	**10.77**	-5.305	-1.237	**-10.61**	**-11.02**
	(< 0.001)	(< 0.001)	(0.019)	(0.080)	(0.808)	(0.006)	(0.018)
TA (µmol kg⁻¹)	**2275.53**	1.108	**-11.70**	**3.318**	1.109	**-5.579**	**-3.872**
	(< 0.001)	(0.472)	(< 0.001)	(0.007)	(0.587)	(< 0.001)	(0.038)
S (-)	**34.65**	**0.1103**	**-5.157·10⁻²**	1.434·10⁻²	4.126·10⁻²	**-5.639·10⁻²**	-9.882·10⁻²
	(< 0.001)	(< 0.001)	(0.007)	(0.252)	(0.052)	(< 0.001)	(0.603)
TotP (µmol kg⁻¹)	**0.4968**	**0.2047**	**8.526·10⁻²**	**-5.046·10⁻²**	-1.775·10⁻²	**-5.861·10⁻²**	**-6.951·10⁻²**
	(<0.001)	(<0.001)	(<0.001)	(<0.001)	(0.482)	(0.002)	(0.004)
$TotNO_3$ (µmol kg⁻¹)	**6.760**	**3.522**	**1.872**	**-0.5442**	4.740·10⁻³	**-0.8536**	**-0.7521**
	(<0.001)	(<0.001)	(<0.001)	(0.019)	(0.990)	(0.004)	(0.034)
TotSi (µmol kg⁻¹)	**2.395**	**1.598**	**0.7516**	-0.1561	**-0.6385**	-0.3093	-0.2590
	(<0.001)	(<0.001)	(<0.001)	(0.215)	(0.004)	(0.054)	(0.181)

$$H = \sum_{k=1}^{m} \left(a_k \sin\left(\frac{2\pi kt}{T}\right) + b_k \cos\left(\frac{2\pi kt}{T}\right) \right) \tag{1}$$

Here, t is Julian day and T is the length of 1 year, i.e. 365 days. Following Keeling et al. (2004) and Gruber et al. (2002), we applied Eq. (1) as a three-harmonic function with periods of 12, 6 and 4 months. Tables 6.2 – 6.4 show the coefficients and corresponding P-values for each parameter, as well as H_0, which represents the annual mean of that parameter. In further calculations, we only included the coefficients that produced a statistically significant fit (i.e. $P < 0.05$, calculated using the *Stats* package in R).

Equation (1) was also applied to fit observed pH values to a harmonic function (pH_{fit}). This pH_{fit} was compared to pH_{pred}, the pH predicted using sensitivity factors.

6.2.2 Sensitivity factors

The factors describing the sensitivity of pH to changes in TA or the total concentration of an acid-base system as described in Chapter 5 are valid for any combination of acid-base systems and any total concentration, or any of the species contributing to the total concentration, as independent state variable, assuming that all other factors remain constant. They are an extension of the work by Frankignoulle (1994) and Egleston et al. (2010) and based on the definition of TA given by Dickson (1981) but include the acid-base systems mentioned by Soetaert et al. (2007). For a detailed derivation the reader is referred to Chapter 5; briefly, the expressions are defined as follows:

Table 6.5a Expressions for $\left(\frac{\partial TA_{TotX}}{\partial [H^+]}\right)_X$ for the major acid-base systems present in natural marine waters. These are valid in case the total concentration of the acid-base system (TotX) is the state variable. The factor n corresponds to the stoichiometric factor in the contribution of X to TA, which is by default 0 for the reference species (X_{ref}).

Acid-base system (TotX)	Reference species (X_{ref})	$\left(\frac{\partial TA_{TotX}}{\partial [H^+]}\right)_X$
Ammonium (TotNH$_4$)	NH_4^+	$\frac{-1}{[H^+]}\left(-n\,TA_{TotNH_4} + [NH_3]\right)$
Borate (TotB)	$B(OH)_3$	$\frac{-1}{[H^+]}\left(-n\,TA_{TotB} + [B(OH)_4^-]\right)$
Carbonate (DIC)	H_2CO_3	$\frac{-1}{[H^+]}\left(-n\,TA_{DIC} + [HCO_3^-] + 4[CO_3^{2-}]\right)$
Phosphate (TotPO$_4$)	$H_2PO_4^-$	$\frac{-1}{[H^+]}\left(-n\,TA_{TotPO_4} + [H_3PO_4] + [H_2PO_4^-] + 4[PO_4^{3-}]\right)$
Nitrate (TotNO$_3$)	NO_3^-	$\frac{-1}{[H^+]}\left(-n\,TA_{TotNO_3} + [HNO_3]\right)$
Nitrite (TotNO$_2$)	NO_2^-	$\frac{-1}{[H^+]}\left(-n\,TA_{TotNO_2} + [HNO_2]\right)$
Sulphide (TotS)	H_2S	$\frac{-1}{[H^+]}\left(-n\,TA_{TotS} + [HS^-] + 4[S^{2-}]\right)$
Silicate (TotSi)	$Si(OH)_4$	$\frac{-1}{[H^+]}\left(-n\,TA_{TotSi} + [SiO(OH)_3^-] + 4[SiO_2(OH)_2^{2-}]\right)$
Fluoride (TotF)	F^-	$\frac{-1}{[H^+]}\left(-n\,TA_{TotF} + [HF]\right)$
Sulphate (TotSO$_4$)	SO_4^{2-}	$\frac{-1}{[H^+]}\left(-n\,TA_{TotSO_4} + 4[H_2SO_4] + [HSO_4^-]\right)$
Water (auto-dissociation)	H_2O	-

$$\frac{\partial pH}{\partial TA} = \frac{-TotX}{\ln(10)\left(TA_{TotX}^2 + \left([H^+]\left(\frac{\partial TA}{\partial [H^+]}\right)_X - n\,TA_{TotX}\right)TotX\right)} \tag{2a}$$

Table 6.5b Expressions for $\left(\frac{\partial TA_{TotX}}{\partial [H^+]}\right)_{TotX}$ for the major acid-base systems present in natural marine waters. These are valid in case the total concentration of the acid-base system (TotX) is the reaction invariant. The factor n corresponds to the stoichiometric factor in the contribution of X to TA, which is by default 0 for the reference species (X_{ref}).

Acid-base system (TotX)	$\left(\frac{\partial TA_{TotX}}{\partial [H^+]}\right)_{TotX}$
Ammonium ($TotNH_4$)	$\frac{-1}{[H^+]}\left([NH_3]\frac{[NH_4^+]}{TotNH_4}\right)$
Borate (TotB)	$\frac{-1}{[H^+]}\left([B(OH)_4^-]\frac{[B(OH)_3]}{TotB}\right)$
Carbonate (DIC)	$\frac{-1}{[H^+]}\left([HCO_3^-]\left(\frac{[H_2CO_3]-[CO_3^{2-}]}{DIC}\right)+2[CO_3^{2-}]\left(\frac{2[H_2CO_3]+[HCO_3^-]}{DIC}\right)\right)$
Phosphate ($TotPO_4$)	$\frac{-1}{[H^+]}\left(\begin{array}{l}-[H_3PO_4]\left(\frac{-[H_2PO_4^-]-2[HPO_4^{2-}]-3[PO_4^{3-}]}{TotPO_4}\right)+[HPO_4^{2-}]\left(\frac{2[H_3PO_4]+[H_2PO_4^-]-[PO_4^{3-}]}{TotPO_4}\right)\\ +2[PO_4^{3-}]\left(\frac{3[H_3PO_4]+2[H_2PO_4^-]+[HPO_4^{2-}]}{TotPO_4}\right)\end{array}\right)$
Nitrate ($TotNO_3$)	$\frac{-1}{[H^+]}\left(-[HNO_3]\frac{[NO_3^-]}{TotNO_3}\right)$
Nitrite ($TotNO_2$)	$\frac{-1}{[H^+]}\left(-[HNO_2]\frac{[NO_2^-]}{TotNO_2}\right)$
Sulphide (TotS)	$\frac{-1}{[H^+]}\left([HS^-]\left(\frac{[H_2S]-[S^{2-}]}{TotS}\right)+2[S^{2-}]\left(\frac{2[H_2S]+[HS^-]}{TotS}\right)\right)$
Silicate (TotSi)	$\frac{-1}{[H^+]}\left([SiO(OH)_3^-]\left(\frac{[Si(OH)_4]-[SiO_2(OH)_2^{2-}]}{TotSi}\right)+2[SiO_2(OH)_2^{2-}]\left(\frac{2[Si(OH)_4]+[SiO(OH)_3^-]}{TotSi}\right)\right)$
Fluoride (TotF)	$\frac{-1}{[H^+]}\left(-[HF]\frac{[F^-]}{TotF}\right)$
Sulphate ($TotSO_4$)	$\frac{-1}{[H^+]}\left(-2[H_2SO_4]\left(\frac{-[HSO_4^-]-2[SO_4^{2-}]}{TotSO_4}\right)-[HSO_4^-]\left(\frac{[H_2SO_4]-[SO_4^{2-}]}{TotSO_4}\right)\right)$
Water (auto-dissociation)	$\frac{-1}{[H^+]}\left([OH^-]+[H^+]\right)$

$$\frac{\partial pH}{\partial TotX}=\frac{TA_{TotX}}{\ln(10)\left(TA_{TotX}^2+\left([H^+]\left(\frac{\partial TA}{\partial [H^+]}\right)_X-n\,TA_{TotX}\right)TotX\right)} \qquad (2b)$$

Here, pH is defined on the free scale, $[H^+]$ is the proton concentration, TotX is the total concentration of the acid-base system of interest (e.g. DIC), X is an acid-base species belonging to this acid-base system (e.g. CO_2), and TA_{TotX} is the contribution of that acid-base system to the definition of TA. For example, $TA_{DIC} = [HCO_3^-] + 2[CO_3^{2-}]$. The factor n is the stoichiometric factor in the contribution of X to TA. By definition, this factor equals 0 in case a change is specified in either the total concentration of an acid-base species or the reference species of that acid-base system with respect to TA. The reference species is the dominant species of an acid-base system under the conditions at which TA is defined. Taking the carbonate system again as an example, if a change in $[CO_2]$ or DIC is considered, then n = 0, if $X = [HCO_3^-]$, then n = 1, and n = 2 for a change in $[CO_3^{2-}]$. Finally, $\left(\frac{\partial TA}{\partial[H^+]}\right)_X$ is a species-specific buffer factor related to the acid-base buffering capacity β_H:

$$\left(\frac{\partial TA}{\partial[H^+]}\right)_X = \beta_H - \left(\frac{\partial TA_{TotX}}{\partial[H^+]}\right)_{TotX} + \left(\frac{\partial TA_{TotX}}{\partial[H^+]}\right)_X \tag{3a}$$

with β_H being defined according to Hofmann et al. (2010a):

$$\beta_H = \sum_{i=1}^{k}\left(\frac{\partial TA_i}{\partial[H^+]}\right)_i \tag{3b}$$

where i represents the total concentration of an acid-base system For each acid-base system, the derivatives $\left(\frac{\partial TA_{TotX}}{\partial[H^+]}\right)_X$ and $\left(\frac{\partial TA_{TotX}}{\partial[H^+]}\right)_{TotX}$ can be found in Tables 6.5a and 6.5b, respectively.

The sensitivity of pH to changes in temperature was determined numerically following Hofmann et al. (2009):

$$\frac{\partial pH}{\partial T} = \frac{1}{\ln(10)[H^+]}\left(\sum_{j=1}^{k}\left(\frac{\partial TA}{\partial K_j^*}\frac{\partial K_j^*}{\partial T}\right) \Big/ \frac{\partial TA}{\partial[H^+]}\right) \tag{4}$$

Here, j refers to the acid-base species of interest and K_j^* to the stoichiometric acid-base dissociation constants corresponding to this species. The sensitivity $\sum_{j=1}^{k}\left(\frac{\partial TA}{\partial K_j^*}\frac{\partial K_j^*}{\partial T}\right)$ was estimated by applying a 10% increase and decrease in T, taking both resulting TA values and calculating the slope. By replacing T in Eq. (4) with S, the same approach can be used to quantify the sensitivity of pH to changes in salinity.

6.2.3 Predicting seasonal pH using sensitivities
For each of the three sites discussed in Sect. 6.2.1 we determined pH_{pred} using Eq. (5), which is basically the total derivative of pH as a function of T, S, DIC, TotB, $TotSO_4$, TotF and nutrients:

$$pH_{pred}\left(T, S, DIC, TA, TotB, TotSO_4, TotF, \sum_{m=1}^{k} nutrient\right) = \overline{pH} + \frac{\partial pH}{\partial T}(\overline{T}-T) + \frac{\partial pH}{\partial S}(\overline{S}-S) + \tag{5}$$

$$\frac{\partial pH}{\partial DIC}(\overline{DIC}-DIC) + \frac{\partial pH}{\partial TA}(\overline{TA}-TA) + \frac{\partial pH}{\partial TotB}(\overline{TotB}-TotB) + \frac{\partial pH}{\partial TotF}(\overline{TotF}-TotF) +$$

$$\frac{\partial pH}{\partial TotSO_4}(\overline{TotSO_4}-TotSO_4) + \sum_{m=1}^{k}\frac{\partial pH}{\partial nutrient}(\overline{nutrient}-nutrient)$$
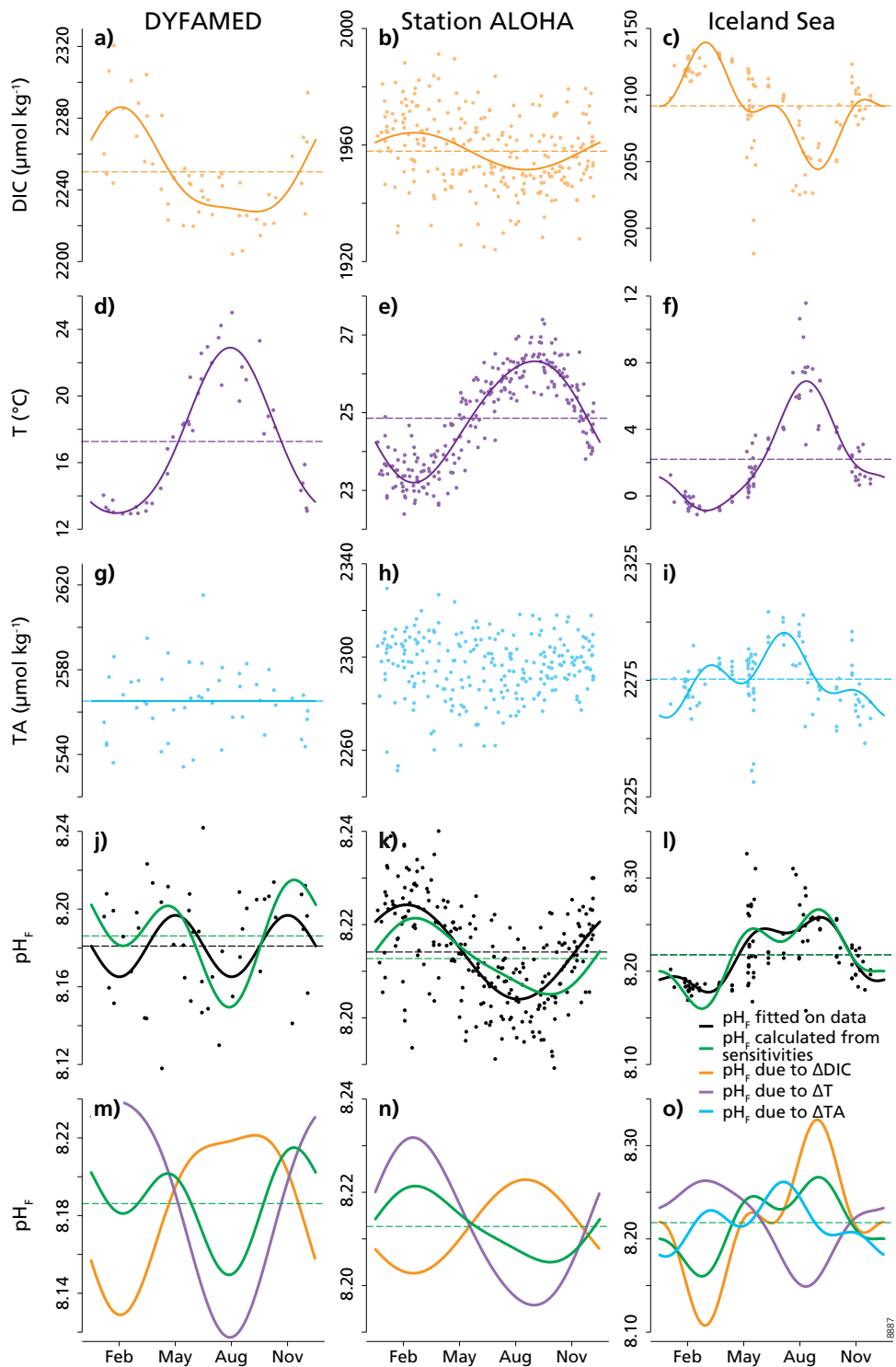
Here, the overbars represent the fitted annual means (H_0), with the exception of pH, where the annual mean is calculated using the H_0 values of the other parameters, and the partial derivatives represent the sensitivities calculated using Eqs. (2a-b). First, we calculated pH_{pred} by varying all parameters concurrently according to Eq. (1), thereby only using the statistically significant coefficients of the fit. Then, to determine which parameters mostly drive seasonality in pH, we varied each of the parameters in Eq. (5) separately, thereby keeping the other parameters at their fitted annual mean values.

All calculations were performed on the free pH scale using the R package *AquaEnv* (Hofmann et al., 2010b). If applicable, nutrient concentrations were converted from µmol L^{-1} to µmol kg^{-1}. As carbonate dissociation constants we used those of Mehrbach et al. (1973) as refitted by Dickson and Millero (1987). This is done as Takahashi et al. (1993), when determining the effect of changes in T on pCO_2, got the best fit between the experimental and computed data when using these constants in combination with the CO_2 solubility expression of Weiss (1974). In addition, these dissociation constants were used in the construction of the GLODAP database (Key et al., 2004) that was used to construct Table 5.4. Since these dissociation constants are not included in *AquaEnv*, they were calculated using CO2SYS (Lewis and Wallace, 1998). For the other acid-base dissociation constants, we chose the default settings of *AquaEnv*.

6.3   Results

6.3.1   Seasonality in the factors driving pH variability

In order to disentangle the effects of the main factors driving seasonal pH variability at these sites, which are DIC, temperature, and TA, we first consider their own seasonal patterns. The average seasonal cycle of DIC at DYFAMED (Fig. 6.1a) shows an increase until late February, reaching a maximum of 2286 µmol kg^{-1}, which is followed by a sharp decline until mid-June. In the second half of the year, DIC slowly decreases to a minimum of 2228 µmol kg^{-1} in late September, after which it increases again. Temperature at DYFAMED (Fig. 6.1d) decreases until early February to a minimum of 13.0°C, increases from early February to mid-August, thereby reaching a maximum of 22.9°C, and declines afterwards. Thus, the temperature extremes are in the opposite direction as the DIC extremes and precede them by a few weeks. The DIC seasonality at Station ALOHA (Fig. 6.1b) is characterised by an increase to 1964 µmol kg^{-1} until early March, followed by a decrease to 1952 µmol kg^{-1} until early September and an increase afterwards. Note that the scatter of DIC measurements around the harmonic fit is much more prominent here than at the DYFAMED and Iceland Sea sites. This indicates that at Station ALOHA there is substantial DIC variability on longer, i.e. interannual, or shorter, i.e. episodic, timescales. The temperature variability at Station ALOHA (Fig. 6.1e) shows a pattern basically opposing that of DIC. Temperature declines until early March until 23.2°C, increases between early March and mid-September until 26.3°C, and decreases again afterwards. In contrast to DYFAMED, the DIC and temperature extremes overlap in timing, but they still occur in contrasting directions. DIC and temperature seasonality at DYFAMED, and temperature seasonality at Station ALOHA, are dominated by the 12-month periodicity on which a minor 6-month signal is superimposed. In contrast, the DIC variability at

DYFAMED — Station ALOHA — Iceland Sea

Legend:
- pH_F fitted on data
- pH_F calculated from sensitivities
- pH_F due to ΔDIC
- pH_F due to ΔT
- pH_F due to ΔTA

Station ALOHA only shows a statistically significant 12-month cyclicity. The maximum peak-to-peak amplitude of the harmonic fit for DIC is 58 µmol kg^{-1} at DYFAMED and 13 µmol kg^{-1} at Station ALOHA. For the seasonal temperature trend, these values are 9.9°C and 3.1°C, respectively. No statistically significant trend could be fitted to the TA data at Station ALOHA and DYFAMED (Figs. 1g-h), indicating that the TA variability is driven by either longer-term or shorter-term processes.

The average seasonal cycle of DIC at the Iceland Sea site (Fig. 6.1c) shows an increase until it reaches its maximum of 2140 µmol kg^{-1} in mid-March. Minimum DIC (2044 µmol kg^{-1}) is found is mid-September; however, the decline between mid-March and mid-September is interrupted by a period of minor DIC increase in May. Similarly, DIC increases from mid-September onwards, but shows a small drawdown in December. Temperature at the Iceland Sea site (Fig. 6.1f) reaches a minimum of -0.9°C in mid-March and a maximum of 6.9°C in late August. The increase in temperature in between is relatively slow until late May and accelerates afterwards. Similarly, the decline from late August onwards is fast until early November, after which it slows down. A closer look at the harmonic fits for DIC and temperature indicates that temperature variability shows a significant 12- and 6-month periodicity, although the 12-month signal is substantially bigger in amplitude, while significant 12- and 4-month signals having similar magnitudes were fitted to the DIC data. The pattern of the timing of the DIC and temperature extremes at the Iceland Sea site is different from both DYFAMED and Station ALOHA. Although the DIC maximum concurs with the temperature minimum, the temperature maximum precedes the DIC minimum by a few weeks. The Iceland Sea is the only site in this study where seasonality in TA was observed (Fig. 6.1l), and detailed analysis revealed that the 12-month, 6-month and 4-month periodicity are all significant, with the 12-month signal being dominant over the others. A maximum TA of 2295 µmol kg^{-1} is reached in mid-July, while TA reaches its minimum of 2259 µmol kg^{-1} in mid-January. The maximum peak-to-peak amplitudes of the harmonic fit for DIC, temperature and TA at the Iceland Sea site are 95 µmol kg^{-1}, 7.8°C and 36 µmol kg^{-1}, respectively.

6.3.2   Comparison of pH estimates

From our comparison between the values of pH$_{fit}$ (Eq. (1), black line) and pH$_{pred}$ (Eq. (5), blue line), it can be seen that using a sensitivity-based approach we can well predict the seasonal evolution of pH. Note that pH$_{pred}$ values were calculated using the seasonal variability of all factors affecting pH, i.e. also including salinity and nutrients, which only have a minor effect on pH variability at these sites. The intra-annual variability of pH$_{fit}$ at DYFAMED (Fig. 6.1j; black line) is dominated by the

(previous page) **Figure 6.1** Composite year data and corresponding harmonic functions (fitted using Eq. (1)) for DIC (µmol kg^{-1}; (a)-(c)), temperature (°C; (d)-(f)), TA (µmol kg^{-1}; (g)-(i)) and pH ((j)-(l)) for DYFAMED (Mediterranean Sea), Station ALOHA (subtropical Pacific Ocean), and the Iceland Sea. No statistically significant function could be fitted to the TA data at DYFAMED (g) and ALOHA (h). The bottom plots ((m)-(o)) show the changes in pH$_{pred}$ over the year resulting from the isolated changes in DIC, temperature and (if relevant) TA, which are calculated using Eq. (5), and the sum of these isolated changes. For comparative purposes, this sum is also added to the plot of the observed pH data and pH$_{fit}$ ((j)-(l)).

6-month period. In fact, this is the only statistically significant coefficient, leading to a seasonality in pH_{fit} of 0.0317. Minima in pH_{fit} of 8.1651 occur in mid-February and mid-August, while pH_{fit} maxima of 8.1968 can be observed in mid-May and mid-November. In between these extremes, the pH_{fit} curve follows a sinusoidal pattern. In contrast, intra-annual variability in pH_{pred} occurs on multiple timescales and its maximum summer-to-wintertime rise is substantially higher (0.0656). The maximum pH_{pred} of 8.2150 occurs in late November and thus supersedes the autumn peak of pH_{fit} by a few days. On the contrary, minimum pH_{pred} (8.1495) occurs in mid-August and thus coincides with the summer minimum of the pH_{fit} values.

The pH_{fit} curve at Station ALOHA (Fig. 6.1k) shows only one statistically significant periodicity as well, but, in contrast to DYFAMED, this is the 12-month signal, which has a peak-to-peak amplitude of 0.0203. At Station ALOHA, pH_{fit} increases until mid-February, when it reaches its maximum of 8.2242. Between mid-February and mid-August, pH_{fit} declines sinusoidally until a minimum of 8.2040, after which it increases again. The curve of pH_{pred} also shows one minimum and one maximum, but the timing of these extremes differs form that of the pH_{fit} curve. Lowest pH_{pred} (8.2050) is found in mid-October, while pH_{pred} peaks in early March at a value of 8.2213. The maximum seasonality of pH_{pred} (0.0163) is thus somewhat lower than that of pH_{fit}.

At the Iceland Sea site (Fig. 6.1l), the pH_{fit} curve is influenced by processes acting on multiple timescales, but its variability is dominated by the 12-month signal. This explains why there is a 6-month difference between the occurrence of the maximum (8.2579, in mid-September) and the minimum pH_{fit} (8.1775, in mid-March). The calculated pH_{pred} values closely match the pattern of pH_{fit}. Although maximum pH_{pred} (8.266) concurs with the peak in pH_{fit}, minimum pH_{pred} (8.1599) occurs in early March and thus slightly precedes the peak in pH_{fit}. The peak-to-peak amplitude of pH_{fit} at the Iceland Sea site is 0.0804, while the seasonality of pH_{pred} is somewhat higher, i.e. 0.1064.

Thus, the comparison between both methods shows that there is a very good to excellent agreement in representing the general trend of annual pH, especially for Station ALOHA and the Iceland Sea where the maximum absolute difference between pH_{pred} and pH_{fit} is 0.00697 and 0.0208, respectively. The deviation in pH between both methods at DYFAMED (0.0215), however, warrants further investigation as it exceeds the peak amplitude in pH_{fit} (0.0158). This moderate fit could be explained by the scarcity in data for DYFAMED (n=51) relative to the other two sites (n=240 and n=105 for Station ALOHA and the Iceland Sea, respectively). Therefore, interannual variability or short-term events may have a relatively big impact on the fitting procedure. In this context it is important to mention that even the 6-month period of pH_{fit} at DYFAMED has a relatively poor statistical significance (P = 0.039; Table 6.3).

6.3.3   Quantifying the mechanisms driving seasonal pH variability

We compared the change in pH induced by the change in a certain parameter (DIC, TA, temperature) with the seasonal pH_{pred} trend that results from combining all parameters (Figs. 1m-o). This analysis reveals how at each site the different driving factors act on various timescales and with various magnitudes on pH. At the beginning of the composite year, pH_{pred} at DYFAMED

(Fig. 6.1m) is close to the annual average and shows a declining trend. As DIC increases until late February, while temperature only decreases slightly, this indicates that the DIC signal, which acts in the opposite direction as the temperature signal, dominates the trend in pH_{pred}. From late February onwards, temperature increases while DIC decreases, having again an opposite effect on pH_{pred}. However, the effect of the drawdown of DIC is stronger, leading to a net increase in pH_{pred}. This situation lasts until late April, when the decrease in DIC slows down, lowering pH_{pred}. Between late April and late November, the effect of temperature dominates that of DIC: pH_{pred} increases until mid-August and declines afterwards, matching the trend in temperature. From late November onwards, DIC strongly increases, leading to a decline in pH_{pred}. The peak-to-peak amplitude of the DIC-driven pH change is 0.0924, while for the temperature-driven pH it is somewhat higher, i.e. 0.1214.

In contrast to DYFAMED, pH_{pred} at the beginning of the composite year at Station ALOHA is mainly driven by temperature, as it is close to the annual average value but shows an increasing trend driven by the decrease in temperature. As we follow the evolution of pH_{pred} over time, we see that it resembles the trend in temperature-driven pH changes in sign, but is attenuated by the changes in DIC that always have an opposite effect on pH_{pred}. The extent to which this dampening occurs varies throughout the year: this is due to the 6-month periodicity that is absent for DIC but present for temperature. Similar to DYFAMED, the seasonality of the DIC-driven pH change is lower (0.0201) than that of the temperature signal (0.0359).

The seasonal variability of pH at the Iceland Sea site is somewhat more complicated to disentangle than at DYFAMED and Station ALOHA, as it is not only driven by temperature and DIC, but also by TA. In addition, seasonal variability in these parameters occurred on more different timescales, as shown by the harmonic fitting procedure. At the beginning of the composite year, pH_{pred} is somewhat lower than average. This is the net result of a lower-than-average temperature, slightly increasing pH, and a lower-than-average TA, which acts to decrease pH, as DIC is around its annual average. Following the evolution of pH_{pred}, we can see that it decreases until early March. This decrease is driven by the strong increase in DIC and modulated by both an increase in both TA and a decrease in temperature. Between early March and the end of May, pH_{pred} increases due to a decrease in DIC, again dampened by the increasing temperature. During this period, the influence of changes in TA is minor compared to the other two drivers. In the following 1.5 months, pH_{pred} slightly decreases, but the influence of the various drivers is not constant during this period. Temperature continuously increases during this period and thereby enforces the net pH_{pred} trend. TA, on the contrary, increases throughout the period and therefore attenuates the net pH_{pred} signal. Finally, DIC slightly increases in June, leading to a small decrease in pH_{pred}, but declines afterwards, thereby dampening the decrease in pH_{pred}. A similar mix of drivers is responsible for the increase in pH_{pred} between mid-July and mid-September. DIC strongly decreases during this period and is therefore the main driver of the net increase in pH_{pred} during this period. TA declines during this period, thereby modulating the net pH_{pred} change. Temperature, finally, increases until late August, by that means driving a decrease in pH, while showing a decline afterwards that leads to an increase in the temperature-driven pH. From mid-September until mid-November, pH_{pred} decreases, which is driven by the increase in DIC and attenuated by the decrease in temperature,

with the effect of changes in TA is negligible. From mid-November onwards, the change in pH_{pred} is negligible and is the net result of a decrease in both DIC and TA, with only a minor temperature signal. In contrast to DYFAMED and Station ALOHA, the seasonality of the DIC-driven change is higher (0.2205) than that of temperature signal (0.1135). Variability in TA leads to the smallest seasonal pH variability (0.0800).

To summarise, throughout the year the DIC and temperature signal have opposing effects on pH at DYFAMED, Station ALOHA and (for most of the year) the Iceland Sea. However, temperature dominates the trend in pH between May and November at DYFAMED, while variation in DIC is the key process controlling pH in the remainder of the year. For Station ALOHA, temperature variability dominates the trend in pH throughout the year. At the Iceland Sea site, DIC changes dominate the trend in pH_{pred} for most of the year. Temperature appears to be the main driver of pH_{pred} between the end of May and mid-July, while from mid-November onwards TA seems to exert the biggest control on pH_{pred}.

6.4 Discussion

6.4.1 Seasonal variability at Station ALOHA

Of the three locations of our study, seasonal carbonate system variability at Station ALOHA has been most extensively studied before. Dore et al. (2009) presented seasonal variability of pH (on the total scale, from now on denoted as pH_T) and temperature at Station ALOHA between 1988-2007. The timing of their minimum and maximum temperature (February-March and September, respectively) concurs with our harmonic fit (Fig. 6.1e). However, their pH_T minimum, which occurs in September, lies in between the minima of the pH_{fit} (Mid-August) and pH_{pred} (mid-October), while the timing of their pH_T maximum concurs with the timing of the pH_{pred} maximum. Previous studies have shown a seasonality in sDIC at Station ALOHA of 14 $\mu mol\ kg^{-1}$ between 1994-1999 (Quay and Stutsman, 2003) and of 15 $\mu mol\ kg^{-1}$ between 1998 and 2002 (Keeling et al., 2004). These values are similar to the 13 $\mu mol\ kg^{-1}$ we derived as peak-to-peak amplitude for DIC. This seems surprising as Bates et al. (2014) showed for several long-term data sets, including Station ALOHA and the Iceland Sea, that seasonal changes in sDIC have smaller amplitudes than seasonal changes in DIC, as the effect of salinity changes on DIC is filtered out by using sDIC. In the Appendix we discuss the reasons for using non-salinity normalised data in this study; here, we focus on the different amplitudes. The data we used for this study spans a bigger period, i.e. 1990-2013, than the data used in Keeling et al. (2004) and Quay and Stutsman (2003). Previous studies have shown the importance of North Pacific subtropical gyre variability, related to both the Pacific Decadal Oscillation and the El Niño-Southern Oscillation (Lukas, 2001), on interannual carbonate system variability at Station ALOHA (Winn et al., 1994; Dore et al., 2003, 2009; Brix et al., 2004). It is evident that, when data of a longer time period are used and interannual variability is not filtered out, this may dampen the seasonality, as is indicated by the scatter of DIC measurements around the harmonic fit. The timings of the sDIC extremes found by Quay and Stutsman (2003) (April and October-November) and Keeling et al. (2004) (early April and October) slightly follow the timings of the DIC extremes in this study.

Similar to the factors driving pH variability at Station ALOHA found in this study, Keeling et al. (2004) showed that the seasonal cycle of pCO_2 is dominated by the temperature-driven pCO_2 changes and modulated by the seasonal DIC variability. Keeling et al. (2004) also used a diagnostic model to attribute the observed seasonality to their driving processes. They found that the seasonality in surface-water sDIC is primarily governed by net community production (NCP), being the only driver of the spring-summer drawdown in sDIC that is modulated by atmospheric CO_2 uptake, diffusion, entrainment and horizontal transport. In autumn and winter, these latter four processes dominate over NCP, with horizontal transport and air-sea gas exchange being the biggest sources. By calculating pH_T at 25°C and comparing this to pH_T at in situ temperature, Dore et al. (2009) observed a similar pattern in the factors driving pH variability at Station ALOHA as in this study, i.e. they found that the effect of DIC on pH_T is smaller than that of temperature and has a reverted seasonal pattern.

6.4.2 Seasonal variability at the DYFAMED site

Previous studies at the DYFAMED site focussing on pCO_2 have show that its seasonal variability, having an amplitude of 120-200 ppmv, is mainly driven by temperature, but is dampened by NCP in spring and vertical mixing in autumn (Copin-Montégut et al., 2004; Hood and Merlivat, 2001; Bégovic and Copin-Montégut, 2002). Temperature is, however, also the primary driver of both the onset of summer stratification and resulting increase in NCP in spring and the reinforcement of vertical mixing in autumn and winter. The drivers for the seasonality in pCO_2 thus differ from those of pH, as we found that pH variability is dominantly temperature-driven between May and November only. Copin-Montégut and Bégovic (2002) presented pH_T, TA and DIC data of the DYFAMED site between 1998-2000. However, as the pH_T are normalised to 25°C (pH_T^{25}), they lack the effect of temperature on pH_T. The seasonality in pH_T^{25} of 0.015 these authors derived was attributed to the same non-temperature drivers, i.e. NCP and vertical mixing, as the seasonality in pCO_2. In line with our results, they found that a clear seasonality in surface-water TA was lacking. The seasonality in DIC they estimated (105 μmol kg^{-1}) is almost twice as high as the peak-to-peak amplitude determined in this study. Similar to Station ALOHA, this may be attributed to the longer timespan of the current data set, thereby including interannual variability. The year-to-year variability in the pCO_2 seasonality at DYFAMED between 1998-2000 has been attributed to differences in temperature distribution with depth that changes the extent of vertical mixing (Copin-Montégut et al., 2004; Copin-Montégut and Bégovic, 2002). Seasonality in pCO_2 can also be substantially affected by short-term variability in mistral winds, especially in winter and spring (Mémery et al., 2002). On a somewhat longer timescale, the Mediterranean Sea is affected by the North Atlantic Oscillation (NAO). A positive NAO leads to both an increased temperature (Krahmann and Schott, 1998) and reduced precipitation (Tsimplis and Josey, 2001). The latter results in an increase in salinity and thereby also increases TA, as they are linearly correlated in the Western Mediterranean Sea (Schneider et al., 2007; Rivaro et al., 2010; Copin-Montégut, 1993). Thus, both the increased temperature and TA may substantially impact the carbonate system at the DYFAMED site.

6.4.3 Seasonal variability at the Iceland Sea site

An earlier paper using the full Iceland Sea data set presented in this study (Olafsson et al., 2009) focusses on long-term pH_T trends but shortly discusses seasonality in pH_T as well. They found a much smaller interannual variability in winter pH_T measurements compared to summer measurements, which they relate to the exact location and timing of the phytoplankton spring bloom. This scatter in summertime pH was also observed in this study (Fig. 6.1l). Previous studies using a small part of the data set have studied the Iceland Sea carbonate system seasonality in more detail (Takahashi et al., 1985, 1993). They showed that surface-water DIC and pCO_2 are lowest in summer and attributed this to high productivity in combination with reduced vertical mixing as a result of strong summer stratification. As productivity is reduced and mixing is reinforced, this leads to high DIC and pCO_2 in winter. Note though, that the basin is a year-round sink for pCO_2. A recent study confirms that, on an annual scale, NCP (5.5-5.6 mol C m^{-2} yr^{-1}) in the Iceland Sea exceeds the CO_2 uptake from the atmosphere (4.4±1.1 mol C m^{-2} yr^{-1}) (Jeansson et al., 2015). CO_2 uptake from the atmosphere varies interannually, however, as a result of variations in atmospheric pCO_2 and wind speed forcing, the latter being driven by the NAO (Olsen et al., 2003).

Takahashi et al. (1985, 1993) also showed that the seasonality in DIC and pCO_2 can actually best be described by a saw-tooth rather than a sinusoidal pattern; the summertime decrease resulting from the phytoplankton spring bloom occurs at a much higher rate than the increase in autumn and winter. The winter-to-summertime drop in sDIC found by Takahashi et al. (1993) was 100-150 μmol kg^{-1}, i.e. again somewhat higher than the 95 μmol kg^{-1} we found for DIC. Several factors might explain this discrepancy. First, we fitted a sinusoidal rather than a saw-tooth curve to the data, which may not capture the actual trend to its full extent. Second, our analysis comprises a longer time period and removing the long-term annual trend from the data. The third reason seems however most important: a detailed analysis on the late spring/early summer data confirms the importance of the timing of the phytoplankton spring bloom on the interannual variability in DIC. Between years DIC in the samples taken in the final week of May or the first week of June can vary by 146 μmol kg^{-1}. This interannual variability in timing cannot be account for by the harmonic fitting procedure, which takes an average timing in DIC extremes for the entire period and therefore smoothens the reproduced trend.

The seasonality in temperature, which was found to be ca. 5°C, appears to be driven by variations in the mixed layer depth (Takahashi et al., 1993). The seasonality in TA is somewhat more difficult to interpret. The majority of the Iceland Sea water mass consists of Arctic Intermediate Water which is partially built up from low-salinity Polar Water (East Greenland Current; Hansen and Østerhus, 2000; Rudels et al., 2012). In combination with local ice melting events, this leads to significant drops in summertime salinity and TA (Takahashi et al., 1985). The influence of the East Greenland Current on the Iceland Sea varies interannually (Hansen and Østerhus, 2000), leading to a wide range in the seasonality in TA (45-127 μmol kg^{-1}) that strongly correlates with salinity (Bellerby et al., 2005; Nondal et al., 2009). However, as sTA also displayed minor temporal variability, the trend in TA found by Takahashi et al. (1985) cannot be attributed to salinity alone. In addition, in our data set we found highest, rather than lowest, TA values in summer (mid-July). Using the linearly detrended data, we found however a weak to moderate correlation between TA and salinity (r^2 =

0.69, P < 0.001, calculated using the R package *Stats*), while no statistical significant correlation could be found between TA and TotP ($r^2 = 0.02$, p = 0.1124) or TA and $TotNO_3$ ($r^2 = 0.02$, p = 0.1806). This implies that NCP cannot be seen as a process responsible for the minor variability in TA.

6.5   Conclusions

We applied recently derived sensitivities describing the change in pH due to changes in TA or the total concentration of an acid-base system to seasonal data sets covering a range of physical and chemical settings. We showed that, by only knowing annual average pH and seasonal cycles of total concentrations of DIC, TA, temperature and salinity, we can well reproduce observed pH values. In addition, we quantified the changes in each of these parameters separately and found contrasting patterns for each of three study sites. pH at the Mediterranean Station DYFAMED is dominated by the DIC signal between November and May and by the temperature-driven pH changes in the remainder of the year. At the subtropical Station ALOHA, temperature variability dominates the trend in pH year-round. In the Iceland Sea, where TA also shows significant seasonal variability, DIC variability dominates the trend in pH for most of the year, with the exception of early summer and early winter, when temperature and TA are the respective dominant drivers.

Acknowledgements

Appendix 6.A. Why no salinity normalisation in this study?

Many papers present DIC and TA data normalised to a salinity of 35 (e.g. Gruber et al., 2002; Thomas et al., 2008). However, previous studies have shown that a simple normalisation method of the form

$$sX = \frac{X}{S} S_{ref} \qquad\qquad (A1)$$

cannot be used in case of a freshwater TA end-member that deviates from zero (Friis et al., 2003; Jiang et al., 2014). This may especially occur in coastal regions where evaporation and precipitation are not the main processes controlling TA at zero salinity ($TA_{S=0}$) (Jiang et al., 2014). The many salinity-TA relationships that have been derived for the western Mediterranean Sea (Copin-Montégut, 1993; Schneider et al., 2007; Touratier and Goyet, 2009; Rivaro et al., 2010) all display a substantially negative $TA_{S=0}$, ranging from -286 μmol kg^{-1} for surface waters only, to -1305 μmol kg^{-1} for whole water-column fits. In the case of DIC, a linear relation with salinity could only be obtained for samples below 40 m depth (Copin-Montégut, 1993). Using our data, we found an intercept of -1095±233 μmol kg^{-1} for TA ($r^2 = 0.85$, P < 0.001, uncertainty represent standard error), while DIC and salinity were not significantly correlated ($r^2 = 0.13$, P = 0.0142). This implies that sDIC cannot be derived, while sTA can only properly be estimated using the relation proposed by Friis et al. (2003). For the Iceland Sea site, we found a statistically significant correlation between TA and salinity ($r^2 = 0.70$, P < 0.001) with $TA_{S=0}$ being estimated at 367±124 μmol kg^{-1}. There was only a weak correlation between DIC and salinity ($r^2 = 0.36$, P < 0.001) with an estimated intercept of -398±327 μmol kg^{-1}. At HOT, a site where salinity normalisation has often been applied (Quay and Stutsman, 2003; Keeling et al., 2004), salinity significantly correlated with both TA ($r^2 = 0.87$, P < 0.001) and DIC ($r^2 = 0.70$, P < 0.001). However, there is substantial uncertainty in the estimates of $TA_{S=0}$ and $DIC_{S=0}$, which were 90±57 μmol kg^{-1} and -17±84 μmol kg^{-1}, respectively. In the case of DIC, this is presumably due to the large scatter in data as previously discussed. Thus, only this latter intercept is not significantly different from zero. Given these uncertainties, in this study we have chosen not to apply any salinity normalisation on the TA and DIC data. This means that we deliberately include the effects of precipitation and evaporation on DIC and TA, in contrast to previous work (Sarmiento and Gruber, 2006; Hauri et al., 2013).

References

Agustí, S., Regaudie-de-Gioux, A., Arrieta, J. M., and Duarte, C. M. (2014). Consequences of UV-enhanced community respiration for plankton metabolic balance. *Limnol. Oceanogr.* 59, 223 – 232. doi:10.4319/lo.2014.59.1.0223.

Álvarez, M., Sanleón-Bartolomé, H., Tanhua, T., Mintrop, L., Luchetta, A., Cantoni, C., Schroeder, K., and Civitarese, G. (2014). The CO_2 system in the Mediterranean Sea: a basin wide perspective. *Ocean Sci.* 10, 69 – 92. doi:10.5194/os-10-69-2014.

Arao, T., and Yamada, M. (1994). Biosynthesis of polyunsaturated fatty acids in the marine diatom, Phaeodactylum tricornutum. *Phytochemistry* 35, 1177 – 1181. doi:10.1016/S0031-9422(00)94817-9.

Arístegui, J., and Harrison, W. G. (2002). Decoupling of primary production and community respiration in the ocean: implications for regional carbon studies. *Aquat. Microb. Ecol.* 29, 199 – 209. doi:10.3354/ame029199.

Bannink, B. A., Van der Meulen, J. H. M., and Nienhuis, P. H. (1984). Lake Grevelingen: from an estuary to a saline lake. An introduction. *Netherlands J. Sea Res.* 18, 179 – 190. doi:10.1016/0077-7579(84)90001-2.

Barber, R. T., and Hiscock, M. R. (2006). A rising tide lifts all phytoplankton: growth response of other phytoplankton taxa in diatom-dominated blooms. *Global Biogeochem. Cycles* 20, GB4S03. doi:10.1029/2006GB002726.

Barranguet, C., Herman, P. M. J., and Sinke, J. J. (1997). Microphytobenthos biomass and community composition studied by pigment biomarkers: importance and fate in the carbon cycle of a tidal flat. *J. Sea Res.* 38, 59 – 70. doi:10.1016/S1385-1101(97)00032-4.

Bates, N. R. (2001). Interannual variability of oceanic CO_2 and biogeochemical properties in the Western North Atlantic subtropical gyre. *Deep Sea Res. Part II Top. Stud. Oceanogr.* 48, 1507 – 1528. doi:10.1016/S0967-0645(00)00151-X.

Bates, N. R. (2007). Interannual variability of the oceanic CO_2 sink in the subtropical gyre of the North Atlantic Ocean over the last 2 decades. *J. Geophys. Res. Ocean.* 112, C09013. doi:10.1029/2006JC003759.

Bates, N. R., Astor, Y. M., Church, M. J., Currie, K., Dore, J. E., González-Dávila, M., Lorenzoni, L., Muller-Karger, F., Olafsson, J., and Santana-Casiano, J. M. (2014). A time-series view of changing ocean chemistry due to ocean uptake of anthropogenic CO_2 and ocean acidification. *Oceanography* 27, 126 – 141. doi:10.5670/oceanog.2014.16.

Bates, N. R., and Peters, A. J. (2007). The contribution of atmospheric acid deposition to ocean acidification in the subtropical North Atlantic Ocean. *Mar. Chem.* 107, 547 – 558. doi:10.1016/j.marchem.2007.08.002.

Batt, R. D., and Carpenter, S. R. (2012). Free-water lake metabolism: addressing noisy time series with a Kalman filter. *Limnol. Oceanogr. Methods* 10, 20 – 30. doi:10.4319/lom.2012.10.20.

Bauer, J. E., Cai, W.-J., Raymond, P. A., Bianchi, T. S., Hopkinson, C. S., and Regnier, P. A. G. (2013). The changing carbon cycle of the coastal ocean. *Nature* 504, 61 – 70. doi:10.1038/nature12857.

Baumann, H., Wallace, R. B., Tagliaferri, T., and Gobler, C. J. (2015). Large natural pH, CO_2 and O_2 fluctuations in a temperate tidal salt marsh on diel, seasonal, and interannual time scales. *Estuaries and Coasts* 38, 220 – 231. doi:10.1007/s12237-014-9800-y.

Beaufort, L., Probert, I., de Garidel-Thoron, T., Bendif, E. M., Ruiz-Pino, D., Metzl, N., Goyet, C., Buchet, N., Coupel, P., Grelaud, M., et al. (2011). Sensitivity of coccolithophores to carbonate chemistry and ocean acidification. *Nature* 476, 80 – 83. doi:10.1038/nature10295.

Bégovic, M., and Copin-Montégut, C. (2002). Processes controlling annual variations in the partial pressure of CO2 in surface waters of the central northwestern Mediterranean Sea (Dyfamed site). *Deep Sea Res. Part II Top. Stud. Oceanogr.* 49, 2031 – 2047. doi:10.1016/S0967-0645(02)00026-7.

Behrenfeld, M. J., Randerson, J. T., McClain, C. R., Feldman, G. C., Los, S. O., Tucker, C. J., Falkowski, P. G., Field, C. B., Frouin, R., Esaias, W. E., et al. (2001). Biospheric primary production during an ENSO transition. *Science* 291, 2594 – 2597. doi:10.1126/science.1055071.

Bellerby, R. G. J., Olsen, A., Furevik, T., and Anderson, L. G. (2005). Response of the surface ocean CO_2 system in the Nordic Seas and northern North Atlantic to climate change, in *The Nordic Seas: An Integrated Perspective (Geophysical Monograph Series 158),* eds. H. Drange, T. Dokken, T. Furevik, R. Gerdes, and W. Berger (Washington, DC: American Geophysical Union), 189 – 197. doi:10.1029/GM15813.

Ben-Yaakov, S. (1973). pH buffering of pore water of recent anoxic marine sediments. *Limnol. Oceanogr.* 18, 86 – 94. doi:10.4319/lo.1973.18.1.0086.

Bergé, J., and Barnathan, G. (2005). Fatty acids from lipids of marine organisms: molecular biodiversity, roles as biomarkers, biologically active compounds, and economical aspects, in *Advances in Biochemical Engineering/Biotechnology: Marine Biotechnology I*, eds. R. Ulber and Y. Le Gal (Springer Berlin Heidelberg), 49 – 125. doi:10.1007/b135782.

Berger, A. (1980). The Milankovitch astronomical theory of paleoclimates: a modern review. *Vistas Astron.* 24, 103 – 122. doi:10.1016/0083-6656(80)90026-4.

Berner, E. K., and Berner, R. A. (1996). *Global Environment: Water, Air, and Geochemical Cycles*. Upper Saddle River, NJ: Prentice-Hall, Inc.

Berner, R. A. (1991). A model for atmospheric CO_2 over Phanerozoic time. *Am. J. Sci.* 291, 339 – 376. doi:10.2475/ajs.291.4.339.

Berner, R. A. (1997). The rise of plants and their effect on weathering and atmospheric CO_2. *Science* 276, 544 – 546. doi:10.1126/science.276.5312.544.

Berner, R. A., and Caldeira, K. (1997). The need for mass balance and feedback in the geochemical carbon cycle. *Geology* 25, 955 – 956. doi:10.1130/0091-7613(1997)025<0955.

Blauw, A. N., Benincà, E., Laane, R. W. P. M., Greenwood, N., and Huisman, J. (2012). Dancing with the tides: fluctuations of coastal phytoplankton orchestrated by different oscillatory modes of the tidal cycle. *PLoS One* 7, e49319. doi:10.1371/journal.pone.0049319.

Bolin, B., and Eriksson, E. (1959). Changes in the carbon dioxide content of the atmosphere and sea due to fossil fuel combustion, in *The Atmosphere and the Sea in Motion: Scientific Contributions to the Rossby Memorial Volume*, ed. B. Bolin (New York: The Rockefeller Institute Press), 130 – 141.

Bopp, L., Resplandy, L., Orr, J. C., Doney, S. C., Dunne, J. P., Gehlen, M., Halloran, P., Heinze, C., Ilyina, T., Séférian, R., et al. (2013). Multiple stressors of ocean ecosystems in the 21st century: projections with CMIP5 models. *Biogeosciences* 10, 6225 – 6245. doi:10.5194/bg-10-6225-2013.

Borges, A. V. (2003). Distribution of surface carbon dioxide and air-sea exchange in the English Channel and adjacent areas. *J. Geophys. Res.* 108, 3140. doi:10.1029/2000JC000571.

Borges, A. V., Delille, B., and Frankignoulle, M. (2005). Budgeting sinks and sources of CO_2 in the coastal ocean: diversity of ecosystems counts. *Geophys. Res. Lett.* 32, L14601. doi:10.1029/2005GL023053.

Borges, A. V., and Gypens, N. (2010). Carbonate chemistry in the coastal zone responds more strongly to eutrophication than ocean acidification. *Limnol. Oceanogr.* 55, 346 – 353. doi:10.4319/lo.2010.55.1.0346.

Boschker, H. T. S. (2004). Linking microbial community structure and functioning: stable isotope (^{13}C) labeling in combination with PLFA analysis, in *Molecular Microbial Ecology Manual*, eds. G. A. Kowalchuk, F. J. de Bruijn, I.

M. Head, A. D. Akkermans, and J. D. van Elsas (Springer Netherlands), 1673 – 1688. doi:10.1007/978-1-4020-2177-0_8.

Boschker, H. T. S., and Middelburg, J. J. (2002). Stable isotopes and biomarkers in microbial ecology. *FEMS Microbiol. Ecol.* 40, 85 – 95. doi:10.1111/j.1574-6941.2002.tb00940.x.

Brewer, P. G., and Peltzer, E. T. (2009). Limits to marine life. *Science* 324, 347 – 348. doi:10.1126/science.1170756.

Brix, H., Gruber, N., and Keeling, C. D. (2004). Interannual variability of the upper ocean carbon cycle at station ALOHA near Hawaii. *Global Biogeochem. Cycles* 18, GB4019. doi:10.1029/2004GB002245.

Brosnan, T. M., and O'Shea, M. L. (1996). Long-term improvements in water quality due to sewage abatement in the lower Hudson River. *Estuaries* 19, 890 – 900. doi:10.2307/1352305.

Brussaard, C. P. D. (2004). Viral control of phytoplankton populations – a review. *J. Eukaryot. Microbiol.* 51, 125 – 138. doi:10.1111/j.1550-7408.2004.tb00537.x.

Buch, K. (1933). Der Borsäuregehalt des Meerwassers und seine Bedeutung bei der Berechnung des Kohlensäuresystems im Meerwasser. *Cons. Perm. Int. Pour L'Exploration la Mer – Rapp. Procès-Verbaux des Réunions* 85, 71 – 75.

Burnett, L. E. (1997). The challenges of living in hypoxic and hypercapnic aquatic environments. *Integr. Comp. Biol.* 37, 633 – 640. doi:10.1093/icb/37.6.633.

Busenberg, E., and Plummer, L. N. (1989). Thermodynamics of magnesian calcite solid-solutions at 25°C and 1 atm total pressure. *Geochim. Cosmochim. Acta* 53, 1189 – 1208. doi:10.1016/0016-7037(89)90056-2.

Byrne, R. H., Mecking, S., Feely, R. A., and Liu, X. (2010). Direct observations of basin-wide acidification of the North Pacific Ocean. *Geophys. Res. Lett.* 37, L02601. doi:10.1029/2009GL040999.

Cadée, G. C., and Hegeman, J. (1991). Historical phytoplankton data of the Marsdiep. *Hydrobiol. Bull.* 24, 111 – 118. doi:10.1007/BF02260427.

Cai, W.-J. (2011). Estuarine and coastal ocean carbon paradox: CO_2 sinks or sites of terrestrial carbon incineration? *Ann. Rev. Mar. Sci.* 3, 123 – 145. doi:10.1146/annurev-marine-120709-142723.

Cai, W.-J., Dai, M., and Wang, Y. (2006). Air-sea exchange of carbon dioxide in ocean margins: a province-based synthesis. *Geophys. Res. Lett.* 33, L12603. doi:10.1029/2006GL026219.

Cai, W.-J., Hu, X., Huang, W.-J., Murrell, M. C., Lehrter, J. C., Lohrenz, S. E., Chou, W.-C., Zhai, W., Hollibaugh, J. T., Wang, Y., et al. (2011). Acidification of subsurface coastal waters enhanced by eutrophication. *Nat. Geosci.* 4, 766 – 770. doi:10.1038/ngeo1297.

Cai, W.-J., Wang, Y., and Hodson, R. E. (1998). Acid-base properties of dissolved organic matter in the estuarine waters of Georgia, USA. *Geochim. Cosmochim. Acta* 62, 473 – 483. doi:10.1016/S0016-7037(97)00363-3.

Calbet, A. (2001). Mesozooplankton grazing impact on primary production: a global comparative analysis in marine ecosystems. *Limnol. Oceanogr.* 46, 1824 – 1830. doi:10.4319/lo.2001.46.7.1824.

Caldeira, K., and Wickett, M. E. (2003). Oceanography: anthropogenic carbon and ocean pH. *Nature* 425, 365. doi:10.1038/425365a.

Cantoni, C., Luchetta, A., Celio, M., Cozzi, S., Raicich, F., and Catalano, G. (2012). Carbonate system variability in the Gulf of Trieste (North Adriatic Sea). *Estuar. Coast. Shelf Sci.* 115, 51 – 62. doi:10.1016/j.ecss.2012.07.006.

Cao, L., Wang, S., Zheng, M., and Zhang, H. (2014). Sensitivity of ocean acidification and oxygen to the uncertainty in climate change. *Environ. Res. Lett.* 9, 064005. doi:10.1088/1748-9326/9/6/064005.

Chen, C.-T. A., and Borges, A. V. (2009). Reconciling opposing views on carbon cycling in the coastal ocean: continental shelves as sinks and near-shore ecosystems as sources of atmospheric CO_2. *Deep Sea Res. Part II Top. Stud. Oceanogr.* 56, 578 – 590. doi:10.1016/j.dsr2.2009.01.001.

Chen, C.-T. A., Huang, T.-H., Chen, Y.-C., Bai, Y., He, X., and Kang, Y. (2013). Air-sea exchanges of CO_2 in the world's coastal seas. *Biogeosciences* 10, 6509 – 6544. doi:10.5194/bg-10-6509-2013.

Chmura, G. L., Anisfield, S., Cahoon, D. R., and Lynch, J. C. (2003). Global carbon sequestration in tidal, saline wetland soils. *Global Biogeochem. Cycles* 17, 1111. doi:10.1029/2002GB001917.

Cloern, J. E., Foster, S. Q., and Kleckner, A. E. (2014). Phytoplankton primary production in the world's estuarine-coastal ecosystems. *Biogeosciences* 11, 2477 – 2501. doi:10.5194/bg-11-2477-2014.

Cole, B. E., and Cloern, J. E. (1987). An empirical model for estimating phytoplankton productivity in estuaries. *Mar. Ecol. Prog. Ser.* 36, 299 – 305. doi:10.3354/meps036299.

Collos, Y., Descolas-Gros, C., Fontugne, M., Mortain-Bertrand, A., Chrétiennot-Dinet, M. J., and Frikha, M. G. (1993). Chemical, isotopic and enzymatic monitoring of free and enclosed seawater: implications for primary production estimates in incubation bottles. *Mar. Ecol. Prog. Ser.* 93, 49 – 54. doi:10.3354/meps093049.

Copin-Montégut, C. (1993). Alkalinity and carbon budgets in the Mediterranean Sea. *Global Biogeochem. Cycles* 7, 915 – 925. doi:10.1029/93GB01826.

Copin-Montégut, C., and Bégovic, M. (2002). Distributions of carbonate properties and oxygen along the water column (0 – 2000m) in the central part of the NW Mediterranean Sea (Dyfamed site): influence of winter vertical mixing on air – sea CO_2 and O_2 exchanges. *Deep Sea Res. Part II Top. Stud. Oceanogr.* 49, 2049 – 2066. doi:10.1016/S0967-0645(02)00027-9.

Copin-Montégut, C., Bégovic, M., and Merlivat, L. (2004). Variability of the partial pressure of CO_2 on diel to annual time scales in the Northwestern Mediterranean Sea. *Mar. Chem.* 85, 169 – 189. doi:10.1016/j.marchem.2003.10.005.

Cox, T. J. S., Maris, T., Soetaert, K., Kromkamp, J. C., Meire, P., and Meysman, F. J. R. (2014). Estimating primary production from oxygen time series: a novel approach in the frequency domain. *Submitted*.

Dauby, P., Frankignoulle, M., Gobert, S., and Bouquegneau, J. M. (1994). Distribution of POC, PON, and particulate Al, Cd, Cr, Cu, Pb, Ti, Zn and ^{13}C in the English Channel and adjacent areas. *Oceanol. Acta* 17, 643 – 657.

Dentener, F. J., and Crutzen, P. J. (1994). A three-dimensional model of the global ammonia cycle. *J. Atmos. Chem.* 19, 331 – 369. doi:10.1007/BF00694492.

Derwent, R. G., Stevenson, D. S., Doherty, R. M., Collins, W. J., Sanderson, M. G., Johnson, C. E., Cofala, J., Mechler, R., Amann, M., and Dentener, F. J. (2005). The contribution from shipping emissions to air quality and acid deposition in Europe. *AMBIO A J. Hum. Environ.* 34, 54 – 59. doi:10.1579/0044-7447-34.1.54.

Diaz, R. J., and Rosenberg, R. (2008). Spreading dead zones and consequences for marine ecosystems. *Science* 321, 926 – 929. doi:10.1126/science.1156401.

Dickson, A. G. (1981). An exact definition of total alkalinity and a procedure for the estimation of alkalinity and total inorganic carbon from titration data. *Deep Sea Res. Part A. Oceanogr. Res. Pap.* 28, 609 – 623. doi:10.1016/0198-0149(81)90121-7.

Dickson, A. G. (1984). pH scales and proton-transfer reactions in saline media such as sea water. *Geochim. Cosmochim. Acta* 48, 2299 – 2308. doi:10.1016/0016-7037(84)90225-4.

Dickson, A. G. (1990). Standard potential of the reaction: $AgCl(s) + \frac{1}{2} H_2(g) = Ag(s) + HCl(aq)$, and the standard acidity constant of the ion HSO_4^- in synthetic sea water from 273.15 to 318.15 K. *J. Chem. Thermodyn.* 22, 113 – 127. doi:10.1016/0021-9614(90)90074-Z.

Dickson, A. G. (2010). The carbon dioxide system in seawater: equilibrium chemistry and measurements, in *Guide to Best Practices for Ocean Acidification Research and Data Reporting*, eds. U. Riebesell, V. J. Fabry, L. Hansson, and J.-P. Gattuso (Luxembourg: Publications Office of the European Union), 17 – 40.

Dickson, A. G., and Millero, F. J. (1987). A comparison of the equilibrium constants for the dissociation of carbonic acid in seawater media. *Deep Sea Res. Part A. Oceanogr. Res. Pap.* 34, 1733 – 1743. doi:10.1016/0198-0149(87)90021-5.

Dickson, A. G., Sabine, C. L., and Christian, J. R. eds. (2007). *Guide to Best Practices for Ocean CO$_2$ Measurements*. PICES Special Publication 3.

Dijkman, N. A., Boschker, H. T. S., Middelburg, J. J., and Kromkamp, J. C. (2009). Group-specific primary production based on stable-isotope labeling of phospholipid-derived fatty acids. *Limnol. Oceanogr. Methods* 7, 612 – 625. doi:10.4319/lom.2009.7.612.

Dijkman, N. A., and Kromkamp, J. C. (2006). Phospholipid-derived fatty acids as chemotaxonomic markers for phytoplankton: application for inferring phytoplankton composition. *Mar. Ecol. Prog. Ser.* 324, 113 – 125. doi:10.3354/meps324113.

Doney, S. C., Fabry, V. J., Feely, R. A., and Kleypas, J. A. (2009a). Ocean acidification: the other CO$_2$ problem. *Ann. Rev. Mar. Sci.* 1, 169 – 192. doi:10.1146/annurev.marine.010908.163834.

Doney, S. C., Lima, I., Feely, R. A., Glover, D. M., Lindsay, K., Mahowald, N., Moore, J. K., and Wanninkhof, R. (2009b). Mechanisms governing interannual variability in upper-ocean inorganic carbon system and air – sea CO$_2$ fluxes: physical climate and atmospheric dust. *Deep Sea Res. Part II Top. Stud. Oceanogr.* 56, 640 – 655. doi:10.1016/j.dsr2.2008.12.006.

Doney, S. C., Mahowald, N., Lima, I., Feely, R. A., Mackenzie, F. T., Lamarque, J.-F., and Rasch, P. J. (2007). Impact of anthropogenic atmospheric nitrogen and sulfur deposition on ocean acidification and the inorganic carbon system. *Proc. Natl. Acad. Sci. U. S. A.* 104, 14580 – 14585. doi:10.1073/pnas.0702218104.

Dore, J. E., Lukas, R., Sadler, D. W., Church, M. J., and Karl, D. M. (2009). Physical and biogeochemical modulation of ocean acidification in the central North Pacific. *Proc. Natl. Acad. Sci. U. S. A.* 106, 12235 – 12240. doi:10.1073/pnas.0906044106.

Dore, J. E., Lukas, R., Sadler, D. W., and Karl, D. M. (2003). Climate-driven changes to the atmospheric CO$_2$ sink in the subtropical North Pacific Ocean. *Nature* 424, 754 – 7. doi:10.1038/nature01885.

Dortch, Q. (1990). The interaction between ammonium and nitrate uptake in phytoplankton. *Mar. Ecol. Prog. Ser.* 61, 183 – 201. doi:10.3354/meps061183.

Driscoll, C. T., Fuller, R. D., and Schecher, W. D. (1989). The role of organic acids in the acidification of surface waters in the Eastern U.S. *Water. Air. Soil Pollut.* 43, 21 – 40. doi:10.1007/BF00175580.

Duarte, C. M., Hendriks, I. E., Moore, T. S., Olsen, Y. S., Steckbauer, A., Ramajo, L., Carstensen, J., Trotter, J. A., and McCulloch, M. (2013a). Is ocean acidification an open-ocean syndrome? Understanding anthropogenic impacts on seawater pH. *Estuaries and Coasts* 36, 221 – 236. doi:10.1007/s12237-013-9594-3.

Duarte, C. M., Middelburg, J. J., and Caraco, N. (2005). Major role of marine vegetation on the oceanic carbon cycle. *Biogeosciences* 2, 1 – 8. doi:10.5194/bg-2-1-2005.

Duarte, C. M., Regaudie-de-Gioux, A., Arrieta, J. M., Delgado-Huertas, A., and Agustí, S. (2013b). The oligotrophic ocean is heterotrophic. *Ann. Rev. Mar. Sci.* 5, 551 – 569. doi:10.1146/annurev-marine-121211-172337.

Dugdale, R. C. (1967). Nutrient limitation in the sea: dynamics, identification, and significance. *Limnol. Oceanogr.* 12, 685 – 695. doi:10.4319/lo.1967.12.4.0685.

Dugdale, R. C., Goering, J. J., Barber, R. T., Smith, R. L., and Packard, T. T. (1977). Denitrification and hydrogen sulfide in the Peru upwelling region during 1976. *Deep Sea Res.* 24, 601 – 608. doi:10.1016/0146-6291(77)90530-6.

Durrieu de Madron, X., Denis, L., Diaz, F., Garcia, N., Guieu, C., Grenz, C., Loÿe-Pilot, M.-D., Ludwig, W., Moutin, T., Raimbault, P., et al. (2003). Nutrients and carbon budgets for the Gulf of Lion during the Moogli cruises. *Oceanol. Acta* 26, 421 – 433. doi:10.1016/S0399-1784(03)00024-0.

Edman, M., and Omstedt, A. (2013). Modeling the dissolved CO_2 system in the redox environment of the Baltic Sea. *Limnol. Oceanogr.* 58, 74 – 92. doi:10.4319/lo.2013.58.1.0074.

Egleston, E. S., Sabine, C. L., and Morel, F. M. M. (2010). Revelle revisited: buffer factors that quantify the response of ocean chemistry to changes in DIC and alkalinity. *Global Biogeochem. Cycles* 24, GB1002. doi:10.1029/2008GB003407.

Eichner, M., Rost, B., and Kranz, S. A. (2014). Diversity of ocean acidification effects on marine N_2 fixers. *J. Exp. Mar. Bio. Ecol.* 457, 199 – 207. doi:10.1016/j.jembe.2014.04.015.

Eilers, P. H. C., and Peeters, J. C. H. (1988). A model for the relationship between light intensity and the rate of photosynthesis in phytoplankton. *Ecol. Modell.* 42, 199 – 215. doi:10.1016/0304-3800(88)90057-9.

Emerson, S., Stump, C., and Nicholson, D. (2008). Net biological oxygen production in the ocean: remote in situ measurements of O_2 and N_2 in surface waters. *Global Biogeochem. Cycles* 22, GB3023. doi:10.1029/2007GB003095.

Engel, A., Borchard, C., Piontek, J., Schulz, K. G., Riebesell, U., and Bellerby, R. (2013). CO_2 increases ^{14}C primary production in an Arctic plankton community. *Biogeosciences* 10, 1291 – 1308. doi:10.5194/bg-10-1291-2013.

Eppley, R. W. (1972). Temperature and phytoplankton growth in the sea. *Fish. Bull.* 70, 1063 – 1085.

Fabry, V. J. (2008). Ocean science. Marine calcifiers in a high-CO_2 ocean. *Science* 320, 1020 – 1022. doi:10.1126/science.1157130.

Fabry, V. J., Seibel, B. A., Feely, R. A., and Orr, J. C. (2008). Impacts of ocean acidification on marine fauna and ecosystem processes. *ICES J. Mar. Sci.* 65, 414 – 432. doi:10.1093/icesjms/fsn048.

Fabry, V., McClintock, J., Mathis, J., and Grebmeier, J. (2009). Ocean acidification at high latitudes: the bellwether. *Oceanography* 22, 160 – 171. doi:10.5670/oceanog.2009.105.

Falkowski, P. G. (1994). The role of phytoplankton photosynthesis in global biogeochemical cycles. *Photosynth. Res.* 39, 235 – 258. doi:10.1007/BF00014586.

Falkowski, P. G., and Raven, J. A. (2013). *Aquatic Photosynthesis*. 2nd ed. Princeton, NJ: Princeton University Press.

Feely, R. A., Alin, S. R., Newton, J., Sabine, C. L., Warner, M., Devol, A., Krembs, C., and Maloy, C. (2010). The combined effects of ocean acidification, mixing, and respiration on pH and carbonate saturation in an urbanized estuary. *Estuar. Coast. Shelf Sci.* 88, 442 – 449. doi:10.1016/j.ecss.2010.05.004.

Feely, R. A., Sabine, C. L., Hernandez-Ayon, J. M., Ianson, D., and Hales, B. (2008). Evidence for upwelling of corrosive "acidified" water onto the continental shelf. *Science* 320, 1490 – 1492. doi:10.1126/science.1155676.

Feistel, R. (2008). A Gibbs function for seawater thermodynamics for –6 to 80°C and salinity up to 120 g kg^{-1}. *Deep Sea Res. Part I Oceanogr. Res. Pap.* 55, 1639 – 1671. doi:10.1016/j.dsr.2008.07.004.

Field, C. B., Behrenfeld, M. J., Randerson, J. T., and Falkowski, P. G. (1998). Primary production of the biosphere: integrating terrestrial and oceanic components. *Science* 281, 237 – 240. doi:10.1126/science.281.5374.237.

Le Floc'h, E., Malara, G., and Sciandra, A. (2002). An automatic device for in vivo absorption spectra acquisition and chlorophyll estimation in phytoplankton cultures. *J. Appl. Phycol.* 14, 435 – 444. doi:10.1023/A:1022338930747.

Fofonoff, N. P., and Millard, R. C. (1983). *Algorithms for Computation of Fundamental Properties of Seawater*. Unesco Technical Papers in Marine Science 44.

Frankignoulle, M. (1994). A complete set of buffer factors for acid/base CO_2 system in seawater. *J. Mar. Syst.* 5, 111 – 118. doi:10.1016/0924-7963(94)90026-4.

Frankignoulle, M., Abril, G., Borges, A. V., Bourge, I., Canon, C., Delille, B., Libert, E., and Théate, J.-M. (1998). Carbon dioxide emission from European estuaries. *Science* 282, 434 – 436. doi:10.1126/science.282.5388.434.

Frankignoulle, M., and Distèche, A. (1984). CO_2 chemistry in the water column above a Posidonia seagrass bed and related air-sea exchanges. *Oceanol. Acta* 7, 209 – 219.

Friedrich, T., Timmermann, A., Abe-Ouchi, A., Bates, N. R., Chikamoto, M. O., Church, M. J., Dore, J. E., Gledhill, D. K., González-Dávila, M., Heinemann, M., et al. (2012). Detecting regional anthropogenic trends in ocean acidification against natural variability. *Nat. Clim. Chang.* 2, 167 – 171. doi:10.1038/nclimate1372.

Friis, K., Körtzinger, A., and Wallace, D. W. R. (2003). The salinity normalization of marine inorganic carbon chemistry data. *Geophys. Res. Lett.* 30, 1085. doi:10.1029/2002GL015898.

Fulweiler, R. W., Emery, H. E., Heiss, E. M., and Berounsky, V. M. (2011). Assessing the role of pH in determining water column nitrification rates in a coastal system. *Estuaries and Coasts* 34, 1095 – 1102. doi:10.1007/s12237-011-9432-4.

Gaarder, T., and Gran, H. H. (1927). Investigations of the production of plankton in the Oslo Fjord. *Cons. Perm. Int. Pour L'Exploration la Mer – Rapp. Procès-Verbaux des Réunions* 42, 1 – 48.

Gaines Jr, A. G., and Pilson, M. E. Q. (1972). Anoxic water in the Pettaquamscutt River. *Limnol. Oceanogr.* 17, 42 – 50. doi:10.4319/lo.1972.17.1.0042.

Galloway, J. N., Townsend, A. R., Erisman, J. W., Bekunda, M., Cai, Z., Freney, J. R., Martinelli, L. A., Seitzinger, S. P., and Sutton, M. A. (2008). Transformation of the nitrogen cycle: recent trends, questions, and potential solutions. *Science* 320, 889 – 892. doi:10.1126/science.1136674.

Garbe, C. S., Rutgersson, A., Boutin, J., Leeuw, G. De, Delille, B., Fairall, C. W., Gruber, N., Hare, J., Ho, D. T., Johnson, M. T., et al. (2014). Transfer across the air-sea interface, in *Ocean-Atmosphere Interactions of Gases and Particles*, eds. P. S. Liss and M. T. Johnson (Springer Berlin Heidelberg), 55 – 112. doi:10.1007/978-3-642-25643-1_2.

Garcia, H. E., Locarnini, R. A., Boyer, T. P., Antonov, J. I., Baranova, O. K., Zweng, M. M., Reagan, J. R., and Johnson, D. R. (2013). *World Ocean Atlas 2013, Volume 4: Dissolved Inorganic Nutrients (phosphate, nitrate, silicate)*. NOAA Atlas NESDIS 76, ed. S. Levitus.

Gattuso, J.-P., Frankignoulle, M., and Wollast, R. (1998). Carbon and carbonate metabolism in coastal aquatic ecosystems. *Annu. Rev. Ecol. Syst.* 29, 405 – 434. doi:10.1146/annurev.ecolsys.29.1.405.

Gattuso, J.-P., Epitalon, J.-M., and Lavigne, H. (2015). seacarb: seawater carbonate chemistry. R package version 3.0.6. http://CRAN.R-project.org/package=seacarb.

Gattuso, J.-P., and Hansson, L. (2011). Ocean acidification: background and history, in *Ocean Acidification*, eds. J.-P. Gattuso and L. Hansson (New York, NY: Oxford University Press Inc.), 1 – 20.

Gazeau, F., Borges, A. V., Barrón, C., Duarte, C. M., Iversen, N., Middelburg, J. J., Delille, B., Pizay, M. D., Frankignoulle, M., and Gattuso, J.-P. (2005a). Net ecosystem metabolism in a micro-tidal estuary (Randers Fjord, Denmark): evaluation of methods. *Mar. Ecol. Prog. Ser.* 301, 23 – 41. doi:10.3354/meps301023.

Gazeau, F., Gattuso, J.-P., Middelburg, J. J., Brion, N., Schiettecatte, L.-S., Frankignoulle, M., and Borges, A. V. (2005b). Planktonic and whole system metabolism in a nutrient-rich estuary (the Scheldt estuary). *Estuaries* 28, 868 – 883. doi:10.1007/BF02696016.

Gazeau, F., Middelburg, J. J., Loijens, M., Vanderborght, J.-P., Pizay, M.-D., and Gattuso, J.-P. (2007a). Planktonic primary production in estuaries: comparison of ^{14}C, O_2 and ^{18}O methods. *Aquat. Microb. Ecol.* 46, 95 – 106. doi:10.3354/ame046095.

Gazeau, F., Quiblier, C., Jansen, J. M., Gattuso, J.-P., Middelburg, J. J., and Heip, C. H. R. (2007b). Impact of elevated CO_2 on shellfish calcification. *Geophys. Res. Lett.* 34, L07603. doi:10.1029/2006GL028554.

Gazeau, F., van Rijswijk, P., Pozzato, L., and Middelburg, J. J. (2014). Impacts of ocean acidification on sediment processes in shallow waters of the Arctic Ocean. *PLoS One* 9, e94068. doi:10.1371/journal.pone.0094068.

Gazeau, F., Smith, S. V., Gentili, B., Frankignoulle, M., and Gattuso, J.-P. (2004). The European coastal zone: characterization and first assessment of ecosystem metabolism. *Estuar. Coast. Shelf Sci.* 60, 673 – 694. doi:10.1016/j.ecss.2004.03.007.

Gilbert, D., Rabalais, N. N., Díaz, R. J., and Zhang, J. (2010). Evidence for greater oxygen decline rates in the coastal ocean than in the open ocean. *Biogeosciences* 7, 2283 – 2296. doi:10.5194/bg-7-2283-2010.

González, N., Gattuso, J.-P., and Middelburg, J. J. (2008). Oxygen production and carbon fixation in oligotrophic coastal bays and the relationship with gross and net primary production. *Aquat. Microb. Ecol.* 52, 119 – 130. doi:10.3354/ame01208.

Grande, K. D., Williams, P. J. L., Marra, J., Purdie, D. A., Heinemann, K., Eppley, R. W., and Bender, M. L. (1989). Primary production in the North Pacific gyre: a comparison of rates determined by the ^{14}C, O_2 concentration and ^{18}O methods. *Deep Sea Res. Part A. Oceanogr. Res. Pap.* 36, 1621 – 1634. doi:10.1016/0198-0149(89)90063-0.

Gruber, N. (2014). Ocean biogeochemistry: Carbon at the coastal interface. *Nature* 517, 148 – 149. doi:10.1038/nature14082.

Gruber, N. (2008). The Marine Nitrogen Cycle: Overview and Challenges, in *Nitrogen in the Marine Environment*, eds. D. G. Capone, D. A. Bronk, M. R. Mulholland, and E. J. Carpenter (Academic Press), 150. doi:10.1016/B978-0-12-372522-6.00001-3.

Gruber, N. (2011). Warming up, turning sour, losing breath: ocean biogeochemistry under global change. *Philos. Trans. A. Math. Phys. Eng. Sci.* 369, 1980 – 1996. doi:10.1098/rsta.2011.0003.

Gruber, N., Gloor, M., Mikaloff Fletcher, S. E., Doney, S. C., Dutkiewicz, S., Follows, M. J., Gerber, M., Jacobson, A. R., Joos, F., Lindsay, K., et al. (2009). Oceanic sources, sinks, and transport of atmospheric CO_2. *Global Biogeochem. Cycles* 23, GB1005. doi:10.1029/2008GB003349.

Gruber, N., Keeling, C. D., and Bates, N. R. (2002). Interannual variability in the North Atlantic Ocean carbon sink. *Science* 298, 2374 – 8. doi:10.1126/science.1077077.

Gruber, N., Keeling, C. D., and Stocker, T. F. (1998). Carbon-13 constraints on the seasonal inorganic carbon budget at the BATS site in the northwestern Sargasso Sea. *Deep Sea Res. Part I Oceanogr. Res. Pap.* 45, 673 – 717. doi:10.1016/S0967-0637(97)00098-8.

Guckert, J. B., Antworth, C. P., Nichols, P. D., and White, D. C. (1985). Phospholipid, ester-linked fatty acid profiles as reproducible assays for changes in prokaryotic community structure of estuarine sediments. *FEMS Microbiol. Lett.* 31, 147 – 158. doi:10.1111/j.1574-6968.1985.tb01143.x.

Guerzoni, S., Chester, R., Dulac, F., Herut, B., Loÿe-Pilot, M.-D., Measures, C., Migon, C., Molinaroli, E., Moulin, C., Rossini, P., et al. (1999). The role of atmospheric deposition in the biogeochemistry of the Mediterranean Sea. *Prog. Oceanogr.* 44, 147 – 190. doi:10.1016/S0079-6611(99)00024-5.

Guinotte, J. M., and Fabry, V. J. (2008). Ocean acidification and its potential effects on marine ecosystems. *Ann. N. Y. Acad. Sci.* 1134, 320 – 342. doi:10.1196/annals.1439.013.

Hagens, M., Hunter, K. A., Liss, P. S., and Middelburg, J. J. (2014). Biogeochemical context impacts seawater pH changes resulting from atmospheric sulfur and nitrogen deposition. *Geophys. Res. Lett.* 41, 935 – 941. doi:10.1002/2013GL058796.

Hagens, M., Slomp, C. P., Meysman, F. J. R., Seitaj, D., Harlay, J., Borges, A. V, and Middelburg, J. J. (2015). Biogeochemical processes and buffering capacity concurrently affect acidification in a seasonally hypoxic coastal marine basin. *Biogeosciences* 12, 1561 – 1583. doi:10.5194/bg-12-1561-2015.

Hall-Spencer, J. M., Rodolfo-Metalpa, R., Martin, S., Ransome, E., Fine, M., Turner, S. M., Rowley, S. J., Tedesco, D., and Buia, M.-C. (2008). Volcanic carbon dioxide vents show ecosystem effects of ocean acidification. *Nature* 454, 96 – 99. doi:10.1038/nature07051.

Hansen, B., and Østerhus, S. (2000). North Atlantic – Nordic Seas exchanges. *Prog. Oceanogr.* 45, 109 – 208. doi:10.1016/S0079-6611(99)00052-X.

Hanson, P. C., Carpenter, S. R., Kimura, N., Wu, C., Cornelius, S. P., and Kratz, T. K. (2008). Evaluation of metabolism models for free-water dissolved oxygen methods in lakes. *Limnol. Oceanogr. Methods* 6, 454 – 465. doi:10.4319/lom.2008.6.454.

Harris, G. P., and Lott, J. N. A. (1973). Light intensity and photosynthetic rates in phytoplankton. *J. Fish. Res. Board Canada* 30, 1771 – 1778. doi:10.1139/f73-286.

Hassellöv, I.-M., Turner, D. R., Lauer, A., and Corbett, J. J. (2013). Shipping contributes to ocean acidification. *Geophys. Res. Lett.* 40, 2731 – 2736. doi:10.1002/grl.50521.

Haugan, P. M., and Drange, H. (1996). Effects of CO_2 on the environment. *Energy Convers. Manag.* 37, 1019 – 1022. doi:10.1016/0196-8904(95)00292-8.

Hauri, C., Gruber, N., Vogt, M., Doney, S. C., Feely, R. A., Lachkar, Z., Leinweber, A., McDonnell, A. M. P., Munnich, M., and Plattner, G.-K. (2013). Spatiotemporal variability and long-term trends of ocean acidification in the California Current System. *Biogeosciences* 10, 193 – 216. doi:10.5194/bg-10-193-2013.

Henry, W. (1803). Experiments on the quantity of gases absorbed by water, at different temperatures, and under different pressures. *Philos. Trans. R. Soc. London* 93, 29 – 42, 274 – 276. doi:10.1098/rstl.1803.0004.

Hernández-Ayon, J. M., Zirino, A., Dickson, A. G., Camiro-Vargas, T., and Valenzuela, E. (2007). Estimating the contribution of organic bases from microalgae to the titration alkalinity in coastal seawaters. *Limnol. Oceanogr. Methods* 5, 225 – 232. doi:10.4319/lom.2007.5.225.

Hillebrand, H., Dürselen, C.-D., Kirschtel, D., Pollingher, U., and Zohary, T. (1999). Biovolume calculation for pelagic and benthic microalgae. *J. Phycol.* 424, 403 – 424. doi:10.1046/j.1529-8817.1999.3520403.x.

Hoegh-Guldberg, O., Mumby, P. J., Hooten, A. J., Steneck, R. S., Greenfield, P., Gomez, E., Harvell, C. D., Sale, P. F., Edwards, A. J., Caldeira, K., et al. (2007). Coral reefs under rapid climate change and ocean acidification. *Science* 318, 1737 – 1742. doi:10.1126/science.1152509.

Hofmann, A. F. (2009). *Quantifying the influences of biogeochemical processes on pH of natural waters*. Geologica Ultraiectina 304.

Hofmann, A. F., Meysman, F. J. R., Soetaert, K., and Middelburg, J. J. (2008). A step-by-step procedure for pH model construction in aquatic systems. *Biogeosciences* 5, 227 – 251. doi:10.5194/bg-5-227-2008.

Hofmann, A. F., Middelburg, J. J., Soetaert, K., and Meysman, F. J. R. (2009). pH modelling in aquatic systems with time-variable acid-base dissociation constants applied to the turbid, tidal Scheldt estuary. *Biogeosciences* 6, 1539 – 1561. doi:10.5194/bg-6-1539-2009.

Hofmann, A. F., Middelburg, J. J., Soetaert, K., Wolf-Gladrow, D. A., and Meysman, F. J. R. (2010a). Proton cycling, buffering, and reaction stoichiometry in natural waters. *Mar. Chem.* 121, 246 – 255. doi:10.1016/j.marchem.2010.05.004.

Hofmann, A. F., Soetaert, K., Middelburg, J. J., and Meysman, F. J. R. (2010b). AquaEnv: An aquatic acid – base modelling environment in R. *Aquat. Geochemistry* 16, 507 – 546. doi:10.1007/s10498-009-9084-1.

Hofmann, G. E., Smith, J. E., Johnson, K. S., Send, U., Levin, L. A., Micheli, F., Paytan, A., Price, N. N., Peterson, B., Takeshita, Y., et al. (2011). High-frequency dynamics of ocean pH: a multi-ecosystem comparison. *PLoS One* 6, e28983. doi:10.1371/journal.pone.0028983.

Holtgrieve, G. W., Schindler, D. E., Branch, T. A., and A'mar, Z. T. (2010). Simultaneous quantification of aquatic ecosystem metabolism and reaeration using a Bayesian statistical model of oxygen dynamics. *Limnol. Oceanogr.* 55, 1047 – 1062. doi:10.4319/lo.2010.55.3.1047.

Hood, E. M., and Merlivat, L. (2001). Annual to interannual variations of fCO_2 in the northwestern Mediterranean Sea: results from hourly measurements made by CARIOCA buoys, 1995-1997. *J. Mar. Res.* 59, 113 – 131. doi:10.1357/002224001321237399.

Hopkinson, C. S., Cai, W.-J., and Hu, X. (2012). Carbon sequestration in wetland dominated coastal systems – a global sink of rapidly diminishing magnitude. *Curr. Opin. Environ. Sustain.* 4, 186 – 194. doi:10.1016/j.cosust.2012.03.005.

Hoppe, C. J. M., Langer, G., Rokitta, S. D., Wolf-Gladrow, D. A., and Rost, B. (2012). Implications of observed inconsistencies in carbonate chemistry measurements for ocean acidification studies. *Biogeosciences* 9, 2401 – 2405. doi:10.5194/bg-9-2401-2012.

Houghton, R. A., Hobbie, J. E., Melillo, J. M., Moore, B., Peterson, B. J., Shaver, G. R., and Woodwell, G. M. (1983). Changes in the carbon content of terrestrial biota and soils between 1860 and 1980: a net release of CO_2 to the atmosphere. *Ecol. Monogr.* 53, 236 – 262. doi:10.2307/1942531.

Howarth, R., Chan, F., Conley, D. J., Garnier, J., Doney, S. C., Marino, R., and Billen, G. (2011). Coupled biogeochemical cycles: eutrophication and hypoxia in temperate estuaries and coastal marine ecosystems. *Front. Ecol. Environ.* 9, 18 – 26. doi:10.1890/100008.

Howarth, R., and Michaels, A. (2000). The measurement of primary production in aquatic ecosystems, in *Methods in Ecosystem Science*, eds. O. E. Sala, R. B. Jackson, H. A. Mooney, and R. W. Howarth (Springer New York), 72 – 85. doi:10.1007/978-1-4612-1224-9_6.

Hunter, K. A. (2007). XLCO2 – Seawater CO_2 equilibrium calculations using Excel. Otago, New Zealand.

Hunter, K. A., Liss, P. S., Surapipith, V., Dentener, F., Duce, R., Kanakidou, M., Kubilay, N., Mahowald, N., Okin, G., Sarin, M., et al. (2011). Impacts of anthropogenic SO_x, NO_x and NH_3 on acidification of coastal waters and shipping lanes. *Geophys. Res. Lett.* 38, L13602. doi:10.1029/2011GL047720.

IPCC (2013). *Climate Change 2013: The Physical Science Basis. Contribution of Working Group I to the Fifth Assessment Report of the Intergovernmental Panel on Climate Change*. Eds. T. F. Stocker, D. Qin, G.-K. Plattner, M. Tignor, S. K. Allen, J. Boschung, A. Nauels, Y. Xia, V. Bex, and P. M. Midgley. Cambridge University Press doi:10.1017/CBO9781107415324.

Jeansson, E., Bellerby, R., Frigstad, H., Ólafsdóttir, S. R., and Olafsson, J. (2015). Fluxes of carbon and nutrients to the Iceland Sea surface waters and inferred primary productivity and stoichiometry. *Biogeosciences* 12, 875 – 885. doi:10.5194/bg-12-875-2015.

Jiang, Z., Tyrrell, T., Hydes, D. J., Dai, M., and Hartman, S. E. (2014). Variability of alkalinity and the alkalinity-salinity relationship in the tropical and subtropical surface ocean. *Global Biogeochem. Cycles* 28, 729 – 742. doi:10.1002/2013GB004678.

Johnson, Z. I., Wheeler, B. J., Blinebry, S. K., Carlson, C. M., Ward, C. S., and Hunt, D. E. (2013). Dramatic variability of the carbonate system at a temperate coastal ocean site (Beaufort, North Carolina, USA) is regulated by physical and biogeochemical processes on multiple timescales. *PLoS One* 8, e85117. doi:10.1371/journal.pone.0085117.

Joint, I., Doney, S. C., and Karl, D. M. (2011). Will ocean acidification affect marine microbes? *ISME J.* 5, 1 – 7. doi:10.1038/ismej.2010.79.

Jury, C. P., Thomas, F. I. M., Atkinson, M. J., and Toonen, R. J. (2013). Buffer capacity, ecosystem feedbacks, and seawater chemistry under global change. *Water* 5, 1303 – 1325. doi:10.3390/w5031303.

Karl, D. M., Hebel, D. V, Bjørkman, K., and Letelier, R. M. (1998). The role of dissolved organic matter release in the productivity of the oligotrophic North Pacific Ocean. *Limnol. Oceanogr.* 43, 1270 – 1286. doi:10.4319/lo.1998.43.6.1270.

Keeling, C. D. (1993). Lecture 2: surface ocean CO_2, in *The Global Carbon Cycle (NATO ASI Series Vol. 15)*, ed. M. Heimann (Springer Berlin Heidelberg), 413 – 429. doi:10.1007/978-3-642-84608-3_17.

Keeling, C. D. (1973). The carbon dioxide cycle: reservoir models to depict the exchange of atmospheric carbon dioxide with the oceans and land plants, in *Chemistry of the Lower Atmosphere*, ed. S. I. Rasool (New York NY: Plenum Press), 251 – 329. doi:10.1007/978-1-4684-1986-3_6.

Keeling, C. D., Brix, H., and Gruber, N. (2004). Seasonal and long-term dynamics of the upper ocean carbon cycle at Station ALOHA near Hawaii. *Global Biogeochem. Cycles* 18, GB4006. doi:10.1029/2004GB002227.

Key, R. M., Kozyr, A., Sabine, C. L., Lee, K., Wanninkhof, R., Bullister, J. L., Feely, R. A., Millero, F. J., Mordy, C., and Peng, T.-H. (2004). A global ocean carbon climatology: results from Global Data Analysis Project (GLODAP). *Global Biogeochem. Cycles* 18, GB4031. doi:10.1029/2004GB002247.

Kim, H.-C., and Lee, K. (2009). Significant contribution of dissolved organic matter to seawater alkalinity. *Geophys. Res. Lett.* 36, L20603. doi:10.1029/2009GL040271.

Kim, H.-C., Lee, K., and Choi, W. (2006). Contribution of phytoplankton and bacterial cells to the measured alkalinity of seawater. *Limnol. Oceanogr.* 51, 331 – 338. doi:10.4319/lo.2006.51.1.0331.

Kirk, J. T. O. (1994). *Light and Photosynthesis in Aquatic Ecosystems*. Cambridge: Cambridge University Press doi:10.1017/CBO9780511623370.

Kitidis, V., Hardman-Mountford, N. J., Litt, E., Brown, I., Cummings, D., Hartman, S., Hydes, D., Fishwick, J. R., Harris, C., Martinez-Vicente, V., et al. (2012). Seasonal dynamics of the carbonate system in the Western English Channel. *Cont. Shelf Res.* 42, 30 – 40. doi:10.1016/j.csr.2012.04.012.

Kitidis, V., Laverock, B., McNeill, L. C., Beesley, A., Cummings, D., Tait, K., Osborn, M. A., and Widdicombe, S. (2011). Impact of ocean acidification on benthic and water column ammonia oxidation. *Geophys. Res. Lett.* 38, L21603. doi:10.1029/2011GL049095.

Kleypas, J. A., Buddemeier, R. W., Archer, D., Gattuso, J.-P., Langdon, C., and Opdyke, B. N. (1999). Geochemical consequences of increased atmospheric carbon dioxide on coral reefs. *Science* 284, 118 – 120. doi:10.1126/science.284.5411.118.

de Kluijver, A., Soetaert, K., Czerny, J., Schulz, K. G., Boxhammer, T., Riebesell, U., and Middelburg, J. J. (2013). A ^{13}C labelling study on carbon fluxes in Arctic plankton communities under elevated CO_2 levels. *Biogeosciences* 10, 1425 – 1440. doi:10.5194/bg-10-1425-2013.

de Kluijver, A., Soetaert, K., Schulz, K. G., Riebesell, U., Bellerby, R. G. J., and Middelburg, J. J. (2010). Phytoplankton-bacteria coupling under elevated CO_2 levels: a stable isotope labelling study. *Biogeosciences* 7, 3783 – 3797. doi:10.5194/bg-7-3783-2010.

Knap, A. H., Michaels, A. F., and Close, A. (1994). *The JGOFS Protocols*. Intergovernmental Oceanographic Commission.

Knull, J. R., and Richards, F. A. (1969). A note on the sources of excess alkalinity in anoxic waters. *Deep Sea Res. Oceanogr. Abstr.* 16, 205 – 212. doi:10.1016/0011-7471(69)90076-X.

Koeve, W., and Oschlies, A. (2012). Potential impact of DOM accumulation on fCO_2 and carbonate ion computations in ocean acidification experiments. *Biogeosciences* 9, 3787 – 3798. doi:10.5194/bg-9-3787-2012.

Krahmann, G., and Schott, F. (1998). Longterm increases in western Mediterranean salinities and temperatures: anthropogenic and climatic sources. *Geophys. Res. Lett.* 25, 4209 – 4212. doi:10.1029/1998GL900143.

Kromkamp, J., Peene, J., van Rijswijk, P., Sandee, A., and Goosen, N. (1995). Nutrients, light and primary production by phytoplankton and microphytobenthos in the eutrophic, turbid Westerschelde estuary (The Netherlands). *Hydrobiologia* 311, 9 – 19. doi:10.1007/BF00008567.

Lam, P., Lavik, G., Jensen, M. M., van de Vossenberg, J., Schmid, M., Woebken, D., Gutiérrez, D., Amann, R., Jetten, M. S. M., and Kuypers, M. M. M. (2009). Revising the nitrogen cycle in the Peruvian oxygen minimum zone. *Proc. Natl. Acad. Sci. U. S. A.* 106, 4752 – 4757. doi:10.1073/pnas.0812444106.

Lana, A., Bell, T. G., Simó, R., Vallina, S. M., Ballabrera-Poy, J., Kettle, a. J., Dachs, J., Bopp, L., Saltzman, E. S., Stefels, J., et al. (2011). An updated climatology of surface dimethlysulfide concentrations and emission fluxes in the global ocean. *Global Biogeochem. Cycles* 25, GB1004. doi:10.1029/2010GB003850.

Lancelot, C., Gypens, N., Billen, G., Garnier, J., and Roubeix, V. (2007). Testing an integrated river – ocean mathematical tool for linking marine eutrophication to land use: the Phaeocystis-dominated Belgian coastal zone (Southern North Sea) over the past 50 years. *J. Mar. Syst.* 64, 216 – 228. doi:10.1016/j.jmarsys.2006.03.010.

Laruelle, G. G., Dürr, H. H., Lauerwald, R., Hartmann, J., Slomp, C. P., Goossens, N., and Regnier, P. A. G. (2013). Global multi-scale segmentation of continental and coastal waters from the watersheds to the continental margins. *Hydrol. Earth Syst. Sci.* 17, 2029 – 2051. doi:10.5194/hess-17-2029-2013.

Laruelle, G. G., Dürr, H. H., Slomp, C. P., and Borges, A. V. (2010). Evaluation of sinks and sources of CO_2 in the global coastal ocean using a spatially-explicit typology of estuaries and continental shelves. *Geophys. Res. Lett.* 37, L15607. doi:10.1029/2010GL043691.

Laruelle, G. G., Lauerwald, R., Pfeil, B., and Regnier, P. (2014). Regionalized global budget of the CO_2 exchange at the air-water interface in continental shelf seas. *Global Biogeochem. Cycles* 28, 1199 – 1214. doi:10.1002/2014GB004832.

Lauvset, S. K., Gruber, N., Landschützer, P., Olsen, A., and Tjiputra, J. (2015). Trends and drivers in global surface ocean pH over the past 3 decades. *Biogeosciences* 12, 1285 – 1298. doi:10.5194/bg-12-1285-2015.

Laws, E. A., Landry, M. R., Barber, R. T., Campbell, L., Dickson, M.-L., and Marra, J. (2000). Carbon cycling in primary production bottle incubations: inferences from grazing experiments and photosynthetic studies using and in the Arabian Sea. *Deep Sea Res. Part II Top. Stud. Oceanogr.* 47, 1339 – 1352. doi:10.1016/S0967-0645(99)00146-0.

Lee, D. Y., Owens, M. S., Doherty, M., Eggleston, E. M., Hewson, I., Crump, B. C., and Cornwell, J. C. (2015). The effects of oxygen transition on community respiration and potential chemoautotrophic production in a seasonally stratified anoxic estuary. *Estuaries and Coasts* 38, 104 – 117. doi:10.1007/s12237-014-9803-8.

Lee, K., Kim, T.-W., Byrne, R. H., Millero, F. J., Feely, R. A., and Liu, Y.-M. (2010). The universal ratio of boron to chlorinity for the North Pacific and North Atlantic oceans. *Geochim. Cosmochim. Acta* 74, 1801 – 1811. doi:10.1016/j.gca.2009.12.027.

Legendre, P., (2014). lmodel2: model II regression. R package version 1.7-2. http://CRAN.R-project.org/package=lmodel2.

Lemaire, E., Abril, G., De Wit, R., and Etcheber, H. (2002). Distribution of phytoplankton pigments in nine European estuaries and implications for an estuarine typology. *Biogeochemistry* 59, 5 – 23. doi:10.1023/A:1015572508179.

Lewis, E. L., and Wallace, D. W. R. (1998). CO2SYS: program developed for CO_2 system calculations. Oak Ridge, Tennessee, USA.

Li, W., and Gao, K. (2012). A marine secondary producer respires and feeds more in a high CO_2 ocean. *Mar. Pollut. Bull.* 64, 699 – 703. doi:10.1016/j.marpolbul.2012.01.033.

Liss, P. S., and Merlivat, L. (1986). Air-sea gas exchange rates: introduction and synthesis," in *The Role of Air–Sea Exchange in Geochemical Cycling (NATO ASI Series Vol. 185)*, ed. P. Buat-Ménard (Springer Netherlands), 113 – 127. doi:10.1007/978-94-009-4738-2_5.

Liu, J., Weinbauer, M., Maier, C., Dai, M., and Gattuso, J. (2010). Effect of ocean acidification on microbial diversity and on microbe-driven biogeochemistry and ecosystem functioning. *Aquat. Microb. Ecol.* 61, 291 – 305. doi:10.3354/ame01446.

Locarnini, R. A., Mishonov, A. V., Antonov, J. I., Boyer, T. P., Garcia, H. E., Baranova, O. K., Zweng, M. M., Paver, C. R., Reagan, J. R., Johnson, D. R., et al. (2013). *World Ocean Atlas 2013, Volume 1: Temperature*. NOAA Atlas NESDIS 73, ed. S. Levitus.

Lovenduski, N. S., Gruber, N., Doney, S. C., and Lima, I. D. (2007). Enhanced CO_2 outgassing in the Southern Ocean from a positive phase of the Southern Annular Mode. *Global Biogeochem. Cycles* 21, GB2026. doi:10.1029/2006GB002900.

Low-Décarie, E., Fussmann, G. F., and Bell, G. (2014). Aquatic primary production in a high-CO_2 world. *Trends Ecol. Evol.* 29, 223 – 232. doi:10.1016/j.tree.2014.02.006.

Lukas, R. (2001). Freshening of the upper thermocline in the North Pacific subtropical gyre associated with decadal changes of rainfall. *Geophys. Res. Lett.* 28, 3485 – 3488. doi:10.1029/2001GL013116.

Luz, B., and Barkan, E. (2000). Assessment of oceanic productivity with the triple-isotope composition of dissolved oxygen. *Science* 288, 2028 – 2031. doi:10.1126/science.288.5473.2028.

MacIntyre, F. (1978). Toward a minimal model of the world CO_2 system. I. Carbonate-alkalinity version. *Thalass. Jugoslavica* 14, 63 – 98.

MacIsaac, J. J., and Dugdale, R. C. (1972). Interactions of light and inorganic nitrogen in controlling nitrogen uptake in the sea. *Deep Sea Res. Oceanogr. Abstr.* 19, 209 – 232. doi:10.1016/0011-7471(72)90032-0.

Mackey, M., Mackey, D., Higgins, H., and Wright, S. (1996). CHEMTAX – a program for estimating class abundances from chemical markers: application to HPLC measurements of phytoplankton. *Mar. Ecol. Prog. Ser.* 144, 265 – 283. doi:10.3354/meps144265.

Mahadevan, A., D'Asaro, E., Lee, C., and Perry, M. J. (2012). Eddy-driven stratification initiates North Atlantic spring phytoplankton blooms. *Science* 337, 54 – 58. doi:10.1126/science.1218740.

Malkin, S. Y., Rao, A. M. F., Seitaj, D., Vasquez-Cardenas, D., Zetsche, E.-M., Hidalgo-Martinez, S., Boschker, H. T. S., and Meysman, F. J. R. (2014). Natural occurrence of microbial sulphur oxidation by long-range electron transport in the seafloor. *ISME J.* 8, 1843 – 54. doi:10.1038/ismej.2014.41.

Marra, J. (2002). Approaches to the measurement of plankton production, in *Phytoplankton Productivity: Carbon Assimilation in Marine and Freshwater Ecosystems*, eds. P. J. le B. Williams, D. N. Thomas, and C. S. Reynolds (Oxford: Blackwell Science Ltd), 78 – 108. doi:10.1002/9780470995204.ch4.

Marra, J., and Barber, R. T. (2004). Phytoplankton and heterotrophic respiration in the surface layer of the ocean. *Geophys. Res. Lett.* 31, L09314. doi:10.1029/2004GL019664.

McGinnis, D. F., Schmidt, M., DelSontro, T., Themann, S., Rovelli, L., Reitz, A., and Linke, P. (2011). Discovery of a natural CO_2 seep in the German North Sea: implications for shallow dissolved gas and seep detection. *J. Geophys. Res.* 116, C03013. doi:10.1029/2010JC006557.

McLeod, E., Chmura, G. L., Bouillon, S., Salm, R., Björk, M., Duarte, C. M., Lovelock, C. E., Schlesinger, W. H., and Silliman, B. R. (2011). A blueprint for blue carbon: toward an improved understanding of the role of vegetated coastal habitats in sequestering CO_2. *Front. Ecol. Environ.* 9, 552 – 560. doi:10.1890/110004.

Van den Meersche, K., Middelburg, J. J., Soetaert, K., van Rijswijk, P., Boschker, H. T. S., and Heip, C. H. R. (2004). Carbon-nitrogen coupling and algal-bacterial interactions during an experimental bloom: modeling a ^{13}C tracer experiment. *Limnol. Oceanogr.* 49, 862 – 878. doi:10.4319/lo.2004.49.3.0862.

Van den Meersche, K., Soetaert, K., and Middelburg, J. J. (2008). A Bayesian Compositional Estimator for microbial taxonomy based on biomarkers. *Limnol. Oceanogr. Methods* 6, 190 – 199. doi:10.4319/lom.2008.6.190.

Mehrbach, C., Culberson, C. H., Hawley, J. E., and Pytkowicz, R. M. (1973). Measurement of the apparent dissociation constants of carbonic acid in seawater at atmospheric pressure. *Limnol. Oceanogr.* 18, 897 – 907. doi:10.4319/lo.1973.18.6.0897.

Meijers, E., and Groot, S. (2007). Deltamodel – hulpmiddel ter ondersteuning van het beheer en beleid van de zuidwestelijke Delta. Delft, Netherlands.

Meinshausen, M., Smith, S. J., Calvin, K., Daniel, J. S., Kainuma, M. L. T., Lamarque, J.-F., Matsumoto, K., Montzka, S. A., Raper, S. C. B., Riahi, K., et al. (2011). The RCP greenhouse gas concentrations and their extensions from 1765 to 2300. *Clim. Change* 109, 213 – 241. doi:10.1007/s10584-011-0156-z.

Melzner, F., Thomsen, J., Koeve, W., Oschlies, A., Gutowska, M. a., Bange, H. W., Hansen, H. P., and Körtzinger, A. (2013). Future ocean acidification will be amplified by hypoxia in coastal habitats. *Mar. Biol.* 160, 1875 – 1888. doi:10.1007/s00227-012-1954-1.

Mémery, L., Lévy, M., Vérant, S., and Merlivat, L. (2002). The relevant time scales in estimating the air – sea CO_2 exchange in a mid-latitude region. *Deep Sea Res. Part II Top. Stud. Oceanogr.* 49, 2067 – 2092. doi:10.1016/S0967-0645(02)00028-0.

Menden-Deuer, S., and Lessard, E. J. (2000). Carbon to volume relationships for dinoflagellates, diatoms, and other protist plankton. *Limnol. Oceanogr.* 45, 569 – 579. doi:10.4319/lo.2000.45.3.0569.

Middelburg, J. J., Barranguet, C., Boschker, H. T. S., Herman, P. M. J., Moens, T., and Heip, C. H. R. (2000). The fate of intertidal microphytobenthos carbon: an in situ ^{13}C-labeling study. *Limnol. Oceanogr.* 45, 1224 – 1234. doi:10.4319/lo.2000.45.6.1224.

Middelburg, J. J., and Herman, P. M. J. (2007). Organic matter processing in tidal estuaries. *Mar. Chem.* 106, 127 – 147. doi:10.1016/j.marchem.2006.02.007.

Middelburg, J. J., and Levin, L. A. (2009). Coastal hypoxia and sediment biogeochemistry. *Biogeosciences* 6, 1273 – 1293. doi:10.5194/bg-6-1273-2009.

Middelburg, J. J., and Nieuwenhuize, J. (2000). Nitrogen uptake by heterotrophic bacteria and phytoplankton in the nitrate-rich Thames estuary. *Mar. Ecol. Prog. Ser.* 203, 13 – 21. doi:10.3354/meps203013.

Middelburg, J. J., and Soetaert, K. (2004). The role of sediments in shelf ecosystem dynamics, in *The Global Coastal Ocean: Multiscale Interdisciplinary Processes (The Sea Vol. 13)*, eds. A. R. Robinson and K. H. Brink (Cambridge, MA: Harvard University Press), 353 – 373.

Midorikawa, T., Inoue, H. Y., Ishii, M., Sasano, D., Kosugi, N., Hashida, G., Nakaoka, S., and Suzuki, T. (2012). Decreasing pH trend estimated from 35-year time series of carbonate parameters in the Pacific sector of the Southern Ocean in summer. *Deep Sea Res. Part I Oceanogr. Res. Pap.* 61, 131 – 139. doi:10.1016/j.dsr.2011.12.003.

Midorikawa, T., Ishii, M., Saito, S., and Sasano, D. (2010). Decreasing pH trend estimated from 25 – yr time series of carbonate parameters in the western North Pacific. *Tellus B* 62, 649 – 659. doi:10.1111/j.1600-0889.2010.00474.x.

Milanković, M. (1941). Kanon der Erdbestrahlung und seine Anwendung auf das Eiszeitenproblem. *Poseńa Izd. Srp. Akad. Nauk.* 132, 1 – 633.

Monteith, D. T., Stoddard, J. L., Evans, C. D., de Wit, H. A., Forsius, M., Høgåsen, T., Wilander, A., Skjelkvåle, B. L., Jeffries, D. S., Vuorenmaa, J., et al. (2007). Dissolved organic carbon trends resulting from changes in atmospheric deposition chemistry. *Nature* 450, 537 – 540. doi:10.1038/nature06316.

Morel, F. M. M., and Hering, J. G. (1993). *Principles and Applications of Aquatic Chemistry*. New York, NY: Wiley-Interscience.

Morris, A. W., and Riley, J. P. (1966). The bromide/chlorinity and sulphate/chlorinity ratio in sea water. *Deep Sea Res. Oceanogr. Abstr.* 13, 699 – 705. doi:10.1016/0011-7471(66)90601-2.

Mucci, A., Starr, M., Gilbert, D., and Sundby, B. (2011). Acidification of Lower St. Lawrence Estuary bottom waters. *Atmosphere-Ocean* 49, 206 – 218. doi:10.1080/07055900.2011.599265.

Muller, F. L. L., and Bleie, B. (2008). Estimating the organic acid contribution to coastal seawater alkalinity by potentiometric titrations in a closed cell. *Anal. Chim. Acta* 619, 183 – 91. doi:10.1016/j.aca.2008.05.018.

Munhoven, G. (2014). Interactive comment on "Improved routines to model the ocean carbonate system: mocsy 1.0" by J. C. Orr and J.-M. Epitalon. *Geosci. Model Dev. Discuss.* 7, C622 – C635.

Nicholson, D., Emerson, S., and Eriksen, C. C. (2008). Net community production in the deep euphotic zone of the subtropical North Pacific gyre from glider surveys. *Limnol. Oceanogr.* 53, 2226 – 2236. doi:10.4319/lo.2008.53.5_part_2.2226.

Nienhuis, P. H. (1978). An ecosystem study in Lake Grevelingen, a former estuary in the SW Netherlands. *Kieler Meeresforschungen. Sonderh.* 4, 247 – 255.

Nienhuis, P. H., and Huis in 't Veld, J. C. (1984). Grevelingen: from an estuary to a saline lake. *Water Sci. Technol.* 16, 27 – 50.

Nilsson, G. E., Dixson, D. L., Domenici, P., McCormick, M. I., Sørensen, C., Watson, S.-A., and Munday, P. L. (2012). Near-future carbon dioxide levels alter fish behaviour by interfering with neurotransmitter function. *Nat. Clim. Chang.* 2, 201 – 204. doi:10.1038/nclimate1352.

Nixon, S. W. (1995). Coastal marine eutrophication: a definition, social causes, and future concerns. *Ophelia* 41, 199 – 219. doi:10.1080/00785236.1995.10422044.

Nolte, A., Troost, T., de Boer, G., Spiteri, C., and van Wesenbeeck, B. (2008). Verkenning oplossingsrichtingen voor een betere waterkwaliteit en ecologische toestand van het Grevelingenmeer. Delft, Netherlands.

Nondal, G., Bellerby, R. G. J., Olsen, A., Johannessen, T., and Olafsson, J. (2009). Optimal evaluation of the surface ocean CO_2 system in the northern North Atlantic using data from voluntary observing ships. *Limnol. Oceanogr. Methods* 7, 109 – 118. doi:10.4319/lom.2009.7.109.

Odum, H. T. (1956). Primary production in flowing waters. *Limnol. Oceanogr.* 1, 102 – 117. doi:10.4319/lo.1956.1.2.0102.

Okin, G. S., Baker, A. R., Tegen, I., Mahowald, N. M., Dentener, F. J., Duce, R. A., Galloway, J. N., Hunter, K., Kanakidou, M., Kubilay, N., et al. (2011). Impacts of atmospheric nutrient deposition on marine productivity: roles of nitrogen, phosphorus, and iron. *Global Biogeochem. Cycles* 25, GB2022. doi:10.1029/2010GB003858.

Okuyama, H., Kogame, K., and Takeda, S. (1993). Phylogenetic significance of the limited distribution of octadecapentaenoic acid in Prymnesiophytes and photosynthetic Dinoflagellates. *Proc. NIPR Symp. Polar Biol.* 6, 21 – 26.

Olafsson, J., Ólafsdóttir, S. R., Benoit-Cattin, A., Danielsen, M., Arnarson, T. S., and Takahashi, T. (2009). Rate of Iceland Sea acidification from time series measurements. *Biogeosciences* 6, 2661 – 2668. doi:10.5194/bg-6-2661-2009.

Olafsson, J., Ólafsdóttir, S. R., Benoit-Cattin, A., and Takahashi, T. (2010). The Irminger Sea and the Iceland Sea time series measurements of sea water carbon and nutrient chemistry 1983 – 2008. *Earth Syst. Sci. Data* 2, 99 – 104. doi:10.5194/essd-2-99-2010.

Oliver, B. G., Thurman, E. M., and Malcolm, R. L. (1983). The contribution of humic substances to the acidity of colored natural waters. *Geochim. Cosmochim. Acta* 47, 2031 – 2035. doi:10.1016/0016-7037(83)90218-1.

Olsen, A., Bellerby, R. G. J., Johannessen, T., Omar, A. M., and Skjelvan, I. (2003). Interannual variability in the wintertime air – sea flux of carbon dioxide in the northern North Atlantic, 1981 – 2001. *Deep Sea Res. Part I Oceanogr. Res. Pap.* 50, 1323 – 1338. doi:10.1016/S0967-0637(03)00144-4.

Omstedt, A., Gustafsson, E., and Wesslander, K. (2009). Modelling the uptake and release of carbon dioxide in the Baltic Sea surface water. *Cont. Shelf Res.* 29, 870 – 885. doi:10.1016/j.csr.2009.01.006.

Orr, J. C., Fabry, V. J., Aumont, O., Bopp, L., Doney, S. C., Feely, R. A., Gnanadesikan, A., Gruber, N., Ishida, A., Joos, F., et al. (2005). Anthropogenic ocean acidification over the twenty-first century and its impact on calcifying organisms. *Nature* 437, 681 – 686. doi:10.1038/nature04095.

Park, P. K. (1969). Oceanic CO_2 system: an evaluation of ten methods of investigation. *Limnol. Oceanogr.* 14, 179 – 186. doi:10.4319/lo.1969.14.2.0179.

Pedersen, S. A., Håkedal, O. J., Salaberria, I., Tagliati, A., Gustavson, L. M., Jenssen, B. M., Olsen, A. J., and Altin, D. (2014). Multigenerational exposure to ocean acidification during food limitation reveals consequences for copepod scope for growth and vital rates. *Environ. Sci. Technol.* 48, 12275 – 12284. doi:10.1021/es501581j.

Peperzak, L., and Poelman, M. (2008). Mass mussel mortality in The Netherlands after a bloom of Phaeocystis globosa (prymnesiophyceae). *J. Sea Res.* 60, 220 – 222. doi:10.1016/j.seares.2008.06.001.

Petit, R. J., Raynaud, D., Basile, I., Chappellaz, J., Ritz, C., Delmotte, M., Legrand, M., Lorius, C., and Pe, L. (1999). Climate and atmospheric history of the past 420,000 years from the Vostok ice core, Antarctica. *Nature* 399, 429 – 436. doi:10.1038/20859.

Philippart, C. J. M., Beukema, J. J., Cadée, G. C., Dekker, R., Goedhart, P. W., van Iperen, J. M., Leopold, M. F., and Herman, P. M. J. (2007). Impacts of nutrient reduction on coastal communities. *Ecosystems* 10, 96 – 119. doi:10.1007/s10021-006-9006-7.

Pierrot, D., Lewis, E., and Wallace, D. W. R. (2006). MS Excel program developed for CO_2 system calculations. Oak Ridge, Tennessee, USA. doi:10.3334/CDIAC/otg.CO2SYS_XLS_CDIAC105a.

Pieters, J. P. F., Bannink, B. A., and Kamer, J. P. G. van de (1985). Een mathematisch model van de chloride- en zuurstofhuishouding van het Grevelingenmeer tijdens de uitwisseling met zeewater. Middelburg, Netherlands.

Pilson, M. E. Q. (2014). Changing pH in the surface ocean. *Oceanography* 27, 120 – 125. doi:10.5670/oceanog.2014.15.

Pinkart, H. C., Ringelberg, D. B., Piceno, Y. M., Macnaughton, S. J., and White, D. C. (2002). "Biochemical approaches to biomass measurements and community structure," in *Manual of Environmental Microbiology*, eds. C. J. Hurst, R. L. Crawford, G. R. Knudsen, M. J. McInerney, and L. D. Stetzenbach (Washington, D. C.: American Society for Microbiology Press), 101 – 113.

Pomeroy, L. R., Sheldon, J. E., and Sheldon Jr, W. M. (1994). Changes in bacterial numbers and leucine assimilation during estimations of microbial respiratory rates in seawater by the precision Winkler method. *Appl. Environ. Microbiol.* 60, 328 – 332.

Provoost, P., van Heuven, S., Soetaert, K., Laane, R. W. P. M., and Middelburg, J. J. (2010). Seasonal and long-term changes in pH in the Dutch coastal zone. *Biogeosciences* 7, 3869 – 3878. doi:10.5194/bg-7-3869-2010.

Quay, P., and Stutsman, J. (2003). Surface layer carbon budget for the subtropical N. Pacific: constraints at station ALOHA. *Deep Sea Res. Part I Oceanogr. Res. Pap.* 50, 1045 – 1061. doi:10.1016/S0967-0637(03)00116-X.

Le Quéré, C., Raupach, M. R., Canadell, J. G., Marland, G., Bopp, L., Ciais, P., Conway, T. J., Doney, S. C., Feely, R. A., Foster, P., et al. (2009). Trends in the sources and sinks of carbon dioxide. *Nat. Geosci.* 2, 831 – 836. doi:10.1038/ngeo689.

R Core Team (2015). R: a language and environment for statistical computing. R Foundation for Statistical Computing, Vienna, Austria. http://www.R-project.org/.

Rabalais, N., Cai, W.-J., Carstensen, J., Conley, D., Fry, B., Hu, X., Quiñones-Rivera, Z., Rosenberg, R., Slomp, C., Turner, E., et al. (2014). Eutrophication-driven deoxygenation in the coastal ocean. *Oceanography* 27, 172 – 183. doi:10.5670/oceanog.2014.21.

Rabalais, N. N., Díaz, R. J., Levin, L. A., Turner, R. E., Gilbert, D., and Zhang, J. (2010). Dynamics and distribution of natural and human-caused hypoxia. *Biogeosciences* 7, 585 – 619. doi:10.5194/bg-7-585-2010.

Redfield, A. C. (1958). The biological control of chemical factors in the environment. *Am. Sci.* 46, 230A, 205 – 221.

Redfield, A. C., Ketchum, B. H., and Richards, F. A. (1963). The influence of organisms on the composition of sea-water, in *The Composition of Seawater. Comparative and Descriptive Oceanography*, ed. M. N. Hill (New York, NY: Interscience Publishers), 26 – 77.

Regaudie-de-Gioux, A., Lasternas, S., Agustí, S., and Duarte, C. M. (2014). Comparing marine primary production estimates through different methods and development of conversion equations. *Front. Mar. Sci.* 1, 19. doi:10.3389/fmars.2014.00019.

Regnier, P., Friedlingstein, P., Ciais, P., Mackenzie, F. T., Gruber, N., Janssens, I. A., Laruelle, G. G., Lauerwald, R., Luyssaert, S., Andersson, A. J., et al. (2013). Anthropogenic perturbation of the carbon fluxes from land to ocean. *Nat. Geosci.* 6, 597 – 607. doi:10.1038/ngeo1830.

Regnier, P., Wollast, R., and Steefel, C. I. (1997). Long-term fluxes of reactive species in macrotidal estuaries: estimates from a fully transient, multicomponent reaction-transport model. *Mar. Chem.* 58, 127 – 145. doi:10.1016/S0304-4203(97)00030-3.

Reum, J. C. P., Alin, S. R., Feely, R. A., Newton, J., Warner, M., and McElhany, P. (2014). Seasonal carbonate chemistry covariation with temperature, oxygen, and salinity in a fjord estuary: implications for the design of ocean acidification experiments. *PLoS One* 9, e89619. doi:10.1371/journal.pone.0089619.

Reuss, N., and Poulsen, L. (2002). Evaluation of fatty acids as biomarkers for a natural plankton community. A field study of a spring bloom and a post-bloom period off West Greenland. *Mar. Biol.* 141, 423 – 434. doi:10.1007/s00227-002-0841-6.

Revelle, R., and Suess, H. E. (1957). Carbon dioxide exchange between atmosphere and ocean and the question of an increase of atmospheric CO_2 during the past decades. *Tellus* 9, 18 – 27. doi:10.1111/j.2153-3490.1957.tb01849.x.

Ridgwell, A., and Zeebe, R. (2005). The role of the global carbonate cycle in the regulation and evolution of the Earth system. *Earth Planet. Sci. Lett.* 234, 299 – 315. doi:10.1016/j.epsl.2005.03.006.

Riebesell, U., Körtzinger, A., and Oschlies, A. (2009). Sensitivities of marine carbon fluxes to ocean change. *Proc. Natl. Acad. Sci. U. S. A.* 106, 20602 – 20609. doi:10.1073/pnas.0813291106.

Riebesell, U., Schulz, K. G., Bellerby, R. G. J., Botros, M., Fritsche, P., Meyerhöfer, M., Neill, C., Nondal, G., Oschlies, A., Wohlers, J., et al. (2007). Enhanced biological carbon consumption in a high CO_2 ocean. *Nature* 450, 545 – 548. doi:10.1038/nature06267.

Riley, G. A. (1939). Plankton studies. II. The western north Atlantic, May-June 1939. *J. Mar. Res.* 2, 145 – 162.

Riley, J. P. (1965). The occurrence of anomalously high fluoride concentrations in the North Atlantic. *Deep Sea Res. Oceanogr. Abstr.* 12, 219 – 220. doi:10.1016/0011-7471(65)90027-6.

Rivaro, P., Messa, R., Massolo, S., and Frache, R. (2010). Distributions of carbonate properties along the water column in the Mediterranean Sea: spatial and temporal variations. *Mar. Chem.* 121, 236 – 245. doi:10.1016/j. marchem.2010.05.003.

Rivkin, R. B., and Legendre, L. (2001). Biogenic carbon cycling in the upper ocean: effects of microbial respiration. *Science* 291, 2398 – 2400. doi:10.1126/science.291.5512.2398.

Roberts, E. C., Legrand, C., Steinke, M., and Wootton, E. C. (2011). Mechanisms underlying chemical interactions between predatory planktonic protists and their prey. *J. Plankton Res.* 33, 833 – 841. doi:10.1093/plankt/fbr005.

Robinson, C., and Williams, P. J. le B. (2005). Respiration and its measurement in surface marine waters, in *Respiration in Aquatic Ecosystems*, eds. P. del Giorgio and P. J. l. B. Williams (Oxford University Press, New York), 147 – 180.

Rodhe, H., Dentener, F., and Schulz, M. (2002). The global distribution of acidifying wet deposition. *Environ. Sci. Technol.* 36, 4382 – 4388. doi:10.1021/es020057g.

Rotty, R. M. (1981). Data for global CO_2 production from fossil fuels and cement, in *SCOPE 16: Carbon Cycle Modelling*, ed. B. Bolin (New York, NY: John Wiley & Sons), 121 – 125.

Roy, S. (1987). High-performance liquid chromatographic analysis of chloropigments. *J. Chromatogr. A* 391, 19 – 34. doi:10.1016/S0021-9673(01)94302-X.

Ruddiman, W. F. (2001). *Earth's climate: past and future*. New York, NY: W.H. Freeman and Company.

Rudels, B., Korhonen, M., Budéus, G., Beszczynska-Möller, A., Schauer, U., Nummelin, A., Quadfasel, D., and Valdimarsson, H. (2012). The East Greenland Current and its impacts on the Nordic Seas: observed trends in the past decade. *ICES J. Mar. Sci.* 69, 841 – 851. doi:10.1093/icesjms/fss079.

Sabine, C. L., Feely, R. A., Gruber, N., Key, R. M., Lee, K., Bullister, J. L., Wanninkhof, R., Wong, C. S., Wallace, D. W. R., Tilbrook, B., et al. (2004). The oceanic sink for anthropogenic CO_2. *Science* 305, 367 – 371. doi:10.1126/science.1097403.

Sakshaug, E., Bricaud, A., Dandonneau, Y., Falkowski, P. G., Kiefer, D. A., Legendre, L., Morel, A., Parslow, J., and Takahashi, M. (1997). Parameters of photosynthesis: definitions, theory and interpretation of results. *J. Plankton Res.* 19, 1637 – 1670. doi:10.1093/plankt/19.11.1637.

Salisbury, J., Green, M., Hunt, C., and Campbell, J. (2008). Coastal acidification by rivers: a threat to shellfish? *Eos, Trans. Am. Geophys. Union* 89, 513. doi:10.1029/2008EO500001.

Santana-Casiano, J. M., González-Dávila, M., Rueda, M.-J., Llinás, O., and González-Dávila, E.-F. (2007). The interannual variability of oceanic CO_2 parameters in the northeast Atlantic subtropical gyre at the ESTOC site. *Global Biogeochem. Cycles* 21, GB1015. doi:10.1029/2006GB002788.

Sarma, V. V. S. S., Abe, O., Hashimoto, S., Hinuma, A., and Saino, T. (2005). Seasonal variations in triple oxygen isotopes and gross oxygen production in the Sagami Bay, central Japan. *Limnol. Oceanogr.* 50, 544 – 552. doi:10.4319/lo.2005.50.2.0544.

Sarmiento, J. L., and Gruber, N. (2006). *Ocean Biogeochemical Dynamics*. Princeton, NJ: Princeton University Press.

Sarmiento, J. L., and Gruber, N. (2002). Sinks for anthropogenic carbon. *Phys. Today* 55, 30 – 36. doi:10.1063/1.1510279.

Sayama, M., Risgaard-Petersen, N., Nielsen, L. P., Fossing, H., and Christensen, P. B. (2005). Impact of bacterial NO_3^- transport on sediment biogeochemistry. *Appl. Environ. Microbiol.* 71, 7575 – 7577. doi:10.1128/AEM.71.11.7575-7577.2005.

Schindler, D. W. (1988). Effects of acid rain on freshwater ecosystems. *Science* 239, 149 – 57. doi:10.1126/science.239.4836.149.

Schneider, A., Wallace, D. W. R., and Körtzinger, A. (2007). Alkalinity of the Mediterranean Sea. *Geophys. Res. Lett.* 34, L15608. doi:10.1029/2006GL028842.

Schulz, K. G., and Riebesell, U. (2013). Diurnal changes in seawater carbonate chemistry speciation at increasing atmospheric carbon dioxide. *Mar. Biol.* 160, 1889 – 1899. doi:10.1007/s00227-012-1965-y.

Seitaj, D., Schauer, R., Sulu-Gambari, F., Malkin, S. Y., Hidalgo Martinez, S., Slomp, C. P., and Meysman, F. J. R. (2015a). Temporal succession of cryptic sulphur cycling in a seasonally hypoxic basin. *In preparation.*

Seitaj, D., Sulu-Gambari, F., Malkin, S. Y., Burdorf, L., Slomp, C. P., and Meysman, F. J. R. (2015b). Sediment mineralization and benthic oxygen dynamics in a seasonally hypoxic basin. *In preparation.*

Shadwick, E. H., Thomas, H., Azetsu-Scott, K., Greenan, B. J. W., Head, E., and Horne, E. (2011). Seasonal variability of dissolved inorganic carbon and surface water pCO_2 in the Scotian Shelf region of the Northwestern Atlantic. *Mar. Chem.* 124, 23 – 37. doi:10.1016/j.marchem.2010.11.004.

Shadwick, E. H., Trull, T. W., Thomas, H., and Gibson, J. A. E. (2013). Vulnerability of polar oceans to anthropogenic acidification: comparison of Arctic and Antarctic seasonal cycles. *Sci. Rep.* 3, 2339. doi:10.1038/srep02339.

Shaw, E. C., McNeil, B. I., Tilbrook, B., Matear, R., and Bates, M. L. (2013). Anthropogenic changes to seawater buffer capacity combined with natural reef metabolism induce extreme future coral reef CO_2 conditions. *Glob. Chang. Biol.* 19, 1632 – 1641. doi:10.1111/gcb.12154.

Shin, K. H., Hama, T., Yoshie, N., Noriki, S., and Tsunogai, S. (2000). Dynamics of fatty acids in newly biosynthesized phytoplankton cells and seston during a spring bloom off the west coast of Hokkaido Island, Japan. *Mar. Chem.* 70, 243 – 256. doi:10.1016/S0304-4203(00)00030-X.

Simpson, H. J., Williams, S. C., Olsen, C. R., and Hammond, D. E. (1977). Nutrient and particulate matter budgets in urban estuaries, in *Estuaries, Geophysics and the Environment*, ed. K. R. Dyer (Washington D.C.: National Academy of Sciences), 94 – 103.

Simpson, J. H. (1981). The shelf-sea fronts: implications of their existence and behaviour. *Philos. Trans. R. Soc. A Math. Phys. Eng. Sci.* 302, 531 – 543. doi:10.1098/rsta.1981.0181.

Skirrow, G. (1975). The dissolved gases – carbon dioxide, in *Chemical Oceanography, Vol. 2*, eds. J. P. Riley and G. Skirrow (London: Academic Press), 1 – 181.

Sluijs, A., Bowen, G. J., Brinkhuis, H., Lourens, L. J., and Thomas, E. (2007). The Palaeocene-Eocene Thermal Maximum super greenhouse: biotic and geochemical signatures, age models and mechanisms of global change, in *Deep-Time Perspectives on Climate Change: Marrying the Signal from Computer Models and Biological Proxies*, eds. M. Williams, A. M. Haywood, F. J. Gregory, and D. N. Schmidt (London: The Geological Society on behalf of The Micropalaeontological Society), 323 – 349.

Van Slyke, D. D. (1922). On the measurement of buffer values and on the relationship of buffer value to the dissociation constant of the buffer and the concentration and reaction of the buffer solution. *J. Biol. Chem.* 52, 525 – 570.

Sobczak, W. V, Cloern, J. E., Jassby, A. D., and Müller-Solger, A. B. (2002). Bioavailability of organic matter in a highly disturbed estuary: the role of detrital and algal resources. *Proc. Natl. Acad. Sci. U. S. A.* 99, 8101 – 8105. doi:10.1073/pnas.122614399.

Soetaert, K., Hofmann, A. F., Middelburg, J. J., Meysman, F. J. R., and Greenwood, J. (2007). The effect of biogeochemical processes on pH. *Mar. Chem.* 105, 30 – 51. doi:10.1016/j.marchem.2006.12.012.

Soetaert, K., Middelburg, J. J., Heip, C., Meire, P., Van Damme, S., and Maris, T. (2006). Long-term change in dissolved inorganic nutrients in the heterotrophic Scheldt estuary (Belgium, The Netherlands). *Limnol. Oceanogr.* 51, 409 – 423. doi:10.4319/lo.2006.51.1_part_2.0409.

Soetaert, K., Petzoldt, T., and Setzer, R. W. (2010). Solving differential equations in R: package deSolve. *J. Stat. Soft.* 33, 1 – 25.

Steemann Nielsen, E. (1952). The use of radio-active carbon (C^{14}) for measuring organic production in the sea. *ICES J. Mar. Sci.* 18, 117 – 140. doi:10.1093/icesjms/18.2.117.

Steinacher, M., Joos, F., Frölicher, T. L., Plattner, G.-K., and Doney, S. C. (2009). Imminent ocean acidification in the Arctic projected with the NCAR global coupled carbon cycle-climate model. *Biogeosciences* 6, 515 – 533. doi:10.5194/bg-6-515-2009.

Strickland, J. D., and Parsons, T. R. (1972). *A Practical Handbook of Seawater Analysis*. 2nd ed. Ottawa: Bulletin 167 of the Fisheries Research Board of Canada.

Stumm, W., and Morgan, J. J. (1996). *Aquatic Chemistry: Chemical Equilibria and Rates in Natural Waters*. 3rd ed. New York, NY: John Wiley & Sons, Inc.

Sullivan, T., Byrne, C., Harman, L., Davenport, J., McAllen, R., and Regan, F. (2014). Determination of spatial and temporal variability of pH and dissolved oxygen concentrations in a seasonally hypoxic semi-enclosed marine basin using continuous monitoring. *Anal. Methods* 6, 5489 – 5497. doi:10.1039/C3AY42162G.

Sunda, W. G., and Cai, W.-J. (2012). Eutrophication induced CO_2-acidification of subsurface coastal waters: interactive effects of temperature, salinity, and atmospheric pCO_2. *Environ. Sci. Technol.* 46, 10651 – 10659. doi:10.1021/es300626f.

Sunda, W. G., and Hardison, D. R. (2010). Evolutionary tradeoffs among nutrient acquisition, cell size, and grazing defense in marine phytoplankton promote ecosystem stability. *Mar. Ecol. Prog. Ser.* 401, 63 – 76. doi:10.3354/meps08390.

Sundquist, E. T., and Plummer, L. N. (1981). Carbon dioxide in the ocean surface layer: some modelling considerations, in *SCOPE 16: Carbon Cycle Modelling*, ed. B. Bolin (New York, NY: John Wiley & Sons), 259 – 269.

Sundquist, E. T., Plummer, L. N., and Wigley, T. M. (1979). Carbon dioxide in the ocean surface: the homogeneous buffer factor. *Science* 204, 1203 – 1205. doi:10.1126/science.204.4398.1203.

Swaney, D. P., Howarth, R. W., and Butler, T. J. (1999). A novel approach for estimating ecosystem production and respiration in estuaries: application to the oligohaline and mesohaline Hudson River. *Limnol. Oceanogr.* 44, 1509 – 1521. doi:10.4319/lo.1999.44.6.1509.

Taguchi, F., and Fujiwara, T. (2010). Carbon dioxide stored and acidified low oxygen bottom waters in coastal seas, Japan. *Estuar. Coast. Shelf Sci.* 86, 429 – 433. doi:10.1016/j.ecss.2009.07.037.

Takahashi, T., Olafsson, J., Broecker, W. S., Goddard, J. G., Chipman, D. W., and White, J. (1985). Seasonal variability of the carbon-nutrient chemistry in the ocean areas west and north of Iceland. *Rit Fiskid.* 9, 20 – 36.

Takahashi, T., Olafsson, J., Goddard, J. G., Chipman, D. W., and Sutherland, S. C. (1993). Seasonal variation of CO_2 and nutrients in the high-latitude surface oceans: a comparative study. *Global Biogeochem. Cycles* 7, 843 – 878. doi:10.1029/93GB02263.

Takahashi, T., Sutherland, S. C., Chipman, D. W., Goddard, J. G., Ho, C., Newberger, T., Sweeney, C., and Munro, D. R. (2014). Climatological distributions of pH, pCO_2, total CO_2, alkalinity, and $CaCO_3$ saturation in the global surface ocean, and temporal changes at selected locations. *Mar. Chem.* 164, 95 – 125. doi:10.1016/j.marchem.2014.06.004.

Takahashi, T., Sutherland, S. C., Sweeney, C., Poisson, A., Metzl, N., Tilbrook, B., Bates, N., Wanninkhof, R., Feely, R. A., Sabine, C., et al. (2002). Global sea – air CO_2 flux based on climatological surface ocean pCO_2, and seasonal biological and temperature effects. *Deep Sea Res. Part II Top. Stud. Oceanogr.* 49, 1601 – 1622. doi:10.1016/S0967-0645(02)00003-6.

Takahashi, T., Sutherland, S. C., Wanninkhof, R., Sweeney, C., Feely, R. A., Chipman, D. W., Hales, B., Friederich, G., Chavez, F., Sabine, C., et al. (2009). Climatological mean and decadal change in surface ocean pCO_2, and net

sea – air CO$_2$ flux over the global oceans. *Deep Sea Res. Part II Top. Stud. Oceanogr.* 56, 554 – 577. doi:10.1016/j. dsr2.2008.12.009.

Tanaka, T., Alliouane, S., Bellerby, R. G. B., Czerny, J., de Kluijver, A., Riebesell, U., Schulz, K. G., Silyakova, A., and Gattuso, J.-P. (2013). Effect of increased pCO$_2$ on the planktonic metabolic balance during a mesocosm experiment in an Arctic fjord. *Biogeosciences* 10, 315 – 325. doi:10.5194/bg-10-315-2013.

Thomas, H., Bozec, Y., Elkalay, K., and de Baar, H. J. W. (2004). Enhanced open ocean storage of CO$_2$ from shelf sea pumping. *Science* 304, 1005 – 1008. doi:10.1126/science.1095491.

Thomas, H., Pempkowiak, J., Wulff, F., and Nagel, K. (2010). Carbon and nutrient budgets of the Baltic Sea, in *Carbon and nutrient fluxes in global continental margins (Global Change – The IGBP Series)*, eds. K.-K. Liu, L. Atkinson, R. Quiñones, and L. Talaue-McManus (Springer Berlin Heidelberg), 334 – 346. doi:10.1007/978-3-540-92735-8_7.

Thomas, H., Prowe, A. E. F., van Heuven, S., Bozec, Y., de Baar, H. J. W., Schiettecatte, L.-S., Suykens, K., Koné, M., Borges, A. V., Lima, I. D., et al. (2007). Rapid decline of the CO$_2$ buffering capacity in the North Sea and implications for the North Atlantic Ocean. *Global Biogeochem. Cycles* 21, GB4001. doi:10.1029/2006GB002825.

Thomas, H., Prowe, A. E. F., Lima, I. D., Doney, S. C., Wanninkhof, R., Greatbatch, R. J., Schuster, U., and Corbière, A. (2008). Changes in the North Atlantic Oscillation influence CO$_2$ uptake in the North Atlantic over the past 2 decades. *Global Biogeochem. Cycles* 22, GB4027. doi:10.1029/2007GB003167.

Thomas, H., Schiettecatte, L., Suykens, K., Koné, Y. J. M., Shadwick, E. H., Prowe, A. E. F., Bozec, Y., de Baar, H. J. W., and Borges, A. V. (2009). Enhanced ocean carbon storage from anaerobic alkalinity generation in coastal sediments. *Biogeosciences* 6, 267 – 274. doi:10.5194/bg-6-267-2009.

Thomsen, J., Gutowska, M. A., Saphörster, J., Heinemann, A., Trübenbach, K., Fietzke, J., Hiebenthal, C., Eisenhauer, A., Körtzinger, A., Wahl, M., et al. (2010). Calcifying invertebrates succeed in a naturally CO$_2$-rich coastal habitat but are threatened by high levels of future acidification. *Biogeosciences* 7, 3879 – 3891. doi:10.5194/bg-7-3879-2010.

Tobias, C. R., Böhlke, J. K., Harvey, J. W., and Busenberg, E. (2009). A simple technique for continuous measurement of time-variable gas transfer in surface waters. *Limnol. Oceanogr. Methods* 7, 185 – 195. doi:10.4319/lom.2009.7.185.

Touratier, F., and Goyet, C. (2009). Decadal evolution of anthropogenic CO$_2$ in the northwestern Mediterranean Sea from the mid-1990s to the mid-2000s. *Deep Sea Res. Part I Oceanogr. Res. Pap.* 56, 1708 – 1716. doi:10.1016/j.dsr.2009.05.015.

Trimborn, S., Brenneis, T., Sweet, E., and Rost, B. (2013). Sensitivity of Antarctic phytoplankton species to ocean acidification: growth, carbon acquisition, and species interaction. *Limnol. Oceanogr.* 58, 997 – 1007. doi:10.4319/lo.2013.58.3.0997.

Tsimplis, M. N., and Josey, S. A. (2001). Forcing of the Mediterranean Sea by atmospheric oscillations over the North Atlantic. *Geophys. Res. Lett.* 28, 803 – 806. doi:10.1029/2000GL012098.

Tsunogai, S., Watanabe, S., and Sato, T. (1999). Is there a "continental shelf pump" for the absorption of atmospheric CO$_2$? *Tellus B* 51, 701 – 712. doi:10.1034/j.1600-0889.1999.t01-2-00010.x.

Tsyro, S., and Berge, E. (1997). The contribution of ship emissions from the North Sea and the north-eastern Atlantic Ocean to acidification in Europe. Oslo, Norway.

Ulfsbo, A., Hulth, S., and Anderson, L. G. (2011). pH and biogeochemical processes in the Gotland Basin of the Baltic Sea. *Mar. Chem.* 127, 20 – 30. doi:10.1016/j.marchem.2011.07.004.

Underwood, G. J. C., and Kromkamp, J. (1999). Primary production by phytoplankton and microphytobenthos in estuaries, in *Estuaries (Advances in Ecological Research Vol. 29)*, eds. D. B. Nedwell and D. G. Raffaelli (London: Academic Press), 93 – 153. doi:10.1016/S0065-2504(08)60192-0.

Uthicke, S., and Fabricius, K. E. (2012). Productivity gains do not compensate for reduced calcification under near-future ocean acidification in the photosynthetic benthic foraminifer species Marginopora vertebralis. *Glob. Chang. Biol.* 18, 2781 – 2791. doi:10.1111/j.1365-2486.2012.02715.x.

Vegter, F., and De Visscher, P. R. M. (1984). Phytoplankton primary production in brackish Lake Grevelingen (SW Netherlands) during 1976 – 1981. *Netherlands J. Sea Res.* 18, 246 – 259. doi:10.1016/0077-7579(84)90004-8.

Verschuur, G. L. (1997). Transparency measurements in Garner Lake, Tennessee: the relationship between Secchi depth and solar altitude and a suggestion for normalization of Secchi depth data. *Lake Reserv. Manag.* 13, 142 – 153. doi:10.1080/07438149709354305.

Veuger, B., Middelburg, J. J., Boschker, H. T. S., Nieuwenhuize, J., van Rijswijk, P., Rochelle-Newall, E. J., and Navarro, N. (2004). Microbial uptake of dissolved organic and inorganic nitrogen in Randers Fjord. *Estuar. Coast. Shelf Sci.* 61, 507 – 515. doi:10.1016/j.ecss.2004.06.014.

Van Vuuren, D. P., Edmonds, J., Kainuma, M., Riahi, K., Thomson, A., Hibbard, K., Hurtt, G. C., Kram, T., Krey, V., Lamarque, J.-F., et al. (2011). The representative concentration pathways: an overview. *Clim. Change* 109, 5 – 31. doi:10.1007/s10584-011-0148-z.

Wallace, R. B., Baumann, H., Grear, J. S., Aller, R. C., and Gobler, C. J. (2014). Coastal ocean acidification: the other eutrophication problem. *Estuar. Coast. Shelf Sci.* 148, 1 – 13. doi:10.1016/j.ecss.2014.05.027.

Waller, K. V., and Makila, P. M. (1981). Chemical reaction invariants and variants and their use in reactor modeling, simulation, and control. *Ind. Eng. Chem. Process Des. Dev.* 20, 1 – 11. doi:10.1021/i200012a001.

Wang, B., Chen, J., Jin, H., Li, H., and Xu, J. (2013). Inorganic carbon parameters responding to summer hypoxia outside the Changjiang Estuary and the related implications. *J. Ocean Univ. China* 12, 568 – 576. doi:10.1007/s11802-013-2239-0.

Wanninkhof, R. (1992). Relationship between wind speed and gas exchange over the ocean. *J. Geophys. Res.* 97, 7373 – 7382. doi:10.1029/92JC00188.

Weger, H. G., Herzig, R., Falkowski, P. G., and Turpin, D. H. (1989). Respiratory losses in the light in a marine diatom: measurements by short-term mass spectrometry. *Limnol. Oceanogr.* 34, 1153 – 1161. doi:10.4319/lo.1989.34.7.1153.

Weiss, R. F. (1974). Carbon dioxide in water and seawater: the solubility of a non-ideal gas. *Mar. Chem.* 2, 203 – 215. doi:10.1016/0304-4203(74)90015-2.

Weiss, R. F. (1981). Determinations of carbon dioxide and methane by dual catalyst flame Ionization chromatography and nitrous oxide by electron capture chromatography. *J. Chromatogr. Sci.* 19, 611 – 616. doi:10.1093/chromsci/19.12.611.

Wetsteyn, L. P. M. J. (2011). Grevelingenmeer: meer kwetsbaar? Lelystad, Netherlands.

Wetsteyn, L. P. M. J., and Kromkamp, J. C. (1994). Turbidity, nutrients and phytoplankton primary production in the Oosterschelde (The Netherlands) before, during and after a large-scale coastal engineering project (1980 – 1990). *Hydrobiologia* 282-283, 61 – 78. doi:10.1007/BF00024622.

Williams, P. J. le B., and Lefevre, D. (1996). Algal ^{14}C and total carbon metabolisms. 1. Models to account for the physiological processes of respiration and recycling. *J. Plankton Res.* 18, 1941 – 1959. doi:10.1093/plankt/18.10.1941.

Williams, P. J. le B., Raine, R. C. T., and Bryan, J. R. (1979). Agreement between the ^{14}C and oxygen methods of measuring phytoplankton production: reassessment of the photosynthetic quotient. *Oceanol. Acta* 2, 411 – 416.

Williams, P. J. le B., and Robertson, J. I. (1989). A serious inhibition problem from a Niskin sampler during plankton productivity studies. *Limnol. Oceanogr.* 34, 1300 – 1305. doi:10.4319/lo.1989.34.7.1300.

Williams, R. G., and Follows, M. J. (2011). *Ocean Dynamics and the Carbon Cycle*. Cambridge: Cambridge University Press.

Williams, R. J. P. (1981). The Bakerian Lecture, 1981: natural selection of the chemical elements. *Proc. R. Soc. B Biol. Sci.* 213, 361 – 397. doi:10.1098/rspb.1981.0071.

Winn, C. D., Mackenzie, F. T., Carrillo, C. J., Sabine, C. L., and Karl, D. M. (1994). Air-sea carbon dioxide exchange in the North Pacific Subtropical Gyre: implications for the global carbon budget. *Global Biogeochem. Cycles* 8, 157 – 163. doi:10.1029/94GB00387.

Wolf-Gladrow, D. A., Zeebe, R. E., Klaas, C., Körtzinger, A., and Dickson, A. G. (2007). Total alkalinity: The explicit conservative expression and its application to biogeochemical processes. *Mar. Chem.* 106, 287 – 300. doi:10.1016/j.marchem.2007.01.006.

Wootton, J. T., and Pfister, C. A. (2012). Carbon system measurements and potential climatic drivers at a site of rapidly declining ocean pH. *PLoS One* 7, e53396. doi:10.1371/journal.pone.0053396.

Wright, S., and Jeffrey, S. (2006). Pigment markers for phytoplankton production, in *The Handbook of Environmental Chemistry: Marine Organic Matter: Biomarkers, Isotopes and DNA*, 71 – 104. doi:10.1007/698_2_003.

Yates, K. K., Dufore, C., Smiley, N., Jackson, C., and Halley, R. B. (2007). Diurnal variation of oxygen and carbonate system parameters in Tampa Bay and Florida Bay. *Mar. Chem.* 104, 110 – 124. doi:10.1016/j.marchem.2006.12.008.

Yi, C., Gong, P., Xu, M., and Qi, Y. (2001). The effects of buffer and temperature feedback on the oceanic uptake of CO_2. *Geophys. Res. Lett.* 28, 751 – 754. doi:10.1029/2000GL011569.

Yool, A., Martin, A. P., Fernández, C., and Clark, D. R. (2007). The significance of nitrification for oceanic new production. *Nature* 447, 999 – 1002. doi:10.1038/nature05885.

Yvon-Durocher, G., Caffrey, J. M., Cescatti, A., Dossena, M., del Giorgio, P., Gasol, J. M., Montoya, J. M., Pumpanen, J., Staehr, P. A., Trimmer, M., et al. (2012). Reconciling the temperature dependence of respiration across timescales and ecosystem types. *Nature* 487, 472 – 476. doi:10.1038/nature11205.

Zeebe, R. E., and Wolf-Gladrow, D. A. (2001). *CO_2 in seawater: equilibrium, kinetics, isotopes*. Amsterdam: Elsevier Ltd. doi:10.1016/S0422-9894(01)80002-7.

Zhai, W., Dai, M., Cai, W.-J., Wang, Y., and Hong, H. (2005). The partial pressure of carbon dioxide and air – sea fluxes in the northern South China Sea in spring, summer and autumn. *Mar. Chem.* 96, 87 – 97. doi:10.1016/j.marchem.2004.12.002.

Zhai, W., Zhao, H., Zheng, N., and Xu, Y. (2012). Coastal acidification in summer bottom oxygen-depleted waters in northwestern-northern Bohai Sea from June to August in 2011. *Chinese Sci. Bull.* 57, 1062 – 1068. doi:10.1007/s11434-011-4949-2.

Zhang, J.-Z. (2000). The use of pH and buffer intensity to quantify the carbon cycle in the ocean. *Mar. Chem.* 70, 121 – 131. doi:10.1016/S0304-4203(00)00024-4.

Zubkov, M. V. (2014). Faster growth of the major prokaryotic versus eukaryotic CO_2 fixers in the oligotrophic ocean. *Nat. Commun.* 5, 3776. doi:10.1038/ncomms4776.

Zweng, M. M., Reagan, J. R., Antonov, J. I., Locarnini, R. A., Mishonov, A. V., Boyer, T. P., Garcia, H. E., Baranova, O. K., Johnson, D. R., Seidov, D., et al. (2013). *World Ocean Atlas 2013, Volume 2: Salinity*. NOAA Atlas NESDIS 74, ed. S. Levitus.

Samenvatting in het Nederlands

Koolstofcyclus in de open oceaan

Het element koolstof is een belangrijke bouwsteen voor organische moleculen en daarom van belang voor het leven op aarde. Koolstof komt ook als gas voor, met name in de vorm van koolstofdioxide (CO_2). Dit gas draagt bij aan de hoeveelheid infrarode straling, en daardoor warmte, die in de atmosfeer wordt opgenomen en wordt daarom een broeikasgas genoemd. Dankzij dit broeikaseffect heeft de aarde een gematigd klimaat en kon er leven op aarde ontstaan. De hoeveelheid CO_2 in de atmosfeer is niet constant en wordt beïnvloed door veranderingen in de koolstofkringloop (Fig. 1.1). Op geologische tijdschaal varieert de hoeveelheid CO_2 door natuurlijke processen, zoals fluctuaties in de hoeveelheid zonnestraling die de aarde bereikt en de mate van chemische verwering. Sinds het begin van de Industriële Revolutie is de hoeveelheid CO_2 in de atmosfeer drastisch toegenomen als gevolg van menselijke activiteit. Het gebruik van fossiele brandstoffen, cementproductie en ontbossing hebben de partiële druk van CO_2 (pCO_2) doen stijgen van 280 ppmv in 1850 tot 400 ppmv in 2015 (Fig. 1.2). In de geologische geschiedenis zijn toenames in pCO_2 meerdere malen opgetreden, echter niet in een vergelijkbaar tempo als de huidige toename. De effecten van de verhoogde atmosferische pCO_2 op het klimaat zijn onmiskenbaar. Door het versterken van het broeikaseffect wordt het warmer, waardoor ijskappen smelten en de zeespiegel stijgt.

Een deel van de antropogene CO_2 wordt opgenomen in de oceanen, omdat er een evenwicht bestaat tussen de pCO_2 in de atmosfeer en in het oppervlaktewater van oceanen. Eenmaal in het water maakt de CO_2 onderdeel uit van het carbonaatsysteem. In combinatie met water vormt de opgeloste CO_2 het zwakke zuur diwaterstofcarbonaat, dat een proton (H^+) kan afgeven om het bicarbonaat-ion (HCO_3^-) te vormen. Bicarbonaat is zelf ook een zwak zuur, dat kan ioniseren en daarbij H^+ en het carbonaat-ion (CO_3^{2-}) vormt. De drie soorten CO_2, HCO_3^- en CO_3^{2-} vormen samen het totaal opgelost anorganisch koolstof (DIC). In welke verhouding de drie soorten anorganisch koolstof voorkomen, hangt samen met de zuurgraad van het water (Fig. 1.3). De zuurgraad wordt meestal uitgedrukt als pH, de negatieve logaritme van de H^+-concentratie, waarbij een waarde lager dan 7 een zuur milieu aanduidt, terwijl een water met een pH hoger dan 7 basisch wordt genoemd. De zuurgraad wordt mede beïnvloed door de temperatuur en het zoutgehalte van het water. Om berekeningen te kunnen doen aan het carbonaatsysteem wordt daarom meestal naast DIC nog een andere grootheid gemeten of gemodelleerd wiens waarde onafhankelijk is van temperatuur of zoutgehalte. Deze grootheid is de totale alkaliteit (TA) en is gedefinieerd als het verschil tussen de concentraties van basen en zuren ten opzichte van een bepaald referentieniveau. Naast het carbonaatsysteem zijn er ook andere zuur-basesystemen in het oceaanwater die bijdragen aan de TA. Voor correcte berekeningen aan het carbonaatsysteem is het dus van belang om ook de totale concentraties van die zuren en basen te weten.

Momenteel nemen de oceanen 1,4 tot 2,2 10^{15} g C per jaar op in de vorm van CO_2, deels van antropogene afkomst. Als gevolg hiervan vinden veranderingen in de chemie van de oceanen plaats: de concentraties van CO_2, DIC en HCO_3^- nemen toe, terwijl de CO_3^{2-}-concentratie en de pH dalen (Fig. 1.4). Deze chemische veranderingen worden gezamenlijk oceaanverzuring genoemd en zijn het onderwerp van dit proefschrift. Een belangrijke consequentie van oceaanverzuring is de verminderde stabiliteit van calciumcarbonaat ($CaCO_3$) als gevolg van de verlaagde CO_3^{2-}-concentraties. Het mineraal $CaCO_3$, dat in drie variëteiten voorkomt, is de bouwsteen van vele organismen met kalkskeletjes. Verschillende studies hebben aangetoond dat mosselen, oesters, koralen, maar ook eencellige algen, zoals coccolithoforen en foraminiferen, negatief worden beïnvloed door oceaanverzuring. Het effect van oceaanverzuring op biologische en biogeochemische processen is momenteel onderwerp van vele studies. Zo lijkt een verhoogde CO_2-concentratie algengroei te stimuleren, al geldt dit niet voor alle algen. Ook zorgt een hogere CO_2-concentratie voor een verstoring van neurologische processen bij clownvissen. Voor de meeste processen kunnen echter nog geen eenduidige conclusies worden getrokken.

Kustzeeën

Uit zowel modelberekeningen als metingen blijkt dat in de open oceaan de pH momenteel met 0,0013 tot 0,0020 per jaar daalt. Met de huidige kennis van het carbonaatsysteem kan dus goed voorspeld kan worden hoe oceaanverzuring in de toekomst de chemie van de open oceaan zal beïnvloeden. Voor het verloop van verzuring in kustzeeën geldt dit echter niet. Kustzeeën vormen de dynamische, verbindende schakel tussen land en oceaan en bestaan uit verschillende onderdelen, zoals estuaria, rivieren, door getijden beïnvloede draslanden en het continentaal plat (Fig. 1.5). Elk van deze onderdelen heeft zijn eigen karakteristieken en daarbij behorend koolstofbudget dat wordt beïnvloed door processen als algengroei, afbraak en begraving van organisch materiaal, temperatuur en lateraal transport. Over het geheel genomen nemen kustzeeën meer CO_2 op dan dat ze uitstoten. Circa 50 tot 100 jaar geleden was dit nog andersom, wat aangeeft dat menselijke activiteit ook het koolstofbudget in deze verbindende schakel verandert.

Doordat kustzeeën zo dynamisch zijn en door veel verschillende processen worden beïnvloed, varieert hun pH sterk op verschillende tijdschalen: gedurende de dag, met de seizoenen en tussen verschillende jaren. Een ander gevolg van deze dynamiek is dat veranderingen in de koolstofkringloop in kustzeeën worden veroorzaakt door meer processen dan alleen de verhoogde atmosferische CO_2-concentratie. Mogelijke oorzaken verschillen per regio en per onderdeel, maar vaak genoemd worden een verhoogde aanvoer van zuur rivierwater, opwelling van CO_2-rijk zeebodemwater, een grotere toevoer van opgelost organisch koolstof, de depositie van atmosferische stikstof en zwavel, en eutrofiëring. Dit laatste proces is de toename van de hoeveelheid organisch materiaal in een ecosysteem, veroorzaakt door de verhoogde toevoer van nutriënten, wat algengroei stimuleert. De concentraties van de nutriënten stikstof en/of fosfor, die net als koolstof essentiële onderdelen van organische moleculen zijn, zijn namelijk meestal de limiterende factoren voor algengroei. In kustzeeën vindt 14 tot 30% van de totale mariene algengroei plaats, terwijl hun oppervlakte slechts 7% van het totaal beslaat. Dit geeft aan dat algengroei een zeer belangrijk proces

is in de koolstofkringloop in kustzeeën. Zowel algengroei als de afbraak van organisch materiaal vormen een link tussen de kringlopen van koolstof en zuurstof (O_2). Tijdens algengroei wordt CO_2 opgenomen en O_2 geproduceerd, terwijl het omgekeerde geldt voor de afbraak van organisch materiaal onder zuurstofrijke omstandigheden. Als gevolg hiervan variëren de concentraties van O_2 en de parameters van het carbonaatsysteem gelijktijdig op verschillende tijdschalen.

Wanneer de productie en afbraak van organisch materiaal in een systeem niet in evenwicht zijn, kan dit leiden tot een verandering van de pH die een orde van grootte hoger is dan de daling van de pH veroorzaakt door de toename in atmosferische CO_2 Daarnaast zijn in veel systemen de productie en afbraak van organisch materiaal van elkaar gescheiden, zowel in de tijd en qua locatie. Algengroei vindt namelijk plaats in het oppervlaktewater, waar licht doordringt. Het gevormde organisch materiaal zinkt in de waterkolom en wordt na enige tijd op diepte afgebroken. In slecht gemengde kustzeeën, waar het bodemwater niet in contact komt met het oppervlaktewater, kan dit leiden tot een sterke daling van de pH in combinatie met het ontstaan van zuurstofarme of zelfs zuurstofloze condities. Zuurstofgebrek en verzuring versterken elkaar en worden nog verder geïntensiveerd door de stijgende temperatuur van de oceanen. Deze drie processen zijn de belangrijkste uitdagingen die kustzeeën en oceanen de komende tientallen jaren zullen moeten overwinnen.

Buffercapaciteit

De versterkte verzuring als gevolg van zuurstofgebrek wordt toegeschreven aan een vermindering van de buffercapaciteit in het bodemwater, een effect dat vooral zichtbaar is in systemen die onderhevig zijn aan een sterke mate van eutrofiëring. De buffercapaciteit is het vermogen van een oplossing om veranderingen in de pH af te zwakken door middel van instantane zuur-basereacties en wordt traditioneel berekend als de inverse helling van een titratiecurve. Er zijn echter meerdere manieren om de bufferintensiteit te beschrijven en in de context van mariene klimaatverandering is de Revelle-factor de meest bekende bufferfactor. Deze factor beschrijft de relatieve verandering in de CO_2-concentratie ten opzichte van het DIC-gehalte. Hoe hoger de waarde van de Revelle-factor, des te moeizamer kan het water de opname van CO_2 bufferen. Er bestaan ook bufferfactoren die de verandering van de pH of de H^+-concentratie als gevolg van een verandering in het DIC-gehalte beschrijven. Deze bufferfactoren hebben echter lang niet altijd betrekking op alle zuur-basesystemen die in het oceaanwater aanwezig zijn en geven daardoor geen compleet beeld van de bufferintensiteit.

Een correcte, complete beschrijving van de buffercapaciteit is van groot belang om zowel de pH-dynamiek op verschillende tijdschalen als de oceaanverzuring te kunnen bestuderen. Dit komt omdat de mate waarin een fysisch of biogeochemisch proces een pH-verandering veroorzaakt sterk afhangt van de mate van buffering. Bij elk proces dat protonen produceert wordt het overgrote deel van deze verzuring direct geneutraliseerd door zuur-basereacties. De buffercapaciteit bepaalt de mate waarin deze neutralisatie plaatsvindt. Om precies te zijn: de netto verandering van de pH als gevolg van een bepaald proces kan worden berekend als de snelheid van dat proces, vermenigvuldigd met de stoichiometrie van de reactie en gedeeld door de buffercapaciteit. Wanneer

meerdere processen tegelijkertijd de pH beïnvloeden, is de totale netto verandering simpelweg de som van de individuele veranderingen. Indien berekeningen aan het carbonaatsysteem worden gedaan met het DIC-gehalte en de TA, zoals meestal het geval is, dan kan alleen de totale netto pH-verandering worden berekend. Om de processen die de seizoensdynamiek van de pH of de verzuring in kustzeeën beïnvloeden, te kunnen identificeren en kwantificeren is echter de hierboven beschreven werkwijze vereist. In deze zogeheten expliciete pH-methode worden berekeningen aan het carbonaatsysteem gedaan met het gehalte DIC en de pH.

Probleemstelling en samenvatting

In dit proefschrift identificeer ik de mechanismen die bepalend zijn voor de dynamiek van pH in mariene systemen. Hierbij focus ik op zowel kustzeeën als de open oceaan en beschrijf ik zowel de seizoensdynamiek als lange-termijnveranderingen in de pH. Om dit doel te bereiken (1) identificeer ik de factoren die de seizoensdynamiek in de pH in een marien bekken met zuurstofarm bodemwater in de zomer bepalen door middel van het opstellen van een protonenbudget; (2) vergelijk ik verschillende meettechnieken om de mate van algengroei te kwantificeren; (3) bediscussieer ik het huidige en toekomstige effect van de atmosferische depositie van stikstof en zwavel op de verzuring in kustzeeën; (4) stel ik generieke definities voor bufferfactoren op die alle zuur-basesystemen aanwezig in kustzeeën kunnen omvatten; (5) pas ik de generieke bufferfactoren op verschillende delen van de open oceaan toe om zo de bepalende factoren van de lokale seizoendynamiek in de pH vast te stellen.

In **hoofdstuk 2** worden de bepalende factoren van de seizoensdynamiek in de pH in een tijdelijk zuurstofarm marien kustbekken geïdentificeerd, met een nadruk op de rol van de buffercapaciteit. Hiertoe zijn in 2012 maandelijks waterkwaliteitsmetingen gedaan in het Grevelingenmeer, gelegen in de delta-regio in het zuidwesten van Nederland. Daarnaast zijn elke maand, of elk seizoen, de snelheden van verschillende biogeochemische processen die de koolstofkringloop beïnvloeden, bepaald. Door de pH expliciet mee te nemen in de berekeningen aan het carbonaatsysteem konden alle metingen gebruikt worden om voor elk seizoen een protonenbudget van het bekken op te stellen, een methode die nauwelijks eerder op gemeten data is toegepast. De resultaten van deze studie tonen duidelijk aan dat, hoewel processen gemiddeld sneller verlopen in de toplaag van het bekken, de schommelingen in de pH door het jaar heen op diepte groter zijn. Dit komt door de substantieel lagere buffercapaciteit van het bodemwater in de zomer, wanneer dit water zuurstofarm is. De protonenbudgetten laten zien dat de totale netto pH-verandering ordes van grootte kleiner is dan de bijdragen van de individuele processen. Daarnaast tonen ze aan dat algengroei en afbraak de seizoensdynamiek van pH domineren.

In **hoofdstuk 3** wordt dieper ingegaan op algengroei in het Grevelingenmeer en met name op de rol van soortendiversiteit in algen op metingen van algengroei. Drie verschillende methoden voor het kwantificeren van algengroei zijn naast elkaar toegepast. Bij de eerste methode werd de opname van koolstof door algen in watermonsters gementen. Deze methode is uitgevoerd in een incubator onder een gradiënt van lichtcondities. Beide andere methoden volgden de verandering

in zuurstofconcentratie. De ene methode maakte hiertoe gebruik van geïncubeerde watermonsters, terwijl bij de andere methode iedere 10 minuten de O_2-concentratie direct in de waterkolom werd gemeten. Daarnaast is het actieve deel van de algenpopulatie geïdentificeerd door het meten van de opname van de stabiele koolstofisotoop ^{13}C in specifieke organische moleculen. Deze organische moleculen zijn aanwezig in alle algensoorten en zijn representatief voor levende algen. De exacte samenstelling van deze moleculen, de zogeheten van fosfolipide afgeleide vetzuren (PLFA), verschilt per algensoort en kan daardoor worden gebruikt om soortendiversiteit te bestuderen. Uit alle drie methoden werden vergelijkbare groeisnelheden verkregen, alhoewel het meten van veranderingen in de zuurstofconcentratie in de waterkolom gemiddeld genomen de hoogste snelheden gaf. De verhouding tussen koolstofopname en zuurstofproductie door algen in watermonsters hangt af van hun groeisnelheid, waarbij een snellere groei zorgt voor relatief meer koolstofopname. Metingen aan de verschillende PLFA tonen aan dat de soortendiversiteit duidelijk varieert door het jaar heen. De groeisnelheden verkregen met deze methode tonen hetzelfde seizoens-patroon als bij de andere methoden, maar zijn significant lager. Ondanks de onzekerheden en aannames die inherent zijn aan alle methoden, zijn ze alle geschikt om algengroei in geëutrofieerde kustzeeën te kwantificeren. De onderlinge verschillen tussen de methoden kunnen echter niet worden gekoppeld aan soortendynamiek.

Hoofdstuk 4 focust op de wisselwerking tussen de opname van atmosferische CO_2 en de depositie van stikstof en zwavel in kustzeeën, en met name op de rol van de biogeochemie van de waterkolom hierin. Hiervoor is een simpel biogeochemisch model in combinatie met het expliciet modelleren van de pH gebruikt. Met dit model is aangetoond dat het relatieve belang van beide processen voor verzuring in kustzeeën afhangt van de CO_2-concentratie in de waterkolom ten opzichte van die in de atmosfeer. Wanneer de CO_2-concentratie in de atmosfeer hoger is dan in het oppervlaktewater, bijvoorbeeld boven het continentaal plat waar gedurende het jaar een netto opname van CO_2 door het water optreedt, dan is dit systeem relatief gezien het meest gevoelig voor verzuring door opname van CO_2, maar het minst gevoelig voor extra verzuring als gevolg van de depositie van stikstof en zwavel. Voor een systeem met een hogere CO_2-concentratie dan de atmosfeer geldt juist het omgekeerde. Het biogeochemisch model is ook gebruikt om veranderingen in deze gevoeligheid in de 21^e eeuw als gevolg van een stijging van de CO_2-concentratie in de atmosfeer te bestuderen. De resultaten hiervan laten zien dat kustzeeën gedurende deze periode tot een factor 4 gevoeliger worden voor verzuring als gevolg van stikstof- en zwaveldepositie De daardoor veroorzaakte extra daling in protonconcentratie is echter slechts maximaal 28%.

In **hoofdstuk 5** is een serie algemene bufferfactoren afgeleid die de gevoeligheid van de pH voor een verandering in oceaanchemie beschrijven. Terwijl eerder afgeleide bufferfactoren alleen toepasbaar zijn onder bepaalde omstandigheden, kunnen deze nieuwe factoren net zoveel zuur-basesystemen omvatten als dat voor het systeem noodzakelijk is. Dit betekent dat deze factoren ook kunnen worden gebruikt in watersoorten waar andere zuur-basesystemen dan het carbonaatsysteem eveneens substantieel bijdragen aan de buffercapaciteit, zoals zuurstofloos bodemwater in kustbekkens. In deze watersoorten worden nauwkeurigere waarden berekend met de nieuwe set bufferfactoren. Daarnaast is de nieuwe set factoren in lijn met de Revelle-factor en andere eerder afgeleide bufferfactoren. Waarden van de nieuwe bufferfactoren zijn berekend voor de toplaag

van de oceaan nu en in 2100, daarbij uitgaande van de voorspelde veranderingen in temperatuur en atmosferische CO_2-concentratie. Deze berekeningen tonen aan dat voor de meeste zuur-baseparameters een verandering in hun concentraties aan het einde van de 21^e eeuw tot een grotere verandering in de pH zal leiden dan nu het geval is. Deze grotere gevoeligheid is het gevolg van de verhoogde atmosferische CO_2-concentratie en wordt enigszins afgezwakt door de opwarming van de aarde. Daarnaast wordt globaal gezien de pH van de toplaag in 2100 minder gevoelig voor veranderingen in de temperatuur.

In **hoofdstuk 6** zijn de nieuwe bufferfactoren verder getest door ze toe te passen op enkele lange-termijndatasets, die metingen van elk seizoen beschikbaar hebben en verschillende fysische en biogeochemische milieus representeren. Indien noodzakelijk werd eerst een lange-termijntrend van de data geëlimineerd, alvorens alle data gecombineerd werden in een modeljaar. Vervolgens werd het verloop in deze data over het jaar heen beschreven met een harmonische functie met verschillende periodiciteiten. Door ten slotte alle parameters volgens deze functie over het jaar te laten variëren, kon de pH worden berekend en vergeleken met de gemeten pH. Wanneer de seizoensdynamiek in temperatuur, zoutgehalte, TA en de totale concentraties van de zuur-basesystemen bekend is, kan op deze manier voor elk van de drie datasets die in dit hoofdstuk zijn gebruikt, de pH goed worden voorspeld. De factoren die bepalend zijn voor het grootste deel van de pH-fluctuaties verschillen echter per locatie. In de Middellandse Zee zijn veranderingen in het DIC-gehalte verantwoordelijk voor de sterkste pH-variabiliteit in de winter en het voorjaar, terwijl temperatuursveranderingen het belangrijkst zijn voor fluctuaties in de pH in de rest van het jaar. In de IJslandse Zee is de seizoensdynamiek in het gehalte DIC in het algemeen de belangrijkste factor die veranderingen in de pH bepaalt, hoewel de temperatuur in het begin van de zomer de dominante factor is en veranderingen in de TA in het begin van de winter de grootste verandering in de pH veroorzaken. De seizoensdynamiek in de pH op een locatie in de subtropische Stille Oceaan dichtbij Hawaï wordt daarentegen vrijwel geheel veroorzaakt door temperatuursschommelingen. Deze studie benadrukt de potentie van de nieuwe set bufferfactoren om verschillende buffermechanismen die gelijktijdig actief zijn te kunnen kwantificeren en toont aan dat deze factoren gebruikt kunnen worden om verder inzicht in de dynamiek van de pH nu en in de toekomst te verkrijgen.

Dit proefschrift toont aan dat buffermechanismen een cruciale rol spelen bij de invloed van biogeochemische of fysische processen op de pH in mariene systemen. Het feit dat in elk marien systeem verschillende processen gelijktijdig de pH beïnvloeden, brengt een zekere complexiteit met zich mee. Dit vraagt erom dat zowel de totale zuur-basebuffercapaciteit als de verschillende bufferfactoren die de gevoeligheid van de pH voor een verandering in de chemische of fysische parameters van de waterkolom beschrijven, accuraat worden gekwantificeerd. In de loop van de 21^e eeuw zullen de oceanen en kustzeeën te maken krijgen met drie elkaar versterkende problemen: verzuring, zuurstoftekort en opwarming. Dit zal ertoe leiden dat de totale zuur-basebuffercapaciteit van het water daalt en als gevolg hiervan zal de gevoeligheid van de pH voor de meeste fysische en chemische veranderingen in de waterkolom toenemen. Daardoor zal de pH op elke tijdschaal een sterkere variatie vertonen.

Streszczenie w języku polskim

Niniejsza praca ma na celu określenie mechanizmów zmian pH w wodach morskich. Praca dotyczy tak sezonowych jak i długoterminowych zmian pH w wodach przybrzeżnych oraz w otwartym oceanie. Aby ten cel osiągnąć; (1) określono czynniki, które sezonowe zmiany pH w nieckach morskich z warstwą wodną ubogą w tlen określają w lecie, poprzez opracowanie bilansu protonowego; (2) porównano różne techniki pomiarowe aby oszacować ilościowy rozwój alg; (3) omówienie obecnego i przyszłego znaczenia opadania z atmosfery siarki i azotu na zakwaszenie wód przybrzeżnych; (4) określenie ważnych ogólnych czynników buforujących, odnośnych do wszystkich systemów wodnych; (5) zastosowanie tych ogólnych czynników buforowych dla różnych części otwartego oceanu, aby ustalić miejscowe przyczyny sezonowych zmian pH.

Celem **Rozdziału 2** jest określenie czynników zmienności sezonowej pH w nieckach przybrzeżnych z wodą przejściowo niedotlenioną z naciskiem na rolę pojemności buforowej. Aby osiągnąć ten cel, w 2012 r. miesięcznie badano jakościowo wodę w jeziorze Grevelingen (Grevelingenmeer), leżącym w południowo-zachodniej delcie Holandii. Oprócz tego co miesiąc i co sezon badano szybkości różnorodnych procesów biogeochemicznych wpływających na cykl obiegu węgla (C). Przy obliczaniu tych szybkości uwzględniano pH, co pozwoliło ustalić dla każdego sezonu bilans protonowy w nieckach. Ten sposób był przedtem prawie nie stosowane. Wyniki wyraźnie wskazują że o ile szybkości procesów średnio wyższe są w wodach powierzchniowych niecek, wychylenia zmian pH w ciągu roku jest większe w głębszych warstwach wód niecek. Wynika to z niższej pojemności buforowej wody w głębszych warstwach w lecie, gdy ta woda jest uboższa w tlen. Bilans protonowy pokazuje, że ogólna zmiana pH jest o wiele mniejsza niż by to wynikało z wkładu sumy poszczególnych procesów. Ponad to bilans protonowy pokazuje że wzrost alg i ich rozkład wpływa na sezonową wartość pH.

W **Rozdziale 3** badano szczegółowo rozwój alg w jeziorze Grevelingen (Grevelingenmeer) z uwzględnieniem różnorodności gatunkowej. Stosowano jednocześnie trzy różne metody pomiaru ilościowego rozwoju alg. W metodzie pierwszej mierzono asymilację węgla (C) przez algi w próbach wodnych inkubowanych ze zmiennym oświetleniem. Dwie inne metody śledziły zmiany w ilości tlenu : jedna używała do pomiarów próbki inkubowane, druga polegała na pomiarze ilości tlenu co 10 minut w kolumnie wodnej. Oprócz tego zidentyfikowano aktywną część fitoplanktonu przez wprowadzenie stabilnego izotopu ^{13}C do organicznych cząsteczek występujących we wszystkich żywych organizmach. Skład tych cząsteczek określany jako kwasy tłuszczowe pochodzi od fosfolipidów (PLFA) i jest charakterystyczny dla każdej grupy fitoplanktonu. Dlatego sposób ten można wykorzystać do badania różnorodności gatunkowej. Te trzy metody pomiarowe dają podobne wyniki ilościowego rozwoju alg, choć metoda pomiarowa tlenu w kolumnie daje wyniki wyższe. Związek między asymilacją węgla a produkcją tlenu zależy od skali produkcji pierwotnej w próbkach inkubowanych. Pomiary PLFA wskazują wyraźnie zmiany w różnorodności gatunkowej fitoplanktonu w ciągu roku i dają ten sam wzorzec, jak i inne metody. Różnice w metodach pomiarowych wskazują ze nie można ich powiązać z rozwojem gatunkowym fitoplanktonu. Mimo

niepewności związanych z każdą metodą te techniki pomiarowe nadają się do określenia produkcji pierwotnej w eutroficznych wodach przybrzeżnych.

Rozdział 4 skupia się na wzajemnym wpływie między poborem z atmosfery dwutlenku węgla (CO_2) i opadaniu siarki i azotu na wody przybrzeżne a przy tym roli biogeochemii w kolumnie wodnej. Do tego celu użyto prostego wzorca biogeochemicznego w kombinacji z modelem przewidywanego pH. W wyniku tego wykazano, że wzajemne znaczenie obu procesów na zakwaszenie wód przybrzeżnych zależy od stężenia CO_2 w kolumnie wodnej w odniesieniu do stężenia CO_2 w atmosferze. Gdy zawartość CO_2 w atmosferze jest wyższa niż w wodach powierzchniowych (np. w szelfie kontynentalnym, gdzie w ciągu roku CO_2 jest absorbowane przez wodę, wtedy ten obszar jest najbardziej wrażliwy na zakwaszenie przez absorpcję CO_2, ale najmniej wrażliwy na dodatkowe zakwaszenie w wyniku opadu siarki i azotu). Dla obszarów z wyższą zawartością CO_2 w wodzie niż w atmosferze – jest odwrotnie. Biogeochemiczny wzorzec jest też używany do badania przewidywanych zmian w 21 wieku w wyniku wzrostu stężenia CO_2 w atmosferze. Wyniki pokazują, że wody przybrzeżne w tym czasie będą czterokrotnie bardziej wrażliwe na zakwaszenie w wyniku opadania siarki i azotu. Wywołane przez to zmniejszenie koncentracji protonowej jest maksymalnie tylko 28% niższe.

Rozdział 5 przedstawia zestaw ogólnych czynników buforowych, które opisują wrażliwość pH na zmiany chemii oceanów. O ile wnioski z wcześniejszych prac na ten temat można stosować tylko w określonych warunkach, ten nowy zestaw można używać bez ograniczeń do wszystkich systemów kwasowo-zasadowych. To sprawia że nadają się one do stosowania w układach wodnych, gdzie systemy kwasowo-zasadowe inne niż system węglanu, znacząco przyczyniają się do kwasowo-zasadowej pojemności buforowej, jak w wodzie dennej ubogiej w tlen w nieckach przybrzeżnych. Nowy zestaw czynników buforowych jest w pełni zgodny ze współczynnikiem Revelle i innymi wcześniejszymi wnioskami o czynnikach buforowych. Nowe wartości czynników buforowych są obliczone dla wód powierzchniowych oceanu teraz i w roku 2100 przy uwzględnieniu zmiany w emisji CO_2 i temperatury. Te obliczenia pokazują że zmiana większości parametrów kwasowo-zasadowych będzie prowadzić do znacznego zwiększenia pH do końca 21 wieku. Ta zwiększona wrażliwość jest wynikiem podwyższonej koncentracji CO_2 w atmosferze i będzie nieznacznie zmniejszona przez ocieplenie Ziemi. Ponadto, w 2100 roku ogólne pH oceanów będzie mniej wrażliwe na zmiany temperatury.

Aby dodatkowo sprawdzić nowy zestaw czynników buforowych, w **Rozdziale 6** zostały one zastosowane przy kilku dostępnych danych z długoterminowych pomiarów z wszystkich sezonów obejmujące różne fizyczne i biogeochemiczne środowiska. Wszystkie dane zostały zgromadzone razem i kierunek zmian modelowego roku jest opisany harmoniczną funkcją. Gdy wszystkie parametry tej funkcji zmieniają się w ciągu roku, można wyliczyć pH i porównać go z pH pomiarów. Gdy znane są sezonowe zmiany: temperatury, zasolenia, całkowitej alkaliczności (TA) i całkowitego stężenia kwasowo-zasadowego systemu, można dla każdego z trzech zestawów czynników buforowych przewidzieć pH. Czynniki, które w większości wpływają na zmienność pH związane są z miejscem. W Morzu Śródziemnym zmiany w ilości rozpuszczonego węgla nieorganicznego (DIC) są w większości odpowiedzialne za zmienność pH zimą i wiosną, natomiast

zmienność temperatury wpływa dominująco na pH w pozostałej części roku. W Morzu Islandzkim sezonowa zmiana DIC jest ogólnie najważniejszym czynnikiem wpływającym na zmiany pH w ciągu roku, choć zmiany temperatury w początku lata znacząco wpływają na pH, a zmiany TA najbardziej zmieniają pH w zimie. Sezonowa zmiana pH w subtropikalnym Oceanie Spokojnym koło Hawajów jest prawie całkowicie spowodowana przez zmiany temperatury. Niniejsza praca podkreśla i pokazuje możliwości powiązania nowego zestawu czynników buforowych z różnymi mechanizmami buforowymi przebiegającymi równocześnie w wodach morskich, i daje możliwość wglądu na ilościowe zmiany wartości pH obecnie i w przyszłości.

Ta praca promocyjna ukazuje kluczową rolę mechanizmów buforowych przy biogeochemicznych i fizycznych procesach na wpływ pH wód morskich. Fakt, że w każdej morskiej wodzie równolegle przebiegające procesy wpływają na pH, ukazuje złożoność tematu. To prosie się aż, o właściwe, dokładne ilościowe ujęcie całkowitej pojemności kwasowo-zasadowej buforowania i pokrewne inne czynniki buforowe, które opisują zmiany czułości pH w wyniku zmian chemicznych i fizycznych parametrów w kolumnie wodnej. W ciągu 21 wieku oceany i wody przybrzeżne będą miały do czynienia z trzema problemami nawzajem się wzmacniającymi: zakwaszenie, niedobór tlenu i ocieplenie. Będzie to prowadzić do obniżenia łącznej kwasowo-zasadowej zdolności buforowania. W rezultacie, czułość pH na zmiany w procesach fizyczno-chemicznych w kolumnie wodnej zwiększy się, przez co amplituda zmienności pH w skali czasowej rozszerzy się.

Acknowledgements

Het dankwoord: voor de meeste mensen het eerste dat ze van een proefschrift lezen, en voor mij vrijwel het laatste deel dat ik schrijf. Dat dit het meest gelezen deel van een proefschrift is, vind ik ook wel terecht. De bijdragen van de hieronder genoemde mensen zijn voor mij namelijk zo belangrijk geweest dat ze deze aandacht simpelweg verdienen.

Allereerst wil ik graag mijn begeleiders Jack Middelburg en Caroline Slomp bedanken voor het vertrouwen dat ik van ze heb mogen ontvangen. Jullie hebben me beide een grote mate van zelfstandigheid gegund, waardoor ik de focus van mijn onderwerp iets kon verleggen en elementen aan mijn proefschrift kon toevoegen die bij mijn interesses en capaciteiten passen. Door iemand met een modelleerachtergrond op een project met veel veldwerk aan te nemen, was dit misschien ook wel onvermijdelijk. Jack, dank je wel voor je vertrouwen, de vrijheid die je me gaf om mijn eigen weg te kiezen en je altijd aanwezige optimisme. Nadat ik jou gesproken had, soms op afspraak maar meestal als ik gewoon je kantoor binnenliep, zagen mijn resultaten er altijd een stukje beter uit. Caroline, bedankt dat je me gewezen hebt op deze positie en voor het betrekken van mijn werk bij het Grevelingenproject, waardoor ik meer inhoudelijk kon samenwerken met de andere mensen in je groep. Ik ben blij dat ik deel uit kan blijven maken van de hechte, ambitieuze en nog altijd groeiende groep mensen die je de afgelopen jaren om je heen hebt verzameld.

De theorie waar mijn proefschrift grotendeels op voortbouwt is in eerder werk op het NIOZ in Yerseke in detail uitgewerkt in het proefschrift van Andreas Hofmann. Andreas, dank je wel voor dit geweldige werk en het prettige contact dat we daarover hebben gehad. In het bijzonder wil ik ook Filip Meysman bedanken, die mij altijd verwelkomde op het NIOZ en nauw betrokken was bij mijn project. Filip, dank je wel voor alle discussies en input die je hebt gegeven, zowel op de hoofdstukken over het Grevelingenproject als de meer theoretische kanten van mijn proefschrift, waardoor ik altijd weer nieuwe ideeën kreeg. Also a special thanks to Helmuth Thomas, who was always available for questions and promoted new and existing collaborations in the North Sea Acidification project. I thank Alberto Borges for his input to Chapter 2, and Keith Hunter and Peter Liss for their enthusiasm to collaborate with me on Chapter 4 of this thesis. Jean-Pierre Gattuso, Karline Soetaert, Wei-Jun Cai, Gert de Lange and Ulf Riebesell: thank you for agreeing to be part of my reading committee, as well as your valuable input.

Een groot deel van het analytisch werk in dit proefschrift heb ik uitgevoerd op het NIOZ in Yerseke, en hier heb ik dan ook flink wat tijd doorgebracht. Ik heb genoten van de open en positieve sfeer die er heerst, en kwam (en kom) er altijd erg graag. Allereerst Pieter, dank je wel voor alle hulp die je mij als relatieve buitenstaander geboden hebt, variërend van de meest basale laboratorium- en veldtechnieken tot de interpretatie van mijn chromatogrammen. Ik krijg spontaan weer last van mijn maag als ik aan de PLFA-pieken terugdenk. Also thanks to Silvia for helping me out with various things in the lab and in the field. Bart, dank je wel voor je uitleg van en hulp bij mijn metingen van nitrificatie-snelheden. Peter, dank je wel voor het meten van zowel mijn PLFA-

your time on the R/V Pelagia and I'm glad you got the opportunity to continue your career in a PhD project! Alissa, wij kenden elkaar natuurlijk al voor je aan je project begon en dat maakte de dynamiek weer heel anders. Ik wist dat het met je werk wel goed zou komen, maar we moesten soms oppassen om het niet te gezellig te maken. Hopelijk kan ik over niet al te lange tijd ook jouw proefschrift lezen! Thomas, bedankt voor je hulp tijdens en na de veldwerken op het Grevelingenmeer, en het feit dat je zo flexibel was in je planning toen bleek dat sommige dingen anders liepen dan gedacht. Zonder jou had het een stuk langer geduurd om al het werk af te krijgen.

For me, a pleasant working atmosphere is very important, and I'm lucky to have had such nice colleagues over the years. Not only to collaborate and discuss data, but also to enjoy doing activities outside office hours. A nice example of the latter is the rUUnning group, which regularly made me come out of my office, even though I felt I didn't always have the time. Thanks for keeping me fit and all the fun, also during the yearly Pheidippidesloop. But also the regular coffee and tea breaks, mostly including sweets or cake (the main reason the running and other sports were necessary), birthday parties, and drinks and other activities in town contributed to the positive atmosphere in the department. So thank you (in random order) Matthias, Nikki, Fatimah, Itzel, Peter, Chiara, Tom, Anna, Marie-Louise, Jiawang, Rick, Amelia, Alwina, Alejandra, Anne, Melanie, Susann, Hamid, Virginia, Mariëtte, Marieke, Loes, Klaas, Gert, Gert-Jan, Tiuri, Helen, Joyce, Jasper, Robin, Linda, Conny, Martijn, Wytze, Marie, Amir, Konstantin, José, Iana, Thilo, Lubos, Regina, Xiaochen, Dirk, Arthur, Lex, Nieves, Carmina, Luis, Jacqueline, Julien, and everyone else I've collaborated or simply had a good time with over the past years. A special thanks should go to my office mates over the years, through whom I've always felt comfortable sitting in N.106: Tom, Virginia, Anne and Fatimah. Many people described our office as quiet and tidy, the latter which was probably true with the exception of my desk. I'd also like to thank my current office mates in PP9, Itzel and Fatimah, for providing again a pleasant working atmosphere and for making our office a cosy place.

Fatimah, thanks so much for everything I've learned from you and we've done together over the past 4.5 years, which is too much to describe here in detail. I'm very honoured that you agreed on being one of my paranymphs. Marie-Louise, Joyce, Itzel and Robin: thanks for allowing me to invade into your Urbino reunion group. I'm still not exactly sure how that happened (I guess it had something to do with EGU 2013), but I'm very pleased to have spent much time with you over the past two years and you've become great friends.

Naast het werken aan mijn proefschrift bleef er gelukkig ook nog af en toe tijd over voor de noodzakelijke afleiding. Nynke en Evelien, als (ex-)collega-promovendi konden we elkaar altijd erg goed begrijpen en steunen, maar bovenal zijn onze gezamenlijke etentjes, koffie-/lunchpauzes en andere activiteiten gewoon altijd leuk. Jeroen, Tim en Tim, dank jullie wel voor alle afleiding en activiteiten die we hebben ondernomen, en natuurlijk voor alle onvergetelijke SST weekendjes. Tessa, dank voor alle gezelligheid, etentjes en andere leuke dingen die we samen hebben gedaan. Lieke, dank je wel voor alle sushi- en spelletjesavonden. Nienke, dank je wel voor alle gezelligheid bij de vele dingen die we samen, al dan niet met andere mensen erbij, hebben gedaan. Daarnaast dank ik Harm Jan, Eva, Wouter, Christien, Menno, Astrid, Rein, Alissa, Richard, Marianne, Janneke, Shanna en alle andere mensen met wie ik de afgelopen 4 jaar een goede tijd heb gehad!

Curriculum Vitae

Mathilde Hagens was born on 18 April 1986 in Soest, Netherlands. She completed her pre-university education (gymnasium) at Het Baarnsch Lyceum in 2004. Being interested in a wide range of subjects, she had difficulties deciding what to study. Ultimately it was a holiday at the beach that stimulated her curiosity about the ocean, and she enrolled in the Bachelor's programme in Earth Sciences at Utrecht University, which she finished cum laude in 2008. During this period, Mathilde was actively involved in the study association, including one year as full-time board member, was member of the Bachelor's programme advisory committee, and participated in a pilot of the Honours Programme in Earth Sciences. In 2008 she started with a Master's programme in Geochemistry at the same university, which she completed cum laude in 2010. During this time she continued organising activities for the study association, and was student representative of the department management board from 2008-2009. Her final Master's research project, in which she investigated zones of high biogeochemical activity in salt marshes, was conducted at the University of Georgia under the supervision of Dr. Christof Meile.

In November 2010, Mathilde started working on a PhD project in the Geochemistry group at Utrecht University under the joint supervision of Prof. Jack Middelburg and Prof. Caroline Slomp and in close collaboration with the Royal Netherlands Institute for Sea Research (NIOZ), resulting in this dissertation. During her years as a PhD candidate, Mathilde was involved in promoting connections between PhD candidates and post docs of the various research groups within the Earth Sciences department by organising several events. She also contributed to a teaching module of the Junior College Utrecht aimed at enhancing the interest of talented high school students for conducting research.

Since March 2015, Mathilde works as a postdoctoral researcher in the Marine Biogeochemistry research group of Prof. Caroline Slomp, where she investigates alkalinity generation and iron cycling in Baltic Sea sediments using numerical modelling.